



**HAL**  
open science

# Freeze-drying of vaccines : Contribution of mathematical modelling for assessing product heterogeneity and scale-up risks

Bernadette Scutella

## ► To cite this version:

Bernadette Scutella. Freeze-drying of vaccines : Contribution of mathematical modelling for assessing product heterogeneity and scale-up risks. Chemical and Process Engineering. Université Paris Saclay (COmUE), 2017. English. NNT : 2017SACLA034 . tel-02366530

**HAL Id: tel-02366530**

**<https://theses.hal.science/tel-02366530>**

Submitted on 16 Nov 2019

**HAL** is a multi-disciplinary open access archive for the deposit and dissemination of scientific research documents, whether they are published or not. The documents may come from teaching and research institutions in France or abroad, or from public or private research centers.

L'archive ouverte pluridisciplinaire **HAL**, est destinée au dépôt et à la diffusion de documents scientifiques de niveau recherche, publiés ou non, émanant des établissements d'enseignement et de recherche français ou étrangers, des laboratoires publics ou privés.

# Freeze-drying of vaccines: Contribution of mathematical modelling for assessing product heterogeneity and scale-up risks

Thèse de doctorat de l'Université Paris-Saclay  
préparée à AgroParisTech -- Institut des sciences et industries du  
vivant et de l'environnement

**École doctorale n° 581 : Agriculture, alimentation, biologie,  
environnement et santé (ABIES)**

Spécialité de doctorat: Génie des procédés

Thèse soutenue à Paris, 15/11/2017 par

**Bernadette Scutellà**

Composition du Jury :

M. Patrick Perré Professeur, CentraleSupélec	Président
Mme Vincenza Calabró Professeur, Università della Calabria	Rapporteur
M. Thomas De Beer Professeur, Ghent University	Rapporteur
M. Romain Jeantet Professeur, AgroCampus-Ouest	Rapporteur
M. Erwan Bourlés Chercheur, GlaxosmithKline Vaccines	Examineur
M. Cristian Trelea Professeur, AgroParisTech	Directeur de thèse
Mme Stéphanie Passot Maître de Conférences, AgroParisTech	Co-encadrant de thèse







*To Domenico*

*Fabrum esse suae quemque fortunae*

from "Carmen de sententiis"

-Appius Claudius Caecus



**DISCLOSURE STATEMENT**

Bernadette Scutellà participated in a postgraduate Ph.D. program at GSK Vaccines. This work was funded by GlaxoSmithKline Biologicals S.A., under a Cooperative Research and Development Agreement with INRA (Institut National de la Recherche Agronomique) via the intermediary of the UMR (Unité Mixte de Recherche) GMPA (Génie et Microbiologie des Procédés Alimentaires) at the INRA Versailles-Grignon research centre.



## ACKNOWLEDGEMENTS

---

My Ph.D. has been a hard, challenging and amazing experience, both personally and professionally, that changed me deeply. The outcome of this work, in several different ways, depended on the participation and the inspiration of many great individuals whom I would like to thank.

Firstly, I would like to express my gratitude to the jury members of this thesis, Thomas De Beer, Vincenza Calabró, Romain Jeantet and Patrick Perré for the review of this manuscript and the insightful comments that improved the final version of this work. I need to thank wholeheartedly my supervisors, Prof. Cristian Trelea, Dr. Stephanie Passot and Dr. Fernanda Fonseca, my "pillars" during these three years, who helped me along all the steps of my project. Everyone in a different way taught me how to be communicative, pedagogic and scientifically critic. I can sincerely say that my experience during this Ph.D., the expertise I have developed, and the final outcome would not have been the same without their support.

I would like also to thank the GlaxoSmithKline Vaccines in Rixensart (Belgium) for funding this research project and giving me the opportunity to perform it. A special mention goes to Dr. Erwan Bourlès, for his commitment in creating this project, for sharing his knowledge with me throughout these years, for the fruitful discussions, but most of all for his presence, his motivation and his patience. I could not have imagined having better, most dedicated mentor during this experience.

I am deeply in debt to the GSK freeze-drying team for hosting me during my first year, and in particular to Vincent Ronsse, Alain Philippart, Olivier Despas for all the cycles run, the vials weighed and the Karl Fisher performed throughout my Ph.D. I am also very grateful to Yves Mayeresse and Benoit Moreau for sharing their expertise and for their contribution to this work.

I would like also to thank Prof. Michel Marin and Prof. Denis Flick, for their insightful comments and feedback. Also, a deeply grateful to Dr. Artemio Plana-Fattori for his friendly approach, our numerous meetings, our discussions about the radiation heat transfer and the precious suggestions in the use of COMSOL.

I am hugely appreciative to the whole unit of Food Engineering and Microbiology (GMPA) of the France National Research Institute of Agronomy (INRA) based Grignon and directed first by François Boué and then by Pascal Bonnarne. I would like especially to thank to all my Ph.D. colleagues, for their hospitality during these years and for their help and patient especially at the very beginning, when my knowledge in French were very (very) basic! More than others, I am grateful to

the whole équipe Malices (Alberto, Nadia, Evelyne and Nathalie), and especially my colleagues Thuy Minh, Thomas, Marc and Benoît for sharing together the good, bad and "hot" moments of our thesis and (in particular) of our office.

My Ph.D. would not have been the same without my interns, Victor, Gwenaël and Cassandre. In particular, I need to thank Cassandre for sharing together the work on the secondary drying, and for being so helpful in the experimental part.

Furthermore, there are some people that made the difference in my life even if they were not directly involved in this work. First, I want to thank Raffaella, my Ci, for her unconditional support, and simply for her presence during these years (and long before). I hope you know how precious you are for me.

From the deepest of my heart, I want to thank my housemate, Anne-Lise, my deputy princess of Europe, for being such an amazing travel companion, for having the patience to stay constantly by me during the up and down of my journey. I will be always ready to leave with you for seeing our little penguins!

Thanks to my beloved friend Laura, who motivated me at first to do a Ph.D., and who introduced me into the world of the academic publications. I will always miss you.

Thanks to Domenico, my soul mate, for encouraging me, for making my success his own, for staying always closely by my side (in different countries of the world), despite the difficulties we went through, and especially for supporting me during this last particularly challenging period of writing. This work is dedicated to us.

However, the most important thank goes (and always will) to my family: my strong dad, my brave mum and my sweet grandmother. I do not need to say anything to them: they already know everything.





## PARTS OF THIS THESIS HAVE BEEN PRESENTED OR PUBLISHED:

### *Publications in peer-reviewed journals*

- **Scutellà, B.**, Trelea, I. C., Bourlès, E., Fonseca, F. and Passot, S. (2017). Determination of the product resistance variability and its influence on the product temperature in pharmaceutical freeze-drying. Submitted to *European Journal of Pharmaceutics and Biopharmaceutics*;
- **Scutellà, B.**, Bourlès, E., Plana-Fattori, A., Fonseca, F., Flick, D., Trelea, I. C and Passot, S. (2017). Effect of freeze-dryer design on heat transfer variability investigated using a 3D mathematical model. Submitted to *Journal of Pharmaceutical Sciences*;
- **Scutellà, B.**, Bourlès, E., Tordjman, C., Fonseca, F., Mayeresse, Y., Trelea, I. C. and Passot, S. (2017). 'Can the desorption kinetics explain the residual moisture content heterogeneity observed in pharmaceuticals freeze-drying process?'. Submitted to *Drying Technology* journal;
- **Scutellà, B.**, Plana-Fattori, A., Passot, S., Bourlès, E., Fonseca, F., Flick, D. and Trelea, I. C. (2017). '3D mathematical modelling to understand atypical heat transfer observed in vial freeze-drying'. *Applied Thermal Engineering*, 126, pp. 226-237;
- **Scutellà, B.**, Passot, S., Bourlès, E., Fonseca, F. and Trelea, I. C. (2017). 'How vial geometry variability influences heat transfer and product temperature during freeze-drying'. *Journal of Pharmaceutical Sciences*, 106 (3), pp. 770-778.

### *Posters and oral communications*

- **Scutellà, B.**, Bourlès, E., Tordjman, C., Fonseca, F., Mayeresse, Y., Trelea, I. C. and Passot, S. (2017). 'Can the desorption kinetics explain the residual moisture content heterogeneity observed in pharmaceuticals freeze-drying process?'. Oral communication with full text at 6<sup>th</sup> *European Drying Conference*, Liège (Belgium);
- **Scutellà, B.**, Bourlès, E., Fonseca, F., Plana-Fattori, A., Flick, D., Trelea, I. C. and Passot, S. (2016). 'How to manage scale-up using the design space approach'. Oral communication at *PDA Conference*, Strasbourg (France);
- **Scutellà, B.**, Passot, S., Bourlès, E., Fonseca, F., Plana-Fattori, A., Flick, D. and Trelea, I. C. (2016). 'Finite elements model of heat transfer predicts the edge vial effect in different freeze-drying configurations'. Poster at *CPPR Conference Freeze-drying of pharmaceuticals and biologicals*, Breckenridge (CO);
- **Scutellà, B.**, Passot, S., Rousseau, V., Davaud, G., Plana-Fattori, A., Flick, D. and Trelea, I. C. (2016). 'Detailed mechanistic modelling of atypical heat transfer condition in freeze-

drying process using COMSOL'. Oral communication at *Ph.D. days ABIES School*, Paris (France);

- **Scutellà, B.**, Passot, S., Bourlès, E., Fonseca, F. and Trelea, I. C. (2015). 'Inter-vial heat transfer heterogeneity during freeze-drying: role of vial geometry and position on the shelf'. Poster at *7th International Conference ISL-FD*, Barcelona (Spain).

#### ***Others***

- 2<sup>nd</sup> prize as best presenter at "Ph.D. days" organized attributed by the ABIES School;
- 3<sup>th</sup> prize at the contest "My professional project in 180 sec" attributed by the ABIES School.

# CONTENTS

---

<b>PREFACE.....</b>	<b>1</b>
<b>I. LITERATURE REVIEW .....</b>	<b>7</b>
<b>I.1 Fundamentals of freeze-drying .....</b>	<b>13</b>
I.1.1 A process as old as time .....	13
I.1.2 The freeze-dryer system .....	15
I.1.3 The process .....	15
I.1.4 The importance of amorphous formulation in freeze-drying.....	19
I.1.5 Importance of heat and mass transfer in freeze-drying.....	23
<b>I.2 Mechanisms of heat and mass transfer in freeze-drying .....</b>	<b>25</b>
I.2.1 Pseudo-steady state in primary drying.....	25
I.2.2 Heat transfer in freeze-drying: the vial heat transfer coefficient .....	25
I.2.3 Mass transfer in primary drying (sublimation).....	35
I.2.4 Mass transfer in secondary drying .....	47
I.2.5 Limits in the use of the classical equations of freeze-drying process.....	49
<b>I.3 Mathematical modelling of freeze-drying .....</b>	<b>51</b>
I.3.1 Pseudo steady state mathematical modelling .....	61
I.3.2 Dynamic mathematical modelling .....	63
I.3.3 Mathematical modelling for process control and product quality assurance.....	67
<b>I.4 Quality-by-Design in freeze-drying process .....</b>	<b>69</b>
I.4.1 What is the "Quality-by-Design"? .....	69
I.4.2 Quality-by-Design in freeze-drying process.....	73
I.4.3 Design space for secondary drying.....	83
I.4.4 Motivations of this project.....	87
<b>II. SCIENTIFIC APPROACH .....</b>	<b>89</b>
<b>II.1 Scientific questions.....</b>	<b>91</b>
<b>II.2 Experimental strategy .....</b>	<b>93</b>
II.2.1 Identification and quantification of the mechanisms responsible for product quality heterogeneity in freeze-drying process .....	93
II.2.2 Complete mathematical model including all considered sources of variability.....	94
<b>III. RESULTS AND DISCUSSION .....</b>	<b>97</b>
<b>III.1 How vial geometry variability influences heat transfer and product temperature during freeze-drying .....</b>	<b>99</b>
III.1.1 Context and objectives.....	99
III.1.2 Paper .....	101
III.1.3 Take-home message .....	124
<b>III.23D mathematical modelling to understand atypical heat transfer observed in vial freeze-drying .....</b>	<b>127</b>

III.2.1	Context and objectives.....	127
III.2.2	Paper .....	129
III.2.3	Take-home message .....	156
<b>III.3</b>	<b>Effect of freeze-dryer design on heat transfer variability investigated using a 3D mathematical model .....</b>	<b>159</b>
III.3.1	Context and objectives.....	159
III.3.2	Paper .....	161
III.3.3	Take-home message .....	180
<b>III.4</b>	<b>Determination of the product resistance variability and its influence on the product temperature in pharmaceutical freeze-drying.....</b>	<b>183</b>
III.4.1	Context and objectives.....	183
III.4.2	Paper .....	185
III.4.3	Take-home message .....	208
<b>III.5</b>	<b>Can the desorption kinetics explain the residual moisture content heterogeneity observed in pharmaceuticals freeze-drying process? .....</b>	<b>211</b>
III.5.1	Context and objectives.....	211
III.5.2	Paper .....	213
III.5.3	Take-home message .....	229
<b>III.6</b>	<b>Multi-vial, dynamic mathematical model to design freeze-drying process of pharmaceuticals through a risk-based approach .....</b>	<b>231</b>
III.6.1	Context and objectives.....	231
III.6.2	Paper .....	235
III.6.3	Take-home message .....	259
<b>IV.</b>	<b>GENERAL CONCLUSIONS .....</b>	<b>261</b>
	<b>GLOSSARY OF FREEZE-DRYING.....</b>	<b>279</b>
	<b>RÉSUMÉ SUBSTANTIEL.....</b>	<b>287</b>
	<b>REFERENCES.....</b>	<b>299</b>
	<b>APPENDIX.....</b>	<b>313</b>





**— PREFACE —**



## PREFACE

---

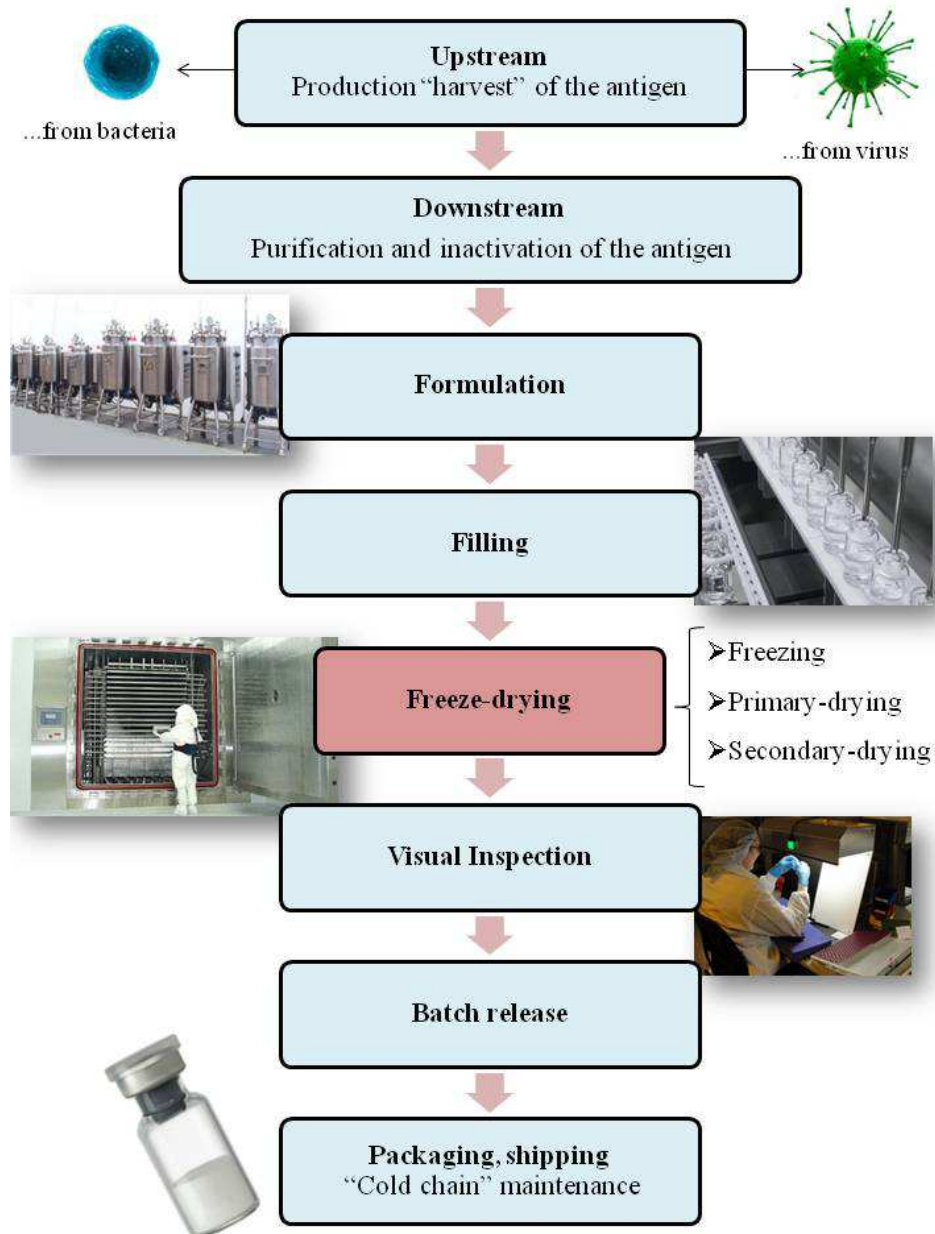
*"Next to clean water, no single intervention has had so profound effect on reducing mortality from childhood diseases as has the widespread introduction of vaccines."*

*- Institute of Medicine Report*

Vaccination is widely considered as one of the greatest achievements of the medical research. Since the first Edward Jenner's development of the vaccine for the smallpox, vaccination was responsible for controlling and greatly reducing the spread of several deadly diseases, such as poliomyelitis, tetanus, pertussis, diphtheria. Nowadays, existing vaccines can be classified in seven groups in function of their active ingredient (named antigen): live attenuated vaccines, subunit vaccines, inactivated vaccines, DNA vaccines, recombinant vector vaccines, toxoid vaccines and conjugate vaccines. The live attenuated vaccines are known to be the most successful and effective class and are made by reducing the virulence of viruses or rarely of bacteria. A schematic representation of their production process is presented in **Figure 0.1**. As live attenuated vaccines are usually more stable in dried form (1 - 3 % of water content) than in aqueous solutions, their production process involves a drying step. However, vaccines are very heat labile products and can be damaged if processed at high drying temperatures, e.g., collapse of the product "cake" can occur, or the vaccine can lose its potency. Thus, due to the combined use of vacuum and low temperatures, freeze-drying is usually the method of choice employed for vaccine production. This process is carried in three successive steps: (i) *the freezing* of the vaccines formulation, previously filled in small glass containers (vials), with the consequent formation of ice crystals and a cryo-concentrated matrix; (ii) *the primary drying*, in which the ice crystals are removed by sublimation; (iii) *the secondary drying*, in which desorption of the water bound to the interstitial matrix is carried out long enough to achieve the target residual moisture content in the product. Due to the combined use of vacuum and low temperatures, this process is recognized to be a gentle method of drying, suitable for heat sensitive products such as vaccines. However, freeze-drying remains a time-consuming and expensive process, difficult to design and scale-up, which often result in product batches of non-homogeneous quality when operating variables are not adequately selected.

Nowadays, vaccines safety and vaccination effectiveness gets understandably more and more public attention. The need of assurance of product quality resulted in more comprehensive regulatory

**Figure 0.1:** Schematic flowchart of the production process of live attenuated vaccines



procedures throughout all the steps of vaccines development and production. One of the newest approach to enhance quality of pharmaceutical products while reducing the regulatory burden is the implementation of the Quality by Design initiative, proposed in the early 2000 by the US Food and Drug Administration. The Quality by Design philosophy states that *the quality of the product should not be tested on the final product but built-in during the process* by means of the determination of quality targets and of a deep understanding of how product and process interacts. One of the critical steps of the implementation of the Quality by Design in the production process of vaccines is the definition of the critical quality attributes (CQAs) of the product, that are for example in a freeze-dried vaccine the stability of the antigen, the final moisture content of the product and the pharmaceutical "elegance" of the cake. These CQAs depend on freeze-drying step, during which the product temperature has to be maintained below a maximum allowed value to avoid the loss of the porous structure of the product, i.e., product collapse. Collapse generally causes a higher final moisture content of the product, longer product reconstitution time and especially the loss of the pharmaceutical "elegance" of the cake required for product acceptance by the authorities. However, a product temperature too far from the optimum leads to a significant increase of the operating time and thus to a decrease of process efficiency.

Optimum operating variables in freeze-drying can be defined by constructing the *design space*. The design space is a key concept of the Quality by Design, defined as the *multidimensional combination of the input variable and process parameter that provide assurance of product quality*. Construction of the design space can be performed by an extensive experimental campaign or by using classical equations of heat and mass transfer in freeze-drying, that can predict an average value of product temperature, sublimation rate and moisture content in the vial batch.

Unfortunately, heat and mass transfer in freeze-drying depend not only on the operating variables of the process (i.e., chamber pressure, shelf temperature) but also on several factors, such as product properties, container geometry, equipment characteristics. Understanding the impact that additional factors can have on the heat and mass transfer phenomena on vials differently located on the shelf is of paramount importance for predicting the product quality variability, and thus allowing to perform a reliable risk assessment of the process during the design and the scale-up steps.

In this context, the present project was realized with the financial contribution of the pharmaceutical company GlaxoSmithKline Vaccines (Belgium).

In line with the Quality by Design initiative, the main objectives of this work were to (i) investigate and quantify the sources responsible for heat and mass transfer variability, and consequently for product quality heterogeneity, within the same vial batch or between batches at different scales in primary and secondary drying and to (ii) implement the previously studied phenomena in a dynamic mathematical model of freeze-drying. The developed model was then used to define an original approach for the prediction of the risk of failure of the process (expressed in terms of percentage of vials potentially rejected) and thus for the selection of process operating conditions leading to desired product quality at acceptable risk.

### Outline of the thesis

This manuscript presents in four main parts the work that was performed during the three years of this Ph.D. project.

In the **first part**, a literature review summarizes the state of art of the mathematical modelling of freeze-drying process. Firstly, this review focuses on the fundamentals of freeze-drying, and describes the main heat and mass transfer phenomena during the different steps of the process. Then, attention is focused on the integration of these phenomena in mathematical models of freeze-drying and on how these models were previously used as tool for the design, scale-up and risk assessment of the process.

The **second part** presents the scientific approach applied during this research for the identification and quantification of the main mechanisms responsible for the product quality variability in the process.

The **third part** is divided in six papers which report the different results obtained. In a *first paper*, the importance of the vial bottom dimensions on the heat transfer variability is analysed. The mechanisms responsible for the difference in heat flow rates between vials located at the periphery and in the centre of the shelf are investigated in a *second paper* by using an original 3D mechanistic mathematical model of heat transfer during sublimation developed in COMSOL Multiphysics. This model is then used in a *third paper* to explore the effect of the loading configurations and of different design elements of the equipment on the heat flow rates received by the vials during the process.

In a *fourth paper*, our attention focuses on mechanisms responsible for the inter-vial mass transfer variability during primary drying related to product structure. Successively, the importance of the desorption rate variability on the distribution of the moisture content in the final product is explored

in a *fifth paper*.

Then, in a *sixth and last paper*, a dynamic mathematical model of freeze-drying is developed including the previously explored mechanisms responsible for heat and mass transfer variability between vials. This model is then used to predict the value and distribution of product temperature, ice fraction and moisture content. Finally, it was proposed an original approach for the development of the primary and secondary drying steps of the freeze-drying process at known risk of failure, expressed as percentage of vials potentially rejected.

Finally, the **IV part** presents the general conclusion of the obtained results through a global analysis of the observed phenomena, and highlights the main future perspectives.

At the end of this manuscript, a small **glossary** of specialized terms in freeze-drying is provided as a tool of reference for the reader.



— I —

## LITERATURE REVIEW



**NOMENCLATURE**

$a_w$	Water activity
$a_c$	Accommodation coefficient
$A$	Cross sectional area ( $m^2$ )
$C_1$	Parameter (contact conduction and radiation contribution to $K_V$ ) of <b>Equation I.2.11</b> ( $W m^{-2}K^{-1}$ )
$C_2$	Parameter (gas conduction contribution to $K_V$ ) of <b>Equation I.2.11</b> ( $W m^{-2}K^{-1} Pa^{-1}$ )
$C_3$	Parameter (gas conduction contribution to $K_V$ ) of <b>Equation I.2.11</b> ( $Pa^{-1}$ )
$E_a$	Activation energy ( $J kg^{-1}K^{-1}$ )
$\Delta H$	Latent heat of sublimation ( $J kg^{-1}$ )
$F$	Visualization factor (-)
$f_I$	Fraction of ice in the product
$K$	Heat transfer coefficient ( $W m^{-2}K^{-1}$ )
$l$	Thickness ( $m$ )
$\dot{m}$	Water vapour flow rate ( $kg s^{-1}$ )
$P$	Pressure ( $Pa$ )
$\dot{Q}$	Heat flow rate ( $W$ )
$R$	Mass transfer resistance ( $Pa s kg^{-1}$ )
$R_g$	Ideal gas constant ( $J K^{-1}kmol^{-1}$ )
$R_p$	Product resistance ( $Pa m^2 s kg^{-1}$ )
$R_{p_0}$	Parameter (initial product resistance at dried layer thickness equal to 0) of <b>Equation I.2.20</b> ( $Pa m^2 s kg^{-1}$ )
$R_{p_1}$	Parameters of <b>Equation I.2.20</b> ( $Pa m s kg^{-1}$ )
$R_{p_2}$	Parameters of <b>Equation I.2.20</b> ( $m^{-1}$ )
$t$	Time ( $s$ )
$T$	Temperature ( $K$ )
$T_g$	Glass transition temperature ( $K$ )
$T'_g$	Glass transition temperature for maximally freeze-concentrated solutions ( $K$ )
$X$	Fraction of moisture content (-)
<b>Greek</b>	
$\lambda$	Thermal conductivity ( $W m^{-1} K^{-1}$ )

$\Lambda_o$	Free molecular flow heat transfer coefficient ( $W m^{-2} K^{-1} Pa^{-1}$ )
$\sigma$	Stefan-Boltzmann constant ( $W m^{-2} K^{-4}$ )
$\tau$	Characteristic desorption time ( <b>Equation I.2.21</b> ) ( $s$ )

**Subscripts and Superscript**

0	Initial
<i>amb</i>	Ambient
<i>B</i>	Bottom
<i>c</i>	Contact
<i>C</i>	Chamber
<i>CN</i>	Condenser
<i>coll</i>	Collapse
<i>d</i>	Dried
<i>des</i>	Desorption
<i>eq</i>	Equilibrium
<i>f</i>	Frozen
<i>gas</i>	Gas
<i>i</i>	Interface
<i>I</i>	Ice
<i>n</i>	Nucleation
<i>r</i>	Radiation
<i>ref</i>	Reference
<i>s</i>	Stopper
<i>S</i>	Shelf
<i>sub</i>	Sublimation
<i>T</i>	Top
<i>v</i>	Vapour
<i>V</i>	Vial

## ABBREVIATIONS

<i>CQA</i>	Critical Quality Attribute
<i>CQP</i>	Critical Quality Parameter
<i>DSC</i>	Differential Scanning Calorimetry
<i>FDM</i>	Freeze-Dry Microscopy
<i>ICH</i>	International Council for Harmonisation of Technical Requirements for Pharmaceuticals for Human Use
<i>NIR</i>	Near Infrared Reflectance
<i>PRT</i>	Pressure Rise Test
<i>QbD</i>	Quality by Design
<i>QbT</i>	Quality by Testing
<i>QTPP</i>	Quality Target Product Profile
<i>TDLAS</i>	Tunable Diode Laser Absorption Spectroscopy



## I.1 Fundamentals of freeze-drying

---

### I.1.1 A process as old as time

The word "freeze-drying" or "lyophilization" generally refers to a drying operation mainly performed by sublimation, which is the direct transition from frozen to gaseous state. The term lyophilization has origin from three ancient Greek word roots, λύω meaning "to break up, to dissolve", φιλέω meaning "to love, to kiss", and -ίζειν meaning "to make". Lyophilisation thus literally means "to make solvent loving", referred to the rapidly reabsorption of the solvent in the dried product (Varshney and Singh, 2015).

The method of freeze-drying can be traced back to prehistoric times, when the Eskimos preserved their fishes in the cold temperatures of arctic by dehydration. Around 1250 BC, the ancient Incas used a rudimental version of the process by storing their crops on the mountains above Machu Picchu. Their food stores were frozen by the cold mountain temperatures during night, and the water inside slowly sublimed under the low air pressure of the high altitudes with the first sun rays (Varshney and Singh, 2015).

During the different centuries, and especially during the II World War, freeze-drying was largely applied in pharmaceutical and medical practice to preserve blood and biological tissues. One of the very first applications of the freeze-drying process in vaccine production was documented in the XX century, with the publication of the freeze-dried formulation of the small pox vaccine in 1909.

However, the first commercialization of a sterile dry formulation for parenteral, the "DryVax" small pox vaccine, took place only in the 1940s (Varshney and Singh, 2015; Riedel, 2005).

Nowadays, freeze-drying is the method of choice in the biotechnology, pharmaceuticals, and biomedical industries for preserving a long list of heat sensitive products such as vaccines, bacteria, nanoparticles, hormones, peptides and proteins (Adams, 1991; Franks, 1998; Pikal *et al.*, 1991; Fonseca *et al.*, 2015; Hansen *et al.*, 2015; Abdelwahed *et al.*, 2006). The process involves three main steps: (i) the freezing of the product, (ii) the sublimation of the ice crystals formed and (iii) the desorption of the residual unfrozen water. Each of these steps is presented in detail thereafter.

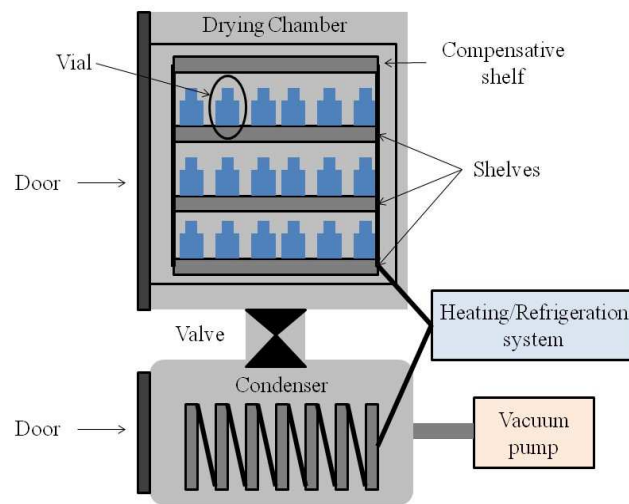


**Figure I.1.1:** Schematic representation of a freeze-dryer.

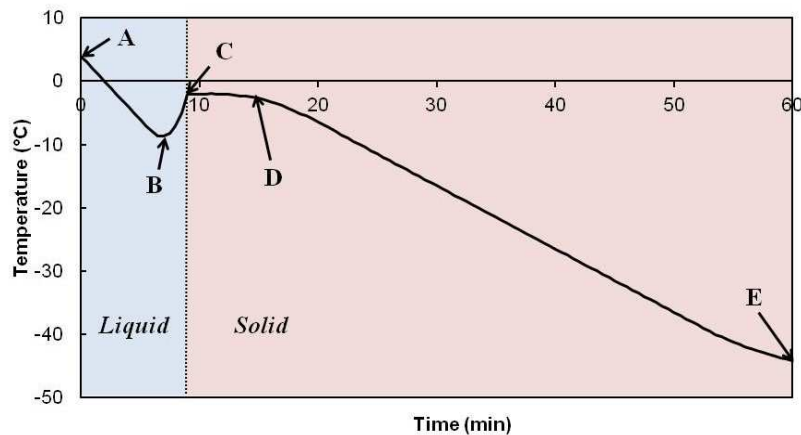


**Figure I.1.2:** An example of the product temperature profile during the freezing step of the process. Point A represents the initial point (product at 4 °C); point B represents the nucleation temperature  $T_n$ ; point C represents the equilibrium freezing temperature  $T_f$ ; the segment C-D represents the freezing plateau at the equilibrium freezing temperature; point E corresponds to the end of the freezing step (Béal and Fonseca, 2015).

## I.1.2 The freeze-dryer system

The freeze-dryer, schematically presented in **Figure I.1.1**, is composed by several elements: the drying chamber, the condenser, the vacuum pump, the heating and refrigeration system, and the supervision and control system. The drying chamber contains usually one or more shelves, on which the vials are directly placed during the three steps of the process. The temperature of the shelves is controlled by means of a heat transfer fluid pumped through built-in channels, which is cooled down or heated up by the heating-refrigeration system. The shelves act as a heat exchanger, removing energy from the product during the freezing and supplying heat during the primary and secondary drying steps. The drying chamber is connected usually by a mushroom or butterfly valve to the condenser, cooled by a refrigeration system. Furthermore, a vacuum pump is connected to the condenser and used to create the vacuum into the system usually at the beginning of the primary drying step. Finally, one or more temperature and pressure sensors help the control system to maintain the selected set point values of the operating variables during the different steps of the cycle.

## I.1.3 The process

### I.1.3.1 The freezing step

In pharmaceutical freeze-drying, the product formulated as aqueous solution is first filled into small glass containers (named vials) and then loaded directly on the pre-cooled shelves at 4 °C of the drying chamber before the beginning of the process. The protocol of the cycle is then implemented into the freeze-dryer software and the process is launched. The first step of the process is the *freezing*. An example of the product temperature profile during freezing is shown in **Figure I.1.2** (Béal and Fonseca, 2015). First, the product temperature decreases until nucleation takes place at the nucleation temperature  $T_n$  with the first ice crystals formation (point B, **Figure I.1.2**). Ice crystallization is an exothermic phenomenon, thus the product temperature abruptly increases to the equilibrium freezing point  $T_f$  (point C, **Figure I.1.2**) (Béal and Fonseca, 2015). The difference between the nucleation temperature  $T_n$  and the equilibrium freezing point  $T_f$  is known as *degree of supercooling* (segment BC, **Figure I.1.2**) (Kasper and Friess, 2011; Rambhatla *et al.*, 2004; Searles *et al.*, 2001b). Then, the product presents a constant temperature at the equilibrium freezing point, due to the equilibrium between the ice formation exothermic phenomenon and the heat removed from the product by the shelf (point CD, **Figure I.1.2**). As ice forms, the concentration of the unfrozen phase in contact with ice increases. Consequently, following shelf's temperature decrease, the freezing temperature progressively drops off according to Raoult's law (segment DE, **Figure I.1.2**).



The concomitant decrease in temperature and increase in solute concentration induces a rapid increase in viscosity. This process continues until the freeze concentrated solution solidifies as a crystalline matrix or a glass (Béal and Fonseca, 2015).

The ice nucleation temperature and the degree of supercooling dictate the size and morphology of ice crystals and thus the final porosity of the dried product (i.e., the fraction of the volume of voids over the total volume). Due to the stochastic nature of the nucleation, a variable degree of supercooling can be observed. A low nucleation temperature (and high degree of supercooling) generates smaller and numerous ice crystals and small pores. Small pores will result in high mass transfer resistance during primary drying and long sublimation time. Conversely, they will lead to short desorption time due to high specific surface area of the dried product.

Once completion of the freezing step, the primary drying starts.

#### **I.1.3.2 The primary drying step**

*Primary drying* is the most critical step of the process and occupies the longest portion of the total cycle time. It consists in the dehydration of the product by means of sublimation under vacuum of the previously formed ice crystals.

At the beginning of primary drying, the condenser is cooled down to temperature lower than  $-50\text{ }^{\circ}\text{C}$  and the pressure in the drying chamber is lowered to create the vacuum. When pressure reaches a value below the saturated vapour pressure of ice at the frozen product temperature, sublimation begins. Since sublimation is an endothermic process, the latent energy necessary for water sublimation is provided to the product by rising the temperature of the shelf. Thus, chamber pressure, shelf temperature and time are the main operating variables controlled during the primary drying.

The water vapour generated during the sublimation process flows from the drying chamber to the condenser. As the temperature of the condenser coils is much lower than the ice temperature in the product, water removal from the sample is achieved by trapping water by condensation on the cold condenser coils.

Primary drying is finished when all ice has been removed from the frozen product, and the process moves to the third and last step of the process, the secondary drying.

#### **I.1.3.3 The secondary drying step**

After completion of primary drying, unfrozen water is still present in the product bound to the dried matrix. The product appears dry, but the residual moisture content may be as high as 10- 20 % depending on the product (Roos, 1997). Further drying step is necessary to reduce the residual moisture content up to the target final value, compatible with storage stability of freeze-dried products.

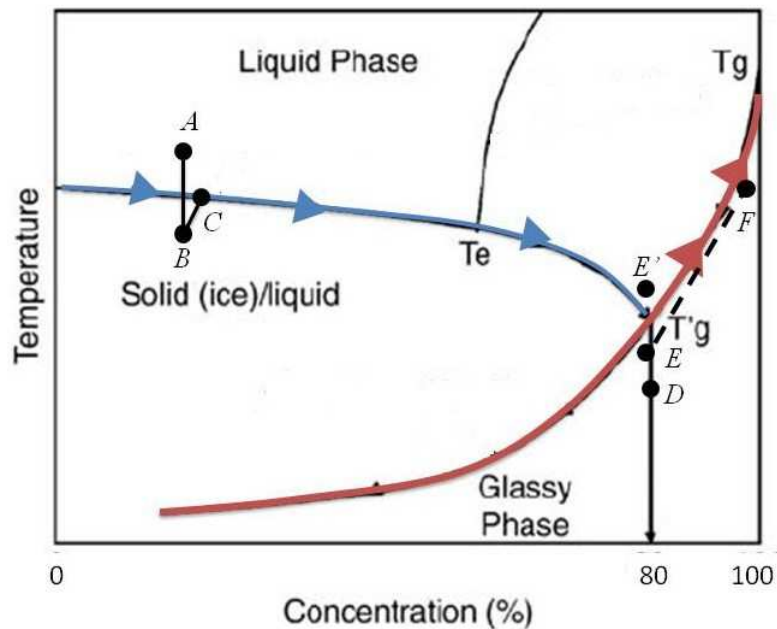


**Figure I.1.3:** Solid-liquid state diagram for the sucrose-water system. Abbreviations:  $T_e$ , eutectic temperature;  $T'_g$ , glass transition temperature for the maximum freeze-concentrated solution;  $T_g$ , glass transition temperature. Point A: initial state of the product; Point B: nucleation at  $T_n$ ; Point C: equilibrium freezing point ( $T_f$ ); Point D: end of the freezing step, product matrix is in glassy state; Point E: primary drying; Point E': primary drying at a temperature higher than  $T'_g$ ; Segment E-F: secondary drying. The % of sucrose is expressed as w/w. The blue line represents the equilibrium freezing curve, the red line represents the glass transition, the black solid line represents the eutectic curve (Abdelwahed *et al.*, 2006).

This last phase of freeze-drying is named *secondary drying* and is performed by desorption of the unfrozen water from the remaining concentrated solute matrix.

Desorption actually begins in a local region of the product once all the ice sublimates from that region, meaning that some secondary drying can occur during primary drying in different regions of the same sample (Pikal and Shah, 1990).

Secondary drying is normally carried out by rising the temperature of the shelf. The chamber pressure is generally kept unmodified, because this step of the process was found to be pressure independent for pressure values below 27 Pa (Pikal *et al.*, 1990).

The product is maintained at this temperature for several hours to reach specified residual moisture content at the end of freeze drying, typically between 1 and 3 %. The final residual moisture content of the lyophilized product needs to be precisely controlled: high values of residual water content impact on the product potency and shelf life, whereas overdrying promotes the protein activity loss upon storage (Pikal, 1994).

The final product, the freeze-dried product, is a solid structure with many very small pores. These pores create a large surface area of the lyophilisates and promote fast reconstitution of the product upon addition of water.

#### I.1.4 The importance of amorphous formulation in freeze-drying

Pharmaceutical freeze-dried products usually exist on the market as amorphous glassy solids (glasses). The use of excipients forming amorphous solids can protect the active ingredients (in particular proteins) against freezing and drying damages by means of two main mechanisms: (i) *the vitrification*, meaning the immobilization and isolation of the critical substances in a rigid glass, to reduce potential for protein aggregation and diffusion of small molecules required to initiate hydrolysis or oxidation; (ii) *the direct interaction between protein and excipient*, by means of hydrogen bonds between stabilizing excipients and the drug, can avoid conformation changes during freeze-drying (Yu, 2001). Crystalline solutes usually look more pharmaceutically elegant and are faster to dry, but can lead to a phase separation and loss of stabilizing power, as well as to the formation of slow dissolving particles, causing slow reconstitution of parenteral product (Akers, 2016; Yu, 2001).

During the freeze-drying process, the formulation solution exists under various states as function of the temperature and solute concentration. The modification of the solution state can be illustrated by a state diagram, as shown in **Figure I.1.3** for the water-sucrose system. The liquid/solid equilibrium freezing temperature (or ice melting point, blue bold line), and the glass transition temperature  $T_g$  (red bold line) are presented.

They respectively indicate the freezing/melting temperature and the reversible transition of a solution



from a rubbery into a glassy state, as a function of the matrix solute concentration. The equilibrium freezing point decreases when the solute concentration increases, whereas the glass transition temperature  $T_g$  decreases when the water content in the product increases.

Before the freezing step, the aqueous solution is in liquid state and contains a fixed concentration of sucrose (point A in **Figure I.1.3**). Then, the temperature is decreased and ice nuclei are formed at the ice nucleation temperature  $T_n$  (point B in **Figure I.1.3**).

As nucleation is an exothermic process, the product temperature rises until the equilibrium freezing temperature  $T_f$  at which ice crystals formation starts (point C in **Figure I.1.3**). Then, the concentration of the solute components of the formulation is progressively increased in the interstitial region between the growing ice crystals and the equilibrium freezing point decreases following the equilibrium freezing curve (Roos and Karel, 2007; Roos, 2010; Abdelwahed *et al.*, 2006). This phenomenon is referred to as "*cryoconcentration*".

As the concentration increases, the solution becomes more and more viscous, thus slowing down ice crystallization until reaching a characteristic temperature after which no further freezing occurs.

This temperature corresponds to the intersection of the equilibrium freezing curve and the glass transition curve and is called the *glass transition temperature of the maximally freeze-concentrated solution* (known as  $T'_g$ ) (Abdelwahed *et al.*, 2006; Roos, 2010).

At the end of the freezing step during freeze-drying process, the product reaches the point D in **Figure I.1.3** and the cryoconcentrated matrix is in glassy states.

During primary drying, the ice crystals are removed by sublimation but the concentration of the interstitial matrix remains constant at  $C'_g$  (point E in **Figure I.1.3**). However, if during primary drying the temperature of the product reaches a critical temperature higher than  $T'_g$  (point E' in **Figure I.1.3**), loss of the pore structure is observed in the dried region adjacent to the ice-vapour interface is due to a decrease of viscosity of the amorphous solute phase (Pikal and Shah, 1990; Roos, 2010). This dynamic phenomenon, known as collapse, takes place at a temperature known as *collapse temperature*  $T_{coll}$  and will normally be at the origin of vial rejection due to the high residual water, the prolonged reconstitution times or simply to the lack of "elegance" of the dried cake (i.e., an "elegant" freeze-dried cake should have the same size and shape as the solution originally filled into the container and should be uniform in color and texture) (Johnson and Lewis, 2011; Pikal and Shah, 1990; Patel *et al.*, 2017). The  $T'_g$  and  $T_{coll}$  do not represent the same parameter. The  $T'_g$  represents the temperature at which the maximally cryoconcentrated matrix follows the reversible transformation from a solid glassy state to a viscous liquid with an increase of temperature. It is generally measured



using the Differential Scanning Calorimetry (DSC) on a frozen sample in closed system, thus the ice crystals are in close contact with the glassy phase during the analysis. In contrast,  $T_{coll}$  is measured by direct observation using the Freeze-Dry Microscopy (FDM), which simulates (at very small scale) the sublimation step of freeze-drying process (Fonseca *et al.*, 2008; Pikal and Shah, 1990).

The collapse temperature thus corresponds to the minimum temperature at which the sublimation of ice is accompanied by a generalized loss of the structure of the lyophilized product. As result, the collapse temperature  $T_{coll}$  is usually slightly higher than  $T_g'$  of about 1 - 5 °C. In the industrial practice, the product temperature has to be maintained below 2 - 5 °C the maximum allowed temperature (Tang and Pikal, 2004), to preserve the product from any damage. The  $T_g'$  can thus be considered a critical threshold and safety value for the product temperature during primary drying to be used for the process design.

Once ice crystals are completely sublimed and secondary drying starts,  $T_g$  will increase as the moisture content will decreased in the product due to desorption (as shown by the red arrows and point F in **Figure I.1.3**). The critical temperature value will evolve during secondary drying according to the  $T_g$  curve.

### I.1.5 Importance of heat and mass transfer in freeze-drying

As evidenced from this analysis, the main constraint imposed to the freeze-drying process is given by the product temperature, which has to be maintained below a maximum allowed value during the primary and secondary drying steps to guarantee an acceptable final product quality. However, the product temperature profile cannot be controlled directly but depends on the values of the operating variables and on several heat and mass transfer phenomena taking place during the process. The understanding of these mechanisms is of paramount importance for a rational selection of the operating variables, i.e., shelf temperature and chamber pressure, and thus for the design and scale-up of the process.

In this regard, the most relevant heat and mass transfer mechanisms taking place during freeze-drying process will be described in the next section.



## I.2 Mechanisms of heat and mass transfer in freeze-drying

---

### I.2.1 Pseudo-steady state in primary drying

In the freeze-drying of pharmaceuticals, primary drying is usually considered to be carried out under pseudo-steady state condition, i.e., the heat flow rate  $\dot{Q}$  (W) received by the vials is completely used for the sublimation of ice crystals (Pisano *et al.*, 2011; Pikal, 1985, 2000; Velardi and Barresi, 2008; Schoen *et al.*, 1995; Pikal *et al.*, 1984). Thus, heat and mass transfer are coupled as:

$$\dot{Q} = \Delta H \dot{m}_{sub} \quad \text{Equation I.2.1}$$

with  $\Delta H$  (W kg<sup>-1</sup>) being the latent heat of sublimation.

### I.2.2 Heat transfer in freeze-drying: the vial heat transfer coefficient

The heat flow rate received by the product bottom is proportional to the difference between the average temperature of the fluid circulating into the shelf  $T_S$  (K) and the product temperature at the vial bottom  $T_{BV}$  (K):

$$\dot{Q} = K_V A_{BV} (T_S - T_{BV}) \quad \text{Equation I.2.2}$$

where  $A_{BV}$  (m<sup>2</sup>) is the vial bottom area and  $K_V$  (W m<sup>-2</sup>K<sup>-1</sup>) is the vial heat transfer coefficient.

Due to the concavity characteristics of the vial bottom, the vial heat transfer coefficient can be defined as the sum of three contributions (Pikal, 2000; Pisano *et al.*, 2011; Pikal *et al.*, 1984; Pikal, 1985):

$$K_V = K_c + K_r + K_g \quad \text{Equation I.2.3}$$

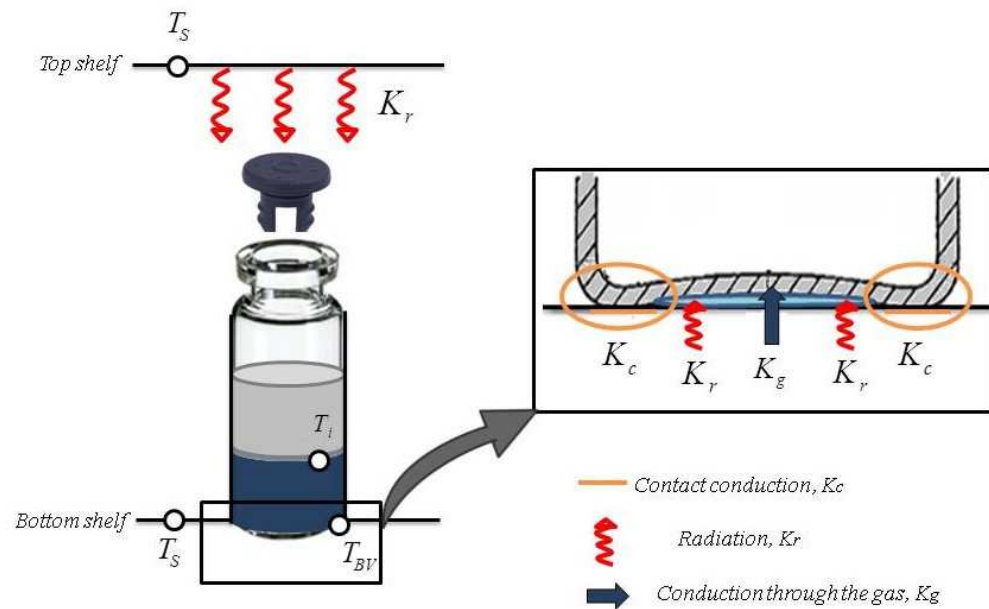


**Figure I.2.1:** Schematic representation of the heat transfer between the shelf and the vial. A zoom on the vial bottom is shown in the inset. The orange line represents the heat transfer by contact conduction ( $K_c$ ), the wavy red arrow the heat transfer by radiation ( $K_r$ ), the blue arrow the heat transfer by conduction through the gas ( $K_g$ ).

Each of those terms represents a different heat transfer mechanisms, as shown in **Figure I.2.1**:

- $K_c$  ( $W m^{-2}K^{-1}$ ) represents the thermal contact conduction through the contact area between the shelf and the vial;
- $K_r$  ( $W m^{-2}K^{-1}$ ) represents the thermal radiation, between the vial and the top and bottom shelves;
- $K_g$  ( $W m^{-2}K^{-1}$ ) represents thermal conduction through the gas entrapped in vial bottom concavity.

Each of those heat transfer contributions will be described in the next section.

### I.2.2.1 Heat transfer by contact conduction

The term  $K_c$  represents the heat transfer by contact conduction from the shelf to the vial bottom. Its contribution is independent on pressure, but it is influenced by the dimension of the contact area (Cannon and Shemeley, 2004; Kuu *et al.*, 2009), which is usually very small due to the presence of the vial bottom concavity. Thus, the value of  $K_c$  can be significantly different in function of the vial type (Kuu *et al.*, 2009).

### I.2.2.2 Heat transfer by radiation

The radiation contribution to the heat flow rate in vials is classically described by the Stefan-Boltzmann equation (Bird *et al.*, 2002; Pikal, 2000; Pikal *et al.*, 1984; Ganguly *et al.*, 2013):

$$\dot{Q}_r = A_r F \sigma (T_1^4 - T_2^4) \quad \text{Equation I.2.4}$$

In **Equation I.2.4**,  $T_1$  ( $K$ ) and  $T_2$  ( $K$ ) are the temperatures of the surfaces involved in the radiation heat exchange,  $A_r$  ( $m^2$ ) is the area exposed to the radiations,  $F$  is the visualization factor and ( $W m^{-2} K^{-4}$ ) is the Stefan-Boltzmann constant.

As presented in **Figure I.2.1**, all the vials on the shelf are affected by two different radiation heat transfer contributions during the process: between (i) the bottom shelf and the bottom of the vial and (ii) the top shelf and the top of the vial (Pikal *et al.*, 1984; Pikal, 2000; Pisano *et al.*, 2011). Thus, the visualization factor  $F$  can be expressed as:

$$F = F_B + F_T \quad \text{Equation I.2.5}$$

The emissivity factor at the bottom of the vial  $F_B$  can be evaluated considering the definition proposed by Bird *et al.* (Bird *et al.*, 2002), and Pikal (Pikal, 2000). For the two surfaces involved in



the exchange, shelf and vial, it is necessary to assume that: (i) the two surfaces are opaque and parallel; (ii) the area of the two surfaces involved in the exchange is equal; (iii) the absorption factor is equal to the emissivity factor for both surfaces; (iv) all the radiations leaving the shelf strike the

vial bottom (Bird *et al.*, 2002; Pikal, 2000). Hence,  $F_B$  can be expressed as in **Equation I.2.6**:

$$F_B = \frac{1}{1 + \left(\frac{1}{e_V} - 1\right) + \left(\frac{1}{e_S} - 1\right)} \quad \text{Equation I.2.6}$$

where  $e_V$  is the emissivity of the vial and  $e_S$  the emissivity of the shelf. Typical values of  $F_B$  may be around 0.1 - 0.3. In contrast, the area of the vial exposed to the top shelf is much smaller than the area of the shelf itself, and the visualization factor  $F_T$  can be estimated as equal to the emissivity of the vial  $e_V$  (Pikal, 2000; Pikal *et al.*, 1984):

$$F_T = e_V \quad \text{Equation I.2.7}$$

The value of visualization factor at the vial top is usually higher than at the vial bottom, being around 0.84 (Pikal *et al.*, 1984).

### I.2.2.3 Heat transfer by conduction through the gas

The vials used in freeze-drying process have a bottom concavity in which some gas is contained. For the typical range of pressure used in pharmaceutical freeze-drying (<10 Pa), the density of the gas is very low and the gas molecules collide more frequently with the solid surface as they do with other molecules. In this condition, the heat transfer takes place under the free-molecular or Knudsen regime (Pikal *et al.*, 1984; Pikal, 2000; Brülls and Rasmuson, 2002).

A relatively simply way of calculating the gas conduction contribution in the vial bottom is a formula derived by Pikal *et al.* (Pikal *et al.*, 1984), from a work of Dushman and Lafferty (Dushman and Lafferty (eds.), 1962):

$$K_g = \frac{C_2 P_C}{1 + C_3 P_C} \quad \text{Equation I.2.8}$$

where  $P_C$  (Pa) is the pressure in the drying chamber whereas  $C_2$  ( $W m^{-2} K^{-1} Pa^{-1}$ ) and  $C_3$  ( $Pa^{-1}$ ) are respectively equal to:

**Table I.2.1:** Most used experimental methods for the determination of the vial heat transfer coefficient  $K_V$ . Local methods allow the determination of  $K_V$  in single vials, global methods lead to the determination of a mean value of  $K_V$  among all the vials on the shelf.

<i>Method</i>	<i>Local/Global method</i>	<i>Measurement</i>	<i>References</i>
Gravimetric method	Local	Average mass flow rate during sublimation in single vials	(Pikal <i>et al.</i> , 1984; Hottot <i>et al.</i> , 2005; Pisano <i>et al.</i> , 2011; Hibler <i>et al.</i> , 2012)
Pressure Rise Test (PRT)	Global	Global mass flow rate profile during sublimation among all the vials on the shelf	(Hottot <i>et al.</i> , 2005; Tang <i>et al.</i> , 2006a; Fissore <i>et al.</i> , 2010)
Tunable Diode Laser Absorption Spectroscopy (TSLAS)			(Kuu <i>et al.</i> , 2009)

$$C_2 = \Lambda_o \frac{\alpha_c}{1-\alpha_c} \left( \frac{273.15}{T_{gas}} \right)^{0.5} \quad \text{Equation I.2.9}$$

$$C_3 = C_2 \frac{l_{BV}}{\lambda_{amb}} \quad \text{Equation I.2.10}$$

where  $\Lambda_o$  ( $W m^{-2} K^{-1} Pa^{-1}$ ) is the free molecular flow heat transfer coefficient of the gas at 0 °C,  $T_{gas}$  (K) the temperature of the gas participating in heat conduction, calculated as the average between the product temperature at the sublimation interface and the shelf temperature values (Pisano *et al.*, 2011),  $\alpha_c$  the accommodation coefficient,  $l_{BV}$  (m) is the depth of bottom curvature,  $\lambda_{amb}$  ( $W m^{-1} K^{-1}$ ) is the conductivity of the gas at atmospheric pressure (1 atm). The accommodation coefficient  $\alpha_c$  will be 1 if the exchange of energy between the shelf and the gas is complete, 0 if there will be no exchange. The value of  $\alpha_c$  can be particularly difficult to calculate, so often it is estimated by regression using experimental data.

The presence of the concavity in the vial bottom accounts for most of the resistance to conductive heat transfer, by reducing the points of direct contact between the vials and the shelf and thus the contact conduction contribution (Nail, 1980; Cannon and Shemeley, 2004; Kuu *et al.*, 2009; Ybema *et al.*, 1995). Furthermore, the value of  $K_V$  has to be characterized for different chamber pressures due to the dependence of the gas conduction contribution  $K_g$  on this parameter.

The dependence of the  $K_V$  on the chamber pressure is usually described in literature by **Equation I.2.11** (Pikal *et al.*, 1984; Hibler *et al.*, 2012; Pisano *et al.*, 2011):

$$K_V = C_1 + \frac{C_2 P_C}{1 + C_3 P_C} \quad \text{Equation I.2.11}$$

where  $C_1$  ( $W m^{-2} K^{-1}$ ) is the sum of  $K_c$  and  $K_r$ .

#### I.2.2.4 Experimental determination of $K_V$

The vial heat transfer coefficient  $K_V$  is usually calculated from experimental data by using **Equation I.2.1** and **I.2.2**. The data needed for the  $K_V$  determination are: (i) the difference between the temperatures of the shelf  $T_S$  and the product  $T_{BV}$ , which are commonly determined by using thermocouples or other temperature sensors, (ii) the outer cross sectional area of the vial  $A_{BV}$ , which can be determined from the dimensions of the container and (iii) the mass flow rate  $\dot{m}_{sub}$ .

An overview of the experimental methods typically used for the evaluation of the  $\dot{m}_{sub}$  ( $kg s^{-1}$ ) in the  $K_V$  determination is presented in (**Table I.2.1**) (Kuu *et al.*, 2009; Tang *et al.*, 2006a; Hibler *et al.*, 2012; Pisano *et al.*, 2011; Pikal *et al.*, 1984; Fissore *et al.*, 2010; Hottot *et al.*, 2005).

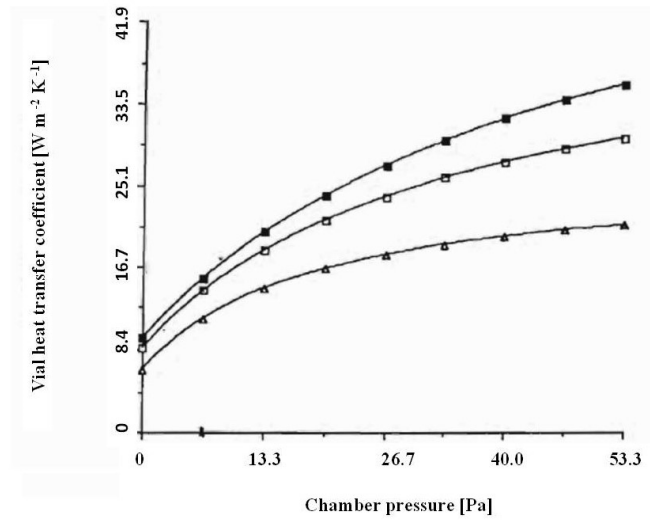
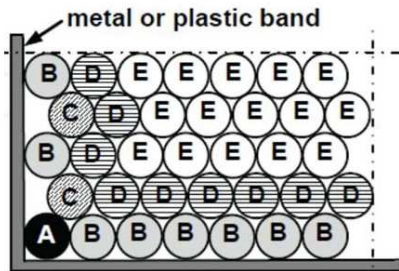


**Figure I.2.2:** Dependence of the vial heat transfer coefficient  $K_V$  on the chamber pressure for central vials. Symbols of empty triangles represent molded vials with a depth of bottom curvature of 0.22 mm, empty and filled squares represent tubing vials with a maximum depth of bottom curvature respectively of 0.11 mm and 0.04 mm (Pikal *et al.*, 1984).



Vial group	Position over the shelf	Additional mechanisms to vial heat transfer		
		radiation from chamber walls	contact with the tray band	contact with "hot" vials
A	corner	yes	yes	yes
B	peripheral	yes	yes	yes
C	peripheral	yes	no	yes
D	core	no	no	yes
E	core	no	no	no

**Figure I.2.3:** Scheme of a batch in which the vials are classified depending on their position and on the additional heat transfer mechanisms involved (Pisano *et al.*, 2011).

Among these, the gravimetric method appeared to be the most used one (Pikal *et al.*, 1984; Hibler *et al.*, 2012; Pisano *et al.*, 2011; Hottot *et al.*, 2005). Commonly, the following procedure is used to determine the average mass flow rate using the gravimetric method. Firstly, the vials are filled with a fixed amount of pure water, weighed and loaded in the drying chamber directly in contact with the shelf. The water is turned into ice crystals during a freezing step. Then, the pressure in the freeze drying chamber is reduced and the shelf temperature is increased to the selected values, so that sublimation of the ice can take place. Product and shelf temperature data are collected throughout this step.

When approximately 30 % of the ice has sublimed, the sublimation step is stopped to avoid loss of contact between the ice and the vial bottom. The vials are unloaded from the equipment and reweighed. Finally, the loss of mass divided by the duration of the sublimation phase gives the mass flow rate.

The vial heat transfer coefficient can be thus calculated from **Equation I.2.1** by using the collected data. This procedure is repeated at different chamber pressure to characterize the dependence of  $K_V$  on this operating variable. An example of the variation of  $K_V$  with the pressure is shown in **Figure I.2.2**. Vials presenting different values of maximum depth of bottom curvatures were used in this study. In agreement with other works (Hibler *et al.*, 2012; Pisano *et al.*, 2011; Kuu *et al.*, 2009), the  $K_V$  values increase with the pressure. However, this dependence is strictly influenced by the vial type, as the container determines the contact conduction contribution  $K_C$  through contact area  $A_C$  and the gas conduction contribution through the depth of bottom curvature  $l_{BV}$ .

Furthermore, other two experimental methods are used in literature for the determination of  $K_V$ : the Pressure Rise Test (PRT) and the Tunable Diode Laser Absorption Spectroscopy (TDLAS) (**Table I.2.1**). Both these methods allow to get a global mass flow rate profile among all the vials on the shelf during sublimation and thus to estimate a global value of  $K_V$  from **Equations I.2.1-2**. Details on the use of the PRT and TDLAS for the determination of the  $\dot{m}_{sub}$  will be given in **§I.2.3.4**. In this case, the curve of  $K_V$  vs.  $P_C$  can be determined in only one run, by varying the chamber pressure during the test (Hottot *et al.*, 2005; Kuu *et al.*, 2009; Velardi *et al.*, 2008).

However, it must be observed that the gravimetric measurement is the only method that allows the determination of  $K_V$  for vials differently located on the shelf and to have a global picture of the vial-to-vial heat transfer variability. During freeze-drying, the vials located at the periphery of the shelf (*edge vials*) present higher heat flow rates than the vials located in the centre of the shelf and surrounded by other vials in the same conditions (*central vials*) (Pikal *et al.*, 1984; Rambhatla and Pikal, 2003; Velardi and Barresi, 2008; Pisano *et al.*, 2011; Zhai *et al.*, 2005; Gan *et al.*, 2005). This position-dependent heat transfer is known as "*edge vial effect*" (Rambhatla and Pikal, 2003), and it is usually ascribed in literature to the additional radiations received by edge vials from the warmer

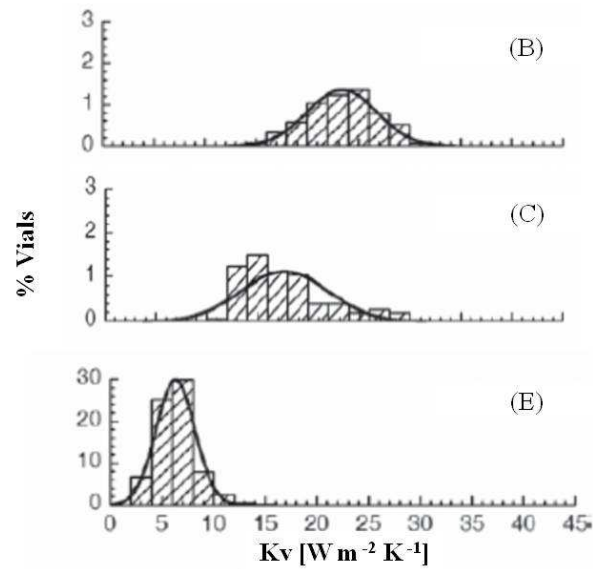


**Figure I.2.4:** Example of vial heat transfer coefficient experimental data (histogram) and normal distributions (solid line) evaluated for (B) edge vials in contact with the rail, (C) edge vials not in contact with the rail and (E) central vials (Pisano *et al.*, 2011). See **Figure I.2.3** for vials classification.

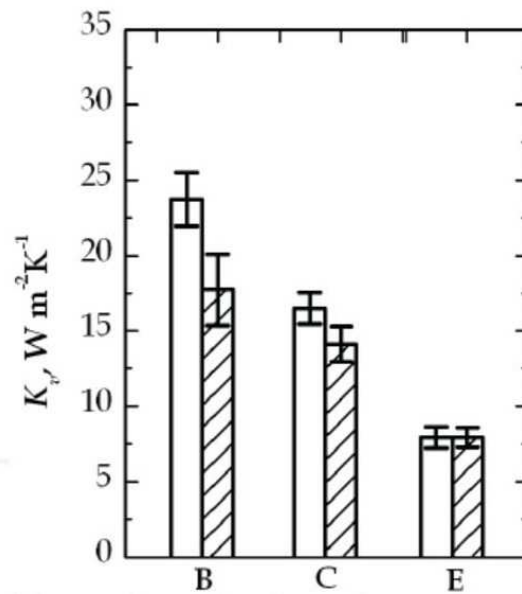


**Figure I.2.5:** Comparison between experimental values of  $K_v$  for edge vials in contact with the rail (B), edge vials not in contact with the rail (C) and central vials (E), measured in two pieces of equipment of different size: (□) laboratory and (///) industrial scale freeze-dryer (Pisano *et al.*, 2011). See **Figure I.2.3** for vials classification.

surface of the drying chamber to which the edge vials are exposed (e.g., walls and door) (Pikal *et al.*, 1984; Rambhatla and Pikal, 2003; Velardi and Barresi, 2008; Pisano *et al.*, 2011; Zhai *et al.*, 2005; Gan *et al.*, 2005). Pisano *et al.* (Pisano *et al.*, 2011), classified the vials in five main groups, as shown in **Figure I.2.3**, in function of their position on the shelf and the heat transfer contributions received: (A) edge vials located in the corner of the shelf, (B) edge vials in contact with the rail, (C) edge vials not in contact with the rail, (D) vials in contact with hot vials, (E) central vials. Due to the different heat transfer conditions, each of those groups can present a different  $K_V$  value. In this regard, **Figure I.2.4** shows the  $K_V$  distributions determined gravimetrically for edge vials B and C in contact and not in contact with the rail and central vials E. The edge vials show higher values of  $K_V$ , due to the additional radiation contributions received by the exposition to the drying chamber walls and the rail (Pisano *et al.*, 2011).

As the radiation heat transfer is strictly related to the emissivity of the components involved in the exchange and the geometry of the system (**Equation I.2.4-7**), the  $K_V$  values of edge vials may depend on the freeze-dryer used. In this regard, **Figure I.2.5** shows that the  $K_V$  values for edge vials located in contact and not in contact with the rail may be significantly different between a laboratory and a manufacturing scale freeze-dryer, whereas central vials show almost the same value (Pisano *et al.*, 2011). As the characteristics of the drying chamber can vary from one equipment to another, differences in  $K_V$  should be evaluated between different freeze-dryers for an effective cycle transfer or the scale-up (Pisano *et al.*, 2011).

It is a common practice in literature to describe heat transfer differences between vials at the edge and in the centre of the shelf by variations in  $K_V$  values. However, this approach does not take into account that the heat flux between the shelf and the vials (described by the vial heat transfer coefficient  $K_V$ , **Equation I.2.2**) and the additional heat fluxes received by edge vials are not due to the same temperature differences. For example, the radiation contribution from the wall to edge vials is due to the temperature difference between the chamber wall and the vial, which may be significantly different from the temperature difference between the shelf and vial.

### I.2.3 Mass transfer in primary drying (sublimation)

The mass transfer in primary drying is usually discussed in terms of resistance offered by a given barrier. **Figure I.2.6** illustrates a typical profile of the partial pressure of water vapour in primary drying and a corresponding graph showing the relative magnitude of each resistance present in the system (Pikal *et al.*, 1984; Pikal, 2000). Considering semi-stoppered or not stoppered vials, the total driving force of the process can be considered equal to the difference between the equilibrium vapour pressure  $P_i$  (Pa) of ice at the sublimation front and the partial pressure of water vapour in the condenser chamber  $P_{CN}$  (Pa).

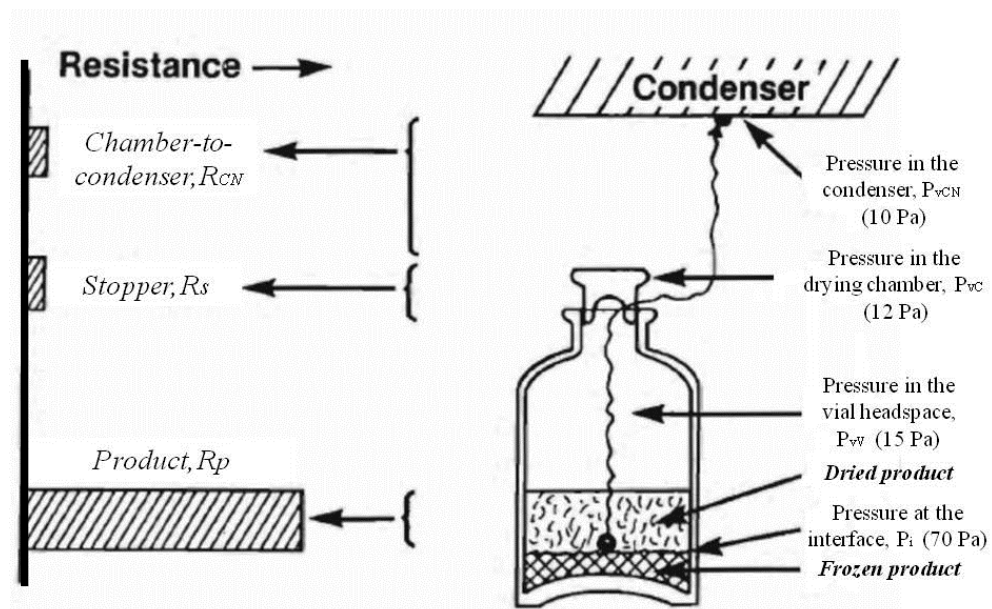


**Figure I.2.6:** A typical profile of the partial pressure of water vapour during primary drying and the relative magnitude of the mass transfer resistances present in the system (Pikal, 2000).

Thus, the mass flow rate  $\dot{m}_{sub}$  can be defined as:

$$\dot{m}_{sub} = \frac{(P_i - P_{CN})}{R} \quad \text{Equation I.2.12}$$

As shown in **Figure I.2.6**, the total mass transfer resistance can be described as the sum of each component resistance in series, which are (i) the dried product, (ii) the stopper and (ii) the chamber-to-condenser pathway. Thus,  $R$  ( $Pa \ s \ kg^{-1}$ ) can be expressed as (Pikal *et al.*, 1984; Pikal, 2000):

$$R = R_p + R_s + R_{CN} \quad \text{Equation I.2.13}$$

where  $R_s$  ( $Pa \ s \ kg^{-1}$ ) is the stopper resistance,  $R_{CN}$  ( $Pa \ s \ kg^{-1}$ ) is the chamber-to-condenser resistance and  $R_p$  ( $Pa \ s \ kg^{-1}$ ) is the product resistance equal to (Pikal *et al.*, 1984; Pikal, 2000):

$$R_p = \frac{\hat{R}_p}{A_i} \quad \text{Equation I.2.14}$$

where  $A_i$  ( $m^2$ ) is the ice-product interface area,  $\hat{R}_p$  ( $Pa \ s \ m^2 \ kg^{-1}$ ) is the area “normalized” product resistance.

### I.2.3.1 Product Resistance

The growing dried layer exhibits the major resistance to the sublimation flow, accounting for more than 80 % of the total resistance, unless the filling volume or concentration of the solute is very low and thus there is essentially no dried layer (Pikal, 2000). The resistance due to the product dried layer, known as product resistance  $\hat{R}_p$ , is classically defined as (Pikal *et al.*, 1984; Pikal, 2000):

$$\hat{R}_p = \frac{A_i(P_i - P_{vV})}{\dot{m}_{sub}} \quad \text{Equation I.2.15}$$

with  $P_{vV}$  ( $Pa$ ) equal to the partial pressure of the vapour into the vial headspace. If the stopper is not present,  $P_{vV}$  ( $Pa$ ) is assumed equal to the partial pressure of the vapour into the drying chamber.



### I.2.3.2 Stopper Resistance

Elastomeric stoppers are usually partially inserted into the vial necks before the process. They usually present one or several openings depending on the stopper design, which allow the outgassing of water vapour during the drying step (Akhilesh and Babu, 2010).

After the process, the stoppers are fully inserted in the vial neck directly into the freeze-dryer by moving the shelves, to guarantee the safety and sterility of the product (Akhilesh and Babu, 2010). The presence of the stopper impose another resistance to the mass flow rate (namely  $R_s$ ), which can be defined as (Pikal, 2000; Pikal *et al.*, 1984):

$$R_s = \frac{(P_{vV} - P_{vC})}{\dot{m}_{sub}} \quad \text{Equation I.2.16}$$

with  $P_{vC}$  (Pa) equal to the partial pressure of the vapour into the drying chamber, usually considered to be equal to the chamber pressure during primary drying as mostly water vapour is supposed to be present in the drying chamber.

The stopper resistance has a small contribution on the total heat transfer resistance, which also depends on the dimension of the vent. In a work of Pikal *et al.* (Pikal *et al.*, 1984),  $R_s$  was found to account to the total mass transfer resistance for 3 - 10 % in function of the dimension of the opening (0.2 to 0.4 cm).

### I.2.3.3 Mass transfer from chamber-to-condenser

The resistance due the chamber-to-condenser pathway  $R_{CN}$  is classically defined as (Pikal, 2000; Pikal *et al.*, 1984):

$$R_{CN} = \frac{(P_{vC} - P_{vCN})}{\dot{m}_{sub}} \quad \text{Equation I.2.17}$$

where  $P_{vCN}$  (Pa) the partial vapour pressure in the condenser, usually determined by the condenser temperature. In a work of Pikal *et al.* (Pikal *et al.*, 1984), the resistance due to the chamber to condenser pathway was found to be in the same order of magnitude of the stopper resistance, and to account for 3 - 6 % to the total mass transfer resistance.

In **Equation I.2.17**,  $R_{CN}$  is defined as a constant parameter. However, experimental evidences showed the value of  $R_{CN}$  may strongly vary in function of the total pressure and of the sublimation flux, which should be obviously impossible (Trelea *et al.*, 2015). Recently, Trelea *et al.* (Trelea *et al.*, 2015) developed a 1D mathematical model of the mass transfer between the chamber and the



condenser based on the mass transfer theory in binary gas mixtures (water vapour and inert gas). This model explained the apparent variation of  $R_{CN}$  with the sublimation rate as due to the mutual diffusion of vapour and inert gas. Thus, a more detailed description of the vapour transfer between the freeze-drying chamber and the condenser should be preferred to the mass transfer resistance approach proposed in **Equation I.2.17** to predict the partial vapour pressure and the sublimation flux during the process.

#### I.2.3.4 Experimental determination of $R_p$

Mass transfer resistance can be evaluated from **Equation I.2.12** knowing (i) the equilibrium vapour pressure at the ice-vapour interface and (ii) the partial vapour pressure in the condenser, usually determined by Clausius Clapeyron equation from the ice and the condenser temperatures, and (iii) the mass flow rate.

However, the resistance due to the chamber to condenser pathway is usually neglected, and the product resistance together with the stopper resistance can be determined as:

$$R_s + A_i R_p = \frac{(P_i - P_{vC})}{\dot{m}_{sub}} \quad \text{Equation I.2.18}$$

Furthermore, as the stopper offers only a small resistance if compared with the product dried layer, this contribution is often neglected or included into  $R_p$  (Oddone *et al.*, 2014; Overcashier *et al.*, 1999; Konstantinidis *et al.*, 2011). Thus, **Equation I.2.18** becomes:

$$\hat{R}_p = \frac{A_i(P_i - P_{vC})}{\dot{m}_{sub}} \quad \text{Equation I.2.19}$$

The following experimental procedure is used for the determination of the mass transfer resistance. The vials are first filled with the selected amount of solution and loaded on the shelf. Then, freezing is carried following the selected protocol. After completion of the freezing step, the sublimation starts. The equilibrium vapour pressure at the ice-vapour interface  $P_i$  is usually determined by Clausius Clapeyron equation from product temperatures, monitored by using sensors such as thermocouples. Furthermore, the mass flow rate profile during sublimation is usually measured by using online methods.

The most common are:

- *The microbalance*: Firstly used by Pikal *et al.* (Pikal *et al.*, 1983), the microbalance is a small balance provided of a holding arm on which one vial is loaded. The balance is placed on the shelf and the holding arm lifts the vial for weighing at fixed time intervals (e.g., about 10



min) during the process. Then, the vial is lowered back on the shelf and released from the holding arm. The difference of vial mass between two consecutive weightings gives the water loss due to sublimation. Finally, the mass flow rate profile can be calculated from the mass losses divided by the time intervals.

- *The pressure rise test (PRT)*: The pressure rise test is carried out by closing the valve in the duct connecting the drying chamber to the condenser for a short time interval (e.g., 30 sec) during sublimation. The pressure in the chamber increases due to the accumulation of the water vapour. Then, the pressure rise data can be analysed by one of the several algorithms developed in literature for the determination of the mass flow rate rate (Milton *et al.*, 1997; Tang *et al.*, 2006a; Velardi *et al.*, 2008; Hottot *et al.*, 2005).
- *The Tunable Diode Laser Absorption Spectroscopy (TDLAS)*: TDLAS is a non-invasive spectroscopic method which mainly consists in the generation of a laser beam by a NIR-Laser launched through the chamber-condenser pathway. The absorption spectrum is recorded and allows accurate measurement of the vapour concentration and of the vapour mass flow rate in the duct connecting the freeze drying chamber with the condenser (Kuu *et al.*, 2006; Gieseler *et al.*, 2007).

The described methods are effective in measuring the mass flow rate evolution in time, and then the product resistance from **Equation I.2.19**. However, it has to be remarked that the measured mass flow rate will be either a local value (e.g., when the microbalance is used) or an average value over all the vials on shelf (e.g., for PRT or TDLAS), and will not give information on the mass transfer variability between the vials. These methods also become unreliable towards the end of the sublimation step where mass flow rate variation is due to other causes than product resistance variation, such as curved sublimation interface or loss of thermal contact between the frozen part of the product and the vial.

The product resistance calculated from **Equation I.2.19**, is usually presented in function of the product dried layer thickness and often described by the following empirical formula (Overcashier *et al.*, 1999; Fissore and Pisano, 2015; Pikal, 2000; Pikal *et al.*, 1983; Kuu *et al.*, 2006; Bosca *et al.*, 2013).

$$\hat{R}_p = \hat{R}_{p_0} + \frac{\hat{R}_{p_1} l_d}{1 + \hat{R}_{p_2} l_d} \quad \text{Equation I.2.20}$$

where  $\hat{R}_{p_0}$  ( $Pa\ m^2\ s\ kg^{-1}$ ),  $\hat{R}_{p_1}$  ( $Pa\ m\ s\ kg^{-1}$ ) and  $\hat{R}_{p_2}$  ( $m^{-1}$ ) are empirical coefficients to be determined from experimental data. The non-zero intercept ( $\hat{R}_{p_0}$ ) accounts for a non-null resistance of the top layer, the exact origin of which remains still unclear.

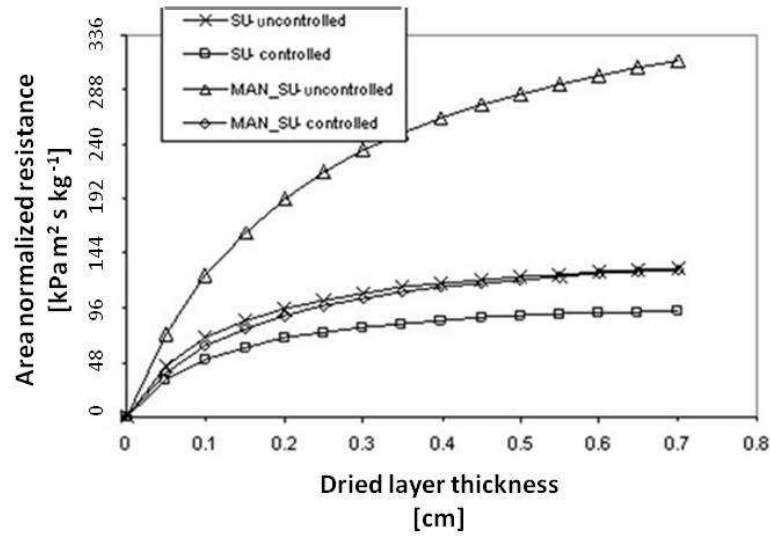


**Figure I.2.7:** Comparison for the area normalized resistance ( $\widehat{R}_p$ ) in  $\text{kPa m}^2 \text{ s h}^{-1}$  for 5 % sucrose (SU in the legend) and 3 % mannitol/2 % sucrose (MAN\_SU in the legend) processed with controlled and uncontrolled nucleation (Konstantinidis *et al.*, 2011).

In some works (Pikal *et al.*, 1984; Pikal and Shah, 1990), the evolution of  $\hat{R}_p$  in function of  $l_d$  ( $m$ ) was expressed as a linear relation ( $\hat{R}_{p_2}=0$ ). The characteristic evolution of  $\hat{R}_p$  with the dried layer thickness strongly depends on the product structure (i.e., solid solution and voids left after the ice crystals have sublimed), which is dictated by the freezing step. A higher value of nucleation temperature and degree of supercooling during the freezing led to bigger ice crystals and dried pores, and can affect the mass transfer resistance during the primary drying step (Searles *et al.*, 2001b; Kasper and Friess, 2011).

Dimensions of the ice crystals can be increased (i) by introducing an annealing step during the freezing, which consists in maintaining the samples at subfreezing temperature for a period of time (Searles *et al.*, 2001a; Lu and Pikal, 2004; Hottot *et al.*, 2005), or (ii) by controlling the ice nucleation (e.g., by inducing nucleation at the desiderate temperature using ultrasounds, vacuum, nucleation agents) (Passot *et al.*, 2009; Oddone *et al.*, 2014; Konstantinidis *et al.*, 2011).

As example, **Figure I.2.7** shows the evolution of the product resistance with the dried layer thickness for two products, a sucrose solution and a mannitol + sucrose solution, processed with and without controlled nucleation (Konstantinidis *et al.*, 2011). In this work (Konstantinidis *et al.*, 2011), ice nucleation was simultaneously induced in all the vials at the desired temperature by manipulating the chamber pressure of the freeze dryer during the freezing step. Both tested products processed under controlled nucleation showed a higher nucleation temperature, bigger radius of dried pores and a lower value of product resistance than products processed with uncontrolled nucleation (Konstantinidis *et al.*, 2011). In agreement with previous works (Searles *et al.*, 2001b; Oddone *et al.*, 2014), this study confirmed that the ice crystal morphology exerts considerable control over the vapour transfer from the ice interface to the top of the dried product layer (Kochs *et al.*, 1991; Searles *et al.*, 2001b).

Furthermore, the glass transition temperature of the product formulation ( $T'_g$ ) and the collapse temperature ( $T_{coll}$ ) can play a role in the definition of  $\hat{R}_p$ . Dried product resistance data had shown a significant temperature dependence as the product temperature becomes higher than  $T'_g$  and approaches  $T_{coll}$  in primary drying. **Figure I.2.8** well illustrates this phenomenon for a 5 % sucrose solution (Fissore and Pisano, 2015). At product temperatures lower or very close to the  $T'_g$  (-34.8 °C),  $\hat{R}_p$  increases with the dried layer thickness  $l_d$  (**Figure I.2.8A, D** and **I.2.8B, E**). In contrast, for a product temperature higher than  $T'_g$ , the magnitude of the product resistance is reduced dramatically, as well as its dependence on the  $l_d$  (**Figure I.2.8C** and **I.2.8F**) (Fissore and Pisano, 2015).

This dependence of the product resistance on the product temperature is due to the so-called "microcollapse", that is the development of larger pores holes in the dried material at temperature higher than  $T'_g$ , as shown in **Figures I.2.8G, I.2.8H** and **I.2.8I** (Fissore and Pisano, 2015).

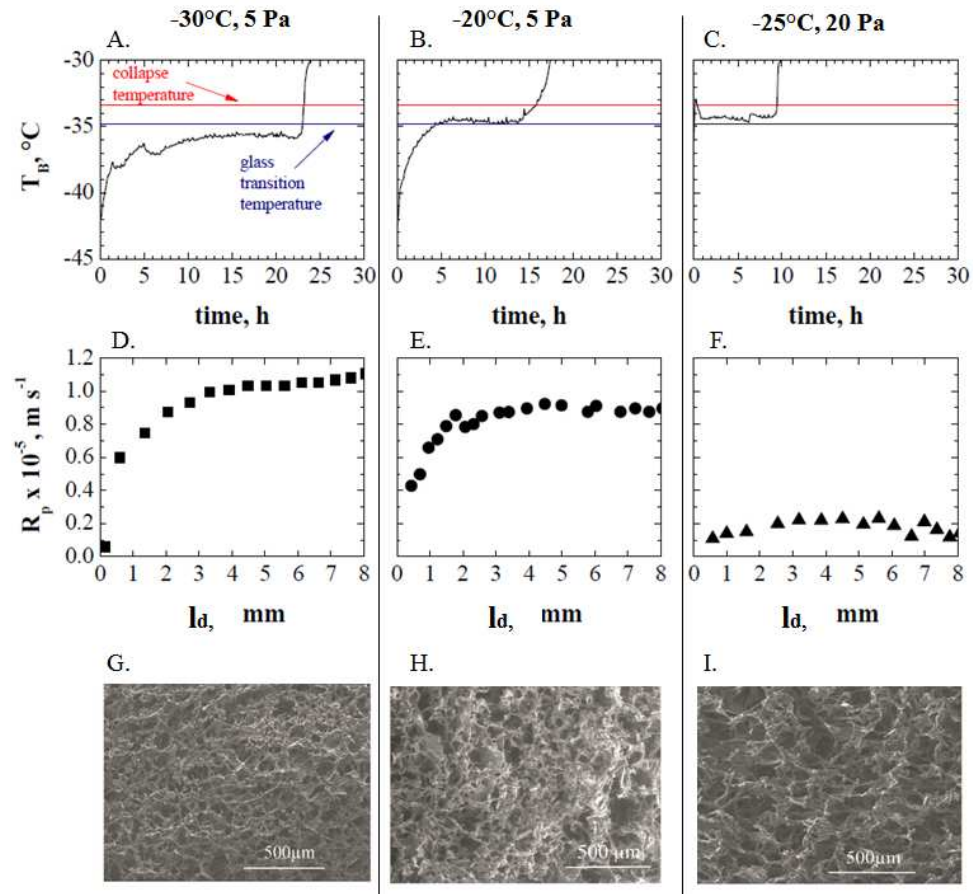


**Figure I.2.8:** Comparison between the values of product temperature at the bottom of the container (A, B, C) with the product resistance (D, E, F) and the cake structure (G., H, I), respectively. Operating conditions are reported on the figure (Fissore and Pisano, 2015).

### I.2.4 Mass transfer in secondary drying

The third and last step of the freeze-drying process is the secondary drying, which governs the final moisture content of the product and thus its stability in time. During this step, the product moisture content is further decreased through desorption of the non-frozen water. In case of most pharmaceutical products, the target moisture content is very low (e.g., 1 - 3 %), and thus secondary drying step may occupy a significant fraction of the process duration (Pikal, 1994). However, despite its importance, only an handful of publications focused on the understanding of secondary drying and on its optimization (Sadikoglu *et al.*, 1998; Pisano *et al.*, 2012; Fissore *et al.*, 2011b; Schneid *et al.*, 2011; Pikal *et al.*, 1990; Sheehan and Liapis, 1998; Lopez-Quiroga *et al.*, 2012; Pikal *et al.*, 2005).

The removal of bound water from the dried matrix to the vial headspace during secondary drying involved two main steps: (i) the mass transfer from the solid matrix surface to the pore channel and (ii) the vapour phase transport through the pores of the dried cake (Pikal *et al.*, 1990).

Contrary to primary drying, the vapour transport in the dried cake was verified to be not rate-limiting, because drying rate resulted to be insensitive to chamber pressure variations for pressures lower than 27 Pa and to cake thickness at constant specific surface area (Pikal *et al.*, 1990). Thus, the rate-determining step is considered to be the desorption of water from the pore surface in most of the works on secondary drying (Pikal *et al.*, 1990; Velardi and Barresi, 2008; Lopez-Quiroga *et al.*, 2012; Pisano *et al.*, 2012; Schneid *et al.*, 2011; Fissore *et al.*, 2011b).

**Figure I.2.9** shows a typical example of the moisture content evolution during secondary drying (Schneid *et al.*, 2011). The decrease of the moisture content  $X$  ( $kg\ kg^{-1}\ wb$ ) proceeds usually along two different kinetics: a first fast desorption, with a sharply decreasing of  $X$ , and a slower one for lower value of  $X$  approaching a plateau (Pikal *et al.*, 1990). The evolution of the product moisture content  $X$  in time during secondary drying is typically described as a single desorption kinetics (Lopez-Quiroga *et al.*, 2012; Pisano *et al.*, 2012; Pikal *et al.*, 2005; Fissore *et al.*, 2015):

$$\frac{dX}{dt} = \frac{1}{\tau} (X^{eq} - X) \quad \text{Equation I.2.21}$$

where  $X$  is the fraction of water per total product,  $X^{eq}$  ( $kg\ kg^{-1}\ wb$ ) is the equilibrium moisture content at a given water activity ( $a_w$ ), which can be calculated from the sorption isotherm (Lopez-Quiroga *et al.*, 2012; Passot *et al.*, 2012), and  $\tau$  (s) is the characteristic desorption time which depends on the product temperature through an Arrhenius type equation (J.H. de Boer, 1953):

$$\tau = \tau_{ref} e^{-\frac{E_a}{R_g} \left( \frac{1}{T_{BV}} - \frac{1}{T_{BVref}} \right)} \quad \text{Equation I.2.22}$$

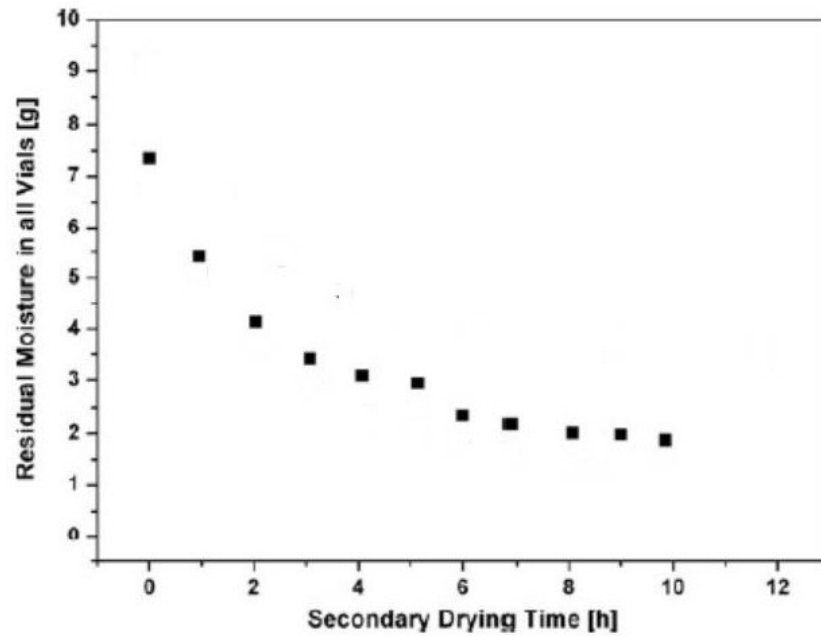


**Figure I.2.9:** Residual moisture content evolution of a BSA/sucrose solution during a secondary drying step performed at 0 °C (Schneid *et al.*, 2011).

where  $T_{BV}$  (K) is the product temperature,  $E_a$  ( $J\ kg^{-1}K^{-1}$ ) is the activation energy,  $R_g$  ( $J\ K^{-1}kmol^{-1}$ ) is the ideal gas constant and  $\tau_{ref}$  (s) is the characteristic desorption time at a reference temperature  $T_{BVref}$  (K).

Furthermore, Trelea et al. (Trelea *et al.*, 2016) recently developed a multilayer desorption model based on the idea that that moisture fractions in different physical states can present different desorption kinetics and thus different characteristic desorption times  $\tau$ . This model (Trelea *et al.*, 2016) accurately describes the evolution of the moisture content during secondary drying by two distinct desorption kinetics, which were assimilated to moisture present as monolayer and as multilayer. Results showed that the desorption of the multilayer was significantly faster than the monolayer, being the ratio of characteristic desorption times (monolayer/multilayer) almost 30.

### I.2.5 Limits in the use of the classical equations of freeze-drying process

In this section, the classical heat and mass transfer equations used to physically describe the primary and secondary drying steps of the freeze-drying process were presented. The two main physical parameters can be identified: (i) the vial heat transfer coefficient  $K_V$ , used to describe the heat transfer from the shelf to the vial, and (ii) the product resistance  $R_p$ , imposed from the dried product layer to the mass flow rate. A correct determination of these parameters together with the use of the presented equations can predict more or less accurately the critical process parameters (e.g. product temperature, sublimation rate). However, this approach has some limitations: it cannot represent the dynamic aspects of the process, and it does not adequately describe the physical mechanisms responsible for heat and mass transfer variability among the vials. In the past years, research in freeze-drying focused on the development of several mathematical models to provide new insights in the understanding of process as well as useful tools for the cycle design and scale-up. In this regard, a review of the main mathematical models of freeze-drying will be outlined in the next session.



### I.3 Mathematical modelling of freeze-drying

---

A number of more or less sophisticated freeze-drying models have been developed in literature to predict the process parameters (e.g., product temperature, sublimation rate, desorption rate) and to describe the progress of the primary and secondary drying steps (Pikal and Shah, 1990; Pikal, 1985; Velardi and Barresi, 2008; Zhai *et al.*, 2005; Gan *et al.*, 2005; Brülls and Rasmuson, 2002; Ybema *et al.*, 1995; Pisano *et al.*, 2012; Sheehan and Liapis, 1998; Lopez-Quiroga *et al.*, 2012; Pikal *et al.*, 2005; Liapis and Litchfield, 1979; Liapis and Bruttini, 1994; Millman *et al.*, 1985; Sadikoglu and Liapis, 1997; Mascarenhas *et al.*, 1997; Trelea *et al.*, 2007; Hottot *et al.*, 2006). **Table I.3.1** resumes the characteristics of the main mathematical models of freeze-drying process published in literature. In **Table I.3.1**, D represents the spatial dimensions of the model (1D, only balances along the axial direction are considered; 2D, balances along the axial and radial directions are considered; no 3D model were developed at the present state for the freeze-drying process). Usually, two different approaches were used to describe the process: the *pseudo-steady state* and the *dynamic state*.

*(Text continues on page 61)*



**Table I.3.1:** Summary of the main mathematical models describing the freeze-drying process. D: dimension. (Continued)

<i>Model (Reference)</i>	<i>Condition</i>	<i>D</i>	<i>Geometry</i>	<i>Product</i>	<i>Steps described</i>	<i>Heat transfer between the shelf and the vial</i>	<i>Additional heat transfer contributions</i>	<i>Inclusion of <math>R_s</math> and <math>R_{CN}</math></i>	<i>Scope of the model</i>
(Liapis and Litchfield, 1979)	Dynamic state	1D	Slab of product placed on a sample holder	-	Primary drying	The product was insulated at the bottom and at lateral walls from the sample holder. Heat flux was fixed, received at the top of the product.	Not described	Not included	Definition of optimal control policy.
	Pseudo-steady state								
(Millman <i>et al.</i> , 1985)	Dynamic state	1D	Slab of product	Skim milk	Primary and secondary drying	Heat transfer by radiation or gas conduction at the product bottom, and/or by radiation at the product top.	Not described	Not included	Study operational policies that can reduce the drying times.
(Pikal, 1985)	Pseudo-steady state	1D	Vial	- KCl solution - Povidone solution - Mannitol solution - DOBUTREX solution	Primary drying	Heat transfer to the vial by contact conduction, radiation and conduction through the gas.	Not described	$R_s$ and $R_{CN}$ are included in the model	Process control and optimization. <u>The model was widely used in literature for the definition of the "classical" design space of primary drying.</u>

**Table I.3.1:** Summary of the main mathematical models describing the freeze-drying process. D: dimension. (Continued)

<i>Model (Reference)</i>	<i>Condition</i>	<i>D</i>	<i>Geometry</i>	<i>Product</i>	<i>Steps described</i>	<i>Heat transfer between the shelf and the vial</i>	<i>Additional heat transfer contributions</i>	<i>Inclusion of <math>R_s</math> and <math>R_{CN}</math></i>	<i>Scope of the model</i>
(Pikal <i>et al.</i> , 1990)	Dynamic state	1D	Vial	- Mannitol solution - Moxalactam disodium/mannitol solution - Povidone solution	Secondary drying (mass transfer)	-	-	Not included	Study of the drying kinetics in secondary drying.
(Liapis and Bruttini, 1994)	Dynamic state	1D	Slab of product placed on a tray	- Cloxacillin Monosodium Salt - Skim milk	Primary and secondary drying	Heat transfer by radiation, gas conduction or convection at the product top, by gas conduction and radiation at the product bottom.	Not described	Not included	Describe primary and secondary drying stages of the freeze-drying of pharmaceutical crystalline and amorphous products.
(Ybema <i>et al.</i> , 1995)	Pseudo-steady state	1D	Vial	Pure water Mannitol solution	Primary Drying (mass transfer is neglected)	Heat transfer by gas conduction at the vial bottom	Not described	Not included	Calculation of the sublimation rate at any pressure or shelf temperature

(Sadikoglu and Liapis, 1997)	Dynamic state	1D	Slab of product placed on a tray	Skim milk	Primary and secondary drying	Heat transfer by gas conduction and radiation to the product bottom, by radiation, gas conduction or convection to the product top.	Not described	Not included	Describe the dynamic behaviour of the primary and secondary drying stages of the freeze-drying of pharmaceuticals in trays.
(Mascarenhas <i>et al.</i> , 1997)	Dynamic state	2D	Slab of product placed on a tray	- Skim milk - Bovine Somatotropin BST protein	Primary and secondary drying	Specific heat fluxes were imposed.	Considered	Not included	Used to calculate the variation of the partial pressure of water vapour, the temperature, and the concentration of sorbed water.
(Sheehan and Liapis, 1998)	Dynamic state	2D	Vial	Skim milk	Primary and secondary drying	Heat transfer by gas conduction at the vial bottom, by radiation at the vial top.	Radiation heat flux from the walls of the drying chamber and the bottom heating plate	Not included	Describe the primary and secondary drying stages of the lyophilisation of a pharmaceutical product in vials for different operational policies.

**Table I.3.1:** Summary of the main mathematical models describing the freeze-drying process. D: dimension. (Continued)

<i>Model (Reference)</i>	<i>Condition</i>	<i>D</i>	<i>Geometry</i>	<i>Product</i>	<i>Steps described</i>	<i>Heat transfer between the shelf and the vial</i>	<i>Additional heat transfer contributions</i>	<i>Inclusion of <math>R_s</math> and <math>R_{CN}</math></i>	<i>Scope of the model</i>
(Schoen <i>et al.</i> , 1995)	Pseudo-steady state	1D	Vial	Glycine in water	Primary drying	Heat transfer by contact and gas conduction at the vial bottom.	Not described	Not included	Process design and scale-up.
(Brülls and Rasmuson, 2002)	Dynamic state	2D	Vial	Pure water	Heat transfer during the process	Heat transfer by radiation and gas conduction at the vial bottom. The top of the vial was considered to be insulated by the stopper.	Additional heat transfer from the walls of the freeze-dryer was considered and experimentally determined.	Not included	Predict the impact on the heat transfer of the vial characteristics (glass, geometry), the total chamber pressure, the filling height, and the position of the vial of the shelf.
(Zhai <i>et al.</i> , 2005)	Dynamic state	2D	Vial	Pure water	Primary drying	Heat transfer by gas conduction at the vial bottom.	Heat transfer by radiation from the drying chamber walls to the vial side	Not included	Understanding heat and mass transfer during primary drying.

(Gan <i>et al.</i> , 2005) (Based on the work of (Sheehan and Liapis, 1998))	Dynamic state	2D	Vial	Not specified	Primary drying	As in (Sheehan and Liapis, 1998)	Heat transfer by radiation from the chamber and (if present) the tray side. This contribution was evaluated in function of the position of the vial on the shelf.	Not included	Study the dynamic behaviour of a freeze-drying system in case of trays with and without lateral sides.
(Pikal <i>et al.</i> , 2005)	Dynamic state	2D	Vial	Sucrose solution	Primary and secondary drying	Heat transfer by contact conduction, gas conduction and radiation at the vial bottom, and radiation at the vial top (if stopper is present, then the top of the vial is considered as insulated)	Radiation heat transfer from the drying chamber walls	Rs and RCN are included in the model	Prediction of product temperature and moisture content.
(Hottot <i>et al.</i> , 2006)	Dynamic state	2D	Vial	Bovine serum albumin BSA aqueous formulation	Freezing and primary drying	Heat transfer by contact and gas conduction at the vial bottom.	Heat transfer by radiation and convection from the drying chamber	Not included	Describe the product temperature and sublimation front velocities.

**Table I.3.1:** Summary of the main mathematical models describing the freeze-drying process. D: dimension. (Continued)

<i>Model (Reference)</i>	<i>Condition</i>	<i>D</i>	<i>Geometry</i>	<i>Product</i>	<i>Steps described</i>	<i>Heat transfer between the shelf and the vial</i>	<i>Additional heat transfer contributions</i>	<i>Inclusion of <math>R_s</math> and <math>R_{CN}</math></i>	<i>Scope of the model</i>
(Trelea <i>et al.</i> , 2007)	Dynamic state	1D	Vial	- Sucrose and Tris-HCl solution -PVP, Sucrose and Tris-HCl solution	Primary and secondary drying	Heat transfer by contact conduction, radiation and conduction through the gas at the vial bottom, radiation at the vial top	Not described	$R_s$ and $R_{CN}$ are included in the model	Optimization of freeze-drying cycles.
(Velardi and Barresi, 2008)	Dynamic state (Detailed model)	1D	Vial	Bovine serum albumin BSA buffered with tris-HCl 0.1M	Primary and secondary drying	Heat transfer by convection and radiation at the vial bottom, and by radiation at the vial top. If the stopper is present, the vial top is considered as thermally insulated. Heat transfer along the vial walls was also described.	Radiation heat transfer from the drying chamber walls	Not included	Description of the primary and secondary drying step.
	Pseudo-steady state (Simplified model I)				Primary drying	Heat exchanged by convection and radiation at the vial bottom.	Not described	Not included	To design model-based algorithms for optimization and control of the process. <u>The model was widely used in literature for the definition of the design space of primary drying.</u>
	Pseudo steady state (Simplified model II)				Primary drying	As for the <i>detailed</i> model	Not described	Not included	

(Pisano <i>et al.</i> , 2012)	Dynamic state	1D	Vial	Sucrose solution	Secondary drying	Heat transfer by contact conduction, radiation and conduction through the gas at the vial bottom, radiation at the vial top.	Not described	Not included	<u>To develop a design space for secondary drying.</u>
(Lopez-Quiroga <i>et al.</i> , 2012)	Dynamic state	1D	Slab of product	Skim milk	Primary and secondary drying	Heat transfer by convection at the vial bottom, and radiation at the vial top.	Not described	Not included	Define operational conditions for minimizing freeze-drying cycle time while preserving product quality.
(Mortier <i>et al.</i> , 2016)	Dynamic state	1D	Vial	Model formulation	Primary drying	Heat transfer by contact conduction, radiation and conduction through the gas at the vial bottom, radiation at the vial top. Described as in (Fissore <i>et al.</i> , 2011a)	Impact of the "Edge vial effect" included in the uncertainty analysis	Not included	Perform uncertainty analysis for the determination of the dynamic primary drying <u>Design Space for pharmaceutical freeze-drying</u>



### I.3.1 Pseudo steady state mathematical modelling

The pseudo-steady state is often employed in literature to describe the primary drying step (Pikal, 1985; Schoen *et al.*, 1995; Liapis and Litchfield, 1979; Velardi and Barresi, 2008; Ybema *et al.*, 1995). Under this condition, the amount of heat entering into the product is assumed to be completely devoted for the sublimation of the ice crystals and energy used for changes in product temperature can be considered as negligible. Pseudo-steady state models are described using algebraic equations, not very time-consuming to be solved, and thus suitable for the process control. A pioneering mathematical model of freeze-drying in pseudo-steady state was developed by Liapis and Litchfield (Liapis and Litchfield, 1979) starting from a more complex dynamic model, in order to define the optimal control policies of the freeze-drying cycles. However, the model described a system which is not normally encountered in pharmaceutical freeze-drying, constituted by a slab of product located in an insulating sample holder and heated in the top by an infrared lamp. Successively, Pikal (Pikal, 1985) developed a model to describe the primary drying step of freeze-drying, which considered a moving planar interface between the dried and frozen product layers. This theoretical model assumed the pseudo-steady state for heat and mass transfer during sublimation, except for a time dependence of the thickness of dried product layer formed above the ice-vapour interface. Pikal (Pikal, 1985) stated that, based on experimental findings, the pseudo-steady state is usually achieved after 30 min of a change in the shelf temperature, and thus it can be applied to the primary drying step which usually takes many hours to complete. The heat exchanged between the shelf and the vial bottom was described in terms of vial heat transfer coefficient  $K_V$ , depending on the contact conduction between the vial bottom and the shelf, the radiation from the bottom and top shelf, and the conduction through the gas entrapped in the vial bottom curvature. The sublimation rate was assumed to be limited by a resistance  $R$  given by the sum of three contributions given by the dried product layer, the stopper and the pathway between the chamber and the condenser.

The two model parameters  $K_V$  and  $R$  can be determined by laboratory experiments, and the precision of their estimation is of paramount importance for the prediction of the critical process parameters given by the model. The model can be thus used for the cycle development and optimization by knowing some additional information, such as the critical temperature of the product. The model proposed in the work of Pikal (Pikal, 1985) was largely applied in successive works for the process design and control and it is nowadays classically employed to describe the heat and mass transfer in primary drying (e.g., in (Overcashier *et al.*, 1999; Ganguly *et al.*, 2013; Hibler *et al.*, 2012; Rambhatla and Pikal, 2003; Rambhatla *et al.*, 2004; Tsinontides *et al.*, 2004; Tang and Pikal, 2004)). In contrast with the results proposed by Pikal (Pikal, 1985), who stated the importance of the growing dried layer thickness during sublimation, Ybema (Ybema *et al.*, 1995) found that the mass transfer was not limiting during this step.



A model was proposed, describing the heat transfer during primary drying as a series of resistance between the shelf and the interface (vial bottom curvature, glass vial, and frozen product). Furthermore, Ybema (Ybema *et al.*, 1995) identified in the vial bottom curvature the major resistance to the heat transfer during the process, as it limits the direct contact between the shelf and the vial.

Later on, Velardi and Barresi (Velardi and Barresi, 2008) developed two simplified models of primary drying in pseudo-steady state conditions, taking as starting point a detailed dynamic model of the process. The so-called "simplified model I" represented the heat and mass transfer during the sublimation step considering only a mass balance into the dried layer and a heat balance into the frozen product layer. The heat transfer in the dried layer and along the vial walls was considered as negligible, thus this model is not suitable to describe the additional heat by radiation from the rail or the chamber walls received by edge vials.

The "simplified model II" was developed considering both the heat transfer in the dried and frozen layer as well as in the vial walls.

However, the radiation heat transfer from the drying chamber walls to the lateral walls of the vials was not taken into account. The mass transfer was simulated as in the simplified model I, without taking into account the impact of the stopper and chamber resistances. The "simplified model I", simpler than the "simplified model II", was found to be sufficient to monitor, control and optimize of freeze-drying process. Conversely, the "simplified model II" allowed to take the advantage of the temperature measurements on the vial wall and was used for development of soft sensors to monitor sublimation during the process (Barresi *et al.*, 2009b).

### I.3.2 Dynamic mathematical modelling

In literature, several mono and bi-dimensional mathematical models of freeze-drying in dynamic state have been developed to describe transient phenomena during the process (Liapis and Litchfield, 1979; Millman *et al.*, 1985; Pikal *et al.*, 1990; Liapis and Bruttini, 1994; Sadikoglu and Liapis, 1997; Mascarenhas *et al.*, 1997; Sheehan and Liapis, 1998; Brülls and Rasmuson, 2002; Zhai *et al.*, 2005; Pikal *et al.*, 2005; Hottot *et al.*, 2006; Trelea *et al.*, 2007; Velardi and Barresi, 2008; Lopez-Quiroga *et al.*, 2012; Pisano *et al.*, 2012), e.g., the shape and velocity of the moving ice vapour interface and the moisture content evolution during the secondary drying step.

Most of the first models developed in dynamic state (Liapis and Litchfield, 1979; Millman *et al.*, 1985; Liapis and Bruttini, 1994; Sadikoglu *et al.*, 1998; Mascarenhas *et al.*, 1997) described the freeze-drying of a slab of a product contained in tray, often skim milk, heated either by an infrared source or by the bottom shelf. Then, Sheehan et Liapis (Sheehan and Liapis, 1998) developed a bi-dimensional dynamic mathematical model to describe the progress of primary and secondary drying performed in an individual vial.



The model included over 30 parameters, most of which had to be determined anew as related to the product formulated, which complicate its use for process design and control.

However, the model of Sheehan et Liapis (Sheehan and Liapis, 1998) took into account the radiation contribution of the drying chamber walls to the lateral side of the vial located at the periphery of the shelf, which was often neglected in previous works. This model (Sheehan and Liapis, 1998) was successfully used by Gan et al. (Gan *et al.*, 2005) to study the effect of the presence of the tray sides on the drying time and moisture content in vials differently located on the shelf.

The study of Gan et al. (Gan *et al.*, 2005) is remarkable as it precisely investigated the additional heat transfer received by the lateral walls of edge vials. This heat transfer contribution was included in some other works by using different approaches (Zhai *et al.*, 2005; Hottot *et al.*, 2006; Pikal *et al.*, 2005; Brülls and Rasmuson, 2002). For example, Brülls and Rasmuson (Brülls and Rasmuson, 2002) developed a bidimensional model taking into consideration the heat transfer from the environment to the lateral vial walls, but the responsible phenomena were not theoretically described and this contribution was experimentally evaluated. In the bidimensional model developed by Zhai et al. (Zhai *et al.*, 2005), the effect of radiation heat transfer was studied, but the model was used to simulated only pure ice and the presence of the dried layer of the product was not considered. Finally, Hottot et al. (Hottot *et al.*, 2006) included the heat transfer by radiation and convection from the drying chamber environment to the vial walls, but the importance of this contribution was not estimated.

The multi-dimensional models developed (Sheehan and Liapis, 1998; Pikal *et al.*, 2005; Zhai *et al.*, 2005; Gan *et al.*, 2005; Hottot *et al.*, 2006) can precisely describe the heat and mass transfer phenomena, but are often not suitable for process control and real time applications, as they are quite complex and time-consuming to solve. More recent publications focused on the development of simplified and control-oriented models.

In particular, Trelea et al. (Trelea *et al.*, 2007) proposed a monodimensional model, which was successfully used for the optimization of the freeze-drying cycles based on the monitoring of process parameters relevant for product quality, such as the product temperature and glass transition temperature at critical points to assess product stability, and the residual moisture content. Velardi and Barresi (Velardi and Barresi, 2008) developed also a dynamic mono-dimensional model, which introduced the transient energy balance to describe the heat transfer in the vial glass. However, this detailed dynamic model was not directly used for process control purposes, but was simplified in the two pseudo-steady state models which were previously discussed (§I.3.1). The models of Trelea et al. (Trelea *et al.*, 2007) and Velardi and Barresi (Velardi and Barresi, 2008) were based on a systematic separation of slow and fast dynamics of the process.



In the work of Lopez-Quiroga et al. (Lopez-Quiroga *et al.*, 2012), characteristic times of freeze-drying dynamics were determined and a monodimensional simplified mathematical model was defined (Millman *et al.*, 1985; Liapis and Bruttini, 1994; Mascarenhas *et al.*, 1997; Sadikoglu and Liapis, 1997; Liapis and Litchfield, 1979). Simplification of the model equations was based on a time-scale reduction approach, which allowed to focus just on the phenomenon of interest, i.e., the time dependent product temperature distribution in the dried layer, and to neglect mechanisms occurring at faster scales (e.g., heat and mass transfer in the water vapour). The model was then used for the optimization of the process by defining optimum operating variables profiles (i.e., chamber pressure and shelf temperature).

### **I.3.3 Mathematical modelling for process control and product quality assurance**

Mathematical models of the freeze-drying process can be developed for different purposes. Firstly, they can provide new insights on heat and mass transfer phenomena taking place during the sublimation and desorption steps. Multi-dimensional dynamic models usually describe precisely the physical mechanisms, although they are more complex to be solved. In contrast, mono-dimensional dynamic or pseudo-steady state models are usually employed for process control purpose, as less time-consuming to be solved. These models can predict key process parameters, such as the product temperature and the sublimation rate, and can be then used to select operating variables (i.e. shelf temperature, chamber pressure, operating time) to guarantee an acceptable product quality (e.g. avoid collapse of the cake maintaining the product temperature below the critical value; reach the target value of final moisture content in the product). In this regard, mathematical modelling is an integral part of the "Quality by Design" approach, which enhance the understanding of the process and product relationship for assuring product quality in pharmaceutical industry. The "Quality by Design" philosophy and its implementation in the freeze-drying process will be discussed in the following section.



## I.4 Quality-by-Design in freeze-drying process

---

### I.4.1 What is the "Quality-by-Design"?

Traditionally, the quality of pharmaceutical drugs is tested on the final product following a regulatory framework known as Quality-by-Testing (QbT). In this system, product quality and performance are ensured by performing extensive tests on the raw material and on the final product, and by using a fixed formulation and manufacturing process fully described in the marketing authorization dossier. However, this framework has several drawbacks. Firstly, QbT gives no attention on how the design of the product formulation and of the manufacturing process can ensure product quality; the causes responsible for product quality variability and/ or failure are not well investigated; finally, the regulatory burden imposed on manufacturers for executing even minor modifications to the manufacturing process inhibits continuous improvement and optimization (Yu, 2008).

The concept of pharmaceutical Quality by Design (QbD) was firstly introduced in the 8 Guidance on Quality of the International Council for Harmonisation of Technical Requirements for Pharmaceuticals for Human Use (ICH Q8) with the following idea: “*the quality cannot be tested into the product, but it should be built into it*” (Food and Drug Administration, 2009). The Food and Drug Administration defined the Quality by Design as a systematic approach to pharmaceutical product development that begins with predefined objectives and emphasizes product and process understanding and process control, based on sound science and quality risk management (Nail and Searles, 2008; Mockus *et al.*, 2011; Yu, 2008; Food and Drug Administration, 2009). In contrast with the Quality by Testing approach, the Quality by Design enhances the assurance of safe, effective drug supply to the consumer, and it promises to significantly improve the manufacturing quality performance (Yu, 2008).

The use of this new approach should offer a reduced manufacturing costs, a greater speed to market, a better allocation of the resources and reduced regulatory burden. **Figure I.4.1** shows a schematic overview of the implementation of the Quality by Design initiative in a pharmaceutical process. A preliminary step for a successful implementation of the QbD in pharmaceutical freeze-drying is the definition of the *quality target product profile* (QTPP), which describes the design criteria of the

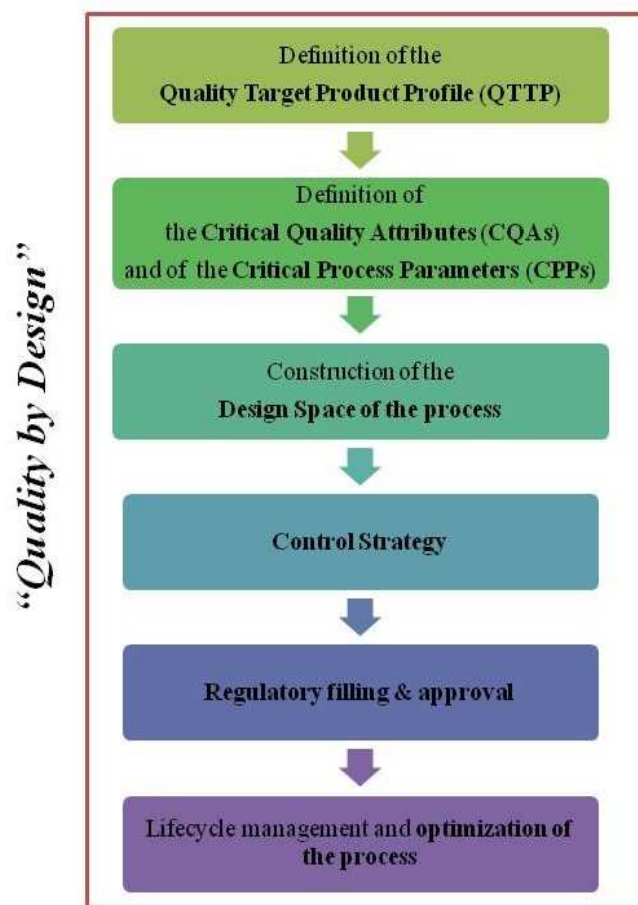


**Figure I.4.1:** Roadmap for the implementation of the Quality-by-Design approach in pharmaceutical processes.

product for quality, safety and efficacy and forms the basis for its development (Food and Drug Administration, 2009). The QTPP could include for example the dosage, the container system, the drug quality criteria (e.g., potency). Once QTPP has been defined, the next step is to identify the relevant *critical quality attributes* (CQAs). The CQAs are the physical, biological, chemical and biological properties of a product that should remain within an appropriate limit, range or distribution to assure the desirerate product quality (Food and Drug Administration, 2009). The CQAs (and thus the quality of the product) are related to the manufacturing process through the *critical process parameters* (CPPs). The CPPs are the process parameters whose variability has an impact on one or more CQAs of the product and therefore should be monitored or controlled to ensure that the process produces the desirerate quality (Food and Drug Administration, 2009). Thus, based on the acceptable range of CQAs, the risk assessment of the process can be performed by constructing the *design space* of CPPs. The design space is defined as "*the multidimensional combination of input variables and process parameters that have been demonstrated to provide assurance of product quality*" (Food and Drug Administration, 2009). The design space is strongly dependent on the product and the equipment considered. It is usually proposed by the applicant and it is subject to regulatory assessment and approval. Working within the FDA approved design space is not considered as a change, whereas a movement out of the design space is considered as a change and requires a regulatory post-approval change process.

The design space for pharmaceutical products can be constructed either through extended experimental campaign at pilot scale or by using mathematical modelling. Successively, a control strategy is defined in order to ensure that a product of required quality is produced consistently. In this regards, the sources of variability that can have an impact on product quality should be identified, appropriately understood, and subsequently controlled. Understanding sources of variability and their impact on the process and product quality can provide an opportunity to minimize the controls and the need for end-product testing (Food and Drug Administration, 2009). Finally, throughout the product lifecycle, the companies have opportunities to evaluate and implement innovative approaches to improve product quality, such as the redefinition of the design space after gaining additional process knowledge (Food and Drug Administration, 2009). The implementation of the QbD in pharmaceutical process is also assisted by the use of the *Process Analytical Tools* (PAT). The FDA defined the PAT as a system for designing, analyzing, and controlling manufacturing through timely measurements (i.e., during processing) of critical quality and performance attributes of raw and in-process materials and processes with the goal of ensuring final product quality (Food and Drug Administration, 2009). The PAT are used to monitor one or more CPPs during the process, and thus can be used for the understanding and control of the process, as well as the development of robust process well-away from the edges of failure.

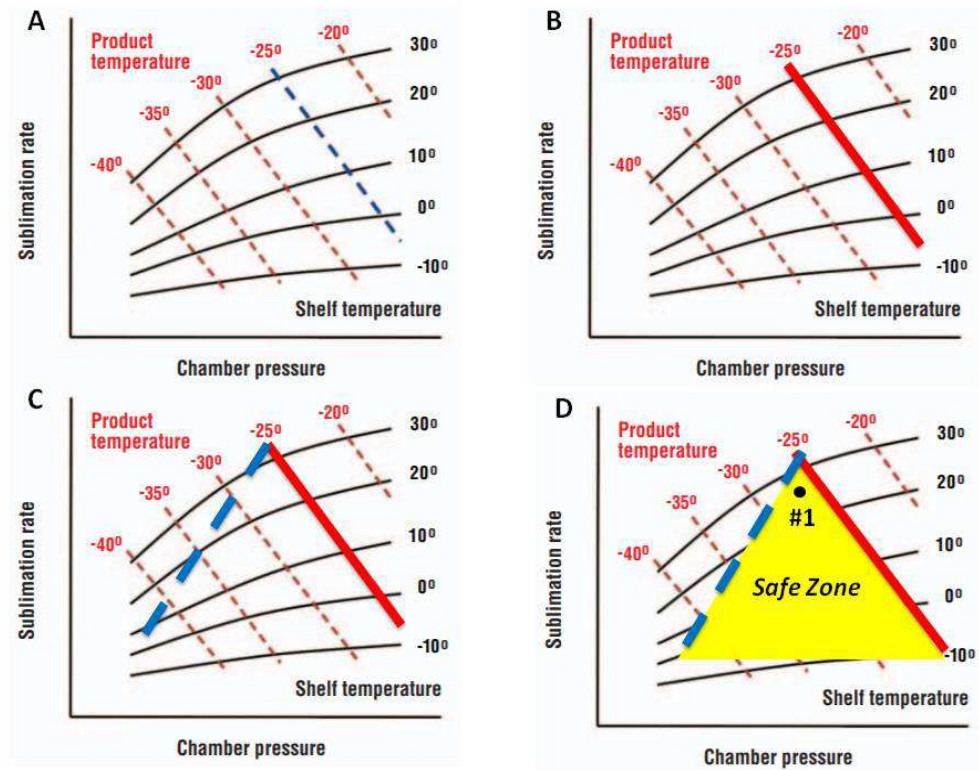


**Figure I.4.2:** Schematic representation of the design space construction for the freeze-drying process. The red solid line represents the maximum allowed product temperature, the blue dashed line the maximum equipment capability. The yellow area represents the safe zone of the process. Black point #1 represents the optimal condition for the cycle design (Nail and Searles, 2008).

## I.4.2 Quality-by-Design in freeze-drying process

### I.4.2.1 The "classical" design space for primary drying

The design space of the freeze-drying process is usually identified with the design space of the primary drying, as it is the most studied and time consuming step of the process. A paper published by Chang et Fischer (Chang and Fischer, 1995) firstly proposed a graph which suggested an approach for the definition of the Design Space for the primary drying step of the freeze-drying process.

This graph, schematically represented in **Figure I.4.2A** (Nail and Searles, 2008), illustrates the relationship of two critical parameters of the process (product temperature and sublimation rate) with the process operating variables (chamber pressure and shelf temperature) at a specific time of the process. In order to define the safe area of the design space, specific constraints have to be considered. The first one is the maximum allowed product temperature and it is shown in **Figure I.4.2B** as a red bold line. The product temperature strongly influences the product quality, as a temperature higher than the maximum allowed value led to the collapse of the product cake. Furthermore, equipment constraints have to be considered to design the process and the sublimation rate should not become higher than the maximum capability of the equipment at a given chamber pressure (represented by the blue dashed line in **Figure I.4.2C**). When the sublimation rate becomes higher than the maximum equipment capability, the chamber pressure rises above the set point and the process runs out of control. This is explained in the literature by the maximum speed at which the water vapour can flow in the duct from the chamber to the condenser is the velocity of sound, which can be reached at high sublimation rates due to low pressure and high volume of vapour (Searles, 2010b; Patel *et al.*, 2010a). Under this specific condition, the vapour flow rate becomes independent of the pressure on the condenser side of the duct connecting the chamber and the condenser, situation termed as "choked flow". The equipment capability depends on the duct geometry between the chamber and the condenser and on the condenser performance (Patel *et al.*, 2010a). Once these process constraints are established, the safe area for the selection of the operating can be identified as the yellow area shown in **Figure I.4.2D** (Nail and Searles, 2008; Patel and Pikal, 2013). Optimization of the freeze-drying process is performed when the selected operating variables leads to the highest possible sublimation rate (and thus to the shortest drying time). In **Figure I.4.2D**, optimal conditions can be found close to the apex of the safe area of the design space (point #1).

Construction of the freeze-drying design space based on experimental investigations would require multiple runs and would be very expensive and time consuming (Chang and Fischer, 1995; Nail and Searles, 2008). For this reason, freeze-drying mathematical models are often used (Pisano *et al.*, 2013; Fissore *et al.*, 2011a; Koganti *et al.*, 2011; Giordano *et al.*, 2011; Oddone *et al.*, 2014). The advantages of the use of the models are the reduced experimental costs, the better risk assessment of

### How to calculate the “classical” design space for primary drying

1. Fix a range of values of  $T_S$  and  $P_C$

$$\dot{Q} = \Delta H \dot{m} \quad \text{Eq. I.2.1}$$

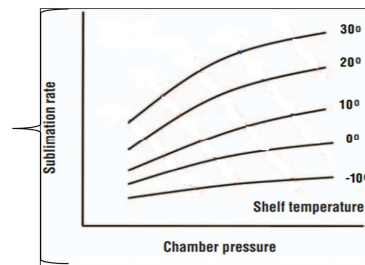
$$\dot{Q} = K_V A_{BV} (T_S - T_{BV}) \quad \text{Eq. I.2.2}$$

2. For each set of  $T_S$  and  $P_C$  solve the system of **Equations I.2.1-2, I.2.11, I.2.19** to calculate  $T_{BV}$  and  $\dot{m}$

$$K_V = C_1 + \frac{C_2 P_C}{1 + C_3 P_C} \quad \text{Eq. I.2.11}$$

$$\dot{m} = \frac{A_i (P_i - P_{vC})}{\widehat{R}_p} \quad \text{Eq. I.2.19}$$

3. The **isotherms of shelf temperature**  $T_{BV}$  are thus determined

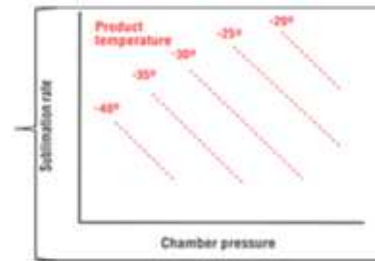


4. Fix a range of values of  $T_{BV}$  and  $P_C$

5. For each set of  $T_{BV}$  and  $P_C$  solve the **Equation I.2.19**

$$\dot{m} = \frac{A_i (P_i - P_{vC})}{\widehat{R}_p} \quad \text{Eq. I.2.19}$$

6. The **isotherms of product temperature** are thus determined



7. Add the *process constraints* (i.e., maximum allowable product temperature and capability of the equipment)

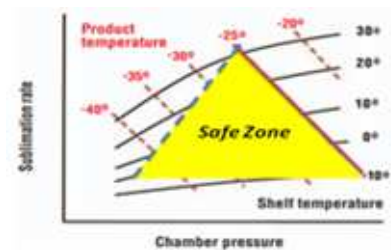


**Figure I.4.3:** Steps for the calculation of the classical design space for primary drying. The pressure at the ice-vapour interface  $P_i$  is usually calculated from the product temperature by using the Clausius Clapeyron relation.

the process and the possibility of deeply explore the relation between operating variables and process parameters.

In this regard, pseudo-steady state model proposed by Pikal (Pikal, 1985) is classically used to construct the design space of primary drying. The two main parameters of the model are  $K_V$  and  $R_p$ , which can be experimentally determined as proposed in §I.2.2.4 and §I.2.3.4. The resistances due to the stopper and to the chamber to the condenser pathway are usually neglected, as significantly lower than  $R_p$ . An average  $K_V$  value for vials located at the centre of the shelf and the maximum value of  $R_p$ , usually observed close to the end of sublimation, are considered for the calculations. The main steps and equations used for the classical design space calculation are reported in **Figure I.4.3**.

However, the use of this model for the definition of the design space presents two important drawbacks: (i) the evolution of the design space with time, mainly due to  $R_p$  variation, is not considered, and (ii) the design space is based on an average vial behaviour, whereas usually the vial batch is not uniform and border vials receive higher heat fluxes.

The use of dynamic models or the evaluation of the process uncertainty have been used in recent works (Fissore *et al.*, 2011a; Giordano *et al.*, 2011; Pisano *et al.*, 2013; Mortier *et al.*, 2016) to improve the definition of the design space.

#### I.4.2.2 Dynamic design space of primary drying

The design space for primary drying is classically constructed by considering the maximum value of the product resistance  $R_p$ , which leads to the calculation of the design space based on the highest values of product temperature during the process. However, for most of the products, the product resistance and the product temperature dynamically increases with the dried layer thickness along with the progress of sublimation. Due to the evolution of these parameters, the design space also varies during the process.

The first time-varying design space was designed by Fissore *et al.* (Fissore *et al.*, 2011a), based on the mathematical model of Velardi and Barresi (Velardi and Barresi, 2008). In this work (Fissore *et al.*, 2011a), the evolution of product resistance  $R_p$  with the dried layer was experimentally determined and calculation of several design spaces was performed at different process times (expressed as evolution of  $\frac{l_d}{l_0}$ , with  $l_0$  being the initial product thickness). An example of the resulting time-varying design space is shown in **Figure I.4.4** for a 5 % w/w mannitol solution. The x and y coordinates were set to be the chamber pressure and shelf temperature, respectively (conversely to the classical design space, where the y coordinate was the sublimation rate). The solid line represents the constraint imposed by the maximum product temperature, the dashed line the constraint imposed by the maximum equipment capability.

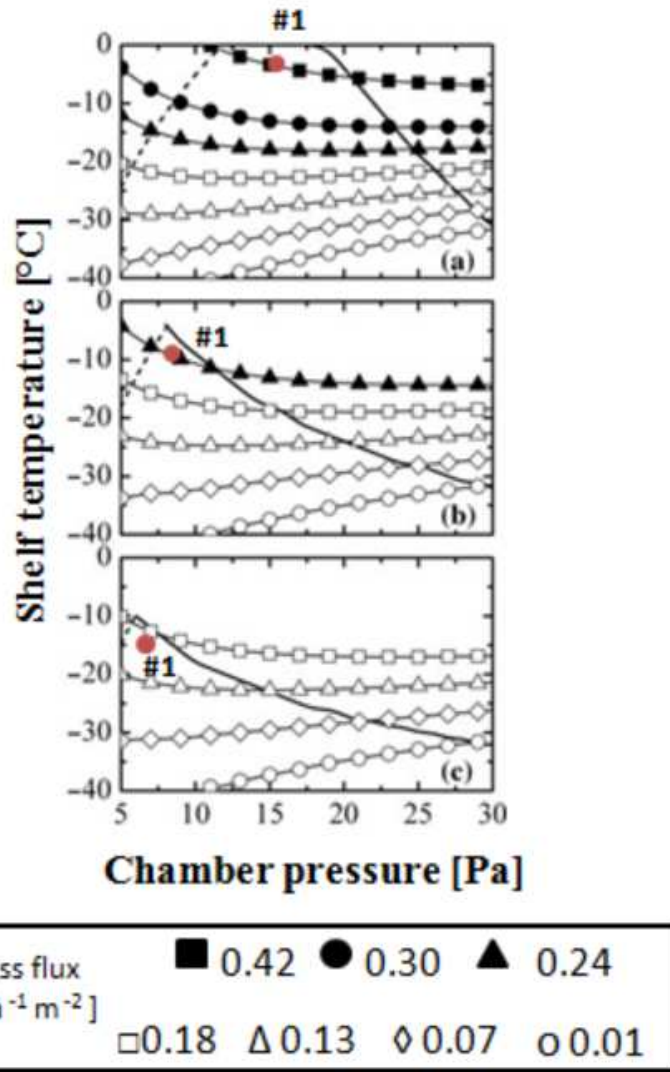


**Figure I.4.4:** Effect of the constraints imposed by product temperature (solid line) and dryer capacity for mass flux (dashed line) on the design space of mannitol solution (Fissore *et al.*, 2011a). Marker represents the mass flux as in the legend. Graphs: (a)  $\frac{l_d}{l_{d_0}} = 0.01$ ; (b)  $\frac{l_d}{l_{d_0}} = 0.55$ ; (c)  $\frac{l_d}{l_{d_0}} = 0.99$ .

The area enclosed below these curves for a certain values of  $\frac{L_d}{l_0}$  represented the "safe area" of the design space at that time instant. As sublimation proceeded in primary drying, the dried layer thickness and the product resistance  $R_p$  increased, the design space "shranked" in time and the area available for the selection of the operating variables became smaller (Fissore *et al.*, 2011a).

This led to conclude that time modifications need to be accounted in the design space, especially for those products whose resistance changes significantly in primary drying. The optimal value of operating conditions (to maximize the sublimation rate and reduce drying time) are given by the red point #1. In order to optimize the process (i.e., to obtain the highest possible sublimation rate throughout the primary drying step and thus the shortest drying time),  $T_S$  and  $P_C$  values should be dynamically updated during the cycle. Operating variable values need to be modified in time accordingly to the design space "shrinkage", to avoid the fall of the set points outside of the space.

#### I.4.2.3 Risk assessment of the primary drying step

The parameters used in the models for the construction of the design spaces (e.g.,  $K_V$ ,  $R_p$ ) can be affected by a degree of uncertainty and variability due for example to measurement errors or to uncontrolled physical phenomena taking place during the process. Thus, the consideration of the parameter uncertainty into the mathematical models used for the design space is of paramount importance to estimate the risk of failure of the process. In this regards, uncertainty analysis is often performed by "interval mathematics". The main assumption of this analysis is that all the possible values of the parameter must lie somewhere within the considered interval, and thus the outputs of the model must lie somewhere between the lower and upper bounds of the solution interval (Broadwater *et al.*, 1994). Then, the 'sampling-based method' is typically used in freeze-drying models to calculate the uncertainty of the model outputs, e.g., Monte Carlo methods, response surface methods (Giordano *et al.*, 2011; Mortier *et al.*, 2016; Pisano *et al.*, 2013; Bosca *et al.*, 2015). The Monte Carlo consists in randomly sampling model parameters from a distribution to obtain successively a distribution of process parameters as output.

A first example of the use of the uncertainty analysis in freeze-drying mathematical models is the work of Giordano *et al.* (Giordano *et al.*, 2011). The authors considered the uncertainty of two model parameters ( $K_V$  and  $R_p$ ) to be distributed around their mean values according to a Gaussian density function. By using the model of Velardi and Barresi (Velardi and Barresi, 2008), the product temperature distribution was simulated and the design space was constructed for various probability of success, that in this work (Giordano *et al.*, 2011) was defined as the probability that the product

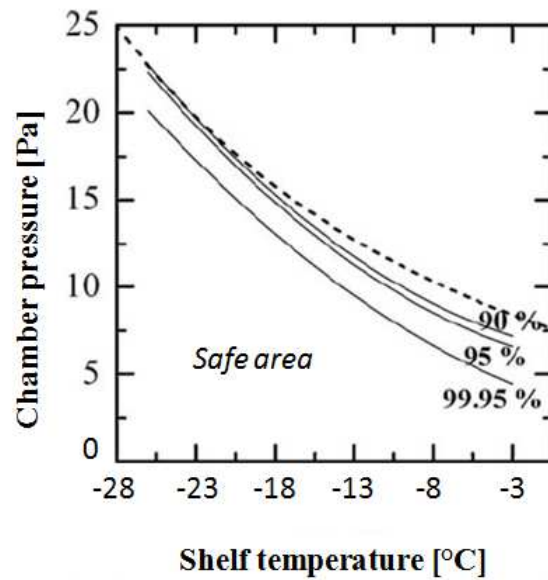


**Figure I.4.5:** Example of design space of a 10 % sucrose solution calculated taking into account a  $K_V$  and  $R_p$  coefficient of variation equal to 10 %. Solid lines identify the design space boundary for different probability of success, whereas the dashed line identify the "classical" design space boundary when parameter uncertainty is not taken into account (Giordano *et al.*, 2011).

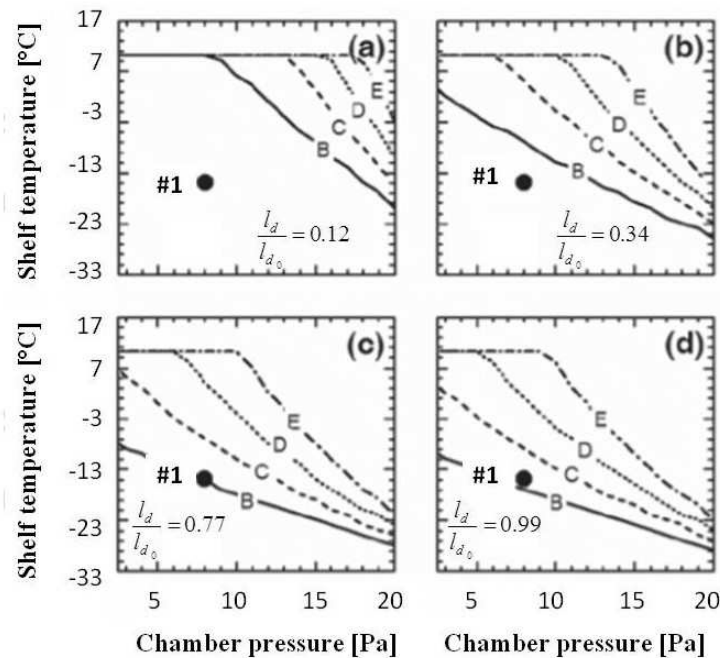


**Figure I.4.6:** Design space of a vaccines formulation evaluated at different  $\frac{l_d}{l_{d0}}$  and for four groups of vials differently located on the shelf (as previously presented in **Figure I.2.3**). Group B: edge vials in contact with the rail; Group C: edge vials not in contact with the rail; Group D: central vials in contact with "hot" vials; Group E: central vials. Condition #1= shelf temperature of -15°C and chamber pressure of 8 Pa (Pisano *et al.*, 2013).

temperature remains below the maximum allowed temperature. **Figure I.4.5** shows an example of a design space calculated by Giordano et al. (Giordano *et al.*, 2011), for a 10 % w/w sucrose solution considering a 10 % of uncertainty of  $K_V$  and  $R_p$ . The safe area is represented by the area below the curves at a fixed probability of success. It results that higher is the probability of success, smaller will be the safe area available for the process design. **Figure I.4.5** also shows that the classical design space (dotted line in **Figure I.4.5**), calculated without considering parameter uncertainty, presents the biggest safe area: this points out that if the operator selects the operating variables without taking into account the parameters uncertainty, the product could be damaged.

Subsequently, Pisano et al. (Pisano *et al.*, 2013), constructed a time variant design space by taking in consideration the uncertainty of the parameters  $K_V$  and  $R_p$  as proposed by Giordano et al. (Giordano *et al.*, 2011). In this work, the quantification of the uncertainty of  $K_V$  and  $R_p$  was based on experimental data. First, the  $K_V$  uncertainty was assessed. Different  $K_V$  distributions were determined gravimetrically for groups of vials differently located on the shelf, classified as edge vials in contact (B) and not in contact with the rail (C), in contact with "hot" vials (D), central vials (E). These experimental distributions were used to evaluate the uncertainty of  $K_V$  for each group, that was expressed in terms of variance of the parameter  $C_1$  only (**Equation I.2.11**). Then,  $R_p$  was calculated by using the pressure rise test. The uncertainty of  $R_p$  was expressed as 10 % of coefficient of variation of the parameter  $R_{p_1}$  (**Equation I.2.20**), which was found to satisfactory represent the variability of  $R_p$  between different runs regardless the freezing protocol used. However, the variability of  $R_p$  between vials processed in same vial batch was not investigated.

Then, the time-variant design space for the different groups of vials was calculated as shown in **Figure I.4.6** for a 9 % w/w vaccine formulation considering average values of the parameters. In agreement with the work of Fissore et al. (Fissore *et al.*, 2011a) the design space shrinks as the dried layer thickness  $l_d$  increases. The edge vials in contact with the shelf (group B) presented the smaller design space due to the higher value of  $K_V$  with respect to central vials (group E), regardless of the process time. The developed design space was then used to select acceptable values of operating variables (condition #1 in **Figure I.4.6**, equal to shelf temperature of about  $-15^\circ\text{C}$  and chamber pressure of 8 Pa), taking as reference the central vials. Finally, the uncertainty of the parameters  $K_V$  and  $R_p$  was used to evaluate the probabilistic distribution of the product temperature and drying time (defined by end of sublimation) of the different vial groups, as shown in **Figure I.4.7**. Only the vials of group B (central vial) showed a maximum product temperature lower than the critical value, and the drying time had to be at least 12.5 h to guarantee that all the vials had completed the primary drying phase.

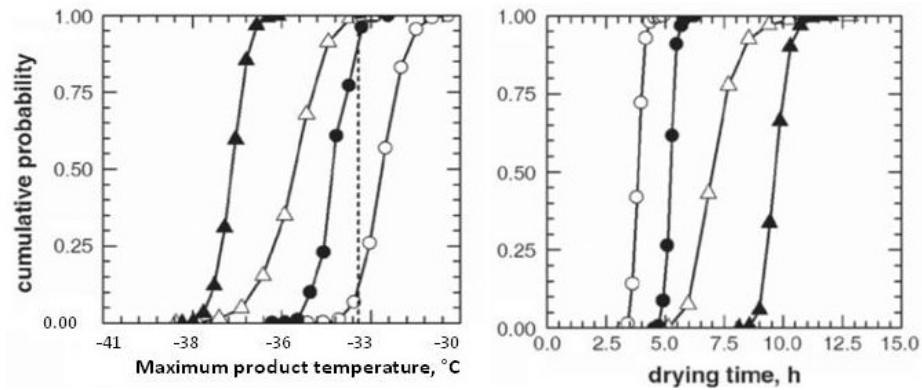


**Figure I.4.7:** Comparison between the probabilistic distribution of the maximum product temperature and drying time for the four families of vials: (○) B, edge vials in contact with the rail; (●) C, edge vials not in contact with the rail; (△) D, central vials in contact with “hot” vials and (▲) E, central vials. The dashed vertical line indicates the maximum allowable product temperature. A shelf temperature of  $-15\text{ }^{\circ}\text{C}$  and a chamber pressure of  $8\text{ Pa}$  were used to run the cycle (Pisano *et al.*, 2013).

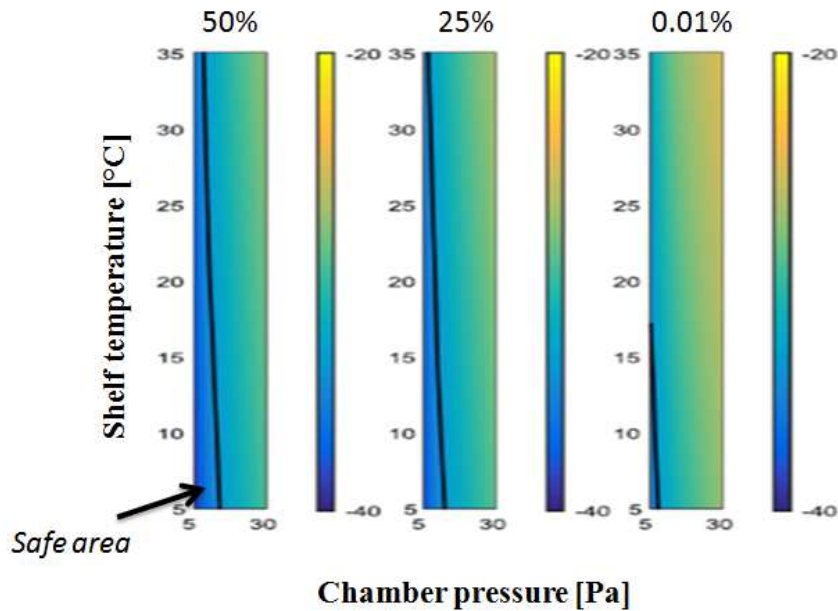


**Figure I.4.8:** Influence of different values for the risk of failure acceptance level on the product temperature at the interface  $T_i$ , and therefore on the resulting dynamic design space evaluated at  $0.78\text{ h}$  from the beginning of primary drying for different risk of failure acceptance levels (50%, 25%, 0.01%). Product temperature  $T_i$  is represented by the colour scale (Mortier *et al.*, 2016).

The presented analysis showed that the consideration of the parameter uncertainty is a key point for the choice of appropriate safety margins for the maximum product temperature and for the primary drying duration to guarantee an acceptable product quality. A step further in the parameter uncertainty analysis was recently performed by Mortier et al. (Mortier *et al.*, 2016), who included in a time-variant design space the uncertainty of 12 parameters in total, e.g.,  $K_V$ ,  $R_p$ , the cross sectional area of the vial and the initial product thickness. Several design spaces were calculated for different risk of failure acceptance levels (i.e., probability that the temperature at the sublimation front of the product exceed the critical value). An example of the influence of the risk of failure acceptance levels on the dynamic design space is shown in **Figure I.4.8**. The "safe area" of the design space shrinks as the risk of failure acceptance levels becomes more conservative. In particular, the process conditions become extremely conservative at 0.01 % risk of failure. Mortier et al. (Mortier *et al.*, 2016) concluded that only the design space built considering 0.01 % risk of failure acceptance level guarantee good cakes without collapse.

In conclusion, variation in time and model parameters uncertainty should be considered into the design space for a successful risk assessment of the process. In this way, cycle design will be performed taking into account not only the optimization of the process, but also its risk of failure usually defined as the probability that the product temperature exceed its critical value.

#### I.4.2.4 Sum-up: the design space "shrinkage"

In summary, the design space based on product quality constraints tends to shrink due to the following factors:

- Product resistance increase in time along with the progress of primary drying due to the increasing dried layer thickness;
- Consideration of edge vial groups which receive additional heat fluxes respect central vials;
- Including model parameter uncertainty which exhibit deviations from average behaviour;
- Increasing the desired percentage of accepted vials towards 100 %.

Reduction of the safe zone in the design space is in opposition with process duration optimisation which favours high sublimation rates and consequently high shelf temperatures and low chamber pressures. High shelf temperatures increase the risk of product collapse (**Figure I.4.5**) while low chamber pressures reduce equipment capability (**Figure I.4.2**).

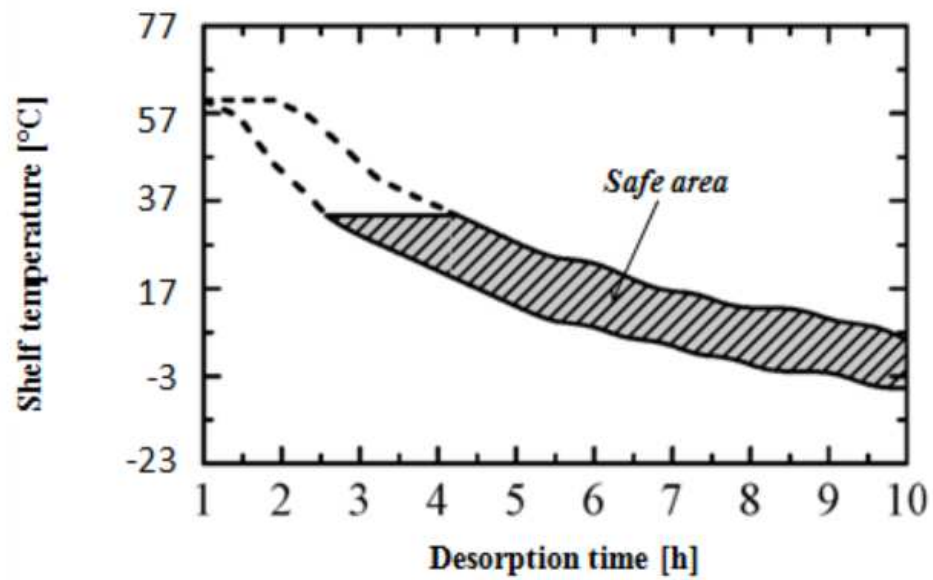


**Figure I.4.9:** Secondary drying design space of a 5% sucrose solution calculated in case an initial moisture content of 6 % and the target moisture content between 1 and 2% (Pisano *et al.*, 2012).

### I.4.3 Design space for secondary drying

The design space for secondary drying can be defined as the set of operating variables (i.e., temperature of the shelf and duration of the secondary drying) that allows to reach the target value of residual moisture in the product while maintaining the product temperature below the glass transition temperature for dried product  $T_g$ . Despite the importance of this step on controlling the final moisture content of the product, only Pisano et al. (Pisano *et al.*, 2012) proposed an approach for the calculation of the secondary drying design space. An example is shown in **Figure I.4.9** for 5 % w/w aqueous sucrose solution. In this model, evolution of moisture content and product temperature with time is described and requires the experimental determination of three model parameters, i.e., the vial heat transfer coefficient  $K_V$ , the product moisture content at the beginning of the secondary drying and the characteristic desorption time (**Equation I.2.21**). Then, the design space can be calculated by considering the combination of shelf temperature and drying time which led to a product temperature lower than  $T_g$  and an acceptable final moisture content. Considering a target moisture content between 1 and 2 %, the safe area in the design space is represented by the gray area limited by the solid lines in **Figure I.4.9**. The dashed lines in **Figure I.4.9** limits the portion of the design space where the constraint on the maximum value of product temperature was not satisfied.

Pisano et al. (Pisano *et al.*, 2012), also verified the impact of  $K_V$  variability and moisture content variability at the beginning of the secondary drying step on the design space. Different values of  $K_V$  did not have an impact on the design space area. Conversely, the safe area of the design space calculated from lower values of initial moisture content is bigger than the one calculated from higher values of moisture content.

The design space can be used to optimize the secondary drying by selecting the value of shelf temperature  $T_S$  that allows minimizing the desorption time  $t_{des}$ . Furthermore, as the critical product temperature depends on the moisture content, the process can be further optimized using different set-points for the shelf temperature during secondary drying, in such a way that product temperature is always close to the limit value as drying goes on.

#### 1.1. A summary of mechanisms responsible for product heterogeneity

The final objective of designing a freeze-drying process is to guarantee product quality within the batch and between different batches. However, different sources of variability present in primary drying can cause a final product quality heterogeneity (i.e., collapse of the product due to a product temperature higher than the critical one during primary or secondary drying, and final moisture content higher than the target value).

The four main sources are:



(i) *the edge vial effect*: the additional heat mechanisms present at the border of the shelf can cause different product temperature and moisture content profiles in edge and central vials during primary drying.

(ii) *the modification of cake structure during the freezing step*: vials differently located on the shelf can present a different temperature of nucleation and degree of supercooling. As consequence, the porous structure of the dried matrix will not be homogeneous within the vial batch, with consequences on mass transfer resistance in primary drying and desorption kinetics in secondary drying (Rambhatla *et al.*, 2004; Passot *et al.*, 2009; Searles *et al.*, 2001b; Konstantinidis *et al.*, 2011);

(iii) *the vial geometry variability*: due to production limits, vial bottom dimensions may be different from one vial to the other. This vial geometry distribution can cause variability of the heat transfer in the batch.

(iv) *local shelf temperature variability and pressure gradient in the drying chamber* could have a more or less marked effect on the batch heterogeneity, depending on the freeze-dryer characteristics (Rasetto *et al.*, 2008).

These un-controlled phenomena cause variability in the heat and mass transfer and thus distributions of the product temperature and moisture content profiles, of the sublimation and desorption rates. Thus, when the primary and secondary drying steps are designed (in terms of shelf temperature, chamber pressure and time), those mechanisms should be taken into consideration.

However, the prediction of critical process parameters such as product temperature, sublimation rate and desorption rate through the mathematical model is often based on the simulation of only average value of the model parameters of heat and mass transfer, which does not adequately represent the complex distribution of the variables in the batch. Only the edge vial effect is often taken into account in mathematical models (e.g., (Velardi and Barresi, 2008; Brülls and Rasmuson, 2002; Hottot *et al.*, 2006; Gan *et al.*, 2005)) whereas cake structure variability as well as vial geometry variability were not considered, probably due to the difficulty in the experimental quantification. The prediction of product temperature and sublimation rate without taken into account the sources of variability can lead to:

1. *An erroneous prediction of critical process parameters, such as the product temperature or the desorption rate.* Heat and mass transfer variability needs to be considered to correctly predict the product temperature and moisture content profile distribution in the batch. As example, edge vials could present a higher product temperature than central vials due to the edge vial effect. If the edge vial effect is not considered and the process run at product temperature closed to the critical one ( $T_g'$ ), collapse in edge vials can occur.



2. *An erroneous detection of the end-point of primary and secondary drying.* Inter-vial mass and heat transfer heterogeneity causes a distribution of the product temperature, sublimation and desorption rates in the vial batch. Regarding the duration of primary drying, vials can end the sublimation at different moments. A more conservative cycle would increase the already long process time, but an early start of the secondary drying step, followed by the increasing of the shelf temperature, can cause the collapse of the vials in which the sublimation is still ongoing. Furthermore, a short duration of the secondary drying step will lead to a higher value of moisture content than the target one, which will affect the shelf life and the stability of the product.
3. *An erroneous scale-up process.* Some mechanisms causing product heterogeneity (e.g., heat transfer by radiation from the drying chamber walls to the edge vials) are dependent on the characteristics of the equipment in which the cycle is run (e.g., emissivity of the walls). Product temperature and sublimation rates distribution over the batch can change from one equipment to another, causing a very poor prediction for the scale-up process.

Deep theoretical understanding together with precise experimental quantification of the phenomena causing heat and mass transfer variability in primary drying could lead to a better prediction of the product quality heterogeneity in the final batch.

#### **I.4.4 Motivations of this project**

The main aim of this literature review was to remark the importance of the mathematical modelling in process design and control, as well as in the description of the heat and mass transfer phenomena taking place during the freeze-drying process. However, there is still a lack of use of the modelling for understanding of physical mechanisms responsible the product quality variability during the process. A correct definition and quantification of those mechanisms could led to a precise prediction of the variability of the critical process parameters, and thus to the definition of safety margins for the cycle development.

In this regards, the present thesis focused on the qualitatively and quantitatively investigation of four sources of product quality variability, previously identified in the review: (i) the variability of the vial geometry, (ii) the edge vial effect, (iii) the modification of cake structure during the freezing step. Mathematical modelling, together with the experimental analysis, was used as powerful tool to describe the physical mechanisms and for the prediction of the impact of on the product quality, through prediction of the product temperature. These mechanisms were then included in a dynamic mathematical model finalized to the development of freeze-drying cycles at a known risk of failure, expressed in term of vials potentially rejected.



— II —

**SCIENTIFIC APPROACH**



## II.1 Scientific questions

---

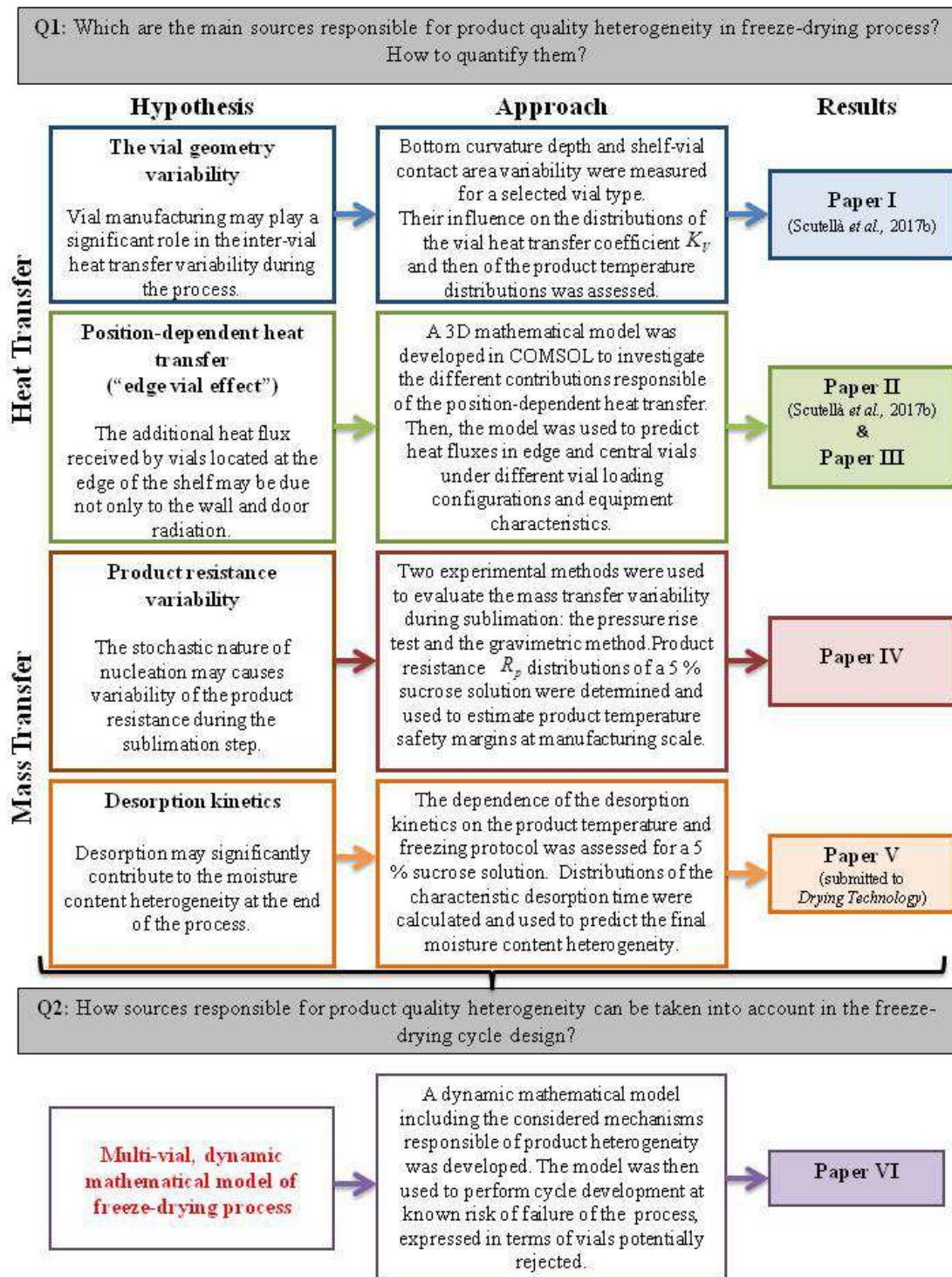
The main aim of the present Ph.D. thesis was to characterize the sources responsible for product quality variability in freeze-drying process within the same batch and from batch to batch in ordinary production and during scale-up, to quantify their relative importance on the risk of product rejection. Based on this analysis, a new approach for the freeze-drying cycles design will be developed in accordance with the Quality by Design concept described in the 8<sup>th</sup> Guidance on Quality of the International Council for Harmonisation of Technical Requirements for Pharmaceuticals for Human Use (ICH Q8).

These objectives were associated with the following two research questions:

- *Q1*: Which are the main sources responsible for product quality heterogeneity in freeze-drying process? How to quantify them?
- *Q2*: How the sources responsible for product quality heterogeneity can be taken into account in the freeze-drying cycle design?

**Figure II.1.1** schematically represents the scientific approach that was used to answer to the previously listed questions. An overview of formulated hypotheses and the main methods used for the research will be presented in the following section.

Figure II.1.1: Schematic representation of the scientific approach used in this project.



## II.2 Experimental strategy

---

### II.2.1 Identification and quantification of the mechanisms responsible for product quality heterogeneity in freeze-drying process

This research has its starting point in the identification of the mechanisms responsible for product quality variability during the different steps of the process. The product quality is usually defined in terms of critical attributes, such as the aspect of the product cake and the residual moisture content. These attributes mainly depend on critical product parameters, such as the product temperature, the sublimation rate and the desorption rate of the product, which are in turn governed by heat and mass transfer phenomena taking place in the drying chamber during the cycle. Based on a preliminary analysis of previous published works (**Part I, Literature Review**), three sources were identified as responsible for the variability of the product temperature and moisture content: (i) the variability of the container dimensions, (ii) the position dependent heat transfer ("edge vial effect"), (iii) the modification of cake structure during the freezing step, which led to variability of the product resistance to the mass transfer during primary drying and of the specific surface area available for desorption during secondary drying.

The *variability of the container dimensions* is mainly due to limits in the container production process to reproduce exactly the same dimensions between one vial to another. Since the heat transfer between the shelf and the vial strictly depends on the vial bottom geometry, variability of the vial bottom dimensions could influence this heat contribution through the vial heat transfer coefficient  $K_V$ . In order to verify this hypothesis, variability of the shelf-vial contact area and the depth of bottom concavity were firstly quantified within one set of 120 vials. The obtained vial dimension distributions were then used to reproduce vial heat transfer coefficient distributions for vials located in the centre of the shelf and not affected by the border heat transfer. Then, the impact on the product temperature of the resulting heat transfer variability was assessed. The results of this investigation are reported in **Paper III.1**.

The *"edge vial effect"* is widely known to be the main source of heat transfer variability within the vial batch. Vials located at the border of the shelf are known to receive additional heat flux compared

to central vials, and radiation from walls and door are often considered to be mainly responsible for this phenomenon. In order to deeply investigate this effect, a 3D mechanistic mathematical model of the heat transfer in edge and central vials was developed by using the software COMSOL Multiphysics, described in detail in **Paper III.2**. Then, the developed model was used to predict the heat transfer variability for different vial loading configurations and equipment characteristics (i.e., thermal characteristic of the freeze-dryer, distances between the shelves and between the wall and the shelf). The results obtained in this analysis are reported in **Paper III.3**.

Furthermore, the *variability of the mass transfer during primary drying was investigated*. Firstly, the importance of the presence of the stopper into the vial neck and of the freezing protocol on the sublimation rate was assessed. To this end, freeze-drying cycles were performed with vials partially stoppered or not stoppered, and using two different freezing protocols, i.e., with and without controlled nucleation. Then, the product resistance variability (expressed in terms of standard deviation) was evaluated for cycles performed with and without controlled nucleation by using two experimental methods: the pressure rise test and the gravimetric method. The obtained product resistance distributions were used to quantify the impact of the mass transfer variability on the product temperature. A 5 % sucrose solution was used throughout the study. The results of this analysis are reported in **Paper III.4**.

Finally, the role of the *desorption kinetics on the moisture content variability* in secondary drying was explored. A second order desorption kinetics was used to describe the moisture content evolution of a sucrose formulation during secondary drying. Controlled and uncontrolled nucleation were used during the freezing step. Then, the value and variability of the characteristic desorption time and their dependence on product temperature and on the freezing protocol were assessed, and used to calculate moisture content distributions during secondary drying. A 5 % sucrose solution was used throughout the study. The results are presented in **Paper III.5**.

### **II.2.2 Complete mathematical model including all considered sources of variability**

Once that the relative importance of several mechanisms on the product heterogeneity was theoretically and experimentally quantified, distributions of relevant physical parameters were included in a multi-vial, dynamic mathematical model describing the heat and mass transfer during the sublimation and desorption steps of the freeze-drying process. This model was then used to develop a new approach for the design of the primary and secondary drying steps of the freeze-drying process at known risk of failure, by considering four main constraint: the maximum allowed product

temperature during primary and secondary drying, the completion of the sublimation step, the target final product moisture content. The risk of failure of the process was estimated in term of percentage of vials potentially rejected. This multi-vial, dynamic developed model is described in **Paper III.6**.

In conclusion, the original approach proposed in this project consisted in (i) a systematic quantification of the variability of heat and mass transfer mechanisms relevant for product quality, and (ii) in the integration of these mechanisms in a new multi-vial, dynamic mathematical model to define a new approach for the development of freeze-drying process at known risk of failure.



— III —

## RESULTS AND DISCUSSION



### III.1 How vial geometry variability influences heat transfer and product temperature during freeze-drying

The present study was published on the Volume 106(3) (March 2017) of the *Journal of Pharmaceutical Science*

#### III.1.1 Context and objectives

Usually vaccines intended to be freeze-dried are processed within glass containers named vials. The vials usually presents a "*champagne bottle*" geometry, with a small concavity in the bottom to improve the stability of the vial on the shelf and to reduce the container breakage. Vials on the shelf are known to receive only the heat flow from the top and bottom shelves through three main mechanisms: (i) the *contact conduction* between the shelf and the vial, (ii) the *radiation* from the top and bottom shelves and (iii) the *conduction through the gas* present in the vial bottom concavity. The heat transfer via contact conduction and conduction through the gas are respectively influenced by the *contact area between the shelf and the vial* and the *depth of vial bottom curvature* in which the gas is entrapped. The presence of a vial bottom curvature limits the heat transfer by reducing the points of direct contact between the vial and the shelf, and represents the major resistance to the heat transfer. Furthermore, due to production limits, the vial bottom dimensions may vary between vials within the same batch and can influence the variability of the heat transfer and thus of the product temperature.

#### Objective

The purpose of the present study was to quantify the importance of the variability of two relevant geometrical dimensions of the vial bottom, i.e. contact area between the shelf and the vial and depth of bottom curvature, on (i) the variability of heat transfer between the shelf and the vial through predictions of vial heat transfer coefficient  $K_v$  distributions and then on (ii) the final product quality heterogeneity through prediction of the product temperature distributions.



### III.1.2 Paper

#### TITLE

How vial geometry variability influences heat transfer and product temperature during freeze-drying

#### AUTHORS

Bernadette Scutella<sup>1,2</sup>, Stephanie Passot<sup>1</sup>, Erwan Bourles<sup>2</sup>, Fernanda Fonseca<sup>1</sup>, Ioan Cristian Trelea<sup>1</sup>

#### AFFILIATIONS

<sup>1</sup> UMR GMPA, AgroParisTech, INRA, Université Paris Saclay, 78850 Thiverval-Grignon, France

<sup>2</sup> Technical R&D Drug Product GSK, 1330 Rixensart, Belgium

#### ABSTRACT

Vial design features can play a significant role in heat transfer between the shelf and the product and, consequently, in the final quality of the freeze-dried product. Our objective was to investigate the impact of the variability of some geometrical dimensions of a set of tubing vials commonly used for vaccine production on the distribution of the vial heat transfer coefficients ( $K_v$ ) and its potential consequence on product temperature. Sublimation tests were carried out using pure water and eight combinations of chamber pressure (4 to 50 Pa) and shelf temperature (-40 °C and 0 °C) in two freeze-dryers.  $K_v$  values were individually determined for 120 vials located in the center of the shelf. Vial bottom curvature depth and contact area between the vial and the shelf were carefully measured for 120 vials and these data were used to calculate  $K_v$  distribution due to variability in vial geometry. At low pressures commonly used for sensitive products (below 10 Pa), the vial-shelf contact area appeared crucial for explaining  $K_v$  heterogeneity and was found to generate, in our study, a product temperature distribution of approximately 2 °C during sublimation. Our approach provides quantitative guidelines for defining vial geometry tolerance specifications and product temperature safety margins.

#### KEYWORDS

Freeze drying/lyophilization; amorphous; drying; vaccines; distribution; vial heat transfer coefficient; sublimation rate; vial design; inter-vial heterogeneity.

## INTRODUCTION

Nowadays, freeze-drying is an essential and valuable preservation method to ensure the long-term stability of the growing list of biopharmaceuticals such as antibodies, hormones, vaccines, therapeutics peptides and proteins. This method makes it possible to remove the majority of water at temperatures far below 0 °C (usually between -40 °C and -20 °C) by sublimation, the phase transition from ice to water vapour (Jennings, 1999).

Due to the really low temperature and pressure typically used, freeze-drying remains a time consuming process often difficult to control and scale-up. The US Food and Drug Administration has recently proposed a new regulatory philosophy to manage product quality: the Quality by Design (QbD) initiative. Quality will be no more tested into the product but designed into the process. The QbD approach is based on pre-defined quality targets and on a deep understanding of how formulations and process interact to influence critical quality attributes of pharmaceutical products (Nail and Searles, 2008). In contrast to tablets, products intended to be freeze-dried are conditioned in their final packaging system (vial or syringe) before the process (Franks, 1998). The vial thus directly influences the freeze-drying process and impacts final product quality (Hibler *et al.*, 2012; Pikal *et al.*, 1984). Furthermore, since the capacity of a manufacturing freeze-dryer can easily reach 100 000 vials, ensuring uniform product quality attributes (potency of the active ingredient, residual moisture content, visual aspect of the freeze-dried cake) within the entire batch represents a real challenge. Any variation in the design of the packaging system or other parameters could result in product quality variation.

Product temperature is a key process parameter governing an important critical product quality attribute, the visual aspect of the freeze-dried cake, which in turn could influence the residual moisture, the stability of the active ingredient and the reconstitution time (Johnson and Lewis, 2011). During the process the product temperature should be maintained below a critical value corresponding to the glass transition temperature in amorphous product (Hibler and Gieseler, 2012; Franks, 1998). However, the product temperature profile cannot be directly controlled and depends on the process operating variables (i.e., shelf temperature, chamber pressure) and on the heat transfer through the container (e.g., vial) (Hibler and Gieseler, 2012; Pikal, 2000; Hibler *et al.*, 2012). Knowledge of the heat transfer characteristics of the vial and the uniformity or non uniformity of this property within vial arrangement inside a freeze-dryer is thus essential to be able to predict final quality of the product batch. Several authors have reported that the heat transfer rate between the shelf and the product is dependent on the vial position on the shelf (Pikal *et al.*, 1984; Rambhatla and Pikal, 2003; Hibler *et al.*, 2012; Pisano *et al.*, 2013; Pikal *et al.*, 2016; Pisano *et al.*, 2011). Pikal *et al.* (Pikal *et al.*, 1984), showed that the vials located at the periphery of the shelf exhibited sublimation rates 15 % higher than vials located in the center. This phenomenon, referred to as "edge effect", has

been ascribed to additional heat transfer by radiation from walls and doors (Rambhatla and Pikal, 2003; Hibler *et al.*, 2012; Pikal, 2000; Pikal *et al.*, 1984, 2016). The higher heat flow rate of these periphery vials could lead to product collapse due to increased product temperatures during the primary drying phase. Furthermore, Pisano *et al.* (Pisano *et al.*, 2013), recently observed a normal distribution in the vial heat transfer coefficient evaluated for vials located in the center of the shelf.

The design of the vial also strongly influences the heat transfer efficiency between the shelf and the product (Pikal *et al.*, 1984; Hibler and Gieseler, 2012; Hibler *et al.*, 2012; Nail, 1980; Ybema *et al.*, 1995; Brülls and Rasmuson, 2002; Pisano *et al.*, 2011). Considering that the vials are placed directly on the shelf, the heat flow transferred to the product can be described by three parallel mechanisms: conduction from the shelf surface to the vial *via* points of direct contact between the vial bottom and the shelf, conduction through the vapour entrapped in the vial bottom concavity and radiation (Pikal *et al.*, 1984; Pikal, 2000; Pisano *et al.*, 2011). Heat transfers *via* contact conduction and conduction through the gas are influenced, respectively, by the dimension of the contact area between the shelf and the vial and the depth of bottom curvature in which the gas is entrapped (Pikal *et al.*, 1984; Pikal, 2000; Pisano *et al.*, 2011). Several studies (Nail, 1980; Cannon and Shemeley, 2004; Kuu *et al.*, 2009) have demonstrated that the vial bottom curvature limits the heat transfer and, thus, the sublimation flow rate that determines the duration of the primary drying. The concavity of the vial bottom limits the direct surface contact between the vial and the shelf, accounting for most of the resistance to conductive heat transfer (Cannon and Shemeley, 2004; Ybema *et al.*, 1995). In pharmaceutical freeze-drying conditions, contact conduction is more efficient than gas conduction, and an increase in the contact area leads to a significant increase in the total heat transfer (Pikal *et al.*, 1984; Ybema *et al.*, 1995).

Our objective was to quantitatively investigate the role of vial geometry distribution on heat transfer heterogeneity and subsequently on product quality by predicting product temperature distribution during the primary drying step induced by variability in vial dimensions. Proposing an approach to understand how vial design and operating variables interact to influence product quality is completely in the scope of the QbD approach.

In the present study, only vials located in the center of the shelf and surrounded by other vials in the same conditions were considered so as to avoid any heterogeneity due to the additional border heat transfer. The analysis of the heterogeneity was conducted in terms of vial heat transfer coefficient ( $K_v$ ) distributions. Based on theoretical analysis (Pikal, 2000; Pikal *et al.*, 1984; Pisano *et al.*, 2011), attention was focused on the role of two vial dimensions, the bottom curvature depth and the contact area between the bottom vial and the shelf.

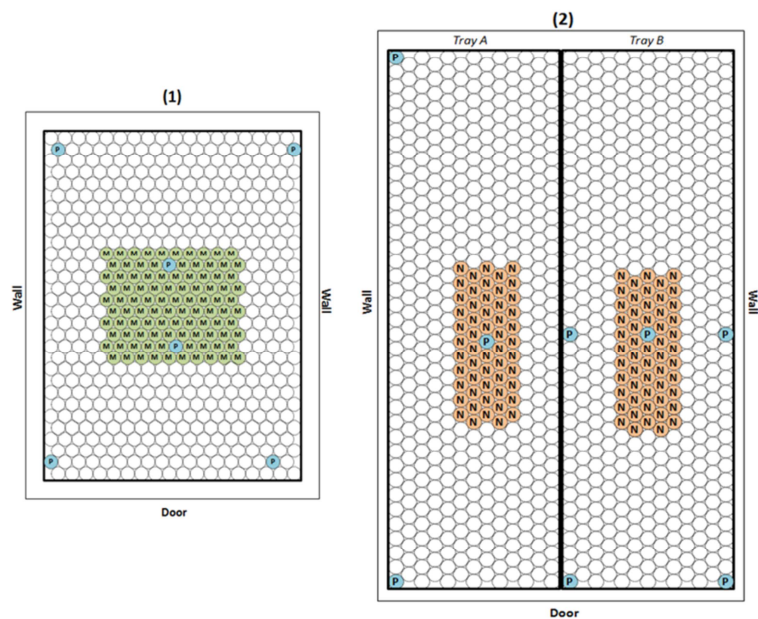


**Figure III.1.1** Vial arrangements in (1) LYO A and (2) LYO B. Gravimetrically-analyzed vials are marked with the letters M and N for LYO A and B, respectively. Vials in which wireless temperature probes were located are marked with the letter P. All vials were filled with 1.8 mL of pure water.

Two shelf temperatures (-40 °C and 0 °C) and six chamber pressures (4, 6, 9, 15, 40 and 50 Pa) were tested in two freeze-dryer pilot plants of similar shelf emissivity to assess the impact of these operative variables on the heat transfer heterogeneity among central vials. Finally, as example of practical application of our work for assessing the pharmaceutical product quality, the impact of the central vial  $K_v$  variability on product temperature was evaluated.

Product temperature distributions for a 5 % sucrose solution were calculated from the simulated  $K_v$  distributions based on the vial geometry for several operating variables.

## MATERIALS AND METHODS

### Materials

Siliconized glass tubing vials (3 mL) were provided by Müller + Müller (Holzminden, Germany). These vials are routinely used in commercial manufacturing. Distilled water was used throughout the experiments.

Two pilot scale freeze-dryers differing mainly by their size, the type of valve connecting the drying chamber to the condenser and their age were used for this study:

- a LyoVac GT6 (Finn-Aqua Santasalo-Sohlberg SPRL, Brussels, Belgium), referred to as LYO A. It included 5 shelves with an area of 0.14 m<sup>2</sup> each, a distance between shelves of 56 mm, a drying chamber volume of 0.061 m<sup>3</sup> and a butterfly valve between the chamber and the condenser.
- an Epsilon 2-25D (Martin Christ Gefriertrocknungsanlagen GmbH, Osterode am Harz, Germany), referred to as LYO B. It included 7 shelves with an area of 0.27 m<sup>2</sup> each, a distance between shelves of 55 mm, a drying chamber volume of 0.38 m<sup>3</sup> and a mushroom valve between the chamber and the condenser.

The pressure in the freeze-dryer chamber was monitored by a capacitive manometer. Since it was not technically possible to install thermocouples in the drying chamber of the two freeze-dryers, Tempris wireless sensors (IQ Mobil Solution GmbH, Holzkirchen, Germany) were positioned in the bottom center of selected vials (**Figure III.1.1**) to record ice temperature during the experiments. The obtained signal was used to define the sublimation starting point.

### Ice sublimation experiments

All experiments were performed using a 1.8 mL fill volume of distilled water (filling height: 11 mm). No stopper was inserted into the vial neck. The middle shelf was fully covered by filled vials for all runs, corresponding to a total of 540 vials in LYO A and 950 vials in LYO B. Bottomless trays were used. The vials were quickly loaded on the pre-cooled shelf at -50°C. The presence of a dry laminar flow in front of the freeze-dryer door made it possible to control the air relative humidity and thus to limit condensation on the shelves.

**Table III.1.1.** Vial dimensions, physical properties and emissivities used in this study

<i>Symbol</i>	<i>Significance</i>	<i>Value ± SD</i>	<i>Units</i>
$A_b$	Outer bottom area of the vial	$(2.07 \pm 0.37) 10^{-4}$	$m^2$
$A_{in}$	Inner bottom area of the vial	$(1.78 \pm 0.29) 10^{-4}$	$m^2$
$A_c$	Vial-shelf contact area	$(1.67 \pm 0.40) 10^{-4}$	$m^2$
$l$	Mean bottom curvature depth <sup>a</sup>	$(1.23 \pm 0.34) 10^{-4}$	$m$
$\Delta H$	Latent heat of sublimation of ice	2763.3	$kJ kg^{-1}$
$\lambda_{amb}$	Molecular conductivity of the water vapour at ambient pressure	0.025	$W m^{-1} K^{-1}$
$\lambda_{ice}$	Ice heat conductivity	2.23	$W m^{-1} K^{-1}$
$\sigma$	Stephen-Boltzmann constant	$5.670367 \times 10^{-8}$	$W m^{-2} K^{-4}$
$R_p$	Product resistance for 5% w/w sucrose solution (Konstantinidis <i>et al.</i> , 2011)	124.8	$kPa s m^2 kg^{-1}$
$e_v$	Vial emissivity	0.78	Dimensionless
$e_s$	Shelf emissivity	0.18	Dimensionless
$\mathcal{F}_b$	Visualization factor at the bottom of the vial ( <b>Equation III.1.10</b> )	0.16	Dimensionless

<sup>a</sup>Calculated as reported in the **Appendix**

After a freezing step of 2 hours, the pressure was decreased and the shelf temperature was increased by 1 °C/min. Experiments were carried out at 4, 6, 9, 15, 40 and 50 Pa with a shelf fluid inlet temperature of 0 °C, and at 4 and 6 Pa with a shelf fluid inlet temperature of -40 °C. The run performed at 0 °C and 6 Pa was repeated three times. The cycles were run long enough to dry up to 20-25 % of the initial fill volume. Subliming a larger quantity of ice could lead to loss of contact between the vial and the ice, introducing uncertainty in the analysis.

The sublimation rate  $\dot{m}$  was measured gravimetrically for each vial and calculated as the mass loss divided by the period of sublimation. A total of 100 vials, placed in the centre of the shelf and surrounded by other vials in the same conditions, were individually weighed before and after the experiment on a precision scale ( $\pm 0.001$  g; Mettler Toledo, Zaventem, Belgium). Sublimation time was measured from the moment when shelf temperature exceeded product temperature, meaning that there was a net heat flux from the shelf towards the vials. The arrangement of the weighed vials within the shelves is shown in **Figure III.1.1** for the two freeze-dryers.

#### Measurement of emissivity of the vial and of the shelf

Emissivity measurements were performed by Themacs Ingénierie (Champs sur Marne, France). The glass vial emissivity was determined using a Fourier transform infrared spectrophotometer (Frontier, Perkin Elmer, Roissy, France) equipped with a Pike integrant sphere (Pike Technologies, Fitchburg, WI, USA). The measured emissivity varied from 0.78 to 0.80 within the range of temperatures tested (from -48 °C to 27 °C). Thus, a constant value corresponding to the average observed product temperatures (between -48 to -24 °C) was used in the data analysis, as reported in **Table III.1.1**.

The shelf emissivity was measured using the emissometer EM-2, making it possible an in situ measurement (Monchau *et al.*, 2013). The emissivity value of the shelves of LYO B was  $0.18 \pm 0.06$  (**Table III.1.1**). Measurements were carried out on several pilot and production freeze-dryers and shelf emissivity values in the range of 0.18-0.3 were obtained. Considering the relative standard deviation of the method (0.06), the measured values are in agreement with values reported in literature (Pikal *et al.*, 1984).

#### Dimensional analysis of a batch of vials

The dimensions of 120 vials were precisely measured by the specialized company Precis&Mans (Le Mans, France) using the micrometer Mitutoyo 3D (Mitutoyo Europe GmbH, Neuss, Germany). The following geometrical parameters were determined with a precision of 0.003 mm: the inner and outer bottom radius and the maximum bottom curvature depth. These values were used to calculate additional vial dimensions: outer and inner vial bottom area, vial shelf contact area ( $A_c$ ) (named radius-based contact area in **Table III.1.1**.) and mean bottom curvature depth ( $l$ ) (**Appendix**).

Furthermore, the vial-shelf contact area was also estimated using the imprint method proposed by Kuu *et al.* (Kuu *et al.*, 2009) and Hibler *et al.* (Hibler *et al.*, 2012). The vials were gently placed on an inkpad and then on a sheet of white paper. ImageJ v.1.49 software (National Institutes of Health, Bethesda, MD, USA) was used for the determination of the vial-shelf bottom contact area in pixels from the imprint images. The scale factor of pixels in mm<sup>2</sup> was determined by evaluating the number of pixels of a black shape of known area and was equal to 0.0153 mm<sup>2</sup> pixel<sup>-1</sup>. The mean value and the relative standard deviation of these geometrical dimensions are reported in **Table III.1.1**. The two methods used for evaluating the vial-shelf contact area gave similar mean values: 16.7 mm<sup>2</sup> for the imprint method and 17.8 mm<sup>2</sup> for the dimensional analysis.

However, the coefficient of variation of these methods appeared different and significantly higher for the imprint method (23.9 % versus 12.0 % for the dimensional analysis). The values of contact area determined using this latter method were selected for the analysis considering that this method better accounts for intimate contact between vial and shelf.

## THEORY AND DATA ANALYSIS

### Evaluation of the vial heat transfer coefficient $K_v$ based on experimental data

As widely reported in literature (Pikal *et al.*, 1984; Pikal, 2000; Pisano *et al.*, 2011; Hibler *et al.*, 2012), the vial heat transfer coefficient  $K_v$  was calculated using the following equation:

$$K_v = \frac{\dot{Q}}{A_b(T_s - T_b)} = \frac{\Delta H \dot{m}}{A_b(T_s - T_b)} \quad \text{Equation III.1.1}$$

where  $\dot{Q}$  is the heat flow received by the vial,  $A_b$  is the outer vial bottom area,  $T_s$  is the average temperature between the inlet and outlet shelf fluid temperatures,  $T_b$  is the bottom product temperature,  $\Delta H$  is the latent heat of sublimation and  $\dot{m}$  is the sublimation rate.

Since it was not possible to implement thermocouples in the freeze-dryer pilot plant to have a precise measurement of the product temperature,  $T_b$  was theoretically determined as:

$$\dot{Q} = \frac{\lambda_{ice}}{L_{ice}} A_{in} (T_b - T_i) \quad \text{Equation III.1.2}$$

where  $\lambda_{ice}$  is the ice thermal conductivity,  $A_{in}$  is the inner bottom area of the vial,  $L_{ice}$  is the ice thickness and  $T_i$  is the ice-vapour interface temperature. The ice thickness was estimated as the mean between the initial and final ice thickness values (calculated using the amounts of initial and sublimed ice).

No stopper and pure water were used in this study in order to assume that the partial pressure of vapour at the sublimation interface was equal to the chamber pressure. The temperature at the ice-vapour interface  $T_i$  was thus calculated as a function of the interface pressure  $P_i$  using the Clausius-Clapeyron relation (Trelea *et al.*, 2007):

$$T_i = \frac{6139.6}{28.8912 - \ln(P_i)} \quad \text{Equation III.1.3}$$

The  $T_b$  value calculated was compared to the product temperature value given by the Tempris probe and an excellent agreement between experimental and theoretical data was observed.

#### Theoretical description of the vial heat transfer coefficient $K_v$

The main objective of this work was to quantify the impact of vial dimensions distribution on heat transfer variability and its resulting consequence on product temperature. To this end, the vial heat transfer coefficient need to be theoretically expressed in function of specific vial dimensions.

The vial heat transfer coefficient  $K_v$  can be described as the sum of three contributions (Pikal, 2000; Pikal *et al.*, 1984; Pisano *et al.*, 2011):

$$K_v = K_c + K_g + K_r \quad \text{Equation III.1.4}$$

where  $K_c$  represents the thermal contact conduction between the shelf and the vial *via* the direct contact area,  $K_g$  the thermal conduction through the gas entrapped in the vial bottom curvature and  $K_r$  the thermal radiation between the vial and the top and bottom shelves.

#### *Heat transfer by thermal contact conduction $K_c$*

The expression of  $K_c$  has been discussed in the literature by only a few authors (Cannon and Shemeley, 2004; Kuu *et al.*, 2009). Kuu *et al.* (Kuu *et al.*, 2009), proposed an evaluation of this parameter and showed that the larger the contact area is, the larger the value of the contact conduction coefficient will be. Thus,  $K_c$  can be assumed to be proportional to the contact area ( $A_c$ , evaluated by the imprint test method) through an empirical constant ( $C_1$ ):

$$K_c = C_1 A_c \quad \text{Equation III.1.5}$$

#### *Heat transfer by conduction through the gas $K_g$*

The coefficient  $K_g$ , representing the contribution of the conduction through the gas in  $K_v$ , can be

expressed as (Pisano *et al.*, 2011; Pikal *et al.*, 1984):

$$K_g = \frac{C_2 P_C}{1 + \frac{C_2 l}{\lambda_{amb}} P_C} \quad \text{Equation III.1.6}$$

where  $P_C$  is the chamber pressure,  $\lambda_{amb}$  is the molecular conductivity of the water vapour at ambient pressure,  $l$  is the mean vial bottom curvature depth calculated as reported in the **Appendix**, and the coefficient  $C_2$  is equal to:

$$C_2 = \Lambda_o \frac{\alpha_c}{2 - \alpha_c} \left( \frac{273.15}{T_{gas}} \right)^{0.5} \quad \text{Equation III.1.7}$$

where  $\Lambda_o$  is the free molecular heat conductivity of the gas at 0 °C,  $T_{gas}$  is temperature of the gas participating to heat conduction, calculated as average between the product temperature at the sublimation interface and the shelf temperature values (Pisano *et al.*, 2011), and  $\alpha_c$  is the accommodation coefficient.

#### *Heat transfer by thermal radiation $K_r$*

The heat transfer by radiation between the shelf and the vial  $\dot{Q}_r^{shelf}$  can be described by the Stephan-Boltzmann equation (Pikal, 2000; Pikal *et al.*, 1984; Bird *et al.*, 2002):

$$\dot{Q}_r^{shelf} = A_r \mathcal{F} \sigma (T_s^4 - T_b^4) \quad \text{Equation III.1.8}$$

where  $A_r$  is the area exposed to the radiation from the shelves to be considered equal to the vial bottom area  $A_b$ ,  $\mathcal{F}$  is the visualization factor and  $\sigma$  the Stephan-Boltzmann constant. After mathematical rearrangement, **Equation III.1.8** can be expressed as:

$$\dot{Q}_r^{shelf} = A_r \mathcal{F} \sigma (T_s^4 - T_b^4) = A_b \mathcal{F} \sigma (T_s + T_b)(T_s^2 + T_b^2)(T_s - T_b) \quad \text{Equation III.1.9}$$

Thus, the heat transfer coefficient  $K_r$  for thermal radiation can be defined as:

$$K_r = \mathcal{F} \sigma (T_s + T_b)(T_s^2 + T_b^2) \quad \text{Equation III.1.10}$$

During the process, central vials are affected by two different radiative heat transfer contributions: between (i) the shelf below the vial and the vial bottom, and (ii) the shelf above the vial and the top of the vial (Pikal, 2000; Pikal *et al.*, 1984; Pisano *et al.*, 2011). Hence, the visualization factor will be the sum of two terms:

$$\mathcal{F} = \mathcal{F}_b + \mathcal{F}_{top} \quad \text{Equation III.1.11}$$

The visualization factor at the bottom of the vial  $\mathcal{F}_b$  can be evaluated considering the definition proposed by Bird *et al.* (Bird *et al.*, 2002) and Pikal (Pikal, 2000) for the heat transfer by radiation between parallel surfaces:

$$\mathcal{F}_b = \frac{1}{1 + \left(\frac{1}{e_v} - 1\right) + \left(\frac{1}{e_s} - 1\right)} \quad \text{Equation III.1.12}$$

where  $e_v$  and  $e_s$  are the emissivities of the vial and shelf, respectively.

Considering vials located in the centre of the shelf and surrounded by other vials in the same conditions, it is possible to assume that (i) the vial area exposed to the top shelf is much smaller than the area of the shelf and (ii) the vial top does not receive radiations from the side walls of the chamber. Thus, the visualization factor between the top of the vials and the shelf  $\mathcal{F}_{top}$  can be estimated equal to the emissivity of the vial (Pikal, 2000; Pikal *et al.*, 1984).

$$\mathcal{F}_{top} = e_v \quad \text{Equation III.1.13}$$

In agreement with the literature, the visualization factor at the vial top (equal to 0.78; **Table III.1.1**) is higher than the one at the vial bottom (equal to 0.16; **Table III.1.1**) (Pikal *et al.*, 1984).

*Dependence of the vial heat transfer coefficient on vial geometry*

**Equations III.1.4, III.1.5 and III.1.6** were combined to highlight the dependence of  $K_v$  on the contact area ( $A_c$ ), and bottom curvature depth ( $l$ ):

$$K_v = C_1 A_c + K_r + \frac{C_2 P_c}{1 + \frac{l}{\lambda_{amb}} C_2 P_c} \quad \text{Equation III.1.14}$$



The term  $K_r$  was calculated from **Equations III.1.10-13** for each experimental condition.

Coefficients  $C_1$  and  $C_2$  were determined by fitting **Equation III.1.14** in a least-squares sense to experimental  $K_v$  values determined by the gravimetric method. Calculations were performed with Matlab R2014b software equipped with the Statistics Toolbox (The Mathworks Inc., Natick, MA, USA). The bottom curvature depth  $l$  and contact area  $A_c$  were evaluated from dimensional analysis of the vial and imprint test, respectively.

#### Calculation of $K_v$ distributions based on vial geometry

Two vial dimensions influence heat transfer: the contact area ( $A_c$ ) and the mean bottom curvature depth ( $l$ ). The absence of correlation between the two geometrical dimensions  $l$  and  $A_c$  was verified by calculating the correlation factor together with its statistical significance (p-value > 0.5). It was thus possible to independently evaluate the impact of those parameters on  $K_v$ . Using **Equation III.1.14**, three  $K_v$  distributions based on vial dimension variations were simulated: (i) curvature-based ( $l$  in **Equation III.1.14**); (ii) contact area-based ( $A_c$  in **Equation III.1.14**); and (iii) their combination. The curvature-based  $K_v$  distribution was obtained by evaluating **Equation III.1.14** with the 120 measured values of the mean bottom curvature depth ( $l$ ), while the contact area was maintained constant at its mean value. The contact area-based  $K_v$  distribution was obtained by evaluating **Equation III.1.14** with the 120 measured values of the imprint-based contact area ( $A_c$ ), whereas the bottom curvature depth was maintained constant at its mean value. Plugging both measured  $l$  and  $A_c$  values into **Equation III.1.14** gave the combined contact area and curvature-based  $K_v$  distribution. The calculation was repeated for all the studied chamber pressures and shelf temperatures. Chi-square goodness-of-fit tests were performed on the simulated  $K_v$  distributions, establishing that the sample data were consistent with a normal distribution at a 0.05 significance level.

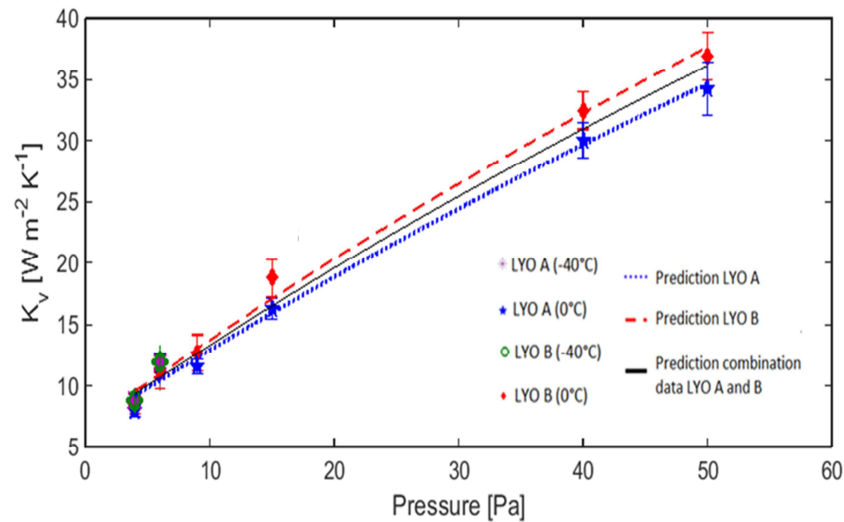


**Figure III.1.2.** Vial heat transfer coefficient ( $K_v$ ) values vs. chamber pressure ( $P_c$ ). The markers refer to the  $K_v$  average values measured in LYO A and B at  $-40^\circ\text{C}$  and  $0^\circ\text{C}$ . The lines correspond to the values calculated with **Equation III.1.14** with the data obtained from LYO A, B and their combination. Error bars represent standard deviations.

**Table III.1.2:** Heat transfer model coefficients evaluated by fitting **Equation III.1.13** to data obtained in (A) LYO A, (B) LYO B and (C) combining both sets of data (mean  $\pm$  standard error).

<i>Set of coefficients</i>	<i>Data</i>	$C_1$ $W K^{-1} m^{-4}$	$C_2$ $W m^{-2} K^{-1} Pa^{-1}$
A	LYO A	$(2.15 \pm 0.30) 10^5$	$0.630 \pm 0.027$
B	LYO B	$(2.25 \pm 0.34) 10^5$	$0.706 \pm 0.032$
C	Combination of data from LYO A and B	$(2.20 \pm 0.27) 10^5$	$0.667 \pm 0.025$

## RESULTS AND DISCUSSION

### Impact of equipment on $K_v$

Vial heat transfer coefficient  $K_v$  of 100 vials located in the centre of the shelf was experimentally determined for different chamber pressures (4 to 50 Pa), shelf temperatures (-40 °C and 0 °C) and freeze-dryers (LYO A and LYO B). **Figure III.1.2** illustrates the evolution of the average value of  $K_v$  with pressure. **Equation III.1.14** was fitted with the experimental data and the resulting coefficients  $C_1$  and  $C_2$  are presented in **Table III.1.2** for the data obtained in LYO A, LYO B and their combination. The accommodation coefficient  $\alpha_c$  was also calculated from **Equation III.1.7**, considering an average value of the gas temperature obtained under the different operating conditions tested ( $T_{gas} = -35$  °C). The obtained values of the accommodation coefficient appear to be in agreement with data in literature (Pikal, 2000).

In **Table III.1.2**, LYO A and LYO B exhibited a similar value of the  $C_1$  coefficient that is related to the contact area coefficient  $K_c$  (**Equation III.1.5**), but distinct values of the  $C_2$  coefficient that is related to  $K_g$  (**Equation III.1.6**). LYO B exhibited a slightly higher accommodation coefficient than LYO A, probably due to a different finish of the freeze-dryer shelf material.

When considering pressure values lower than 10 Pa (**Figure III.1.2**), the  $K_v$  values obtained in the two freeze-dryer appeared similar. This result was confirmed also by Pisano et al. (Pisano *et al.*, 2011), who reported no significant difference in  $K_v$  value of central vials processed in a pilot and manufacturing freeze-dryer at a pressure of 10 Pa. For pressure value higher than 10 Pa, the influence of freeze-dryer configuration became significant with slightly higher values obtained in LYO B (**Figure III.1.2**). At 50 Pa, the  $K_v$  value was approximately 8 % higher in LYO B than in LYO A. Considering the different values of  $C_2$  coefficient, the  $K_v$  difference between freeze-dryers at high pressure can thus be ascribed to the increased rate of heat transfer through the gas over the total heat flow.

However, the physical origin of the differences in the pressure-dependent component of  $K_v$  remains unclear. Possible hypotheses include: (i) differences in the shelf surface finish that could induce differences in the gas-shelf heat transfer through the accommodation coefficient (Pikal, 2000) (**Equation III.1.6-III.1.7**) as well as (ii) differences in the gas convection conditions, a mechanism responsible for a small part of the pressure-dependent heat transfer (Ganguly *et al.*, 2013). These results suggest that small differences between devices might become more apparent at high pressures. When considering only vials not exposed to edge effect a cycle designed with low operating pressure (below 10 Pa) could therefore be more suitable for safe scale-up. However the behavior of the edge vials located at the periphery of the shelf or in contact with metallic band need also to be considered and some elements were recently proposed by Pikal et al. (Pikal *et al.*, 2016), to investigate the impact of the freeze-dryer configuration.

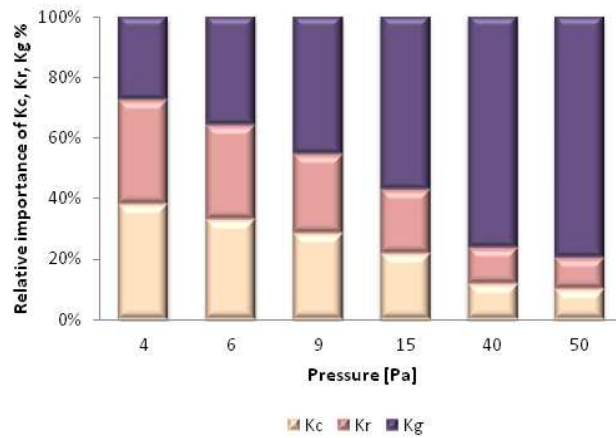


**Figure III.1.3.** Relative importance of the heat transfer coefficients by contact conduction ( $K_c$ ), radiation ( $K_r$ ) and conduction through the gas ( $K_g$ ) as percentages of the total heat transfer coefficients ( $K_v$ ). Average values of the contact area ( $A_c$ ) and mean bottom curvature depth ( $l$ ) were considered in this calculation. The set of coefficients C (Table III.1.2.) was used to evaluate  $K_c$  and  $K_g$ .

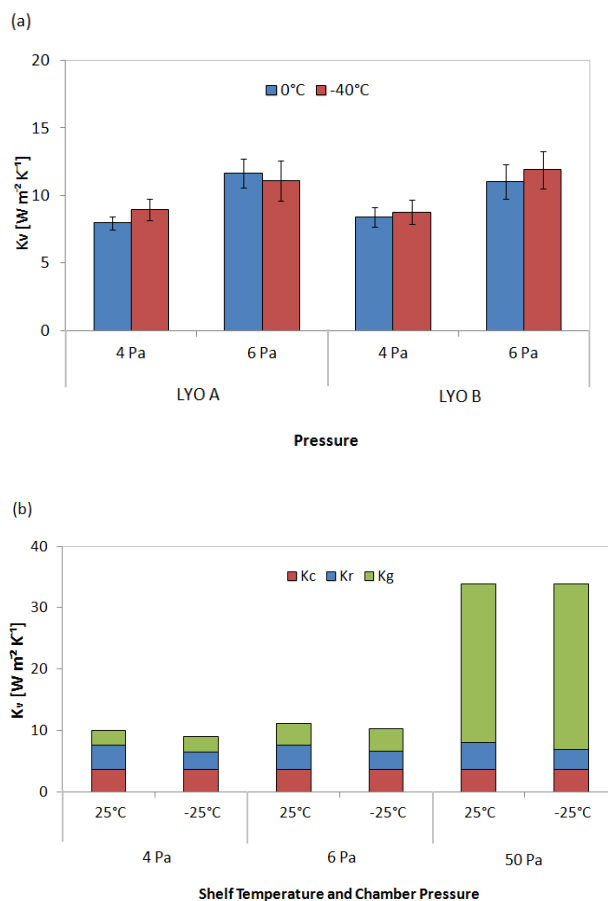


**Figure III.1.4.** Influence of the shelf temperature on the vial heat transfer coefficients  $K_v$ .  $K_v$  values were evaluated at different shelf temperatures and chamber pressures (a) from experimental data obtained in LYO A and B and (b) from the coefficients  $K_c$ ,  $K_r$  and  $K_g$ , calculated using Equations III.1.5, III.1.6 and III.1.10.

### Impact of chamber pressure and shelf temperature on $K_v$

As reported in the literature and shown in **Figure III.1.2**, chamber pressure had a strong impact on  $K_v$  (Pikal, 2000; Pikal *et al.*, 1984; Pisano *et al.*, 2011; Nail, 1980; Hibler *et al.*, 2012; Brülls and Rasmuson, 2002). The vial heat transfer coefficient increased approximately four times between 4 and 50 Pa. At the vial bottom, the presence of the curvature limits the intimate contact between the shelf and the vial and create an empty space between the shelf and the vial that acts as an insulator (Nail, 1980; Cannon and Shemeley, 2004; Kuu *et al.*, 2009). At very low pressures typically used in the process, the heat transfer contribution by gas convection is usually neglected (Pikal *et al.*, 2016), whereas the contribution of gas conduction has to be considered. This heat transfer mechanism, represented by the coefficient  $K_g$ , is dependent on the chamber pressure and increases when increasing pressure, as shown in **Equation III.1.6** (Pikal, 2000; Pikal *et al.*, 1984; Pisano *et al.*, 2011; Brülls and Rasmuson, 2002). **Figure III.1.3** shows the relative contributions of  $K_c$ ,  $K_r$  and  $K_g$  on the total  $K_v$ , calculated using the set C of the fitting coefficients reported in **Table III.1.2**. The  $K_c$  and  $K_r$  contributions go from about 30 % at 4 Pa to 10 % at 50 Pa, whereas the  $K_g$  contribution goes from about 25 % at 4 Pa to 80 % at 50 Pa.

A moderate effect of shelf temperature on  $K_v$  was expected theoretically due to  $K_r$  (**Equation III.1.10**) and to  $K_g$  through the gas temperature (**Equations III.1.6- 7**). **Figure III.1.4A** displays the influence of shelf temperature on  $K_v$ . Differences in  $K_v$  values due to temperature remained within the standard deviation when considering pressure values lower than 10 Pa and when the contribution of  $K_g$  in the total  $K_v$  is moderate (around 25 %, **Figure III.1.3**).

In order to clarify the impact of the shelf temperature, the contributions of the single coefficients  $K_c$ ,  $K_r$  and  $K_g$  on  $K_v$  were calculated for two shelf temperatures (25 °C and -25 °C) and three chamber pressures (4, 6 and 50 Pa), as show in **Figure III.1.4B**. The contact conduction coefficient  $K_c$  does not depend on the shelf temperature (**Equation III.1.5**) and thus has a constant contribution in  $K_v$  for all the temperatures tested. The radiative coefficient  $K_r$  depends on the third power of the shelf temperature and increases by about  $1 \text{ W m}^{-2} \text{ K}^{-1}$  between -25 °C and 25 °C for all pressures considered.

The gas conduction coefficient  $K_g$  depends on the gas temperature and decreases by 0.1-0.2  $\text{W m}^{-2} \text{ K}^{-1}$  at low pressures (4-6 Pa) and by 1.1  $\text{W m}^{-2} \text{ K}^{-1}$  at 50 Pa, between the two considered values of shelf temperature.

When increasing shelf temperature, the increase of  $K_r$  is partly compensated by the decrease of  $K_g$ . These results confirm that the dependence of  $K_v$  on the shelf temperature is negligible, especially if compared with the role played by the chamber pressure. Pisano *et al.* (Pisano *et al.*, 2011), and Hottot *et al.* (Hottot *et al.*, 2005), reported similar  $K_v$  values for different shelf temperature conditions.

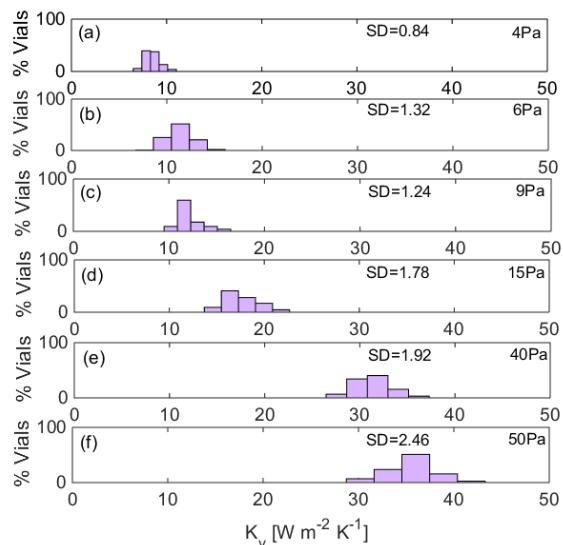


**Figure III.1.5.** Experimentally-measured distribution of the vial heat transfer coefficients at 4 Pa (a), 6 Pa (b), 9 Pa (c), 15 Pa (d), 40 Pa (e) and 50 Pa (f). Data of LYO A and LYO B at different shelf temperatures ( $0^\circ\text{C}$  and  $-40^\circ\text{C}$ ) were combined.

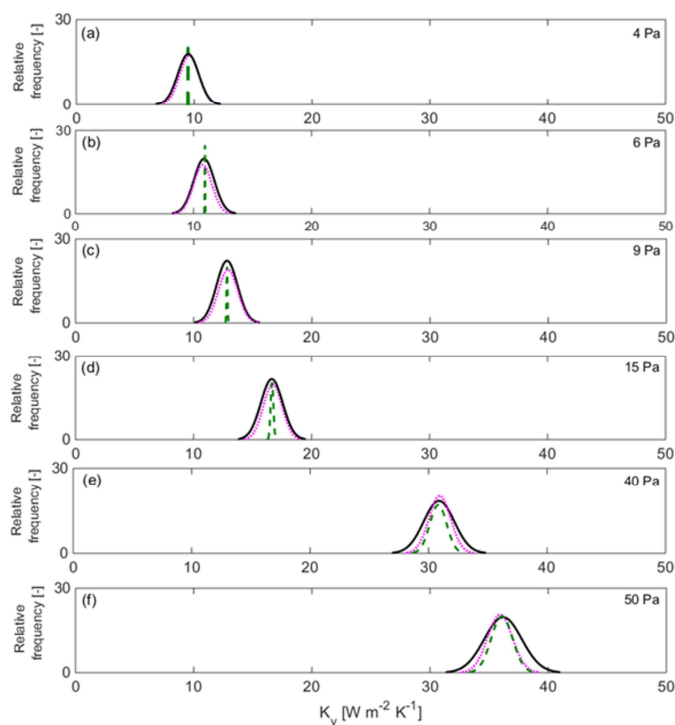


**Figure III.1.6** Calculated  $K_v$  normal distributions: curvature-based (dashed green line - -), contact area-based (dotted red line - -) and combined curvature and contact area-based (solid black line —) at 4 Pa (a), 6 Pa (b), (c) 9 Pa (c), 15 Pa (d), 40 Pa (e) and 50 Pa (f).

### Inter-vial heat transfer heterogeneity and the role of vial dimensions

**Figure III.1.5** presents the experimentally observed distributions of the vial heat transfer coefficient data of central vials at six chamber pressures. Since temperature- and equipment-induced variations were minor, data obtained in LYO A and B and for the two shelf temperatures were merged.

A significant variability in the  $K_v$  values evaluated for central vials was observed, the standard deviation increasing with pressure from 0.84 to 2.46  $W m^{-2} K^{-1}$ . The values of standard deviation corresponded to coefficient of variation comprised between 4 and 8 % depending on the operating conditions. The measurement error associated to the determination of  $K_v$  was evaluated as the sum of the individual measurement accuracy of each parameter entering in the calculation of  $K_v$  (**Equation III.1.1**). The measurement uncertainty was estimated to be  $\sim 1$  %. This value is in agreement with the value reported by Pikal et al. (Pikal *et al.*, 1984), who reported an uncertainty value of  $\sim 1.2$  %. The measurement uncertainty alone did not allow to completely explain the variability of the  $K_v$  data. An external factor responsible for inter-vial heat transfer heterogeneity had thus to be considered.

Attention was focused on the container: the geometrical difference among the vials was considered as a possible source of the heat transfer heterogeneity. This variability in the vial dimensions can be due to production limits and could change as a function of the container model and provider. For the tested vial set, the coefficient of variation was approximately 27.7 % for the mean bottom curvature depth ( $l$ ) and 23.9 % for the imprint-based contact area ( $A_c$ ). Hence, the effect of the variability of these geometrical dimensions on  $K_v$  was evaluated as proposed in the **Theory and data analysis** section using the set of coefficients C reported in **Table III.1.2**.

**Figure III.1.6** displays the simulated distributions of  $K_v$  based on the vial bottom dimensions. These distributions showed a trend and range of  $K_v$  values similar to the experimental ones. At low pressure,  $K_v$  variability is almost completely due to the contact area variability. The importance of the contact area on the  $K_v$  value was also confirmed by Pikal et al. (Pikal *et al.*, 1984), and Cannon et al. (Cannon and Shemeley, 2004). Regarding the vial bottom curvature, the importance of its variability increased when the pressure rose. This is due to the coefficient  $K_g$  that plays a major role in the total value of  $K_v$  at 40 and 50 Pa, as shown in **Figure III.1.3**. The role of the bottom curvature dimension was previously investigated by Brülls and Radsmuson (Brülls and Rasmuson, 2002) and Cannon et al. (Cannon and Shemeley, 2004). Brülls and Radsmuson (Brülls and Rasmuson, 2002) have shown that the bottom curvature has an impact on the heat transfer only at chamber pressures higher than 30 Pa. This conclusion was confirmed by Cannon et al. (Cannon and Shemeley, 2004), who found that bottom curvature had little impact when considering low pressure ( $< 27$  Pa). Our results agree with these conclusions (Brülls and Rasmuson, 2002; Cannon and Shemeley, 2004), confirming that the variability of the bottom curvature depth has to be taken into consideration only if cycles at high chamber pressure are performed ( $> 30$  Pa).

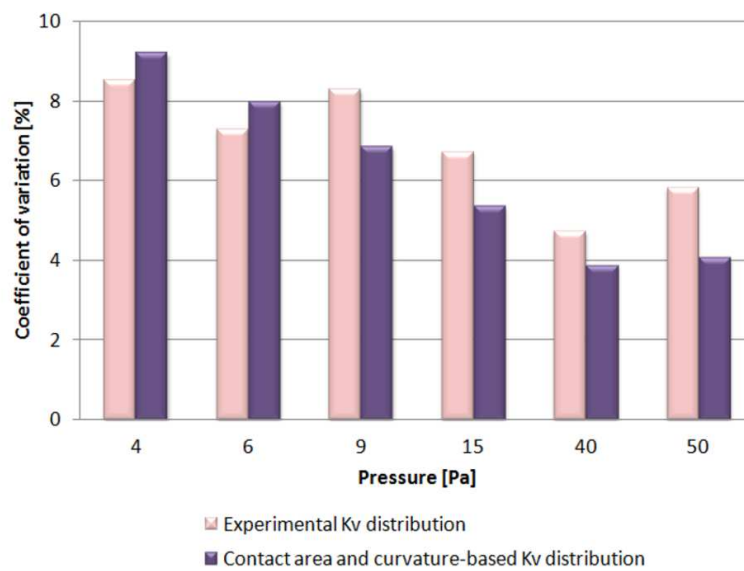


**Figure III.1.7.** Coefficients of variation of experimentally-measured  $K_v$  distribution (LYO A and B; light bars) and calculated (combined contact area and curvature-based)  $K_v$  distribution (dark bars) and at different pressures.

**Figure III.1.7** displays the coefficient of variation of the experimental and calculated  $K_v$  distributions at different pressures. For the experimental distributions, the coefficient was calculated as an average between the LYO A and B datasets. The trend of the observed coefficient of variations for both experimental and simulated  $K_v$  distributions decreased from approximately 9 % to 4 % when increasing the chamber pressure. The variability of the experimental  $K_v$  distributions is completely explained by the geometrical variability at low pressures (i.e., 4, 6 Pa), whereas at higher pressures, the experimental coefficient of variation appears to be slightly higher than the one calculated based on vial geometry. It is thus possible that other sources of variability should be taken into consideration, for example convection in the drying chamber could play a role if higher pressures are considered (Ganguly *et al.*, 2013).

These considerations can guide the selection of the container as a function of the variability of the vial dimensions. The results obtained show that at low chamber pressure (i.e., 4, 6, 9, 15 Pa), it is important to assess the variability of the contact area between the vial and the shelf, whereas for cycles performed at high pressure (i.e., 40, 50 Pa), the variability of the bottom curvature depth becomes a relevant parameter. Consequently, for pharmaceutical processes that are usually carried out at pressures lower than 10 Pa, the contact area needs to be taken into account more than the bottom curvature depth.

#### **Impact of $K_v$ heterogeneity on the product temperature distribution within a batch of vials located in the centre of the shelf and not exposed to edge effect**

In the case of freeze-drying, product temperature is one of the most important critical quality parameters. During the process, product temperature must be maintained close to a limit value (i.e., glass transition temperature for amorphous products,  $T_g$ ) in order to optimize the process time but not to exceed it so as to guarantee the visual aspect of the cake and the product quality. The vial-to-vial heat and mass transfer heterogeneity during the sublimation step causes variability in the product temperature. Considering a constant and fixed value of mass transfer resistance, it would be interesting to estimate the product temperature distribution during the primary drying step resulting only from the variability in vial geometry.

Product temperature distributions were thus evaluated considering the contact area and curvature-based  $K_v$  distributions. For this analysis, a 5 % w/w sucrose solution was considered, processed at -25 °C and four different pressures (4, 6, 9 and 15 Pa). Relevant data concerning product resistance and glass transition temperature (-32 °C) were found in the literature (Konstantinidis *et al.*, 2011). As expected, product temperature increased from 4 Pa to 15 Pa because of the higher value of the vial heat transfer coefficient and higher ice sublimation temperature.

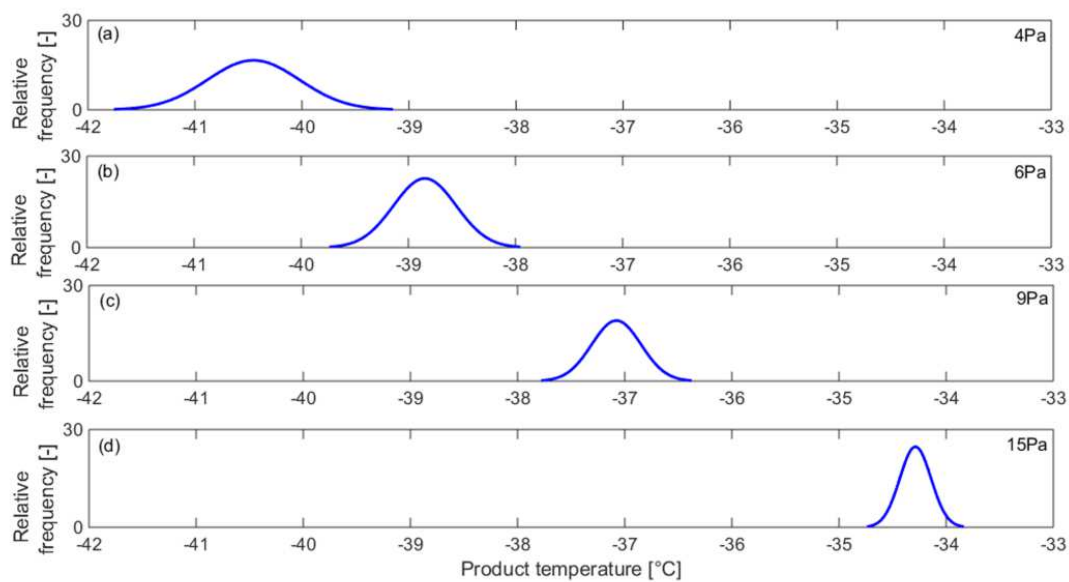


**Figure III.1.8.** Product temperature distributions obtained from the contact area and curvature-based distribution for a 5 % w/w sucrose solution processed at a shelf temperature of  $-25\text{ }^{\circ}\text{C}$  and four chamber pressures: (a) 4 Pa, (b) 6 Pa, (c) 9 Pa and (d) 15 Pa.

The variability of the product temperature was estimated to be approximately 0.9 °C at 15 Pa and as large as 2.2 °C at 4 Pa, considering  $\pm 3$  times the standard deviation that includes 99 % of the vials (**Figure III.1.8**). A practical implication of these results is that, at the low pressures commonly encountered in vaccine freeze-drying, a temperature safety margin of approximately 2 °C has to be considered with respect to cycles designed on the basis of an average  $K_v$  value and to vials not exposed to edge effect.

Vials located at the periphery of the shelf (i.e., edge vials) receive additional heating due to the radiation from the chamber walls and the contact with the metallic guardrail. Thus, edge vials present a higher sublimation rate and a higher product temperature respect central vials (Pikal *et al.*, 1984). Tang et al. (Tang *et al.*, 2006b), reports that the temperature difference between edge vials and central vial can be up to 2 °C at a shelf temperature of 20 °C and up to 4 °C at -30 °C for a chamber pressure of about 10 Pa. Depending on the operating conditions of the process, the safety product temperature margin resulting from variability in vial dimensions could be in the same order of magnitude than the safety margin imposed by the "edge effect".

## CONCLUSIONS

Implementation of the Quality by Design initiative require a precise definition of the acceptable range for all product and process parameters ensuring the fulfilment of the critical quality attributes of the final product. The impact of any variation of these parameters on the final quality need to be quantified in advance. In this work, the effect of the variability of geometrical dimensions observed within a batch of vials (i.e., contact area between the shelf and the vial and the mean bottom curvature depth) on product quality was explored. The product quality was evaluating by predicting the product temperature knowing the vial heat transfer coefficient  $K_v$ . An original approach was proposed to calculate  $K_v$  distribution based on geometrical dimensions when considering a batch of vials located in the center of the shelf not exposed to any edge effect. The impact of freeze-dryer configuration and operating conditions was also considered. When considering low pressure (< 10 Pa), commonly used for freeze-drying biopharmaceuticals, the influence of freeze-dryer configuration and shelf temperature on heat transfer characteristics can be neglected and  $K_v$  distribution is completely explained by the contact area distribution. Furthermore the variability of vial dimension results in the definition of a product temperature safety margin of 2 °C. However, additional sources of variability need to be included in QbD approach. In particular, a study focused on the variability between edge and central vials and its role in cycle scale-up is presently ongoing.

## **ACKNOWLEDGMENTS**

This research was supported by GlaxoSmithKline Biologicals. The authors would also like to thank Yves Mayeresse and Benoit Moreau for their help in reviewing this work. All authors have no personal financial or non financial conflicts of interests.

## **CONFLICT OF INTEREST**

Erwan Bourlés is an employee of the GSK group of companies. Bernadette Scutellà participated in a postgraduate Ph.D. program at GSK Vaccines. Stephanie Passot, Fernanda Fonseca and Ioan Cristian Trelea report no financial conflicts of interest.

## **FUNDING**

This work was funded by GlaxoSmithKline Biologicals S.A., under a Cooperative Research and Development Agreement with INRA (Institut National de la Recherche Agronomique) via the intermediary of the UMR (Unité Mixte de Recherche) GMPA (Génie et Microbiologie des Procédés Alimentaires) at the INRA Versailles-Grignon research center.

## **AUTHORS CONTRIBUTIONS**

Bernadette Scutellà, Stephanie Passot, Erwan Bourlés, Fernanda Fonseca and Ioan Cristian Trelea were involved in the conception and design of the study. Bernadette Scutellà and Erwan Bourlés acquired the data. Bernadette Scutellà, Stephanie Passot, Erwan Bourlés, Fernanda Fonseca and Ioan Cristian Trelea analyzed and interpreted the results. All authors were involved in drafting the manuscript or revising it critically for important intellectual content. All authors had full access to the data and approved the manuscript before it was submitted by the corresponding author.

### III.1.3 Take-home message

- The main result of this work showed that, for vaccine production typically carried at pressures lower than 10 Pa, the variability of the contact area between the shelf and the vials should be taken into account more than the bottom curvature depth in the selection of the vial as it strongly influences the heat transfer at low chamber pressure (< 30 Pa). Conversely, the variability of the bottom curvature depth becomes relevant only in cycles performed at higher chamber pressure (>30 Pa).
- For pressure values typically used in pharmaceuticals freeze-drying (<10 Pa), the variability of the contact area between the shelf and the vial and the depth of bottom curvature can lead to a product temperature safety margin of about 2 °C.

Differences in the geometry of the vials nearly explain the heat transfer variability in vials located in the centre of the shelf. However, vials located at the periphery of the shelf and exposed to other components of the drying chamber (e.g., walls, rail) receive a heat flow rate significantly higher than central vials. The mechanisms responsible for the differences in heat transfer between peripheral and central vials will be explored in the following paper.



## III.2 3D mathematical modelling to understand atypical heat transfer observed in vial freeze-drying

---

The present study was published on the Volume 126 (November 2017) of the *Applied Thermal Engineering* journal

### III.2.1 Context and objectives

It is known that the heat flow rates received by the vials during freeze-drying are sensitive to the position of the vials on the shelf, and may be also significantly different between one equipment and another. Vials located at the periphery of the shelf (named *edge vials*) usually receive a higher heat flow rate than central vials. This phenomenon, named *edge vial effect*, is classically ascribed in literature to the exposition of the edge vials to the additional radiations from the warmer chamber surfaces (e.g., chamber wall). Consequently, edge vials can present a higher product temperature than central vials due to the edge vial effect. If the process runs close to the critical product temperature, edge vials can collapse leading to differences in the final product quality within the vial batch and rejection of a part of the vials.

Usually, characterization of the heat transfer variability between edge and central vials is performed through experimental evaluation of the vial heat transfer coefficient  $K_v$  in these two groups of vials. However, mathematical models of heat transfer during freeze drying can precisely predict the heat flow rates variability in vials differently located on the shelf with a significantly reduced experimental effort, and can help the understanding the mechanisms responsible for it.

#### Objective

The aim of this work was to develop a 3D, steady state mechanistic model using the modelling software COMSOL Multiphysics in order to (i) simulate the heat transfer phenomena during the sublimation step in vials located on the shelf more or less close to the chamber walls and thus (ii) to predict the relative importance of the different heat transfer mechanisms on the total heat transfer received by edge vials.



## III.2.2 Paper

### TITLE

3D mathematical modelling to understand atypical heat transfer observed in vial freeze-drying

### AUTHORS

B. Scutellà<sup>1,2</sup>, A. Plana-Fattori<sup>3</sup>, S. Passot<sup>1</sup>, E. Bourlès<sup>2</sup>, F. Fonseca<sup>1</sup>, D. Flick<sup>3</sup>, I.C. Trelea<sup>1</sup>

### AFFILIATIONS

<sup>1</sup> UMR GMPA, AgroParisTech, INRA, Université Paris Saclay, 78850 Thiverval-Grignon, France

<sup>2</sup> GSK Vaccines, Rixensart, Belgium

<sup>3</sup> UMR Ingénierie Procédés Aliments, AgroParisTech, INRA, Université Paris-Saclay, 91300 Massy, France

### ABSTRACT

In pharmaceutical freeze-drying, the position of the product container (vial) on the shelf of the equipment constitutes a major issue for the final product quality. Vials located at the shelf edges exhibit higher product temperature than vials located at the centre, which in turn often results in collapsed product. A physics-based model was developed to represent heat transfer phenomena and to study their variation with the distance from the periphery of the shelf. Radiation, conduction between solids, and conduction through low-pressure water vapour were considered. The modelling software package COMSOL Multiphysics was employed in representing these phenomena for a set of five vials located at the border of the shelf, close to the metallic guardrail. Model predictions of heat fluxes were validated against experimental measurements conducted over a broad range of shelf temperatures and chamber pressures representative for pharmaceutical freeze-drying. Conduction through low-pressure water vapour appeared as the dominant mechanism explaining the additional heat transfer to border vials compared to central ones. The developed model constitutes a powerful tool for studying heterogeneity in freeze-drying while reducing experimental costs.

### HIGHLIGHTS

- A 3D mathematical model of heat transfer in freeze-drying is proposed.
- The role of several heat transfer mechanisms is explored.
- Knudsen effect is considered for conduction inside low-pressure water vapour.
- Radiation heat transfer is evaluated using the surface-to-surface model.

- Atypical heat transfer is explained mainly by gas conduction rather than radiation.

**KEYWORDS**

Lyophilization, edge vial effect, radiation heat transfer, Knudsen conduction, low-pressure gas, vacuum heat transfer.

**NOMENCLATURE**

$A$	Area ( $m^2$ )
$e$	Emissivity
$F$	Visualization factor
$\Delta H$	Latent heat of sublimation ( $J kg^{-1}$ )
$\dot{m}$	Mass flow rate ( $kg s^{-1}$ )
$K$	Heat transfer coefficient ( $W m^{-2} K^{-1}$ )
$l$	Thickness ( $m$ )
$m$	Mass of the vial ( $kg$ )
$P$	Pressure ( $Pa$ )
$\dot{Q}$	Heat flow rate ( $J s^{-1}$ )
$q$	Heat flux ( $J m^{-2} s^{-1}$ )
$T$	Temperature ( $^{\circ}C$ )
$t$	Sublimation time ( $s$ )

**Greek symbols**

$\alpha$	Semi-empirical constant
$\delta$	Average vial bottom concavity thickness ( $m$ )
$\Lambda_o$	Free molecular flow heat transfer coefficient ( $W m^{-2} K^{-1} Pa^{-1}$ )
$\lambda$	Thermal conductivity ( $W m^{-1} K^{-1}$ )
$\sigma$	Stefan-Boltzmann constant ( $W m^{-2} K^{-4}$ )

**Subscripts**

$1,2$	Body 1 and 2
$BS$	Bottom shelf
$BV$	Bottom vial
$c$	Heat transfer by conduction (general)
$C$	Chamber
$cc$	Heat transfer by contact conduction between solids
$CV$	Contact between the shelf and the vial
$G$	Glass
$i$	Interface
$I$	Ice
$IN, FIN$	Before and after sublimation
$Kn$	Knudsen
$r$	Heat transfer by radiation

<i>R</i>	Rail
<i>S</i>	Shelf
<i>TS</i>	Top shelf
<i>V</i>	Vial
<i>W</i>	Wall
<i>w</i>	Water vapour

## INTRODUCTION

Freeze-drying is a drying process involving three successive steps: freezing of the aqueous solution, followed by primary drying to remove ice by sublimation and, finally, secondary drying to remove unfrozen or sorbed water (Jennings, 1999). Due to the very low temperatures involved, freeze-drying process is particularly suitable for preservation of a wide variety of heat-sensitive products such as high-value foods, cultured microorganisms, pharmaceuticals and nanoparticles (Ratti, 2001; Abdelwahed *et al.*, 2006; Tang and Pikal, 2004; Fonseca *et al.*, 2015). This work is focused on pharmaceutical products (e.g., vaccines, proteins, peptides), which are usually processed in small containers (vials) loaded on the shelf of the equipment. During the primary drying step, the total heat transfer towards the sublimation interface is mainly dependent on the operating variables (shelf temperature, chamber pressure, step duration), but also on the vial geometry and on the position of the vial on the shelf (Pikal *et al.*, 1984; Rambhatla and Pikal, 2003; Pikal *et al.*, 2016; Scutellà *et al.*, 2017a). Vials located at the periphery of the shelf (named edge vials) receive an additional heat flow and present a product temperature up to 4 °C higher compared to vials located in the centre of the shelf (named central vials) and surrounded only by other vials at the same conditions (Pikal *et al.*, 1984; Rambhatla and Pikal, 2003; Pikal *et al.*, 2016; Tang *et al.*, 2006b). This atypical heat transfer characteristic is usually known as "edge vial effect" (Rambhatla and Pikal, 2003).

The "edge vial effect" represents a serious issue in process control because it causes variability in terms of heat flow and product temperature in the vial batch (Rambhatla and Pikal, 2003). If product temperature exceeds a critical value (e.g., glass transition temperature for amorphous products) the product will lose its porous structure and then will collapse (Pikal and Shah, 1990; Barresi *et al.*, 2009a; Johnson and Lewis, 2011; Overcashier *et al.*, 1999; Passot *et al.*, 2007). Due to the additional heat flow received and the higher product temperature, collapse can take place in vials located at the periphery of the shelf rather than in central vials. For this reason, the understanding of the mechanisms causing the heat flow variability with respect to the position of the vial on the shelf is a key point for a successful process design.

Several mono- and multi-dimensional mathematical models of freeze-drying were developed in the past years (Pikal, 1985; Millman *et al.*, 1985; Gan *et al.*, 2005; Velardi and Barresi, 2008; Hottot *et al.*, 2006; Brülls and Rasmuson, 2002; Zhai *et al.*, 2005; Trelea *et al.*, 2007; Liu *et al.*, 2008; Sheehan and Liapis, 1998), but only few of them explore the sources of the atypical heat flow rate in edge vials. In most of the studies (Velardi and Barresi, 2008; Zhai *et al.*, 2005; Hottot *et al.*, 2006; Sheehan and Liapis, 1998), the heat transfer by radiation from the door and walls of the drying chamber was considered completely responsible for the higher product temperature observed in edge vials. However, Gan *et al.* (Gan *et al.*, 2005), and Rambhatla *et al.* (Rambhatla and Pikal, 2003),

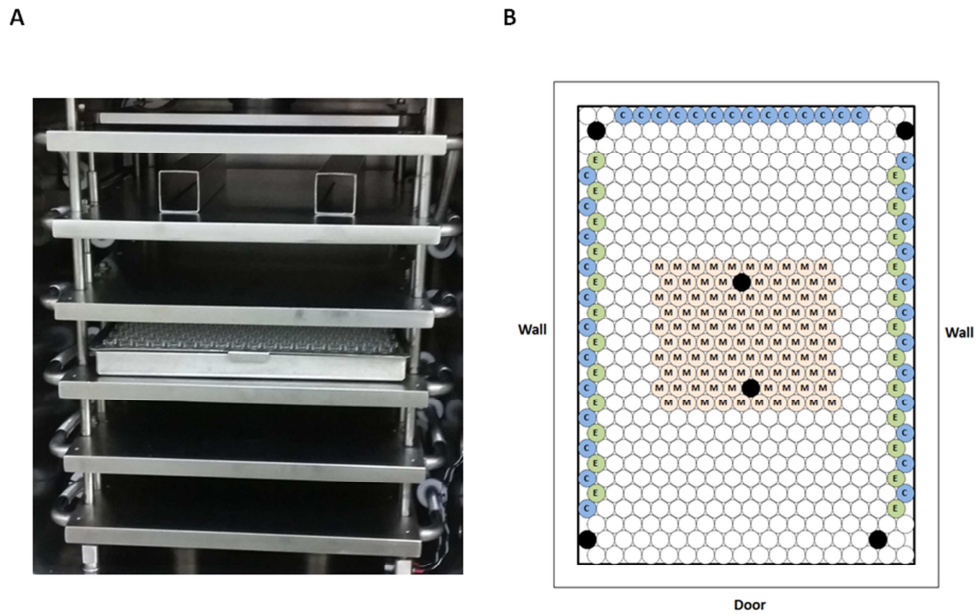


**Figure III.2.1.** Arrangement of the vials on the shelf in the drying chamber: (A) real view of the chamber; (B) position of the vials weighted in the gravimetric method. Marker "C" indicate vials in contact with the rail, "E" vials exposed but not in contact with the rail and "M" central vials. Black circles represent vials in which Tempris sensors were placed to monitor ice temperature.

showed that the presence of the metallic rail surrounding vials also contributes to the heat transfer by means of contact conduction and radiation.

Due to the very low pressures used during the process, the conduction through the gas in freeze-drying partly takes place under Knudsen regime and it is thus dependent on the chamber pressure. Recently, a study of Pikal et al. (Pikal *et al.*, 2016), showed that the conduction through the low-pressure water vapour contained in the gap between the metallic rail and the vial could play a relevant role in the additional heat transfer in edge vials.

The main objective of this work was to develop a 3D mathematical model in order to (i) predict the heat flow received by the vials located at the border of the shelf under different operating conditions and (ii) assess the relative importance of the involved mechanisms in the heat transfer, with particular attention to the radiation heat transfer and conduction through the low-pressure water vapour present in the drying chamber. The COMSOL Multiphysics software was used to design a 3D mechanistic mathematical model of the heat transfer during the sublimation step of the freeze-drying process. The geometry was defined to represent a portion of the drying chamber, including metallic rail, shelves, wall and an array of five vials.

The presence of the gas in the drying chamber was considered and an original approach was used to represent the heat transfer through the gas in Knudsen regime near solid surfaces. The model was then validated with experimental data obtained from sublimation tests performed in a pilot scale freeze dryer at two shelf temperatures (-40 °C and 0 °C) and four chamber pressures (4, 6, 9, 15 Pa) covering the usual range of conditions in pharmaceutical freeze-drying. Then, the contributions of the individual heat transfer mechanisms were quantified specifying the effect of chamber walls, rail and shelves. The developed model predicted in an accurate way the heat flow rates in edge and central vials and can be used for investigating different vials loading configurations and the impact of equipment design.

## MATERIALS AND METHODS

### Materials

The experimental determination of the sublimation heat flow rates was carried out on a pilot freeze-dryer (LyoVac GT6 Finn-Aqua Santasalo-Sohlberg SPRL, Bruxelles, Belgium; **Figure III.2.1A**). This equipment had 5 shelves with an area of 0.14 m<sup>2</sup> each. The distance between shelves was 62 mm whereas the distance between shelf and wall was 55 mm. Measurements of the shelf, wall and rail emissivity were performed by Themacs Ingénierie (Champs sur Marne, France) using the emissometer EM-2 (Monchau *et al.*, 2013). The measured values are reported in **Table III.2.1**.

**Table III.2.1:** Relevant thermal properties and constants used in the model

<i>Property</i>	<i>Symbol</i>	<i>Value</i>	<i>Reference</i>
Stefan-Boltzmann constant	$\sigma$	$5.7 \cdot 10^{-8} \frac{W}{m^2 K^4}$	
Latent heat of ice sublimation	$\Delta H$	$2.8 \cdot 10^6 \frac{J}{kg}$	(Perry <i>et al.</i>
Thermal conductivity of the rail stainless steel	$\lambda_R$	$16.5 \frac{W}{m K}$	(eds.), 1997)
Thermal conductivity of the vial glass	$\lambda_G$	$1.1 \frac{W}{m K}$	
Thermal conductivity of the water vapour at atmospheric pressure	$\lambda_w$	$2.5 \cdot 10^{-2} \frac{W}{m K}$	(Haynes <i>et al.</i> (eds.), 2014)
Thermal conductivity of the ice	$\lambda_I$	$2.2 \frac{W}{m K}$	(Fukusako, 1990)
Ice emissivity	$\varepsilon_I$	0.98	(Heldman (ed.), 2010)
Vial glass emissivity	$\varepsilon_V$	0.78	(Scutellà <i>et al.</i> , 2017a)
Rail stainless steel emissivity	$\varepsilon_R$	0.14	
Shelf stainless steel emissivity	$\varepsilon_S$	0.18	
Wall stainless steel emissivity	$\varepsilon_W$	0.13	
Temperature of the wall when $T_s = 0 \text{ }^\circ\text{C}$		5.7 °C	Measured in this study
Temperature of the wall when $T_s = -40 \text{ }^\circ\text{C}$	$T_W$	0.9 °C	

Glass siliconized tubing vials (3 mL, Müller & Müller, Holzminden, Germany) filled with 1.8 mL of distilled water were used. A detailed dimensional analysis of vial geometry was performed on a batch of 120 vials by a specialized company Precis&Mans (Le Mans, France), using the micrometer Mitutoyo 3D (accuracy  $\pm 0.003\text{mm}$ ; Mitutoyo Europe GmbH, Neuss, Germany).

The pressure in the freeze-dryer chamber was monitored and controlled by a capacitive manometer. A number of six temperature wireless sensors (Tempris IQ Mobil Solution GmbH, Holzkirchen, Germany) were positioned in the bottom centre of selected vials to record ice temperature during the experiments (**Figure III.2.1B**). In some tests, the temperatures of the drying chamber wall was measured by sticking additional sensors by means of aluminium tape. The values of the wall temperatures measured for shelf temperatures of  $-40\text{ }^{\circ}\text{C}$  and  $0\text{ }^{\circ}\text{C}$  are reported in **Table III.2.1**.

### Sublimation heat flow evaluation

The sublimation heat flow was experimentally determined by following the method previously described by Scutellà *et al.* (Scutellà *et al.*, 2017a). A number of 540 vials in hexagonal arrangement were loaded on the middle shelf of the freeze-dryer pre-cooled at  $-50\text{ }^{\circ}\text{C}$  using a bottomless tray. Vials were directly in contact with the shelf and surrounded by a stainless steel rail, as shown in **Figure III.2.1**. After a freezing step of 2 hours, the pressure was decreased and the shelf temperature was increased at a rate of  $1\text{ }^{\circ}\text{C}/\text{min}$  to the set point. Six sublimation tests in total were carried out: four at the shelf temperature of  $0\text{ }^{\circ}\text{C}$  and chamber pressures of 4, 6, 9, 15 Pa and two at the shelf temperature of  $-40\text{ }^{\circ}\text{C}$  and chamber pressures of 4 and 6 Pa. The cycle was allowed to run long enough to sublimate up to 20-25 % of the initial mass of water. Subliming a larger quantity of the ice may lead to loss of contact between the vial and the ice, introducing uncertainty in the analysis.

The sublimation rates were measured gravimetrically. As reported by Pisano *et al.* (Pisano *et al.*, 2011), the vials located after the second row from the border of the shelf can be considered as equivalent to central vials.

Thus, a number of 100 central vials (named M in **Figure III.2.1B**) and 62 edge vials, among which 38 were in contact (C vials in **Figure III.2.1B**) and 24 were not in contact with the rail (E vials in **Figure III.2.1B**), were weighed before and after the run using a PG503-S DeltaRange balance (accuracy  $\pm 0.001\text{g}$ ; Mettler Toledo, Zaventem, Belgium).

After the sublimation tests, the mass flow rate  $\dot{m}$  was calculated as:

$$\dot{m} = \frac{m_{IN} - m_{FIN}}{t} \quad \text{Equation III.2.1}$$

where  $m_{IN}$  and  $m_{FIN}$  are the initial and final masses of the vial and  $t$  is the sublimation time measured from the moment when shelf temperature exceeded the product temperature, meaning that

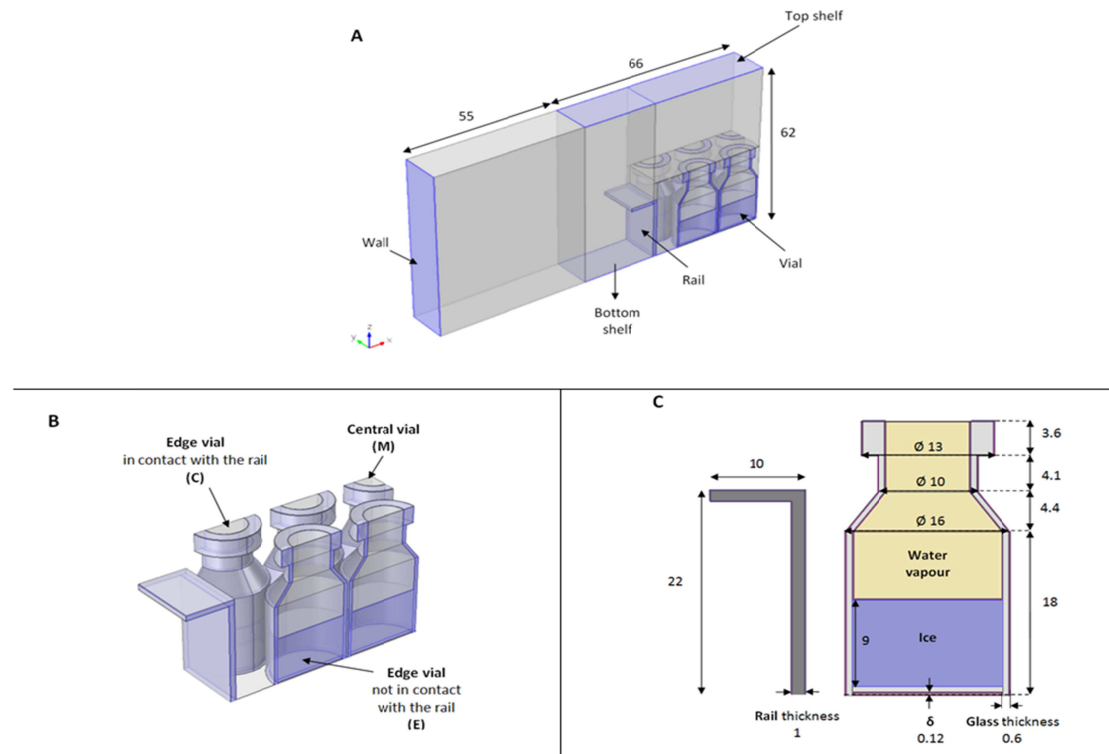


**Figure III.2.2:** Three views of the built geometry with relevant dimensions (in mm): (A) global view of the vials, shelves, rail and wall; (B) zoom on the vials and rail system and classification of the vials; (C) detail of the vial and rail geometry.

there was a net heat flux from the shelf towards the vials.

In freeze-drying, pseudo-stationary state can be assumed because of the slow dynamics of the process (Pikal, 2000; Pikal *et al.*, 1984; Trelea *et al.*, 2007; Pisano *et al.*, 2011). Under this condition, the net heat flow rate  $\dot{Q}$  at the sublimation interface is directly proportional to the mass flow rate  $\dot{m}$ :

$$\dot{Q} = \Delta H \dot{m} \quad \text{Equation III.2.2}$$

$\Delta H$  being the latent heat of sublimation (**Table III.2.1**).

## MATHEMATICAL MODEL

### Geometry

The 3D geometry, representing a portion of the drying chamber, was built in COMSOL Multiphysics (**Figure III.2.2A**). It included wall, rail, bottom and top shelves and five vials. The geometry was considered to be symmetric about the x-z plane. **Figure III.2.2B** focuses on the hexagonal arrangement of vials, which were placed in direct contact with the bottom shelf. The vials located at the border of the shelf were alternatively in contact (vial C) and not in contact (vial E) with the rail. The detailed vial and rail geometry is presented in **Figure III.2.2C**. All the vials were made of borosilicate glass and were filled with pure ice. The vial bottom was designed to have an area in contact with the shelf and a cylindrical concavity. The thickness of this concavity  $\delta$  was considered equal to the mean bottom curvature depth calculated by Scutellà *et al.* (Scutellà *et al.*, 2017a) (0.12 mm).

### Problem statement and boundary conditions

In this model, heat transfer during pure ice sublimation was simulated. A flat ice-vapour interface and a constant ice thickness were defined. The drying chamber was considered to be completely saturated with vapour water during sublimation. The temperatures of several surfaces were imposed: (i) the top and bottom shelves temperature, imposed as operating condition; (b) the wall temperature, determined from experimental data; (c) the ice-vapour interface temperature  $T_i$ , evaluated from the Clausius-Clapeyron relation (Trelea *et al.*, 2007):

$$T_i = \frac{6139.6}{28.8912 - \ln(P_i)} \quad \text{Equation III.2.3}$$

where  $P_i$  was taken equal to the chamber pressure since no mass transfer resistance between the ice-vapour interface and the chamber was considered.

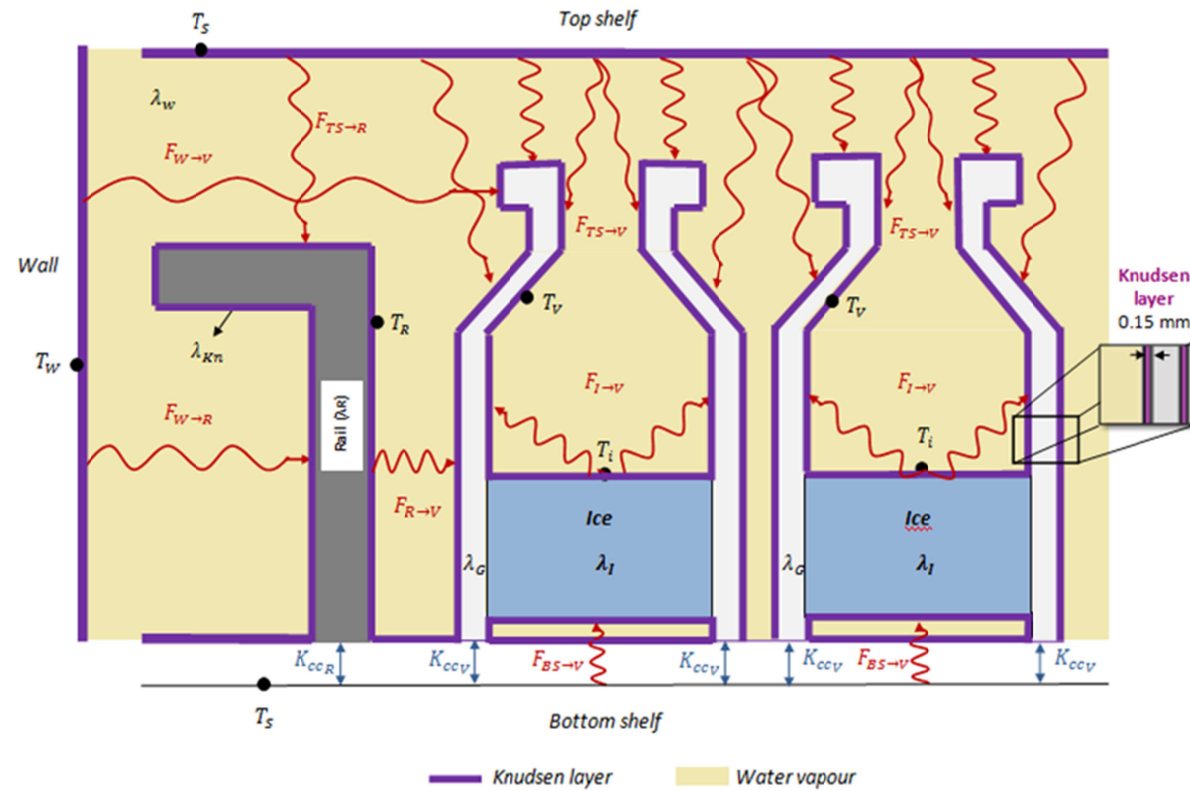


**Figure III.2.3:** Schematic representation (not in scale) of the main heat transfer mechanisms, corresponding coefficients and relevant body temperatures in the analyzed system. Radiation mechanisms considered in the simplified model are shown.

During the process, several sources contribute simultaneously to the heat transfer toward the sublimation interface.

The main heat transfer mechanisms and their characteristic coefficients are schematized in **Figure III.2.3** and can be synthesized as follows:

1. *Conduction through the gas in the drying chamber.* A fictitious layer was defined, named Knudsen layer, which covers all the solids (i.e., ice, vial glass, rail, wall, top and bottom shelves), represented as a violet bold line in **Figure III.2.3**. The thickness of the Knudsen layer  $l_{Kn}$  was arbitrarily set to be equal to 1/4 of the vial glass thickness;
2. *Conduction between solids.* Only the conductive exchanges which were expected to be the most relevant were considered, i.e., (i) the conduction between the bottom shelf and the vials ( $K_{ccv}$ ) and (ii) the conduction between the bottom shelf and the rail ( $K_{ccr}$ );
3. *Radiation.* A number of radiation fluxes were taken into account, as shown in **Figure III.2.3**:
  - from the top ( $F_{TS \rightarrow V}$ ) and bottom shelves ( $F_{BS \rightarrow V}$ ) to the vials;
  - from the top shelf to the rail ( $F_{TS \rightarrow R}$ );
  - from the chamber wall to the rail ( $F_{W \rightarrow R}$ ) and to the parts of the vials which face the wall ( $F_{W \rightarrow V}$ );
  - between the rail and the vials (E and C) facing it ( $F_{R \rightarrow V}$ );
  - between the vial internal walls and the ice ( $F_{I \rightarrow V}$ ).

Heat transfer by convection was not considered in the model. Even if a debate is ongoing in literature on the importance of convection during freeze-drying (Rambhatla and Pikal, 2003; Pikal *et al.*, 2016; Ganguly *et al.*, 2013), a recent work of Pikal *et al.* (Pikal *et al.*, 2016), has shown that convection can be considered negligible at the low pressures typically encountered during the freeze-drying of pharmaceuticals (usually below 10 Pa).

Under those hypotheses, modelling heat transfer in freeze-drying involved the simultaneous solution of conduction in solid, in gas and radiation heat transfer equations.

#### *Heat transfer by conduction*

The heat transfer by conduction occurring inside different materials (i.e., vial glass, ice, rail, gas) was described by the first Fourier law (Bird *et al.*, 2002):

$$\vec{q}_c = -\lambda \nabla T \quad \text{Equation III.2.4}$$

$\vec{q}_c$  being the heat flux,  $\nabla T$  the temperature gradient and  $\lambda$  the thermal conductivity of the materials, reported in **Table III.2.1**

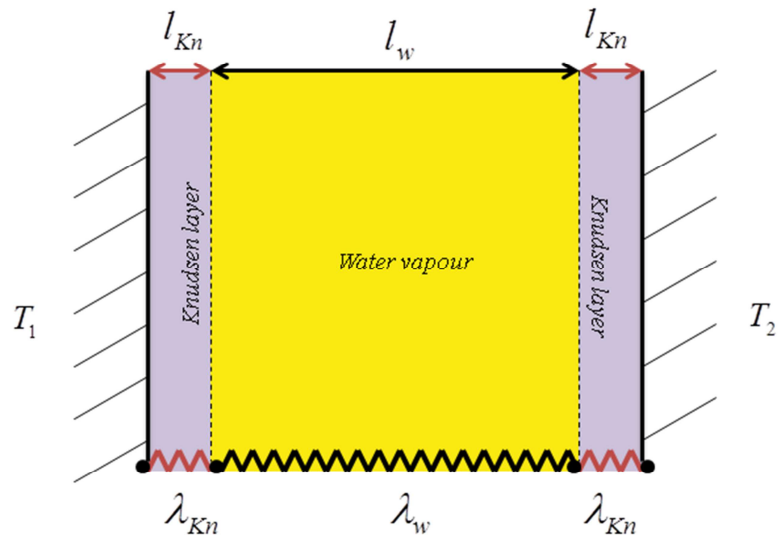


**Figure III.2.4:** Schematic representation of the heat transfer resistances in the gas, as given by **Equation III.2.6**.

### *Thermal conductivity of the gas in the drying chamber*

Usually freeze-drying of pharmaceuticals is carried out at very low chamber pressure, in a range of 4 to 10 Pa. Under this condition, the density of the gas is very low and the gas molecules collide more frequently with solid surfaces than among them at distances from the solid surface lower than the free molecular path (equal to about 0.6 mm at 10 Pa for water vapour) (Pikal, 2000). Thus, in typical ranges of freeze-drying operating variables (i.e., chamber pressure < 10 Pa and shelf temperature < 0 °C), the heat transfer regime is classified as the free-molecular or Knudsen regime near solids surfaces (Pikal *et al.*, 1984; Pikal, 2000; Brülls and Rasmuson, 2002; Dushman and Lafferty (eds.), 1962). In the present model, the heat transfer under Knudsen regime was simulated by building a fictitious layer (named Knudsen layer) around all solids in contact with gas.

According to previous works of Pikal *et al.* (Pikal, 2000; Pikal *et al.*, 1984), the heat transfer by conduction through the water vapour during freeze-drying can be described as:

$$q_w = K_w (T_1 - T_2) \quad \text{Equation III.2.5}$$

where  $q_w$  is the heat flux by conduction through the water vapour,  $T_1$  and  $T_2$  are respectively the temperatures of the two solids between which the gas is contained and  $K_w$  is the global heat transfer coefficient by conduction through the water vapour.

The global resistance to heat transfer through the gas ( $\frac{1}{K_w}$ ), as described in the model and shown in **Figure III.2.4**, can be defined as (Pikal, 2000; Pikal *et al.*, 1984):

$$\frac{1}{K_w} = \frac{l_w}{\lambda_w} + 2 \frac{l_{Kn}}{\lambda_{Kn}} \quad \text{Equation III.2.6}$$

In **Equation III.2.6**,  $l_w$  is the distance among the two solid surfaces between which the gas is contained,  $\lambda_w$  is the water vapour thermal conductivity,  $l_{Kn}$  is the Knudsen layer thickness whereas  $\lambda_{Kn}$  is the Knudsen layer conductivity. The resistance to the heat transfer in the Knudsen layers ( $2 \frac{l_{Kn}}{\lambda_{Kn}}$ ) was defined by Pikal *et al.* (Pikal, 2000; Pikal *et al.*, 1984) as:

$$2 \frac{l_{Kn}}{\lambda_{Kn}} = \frac{1}{\alpha \Lambda_o P_C} \quad \text{Equation III.2.7}$$

where  $\alpha$  is a semi-empirical constant related to the quality of energy exchange between the solid surface and the gas and usually estimated by regression from experimental data,  $\Lambda_o$  is the free molecular flow heat transfer coefficient and  $P_C$  is the chamber pressure.

**Table III.2.2:** Relevant model parameters for heat transfer

<i>Parameter</i>	<i>Symbol</i>	<i>Value</i>	<i>Reference</i>
Free molecular flow heat transfer coefficient	$\Lambda_o$	$1.99 \frac{W}{m^2 K Pa}$	(Pikal, 2000)
Semi-empirical constant (equal to $C_2/\Lambda_o$ in Scutellà et al. (Scutellà <i>et al.</i> , 2017a))	$\alpha$	0.34	Calculated from data presented in (Scutellà <i>et al.</i> , 2017a)
Heat transfer coefficient by conduction shelf-vial	$K_{CCV}$	$25.80 \frac{W}{m^2 K}$	
Heat transfer coefficient by conduction shelf-rail	$K_{CCR}$	$10 \frac{W}{m^2 K}$	
Visualization factor wall-rail <sup>(a)</sup>	$F_{W \rightarrow R}$	0.07	Evaluated in this study
Visualization factor wall-vial <sup>(a)</sup>	$F_{W \rightarrow V}$	0.12	
Visualization factor rail-vial <sup>(a)</sup>	$F_{R \rightarrow V}$	0.13	
Visualization factor shelf-vial <sup>(a)</sup>	$F_{TS \rightarrow V}, F_{BS \rightarrow V}$	0.17	
Visualization factor vial-ice <sup>(b)</sup>	$F_{I \rightarrow V}$	0.98	

<sup>(a)</sup> Parallel surfaces case (calculated from **Equation III.2.11**)

<sup>(b)</sup> Black body case ( $F_{I \rightarrow V} = \epsilon_I$ )

In the present work, the coefficient  $\alpha$  was determined considering experimental data of sublimation tests presented by Scutellà *et al.* (Scutellà *et al.*, 2017a) (where  $\alpha = C_2/\Lambda_o$ , with  $C_2$  equal to 0.67). The determined  $\alpha$  value and other relevant parameters for heat transfer modelling are reported in **Table III.2.2**.

Thus, the thermal conductivity of the Knudsen layer  $\lambda_{Kn}$  was estimated from **Equation III.2.7** as follows:

$$\lambda_{Kn} = 2 \alpha \Lambda_o P_C l_{Kn} \quad \text{Equation III.2.8}$$

#### *Heat transfer by contact conduction between solid bodies*

The heat flux by contact conduction between two bodies in contact (e.g., vial-shelf or rail-shelf, **Figure III.2.3**) can be defined as (Pikal *et al.*, 1984):

$$q_{cc} = K_{cc} (T_1 - T_2) \quad \text{Equation III.2.9}$$

where  $q_{cc}$  is the heat flux from body 1 to body 2 transmitted by contact conduction,  $T_1$  and  $T_2$  are respectively the temperatures of the two bodies and  $K_{cc}$  is the heat transfer coefficient by contact conduction, which depends on the quality of the contact. The heat transfer coefficient by contact conduction between the shelf and the vial ( $K_{ccv}$ ) was evaluated from the work of Scutellà *et al.* (Scutellà *et al.*, 2017a): a coefficient  $K_c$  (equal to  $3.67 \text{ W m}^{-2} \text{ K}^{-1}$ ) was evaluated, with reference to the entire vial bottom area ( $A_{BV}$ ). In order to obtain the heat transfer coefficient by contact conduction applicable to the contact area only ( $A_{CV}$ ),  $K_{ccv}$  was considered equal to  $K_c \frac{A_{BV}}{A_{CV}}$ . In contrast, the heat transfer coefficient by contact conduction between shelf and rail ( $K_{ccR}$ ) was determined by fitting model predictions to the rail temperature measured in a separate experiment. The values of these coefficients are reported in **Table III.2.2**.

#### *Heat transfer by radiation*

In the considered low-pressure environment, heat transfer by radiation is expected to play a non negligible role (Rambhatla and Pikal, 2003; Pikal *et al.*, 2016). In the present model, it was considered that the solid surfaces are opaque, that the radiation and the absorption occur in the same spectral range and that the absorption and radiation of the low pressure water vapour are negligible (Brülls and Rasmuson, 2002; Bird *et al.*, 2002). Thus, the heat flux by radiation  $q_r$  can be described by the Stefan-Boltzmann equation (Pikal, 2000; Bird *et al.*, 2002):

**Table III.2.3:** Heat flow rates at the ice sublimation interface in vials C, E, M for a chamber pressure of 4 Pa and a shelf temperature of 0 °C versus the number of mesh elements and the maximum element size evaluated for a radiation resolution of 64 streams.

<i>Number of mesh elements</i>	<i>Maximum element size [m]</i>	<b>Heat flow rates [W]</b>		
		<b>Vial C</b>	<b>Vial E</b>	<b>Vial M</b>
189 628	0.0134	0.1219	0.09522	0.08105
259 433	0.0107	0.1222 (-0.2 %)	0.09525 (-0.03 %)	0.08108 (-0.04 %)

$$q_r = F_{1 \rightarrow 2} \sigma (T_1^4 - T_2^4) \quad \text{Equation III.2.10}$$

where  $T_1$  and  $T_2$  are the absolute temperatures of the surfaces 1 and 2 respectively,  $\sigma$  is the Stefan-Boltzmann constant and  $F_{1 \rightarrow 2}$  the visualization factor between the two surfaces under consideration. The surface-to-surface radiation model proposed by COMSOL was used to evaluate the radiation heat transfer by the hemicube method. This method takes into account the shadowing effect in the system, automatically calculating the view factors for all the bodies present in the geometry. The surface-to-surface model results in very accurate computation, including all the possible contributions to radiation heat transfer, even if it remains time-consuming. Furthermore, a simplified radiation model was developed. In this model, only the main radiation contributions were considered, as schematized in **Figure III.2.3**. Each part of the rail and vial surface was assumed to exchange by radiation with one of the imposed temperature surfaces (wall, shelves, ice interface). The visualization factors were estimated as for parallel plates (Bird *et al.*, 2002; Pikal, 2000):

$$F_{1 \rightarrow 2} = \frac{1}{\frac{1}{e_1} + \frac{1}{e_2} - 1} \quad \text{Equation III.2.11}$$

The internal walls of the vials were assumed to act as a black body. The radiation rays coming from the top shelf are eventually trapped by the internal vial walls after several reflections. Values of the visualisation factors used in the simplified radiation model are given in **Table III.2.2**.

### Numerical solution

The developed model was solved by means of Comsol Multiphysics 5.2 (COMSOL, Inc, Burlington, USA). This commercial software was ran on a PC, equipped with Intel(R) Core(TM) i7-490 CPUs, at 3.6 GHz, 64-bits, with 32 Gb of RAM, under Windows 10.

Governing equations were solved under steady-state condition by applying the finite-element method. The solution of the large linear system resulting from the linearization of the coupled equations was reached with the help of the Multifrontal Massively Parallel Sparse Direct Solver (MUMPS) (Amestoy *et al.*, 2001). The relative tolerance was set to  $10^{-5}$ . Numerical tests were based on non-structured meshing (tetrahedral elements).

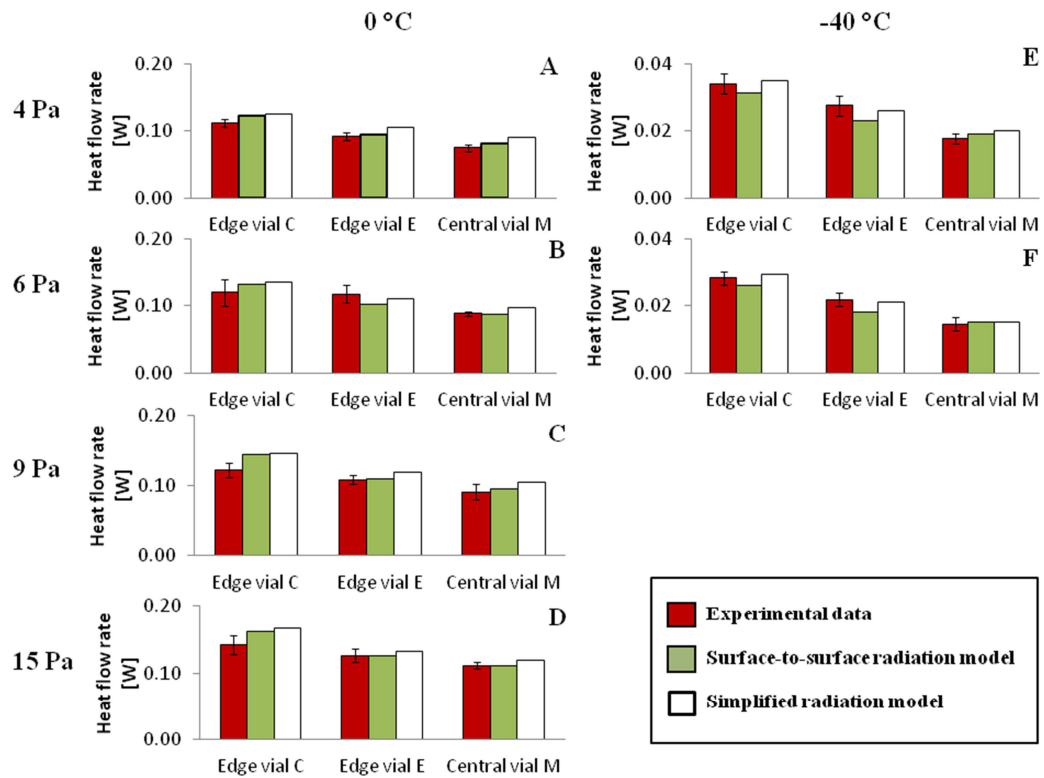


**Figure III.2.5:** Comparison of experimental and simulated heat flow rates for edge vial in contact (C) and not in contact (E) with the rail and for central vial (M). Several combinations of shelf temperatures (-40 °C and 0 °C) and chamber pressures (4, 6, 9, 15 Pa) were tested. Error bars in experimental data represent standard deviations.

**Table III.2.4:** Relative mean error (RME) and the root mean square deviation (RMSD) for the surface-to-surface and simplified radiation models considering the vials C, E, M.

	RME %		RMSD [W]	
	<i>Surface-to-Surface model</i>	<i>Simplified model</i>	<i>Surface-to-Surface model</i>	<i>Simplified model</i>
<i>Vial C</i>	11	11	0.014	0.016
<i>Vial E</i>	9	7	0.007	0.008
<i>Vial M</i>	4	11	0.003	0.009

## RESULTS

### Mesh and radiation resolution sensitivity analysis

A sensitivity test was performed since the numerical solution of the problem depends on the resolution adopted in discretizing the equations.

Regarding the mesh resolution used for discretizing the conduction equations, an increase of the number of elements by about 40 % resulted in a weak impact on heat fluxes with a difference of maximum 0.2 % (**Table III.2.3**) for the different vials (C, E, M). The increase of the angular discretization applied for radiation calculations (from 64 to 4096 streams) did not modify the predicted values of heat fluxes (0.002 %). COMSOL simulations were thus considered robust, and lower values of mesh elements (189,628) and radiation streams (64) were selected to reduce computation time.

### Model validation

The model was validated based on sublimation experiments carried out at four chamber pressures (4, 6, 9 and 15 Pa) and two shelf temperatures (-40 °C and 0 °C) selected in the range typically used in freeze-drying of pharmaceuticals.

**Figure III.2.5** displays the comparison between the mean values of the experimental heat flow rates toward the ice-vapour interface and their standard deviations (38, 24 and 100 vials in configuration C, E and M, respectively) and the model predictions for all the combinations of shelf temperature and chamber pressure tested.

The agreement between measurements and model predictions was satisfactory. Deviations were less than 21 % of the mean heat flow rate and close to the experimental coefficients of variation of each vial group. For the experiments performed at a shelf temperature of 0 °C and higher pressures (9 and 15 Pa), the simulated heat flow rates of the vial C in contact with the rail appeared to be slightly overestimated with respect to the mean experimental value for both radiation models. Simulated and experimental heat flow rates of vial E not in contact with the rail showed a good agreement, as well as the simulated heat flow rates of the central vial, for all 6 combinations of applied operating conditions.

These results were confirmed by the calculation of the relative mean error (RME) and the root mean square deviation (RMSD), presented **Table III.2.4**.

Simulated heat flow rates in vial C at high shelf temperature showed higher RME and RMSD values than vial E and M. However, the RME values remained below 11 % for both the surface-to-surface model and the simplified model. The quality of the models was also statistically assessed by the calculation of the coefficient of determination  $R_{pred}^2$ .

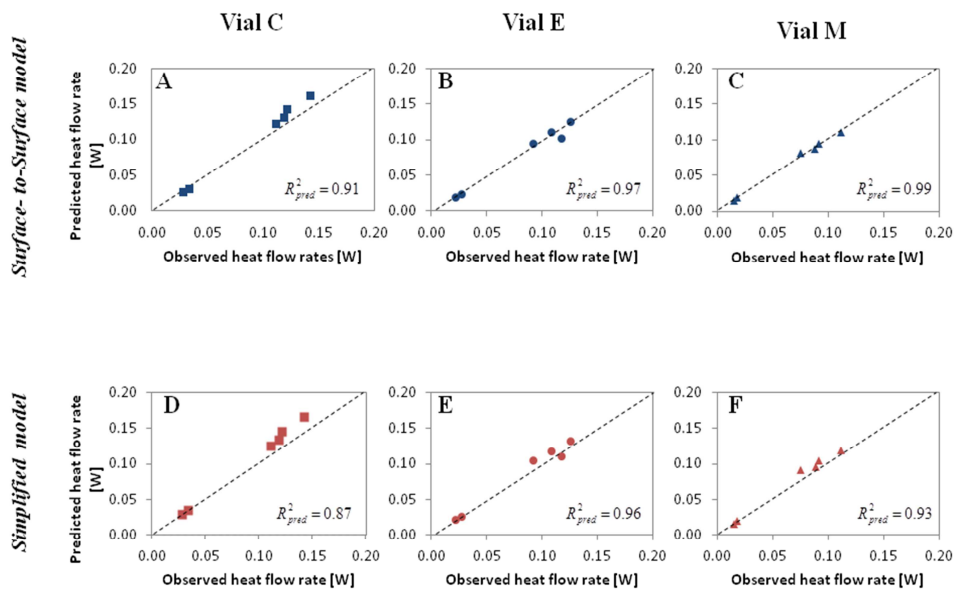


**Figure III.2.6:** Predicted vs. observed heat flow rates for both surface-to-surface (A, B, C) and simplified radiation models (D, E, F). Square, circle and triangle markers represent respectively the edge vials C, E and the central vials M. The 1:1 dotted line represents perfect agreement between predicted and observed value. The values of the coefficient of determination ( $R^2_{pred}$ ) are reported on the figure.

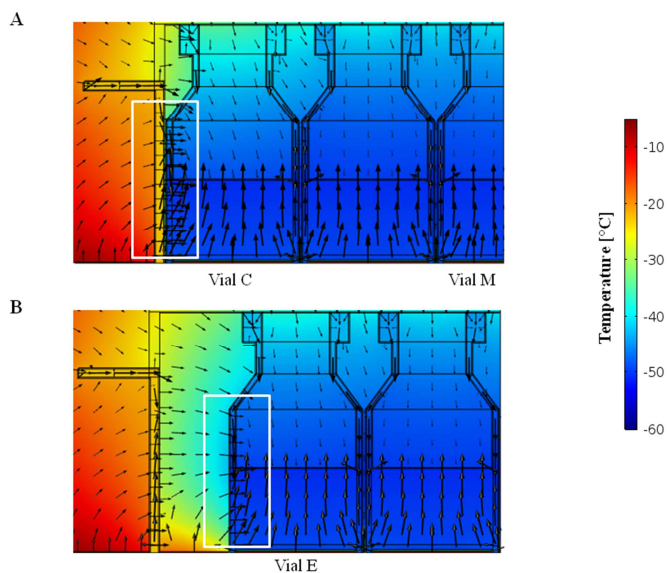


**Figure III.2.7:** Temperature profiles and heat fluxes in the vial in contact (view A) and not in contact (view B) with the rail at a shelf temperature of 0 °C and a chamber pressure of 4 Pa. White rectangles indicate the lateral heat fluxes in edge vials C and E. Arrow length indicates flux magnitude on a logarithmic scale, to improve the visualisation of smaller fluxes from top, wall and rail.

**Figure III.2.6** presents predicted versus observed net heat flow rates for edge vials in contact (Vial C) and not in contact (Vial E) with the rail and for central vials (Vial M), both for the surface-to-surface (**Figure III.2.5A, B and C**) and simplified radiation models (**Figure III.2.5 D, E and F**). The distribution of the data around the 1:1 line and the value of  $R_{pred}^2$  close to 1 confirmed the goodness of the simulations.

The surface-to-surface model presented higher  $R_{pred}^2$  values and appeared to better predict the heat flow rates in both edge and central vials than the simplified radiation model. However, the computational time was much longer for the surface-to-surface model (about 1 h, physical memory 30 GB) than for the simplified model (about 5 min, physical memory 6 GB). These results confirm that the developed models represent well not only the usually considered heat transfer from the top and bottom shelves but also the border heat transfer from the wall and rail to the edge vials.

Even if the results obtained from the two models were both accurate and comparable, it was decided to perform the further analysis using the surface-to-surface radiation model only.

### Temperature profile and heat fluxes distribution

The developed 3D geometry allowed to visualize the temperature profile and the heat fluxes in the modelled system. An example is given in **Figure III.2.7** for the set of operating conditions (0 °C and 4 Pa and a wall temperature equal to 5.7 °C).

The temperature profile is represented by colour scale, whereas the heat flux distribution is represented by arrows whose length is proportional to the logarithm of the flux magnitude, to enhance the visualisation of small fluxes.

Two different views of the system, showing the vial in contact (A) and not in contact (B) with the rail, are presented. The vial located at the center of the shelf (vial M) is also represented in **Figure III.2.7A**. When considering the central vial M, product received heat fluxes from the bottom and the top shelves (upward and downward arrows). The temperature of the ice-vapour interface was equal to about -50.7 °C (**Equation III.2.3**). A small temperature difference was observed inside the product (e.g., about 1.5 °C difference between the ice bottom and the ice-vapour interface), which was in agreement with experimental results. In contrast, the temperature difference between the shelf and the vial bottom was close to 49 °C. Due to the concave shape of the bottom, only a small portion of the vial bottom area was directly in contact with the shelf, whereas some gas was entrapped in the concavity between the shelf and the vial. Hence, the heat transfer was limited by the presence of the Knudsen layer, which caused an important temperature gradient between the shelf and the vial bottom, especially at low pressure as in this case (4 Pa). The downward arrows coming from the top shelf represented heat fluxes by conduction through the gas present the drying chamber and by radiation from the top shelf.

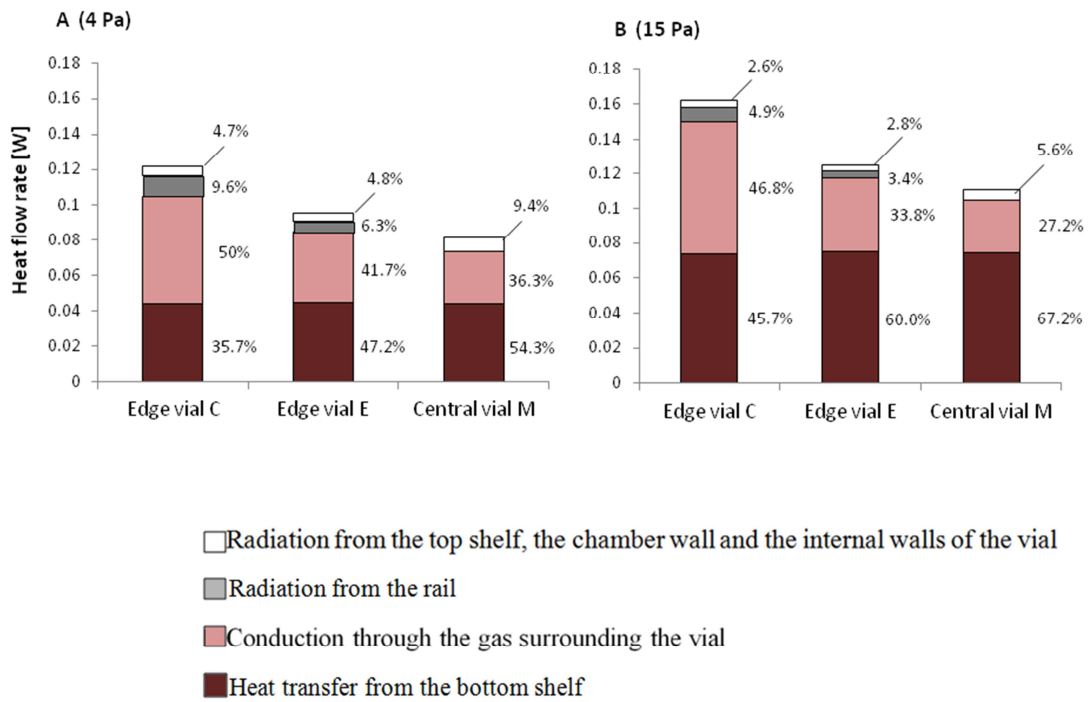


**Figure III.2.8:** Heat flow rate contributions and their relative importance (in %) of the single heat transfer mechanisms to the total heat transfer. Results are shown for edge vials in contact (C) and not in contact (E) with the rail and in central vial (M) at a shelf temperature of 0 °C and two different pressures (4 and 15 Pa).

The edge vials (C and E) received additional lateral heat fluxes (highlighted by white rectangles in **Figure III.2.7**) which resulted in an increase of the temperature of the vial lateral wall when increasing the proximity with the rail (-48 °C for central vial M, -47 °C for vial E and -46 °C for vial C in contact with the rail). These lateral heat fluxes involved conduction through the gas present in the chamber and radiation from the rail and the wall.

Furthermore, the heat flux received by the rail exhibiting a temperature of -23 °C depends on the direct contact between the rail bottom and the shelf (upward arrows from the bottom shelf) but also on the exposure to the chamber wall (lateral arrows) from which heat was transmitted by radiation and gas conduction.

#### **Relative importance of individual heat transfer mechanisms**

As shown in **Figure III.2.7**, vials located in different positions on the shelf receive different heat transfer contributions from the wall, the rail, the shelves and the gas surrounding the vials through several heat transfer mechanisms (i.e., radiation, contact conduction, conduction through the gas). Understanding of the role played by each element of the drying chamber in the heat transfer could help reducing the "edge vial effect".

Thus, using the developed model, it was possible to evaluate the relative importance of four heat transfer contributions: (i) heat transfer from the bottom shelf by radiation, contact conduction and gas conduction (the latter related to the bottom concavity of the vial); (ii) heat transfer by conduction through the water vapour surrounding the vial (related to the top and the lateral side of the vial); (iii) heat transfer by radiation from the rail; (iv) heat transfer by radiation from the top shelf, the wall and the internal walls of the vial. **Figure III.2.8** displays the heat flow rates as well as the relative importance of these different elements calculated for a value of shelf temperature of 0 °C and the two extreme pressures in the explored range.

The heat flow rate from the bottom shelf was the same for all vials at a given pressure, but its relative importance in the total heat flow rate was higher in central vials than in edge vials. For example, at 4 Pa the relative importance of the heat transfer from the bottom shelf was about 54 % for the central vial M but it decreases until about 47 % for the edge vial E and about 36 % for the edge vial C. Furthermore, the heat flow rate from the bottom shelf increased at higher pressure by about 70 %, because the heat transfer by conduction through the gas entrapped in the vial bottom curvature is a pressure dependent mechanism.

The conduction through the gas surrounding the vial appeared as a significant phenomenon and became the most important contribution to the heat transfer for the vials located at the border of the shelf. The edge vial C was particularly affected by the gas conduction, which contributes to the 50 % of the total heat flow rate, due to the proximity to the rail.

The heat transfer by radiation from the rail, the wall and the top shelf had a relatively minor contribution to the total heat flow rate: from 5.6 % to 14.3 %. The most important role was played by radiation from rail in vial C (about 10 % at low pressure) and followed by vial E (about 6 %). This result is original, as the mainstream of the literature more or less implicitly ascribed the edge vial effect to radiation. The limited role of radiation is supported by some previous studies (Rambhatla and Pikal, 2003; Gan *et al.*, 2005), who found that the heat transfer difference between edge and central vials is not eliminated by the presence of a shielding rail.

## CONCLUSIONS

The tri-dimensional, steady state mathematical model developed in this work successfully predicted the atypical heat transfer affecting the vials located at the periphery of the shelf in the freeze-drying process. The numerical solution of the model was validated with experimental results obtained in conditions relevant for pharmaceutical applications. The model made it possible to investigate the relative heat transfer contributions of the elements present in the drying chamber, i.e., wall, shelves and rail. In the range of operating conditions considered, the atypical heat transfer was mainly ascribed to gas conduction rather than radiation, as often stated in the literature. Furthermore, the radiation from the rail counts more than the radiation from the wall in the present configuration (height of the rail close to that of the vials). The use of rails made of a low emissivity and conductivity material could help in reducing the edge vial effect.

The developed model can be used to predict the heat flow rates in edge and central vials for different loading configurations and equipment characteristics, providing useful information for the freeze-drying cycle design and scale-up.

## **ACKNOWLEDGMENTS**

The authors would like to thank Benoit Moreau and Yves Mayeresse (GSK Vaccines) for reviewing this manuscript, Vincent Ronsse (technician) and Alain Philippart (operator) (GSK Vaccines) for their help in the data acquisition, and Victor Rousseau and Gwenael Davaud (AgroParisTech) for their help in developing the model.

## **CONFLICT OF INTEREST**

Erwan Bourlès is an employee of the GSK group of companies. Bernadette Scutellà participated in a postgraduate Ph.D. program at GSK Vaccines. Stephanie Passot, Fernanda Fonseca, Artemio Plana-Fattori, Denis Flick and Ioan Cristian Trelea report no financial conflicts of interest.

## **FUNDING**

This work was funded by GlaxoSmithKline Biologicals S.A., under a Cooperative Research and Development Agreement with INRA (Institut National de la Recherche Agronomique) via the intermediary of the UMR (Unité Mixte de Recherche) GMPA (Génie et Microbiologie des Procédés Alimentaires) at the INRA Versailles-Grignon research centre.

## **AUTHORS CONTRIBUTIONS**

All authors were involved in the conception of the model and design of the study. Bernadette Scutellà and Erwan Bourlès acquired the data. Bernadette Scutellà, Stephanie Passot, Erwan Bourlès, Fernanda Fonseca and Ioan Cristian Trelea analyzed and interpreted the experimental results. Bernadette Scutellà, Artemio Plana-Fattori, Denis Flick, and Ioan Cristian Trelea were involved in the model development. All authors were involved in drafting the manuscript or revising it critically for important intellectual content. All authors had full access to the data and approved the manuscript before it was submitted by the corresponding author.

### III.2.3 Take-home message

- A 3D, steady state mathematical model of heat transfer in freeze-drying was developed to precisely predict the heat flow rates in vials differently located on the shelf. The goodness of the model was confirmed by comparing experimental and simulated heat flow rates in edge and central vials in a broad range of shelf temperatures and chamber pressures.
- The conduction through the water vapour was found to be the major responsible for the atypical heat transfer observed in vials located closer to the freeze-dryer walls. In contrast to what is usually claimed in literature, heat transfer by radiation from the rail and the walls have only a limited contribution on the total heat flow rate in edge vials in the configuration tested, i.e., vials partially shielded by the rail.

In the presented work, model prediction of heat flow rates in edge and central vials were shown considering only a single pilot freeze-dryer and one vial loading configuration. In the following paper, our 3D model of heat transfer in freeze-drying will be used to explore the impact of the freeze-dryer design on the heat transfer variability during the process.





### III.3 Effect of freeze-dryer design on heat transfer variability investigated using a 3D mathematical model

---

The present study was submitted to the *Journal of Pharmaceutical Science*.

#### III.3.1 Context and objectives

The use of the 3D mathematical model of heat transfer in freeze-drying previously developed in **Paper III.2** allowed to identify two main mechanisms responsible for the heat transfer variability between edge and central vials: (i) the *conduction through the gas present in the drying chamber* and (ii) the *radiations from the rail and the walls*. However, these heat transfer contributions can be strongly influenced by the vial loading configuration used and by the thermal characteristics and the dimensions of the drying chamber components (e.g., walls, shelves). As these features may change from one freeze-dryer to another, prediction of their impact on the heat transfer phenomena during the process is paramount importance for a successful cycle transfer or scale-up.

#### Objective

Our 3D mathematical model was used in the present study to investigate the importance of several design elements of the equipment on the inter-vial heat transfer variability, such as the vial loading configuration, the thermal characteristics of the rail, the wall and shelf emissivity and the distance between the shelves and between the shelf and the wall.



### III.3.2 Paper

#### TITLE

Effect of freeze-dryer design on heat transfer variability investigated using a 3D mathematical model

#### AUTHORS

B. Scutellà<sup>1,2</sup>, E. Bourlés<sup>2</sup>, A. Plana-Fattori<sup>3</sup>, F. Fonseca<sup>1</sup>, D. Flick<sup>3</sup>, I.C. Trelea<sup>1</sup>, S. Passot<sup>1</sup>

#### AFFILIATION

<sup>1</sup> UMR GMPA, AgroParisTech, INRA, Université Paris Saclay, 78 850 Thiverval-Grignon, France

<sup>2</sup> GSK Vaccines, Rixensart, Belgium

<sup>3</sup> UMR Ingénierie Procédés Aliments, AgroParisTech, INRA, Université Paris-Saclay, 91300 Massy, France

#### ABSTRACT

During the freeze-drying process, vials located at the border of the shelf usually present higher heat flow rates that, in turn, result in higher product temperatures than vials in the center. This phenomenon, referred to as edge vial effect, can lead to product quality variability within the same batch of vials and between batches at different scales. Our objective was to investigate the effect of various freeze-dryer design features on heat transfer variability. A 3D mathematical model previously developed in COMSOL Multiphysics and experimentally validated was used to simulate the heat transfer of a set of vials located at the edge and in the center of the shelf. The design features considered included the loading configurations of the vials, the thermal characteristics of the rail, the walls and the shelves, and some relevant dimensions of the drying chamber geometry. The presence of the rail in the loading configuration and the value of the shelf emissivity strongly impacted the heat flow rates received by the vials. Conversely, the heat transfer was not significantly influenced by modifications of the thermal conductivity of the rail, the emissivity of the walls or by the geometry of the drying chamber. The model developed turned out to be a powerful tool to predict the heat transfer variability between edge and central vials for cycle

development and scale-up and to compare various freeze-dryer design features.

**KEY WORDS**

Freeze drying/lyophilisation, vaccines, injectables, amorphous, mathematical model, processing.

## INTRODUCTION

The freeze-drying process is widely used today in the pharmaceutical industry as an essential step for extending the product shelf life of several parenteral drugs and biologicals. Due to the combined use of vacuum and low temperatures, this process is recognized to be a gentle method to convert solutions of heat labile drugs, such as vaccines, into solid forms with sufficient stability for shipping and long-term storage (Hansen *et al.*, 2015; Pikal, 1994).

The objective of designing a freeze-drying cycle is to guarantee a high and consistent product quality within the vial batch and from different batches that could be manufactured in various freeze-dryers (Patel *et al.*, 2010b; Tchessalov *et al.*, 2007; Kremer *et al.*, 2009; Fissore and Barresi, 2011). Since the product quality is known to be highly correlated to the product temperature, the product thermal history should be as similar as possible between vials and between cycles run at pilot and commercial scales (Tchessalov *et al.*, 2007). However, product temperature profile depends not only on the process operating conditions (i.e., chamber pressure and shelf temperature) but also on the position-dependent heat transfer (Rambhatla and Pikal, 2003; Pikal *et al.*, 2016; Pisano *et al.*, 2011). Vials on the shelf may be approximately divided into two groups: vials located at the periphery of the shelf (referred to as "edge vials") and vials located in the center (referred to as "central vials"). Edge vials usually receive an additional heat flow rate and present a product temperature higher than central vials of up to 4 °C (Rambhatla and Pikal, 2003; Pikal *et al.*, 2016; Pisano *et al.*, 2011; Tang *et al.*, 2006b). This heat transfer variability, known as the "edge vial effect", could be a serious problem in process design if not accurately predicted, since edge vials are likely to collapse if the product is processed at a temperature close to the limit (e.g., glass transition temperature for amorphous products) (Rambhatla and Pikal, 2003). Furthermore, differences in heat transfer may exist among the edge vials. In this regard, Pisano *et al.* (Pisano *et al.*, 2013, 2011) proposed an effective sub-classification of the edge vials according to their positions on the shelf (e.g., vial located at the corner or at the sides of the shelf ) and also to the heat transfer mechanisms involved (i.e., radiation from the walls, contact conduction from the rail, contact conduction from hotter vials). Such classification was used for the characterization of the inter-vial heat transfer variability within the same batch, which was performed by determining gravimetrically the vial heat transfer coefficient  $K_V$  for each group of vials at different pressures (Pisano *et al.*, 2011). No relationship has been reported between the  $K_V$  value for central vials and the freeze-dryer unit (Pisano *et al.*, 2011; Scutellà *et al.*, 2017a). In contrast, the  $K_V$  values for the edge vial groups should be separately evaluated in every freeze-dryer used, as they could depend on the characteristics of the freeze-dryer and on the loading configuration, e.g., presence or not of the rail. This evaluation may require considerable experimental investment in terms of time and costs (Fissore and Barresi, 2011; Pikal *et al.*, 2016; Pisano *et al.*, 2011).

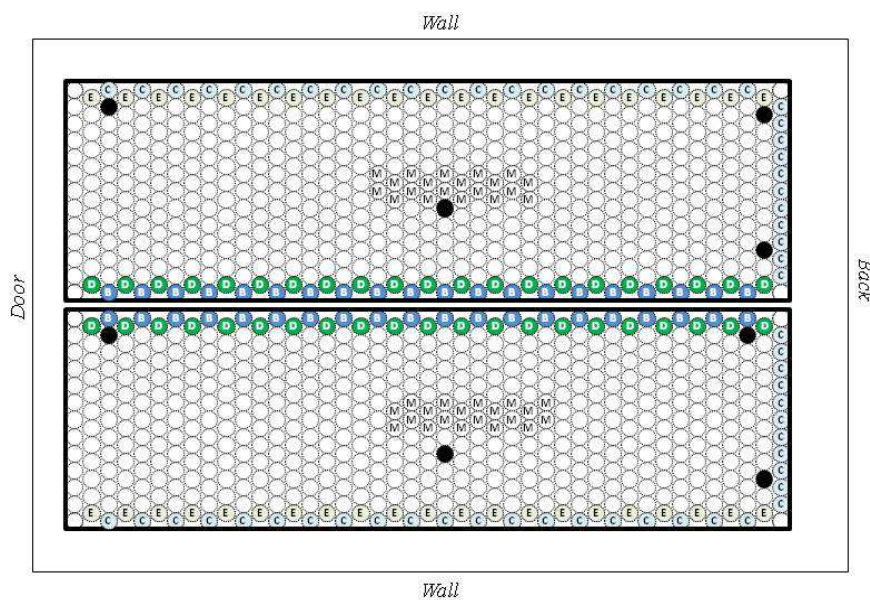


**Figure III.3.1:** Vial arrangement used for experimental validation in the freeze-dryer. Edge vials C and E are respectively in contact and not in contact with the rail and located at the periphery of the shelf; edge vials B and D are respectively in contact and not in contact with the rail and located in the middle of the shelf; vials M are located in the centre of the shelf and surrounded by other vials in the same conditions. Black circles represent the vials in which Tempris probes were placed to monitor the product temperature.

Mathematical models of heat transfer during freeze-drying can be used to predict heat flow rates in vials differently located on the shelf and to investigate the mechanisms responsible for the heat transfer variability between edge and central vials. However, only few models or algorithms have been presently proposed to predict the heat transfer in edge vials processed with different loading configurations or in different dryers (Gan *et al.*, 2005; Pikal *et al.*, 2016; Scutellà *et al.*, 2017b).

Recently, we have developed a 3D mechanistic model of the heat transfer in the drying chamber during sublimation by using the COMSOL software (Scutellà *et al.*, 2017b). It allowed to precisely simulate the radiation heat transfer from the drying chamber components (walls, shelves, rail) as well as the conduction through the gas surrounding the vials. As the logical continuation of our previous work (Scutellà *et al.*, 2017b), the present article is devoted to the assessment of selected factors that drive heat transfer inside a freeze-dryer unit, including the vial loading configuration, the geometry and the thermal properties of the freeze-dryer chamber.

## MATHEMATICAL MODEL

The freeze-drying process can be carried out using several vial loading configurations, in which the vials may receive different heat flow rates depending on the heat transfer mechanisms involved. As an example, **Figure III.3.1** illustrates a typical scenario, in which two vial batches are loaded on the shelf using two bottomless trays. Three main groups of vials can be identified: (i) vials located at the periphery of the shelf and exposed to the wall and the rail (marked in light colours respectively as C and E in **Figure III.3.1**), (ii) vials located in the middle of the shelf and exposed to the rail (marked in dark colours respectively as B and D in **Figure III.3.1**) or (iii) vials located in the centre of the tray and surrounded by other vials in the same conditions (vials M). The 3D mathematical model of vial freeze-drying fully described by Scutellà *et al.* (Scutellà *et al.*, 2017b) was used to predict the heat flow rates received by the vials in different configurations. The model describes the heat transfer phenomena that take place during sublimation in the drying chamber for a set of 5 representative vials. It was developed using the software COMSOL Multiphysics, which is able to precisely compute the radiation, contact and gas conduction heat flow rates in the considered system. The reference configuration is shown in **Figure III.3.2A**. It included the drying chamber wall, bottom and top shelves, rail and five vials arranged in a hexagonal configuration. Edge vials were placed alternatively in contact (vial C) and not in contact with the rail (vial E). The vial placed after the second row from the border of the shelf was considered to be a central vial (vial M). The rail in the reference configuration was designed to partially shield the edge vials C and E. The vial bottom was designed to have an area directly in contact with the shelf and a cylindrical concavity. All the vials were filled with 1 cm of ice.

The main heat transfer mechanisms considered in the model were:

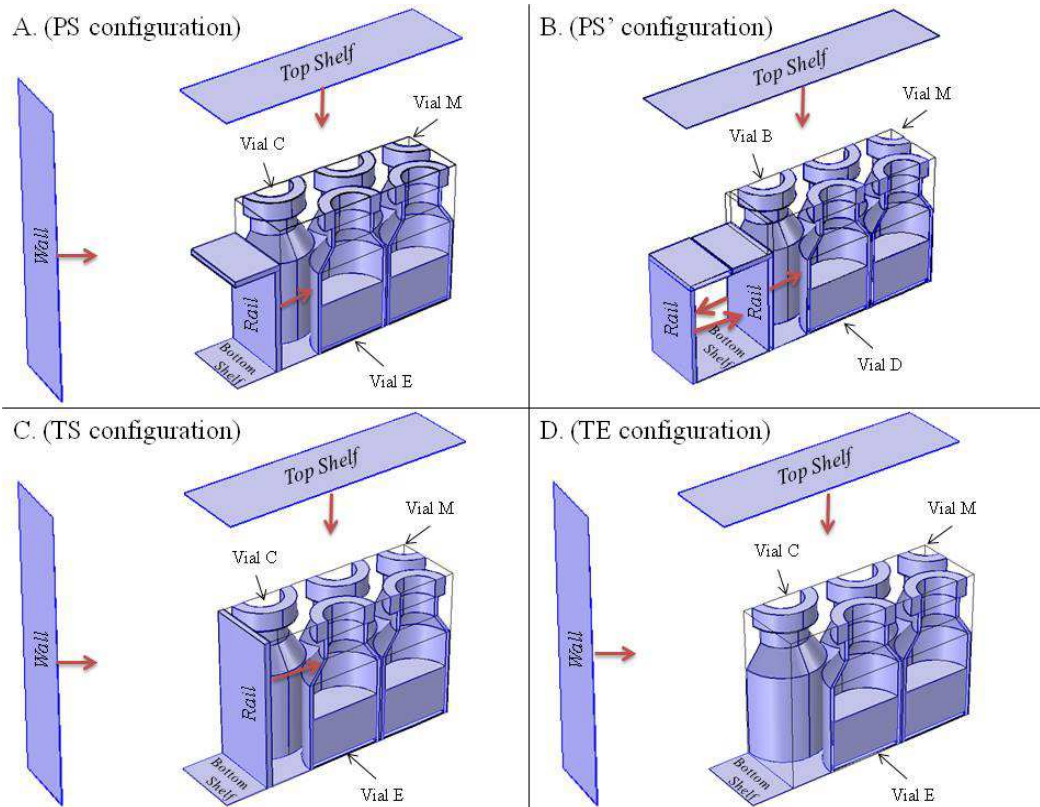


**Figure III.3.2:** Loading configurations studied in this work and typically used in freeze-drying process: (A) edge vials "partially shielded by the rail", named PS; (B) vials "partially exposed to the rail and located in the middle of the shelf", named PS'; (C) edge vials "totally shielded by the rail", named TS; (D) edge vials "totally exposed to the wall", named TE. In function of their positions, the vials are classified as edge vial C and E or B and D and central vial M.

(a) *Contact conduction*. The contact conduction between the shelf and the vials and the shelf and the rail was simulated;

(b) *Conduction through the gas*. The conduction through the low-pressure water vapour entrapped in the vial bottom concavity and surrounding the vial in the drying chamber was taken into account in the model;

(c) *Radiation*. The surface-to-surface radiation model proposed by COMSOL was used to simulate the radiation heat transfer inside the system. This method automatically includes all the possible contributions to radiation heat transfer in the drying chamber and calculates the view factors for all the bodies present in the geometry, resulting in very accurate computation.

Four different vial loading configurations were studied in this work:

-*Edge vials "partially shielded by the rail" (PS)*: This configuration was originally described by Scutellà et al. (Scutellà *et al.*, 2017b), and is shown in **Figure III.3.2A**. Vials are arranged on a tray surrounded by a metallic rail (known as "bottomless tray") and loaded on the freeze-dryer shelf. Then, the bottom of each tray is removed but the metallic rail remains. If the height of the rail is lower than the total height of the vial, edge vials C and E are partially exposed to the chamber wall. In the simulated configuration, the height of the rail was 2.2 cm whereas the height of the vial was 3 cm. Thus, the rail shielded approximately 70 % of the vial height (**Figure III.3.2A**);

- *Vials "partially exposed to the rail and located in the middle of the shelf" (PS')*: Depending on the dimension of the shelf, several "bottomless trays" may be loaded on the same shelf of a freeze-dryer. In this case, one of the rail sides is not exposed to the wall, but to the rail of another tray, as shown in **Figure III.3.2B**. In the present configuration, vials B and D represent vials partially exposed to the rail and placed alternatively in contact (vial B) and not in contact with the rail (vial D);

-*Edge vials "totally shielded by the rail" (TS)*: In the "bottomless tray" configuration, if the height of the rail is equal to the height of the vials, only the rail is directly exposed to the chamber wall, as shown in **Figure III.3.2C**;

-*Edge vials "totally exposed to the wall" (TE)*: In manufacturing freeze-dryers, auto-loading systems of vials are often used. Here, the vials are loaded directly on the shelves, without the aid of any tray or rail, as represented in **Figure III.3.2D**. In this configuration, the lateral walls of the edge vials (C and E) are completely exposed to the heat transfer from the wall.

## EXPERIMENTAL

An experimental procedure similar to the one proposed by Scutellà et al. (Scutellà *et al.*, 2017b), was used to validate the simulated results of the PS and PS' configurations. Sublimations tests were carried out in the pilot freeze-dryer Epsilon 2-25D (Martin Christ Gefriertrocknungsanlagen GmbH, Osterode am Harz, Germany).

**Table III.3.1:** Thermal properties and relevant dimensions of the freeze-dryer used

<i>Characteristic</i>	<i>Value</i>
Number of shelves	7
Area of each shelf	0.27 m <sup>2</sup>
Distance between shelves	0.06 m
Distance between the wall and the shelf	0.11 m
Thermal conductivity of the rail	16.5 W m <sup>-1</sup> K <sup>-1</sup>
Emissivity of the walls and the rail	0.13 <sup>a</sup>
Emissivity of the shelf	0.18 <sup>b</sup>
Emissivity of the vial glass	0.78 <sup>b</sup>

<sup>a</sup> Evaluated in this study<sup>b</sup> Scutellà et al. (Scutellà *et al.*, 2017a)

Relevant geometrical dimensions and thermal properties of the freeze-dryer are reported in **Table III.3.1**. The pressure in the drying chamber was monitored by a capacitive manometer, whereas the product temperature was monitored using six Tempris wireless sensors (IQ Mobil Solution GmbH, Holzkirchen, Germany), placed in the bottom centre of selected vials (**Figure III.3.1**).

A number of 1076 glass siliconized tubing vials of 3 mL (Müller & Müller, Holzminden, Germany) were arranged in two bottomless trays and surrounded by a stainless steel rail shielding 70 % of the vial lateral walls, as shown in **Figure III.3.1**. Vials were filled with 1.8 mL of distilled water, and loaded on the middle shelf of the freeze-dryer. The bottom metallic trays were removed, to allow the direct contact of the vials bottom with the shelf. After loading, a freezing step of 2 h at -50 °C was performed. Then, the pressure was decreased and the shelf temperature was increased by 1 °C min<sup>-1</sup> to the set point, starting the sublimation step.

Two sublimation experiments were carried out at 4 Pa with a shelf fluid inlet temperature of 0 °C and -40 °C. The tests were ended after sublimation of about 20 % of the ice.

Sublimation time was measured from the moment when shelf temperature exceeded product temperature, meaning that there was a net heat flow rate from the shelf towards the vials (Scutellà *et al.*, 2017b).

Sublimation rates were measured gravimetrically. A number of 226 vials, located as shown in **Figure III.3.1**, were weighed before and after the runs using a PG503-S DeltaRange balance (accuracy ±0.001 g; Mettler Toledo, Zaventem, Belgium). The heat flow rates  $\dot{Q}$  were calculated as:

$$\dot{Q} = \frac{m_{IN} - m_{FIN}}{t} \Delta H \quad \text{Equation III.3.1}$$

where  $m_{IN}$  and  $m_{FIN}$  are the masses of the vial respectively before and after sublimation,  $t$  is the sublimation time and  $\Delta H$  is the latent heat of sublimation.

## RESULTS AND DISCUSSION

### Effect of the rail position on the shelf on heat flow rate received by the vials: comparison between PS and PS' configurations

In a manufacturing environment, several bottomless trays may be placed on the same shelf of the freeze dryer (**Figure III.3.1**). Thus, vials located either at the edge or in the middle of the shelf are exposed to the rail as shown in the PS and PS' configurations, respectively. The effect of the rail in the PS and PS' vial loading configurations was assessed both by predicting the heat flow rates in edge (vials C, E, B and D) and central vials (vials M) using the COMSOL model and by performing sublimation tests in the freeze-dryer at a chamber pressure of 4 Pa and two shelf temperatures of 0 °C and -40 °C. Comparison of experimental data and simulations is shown in **Figure III.3.3**.

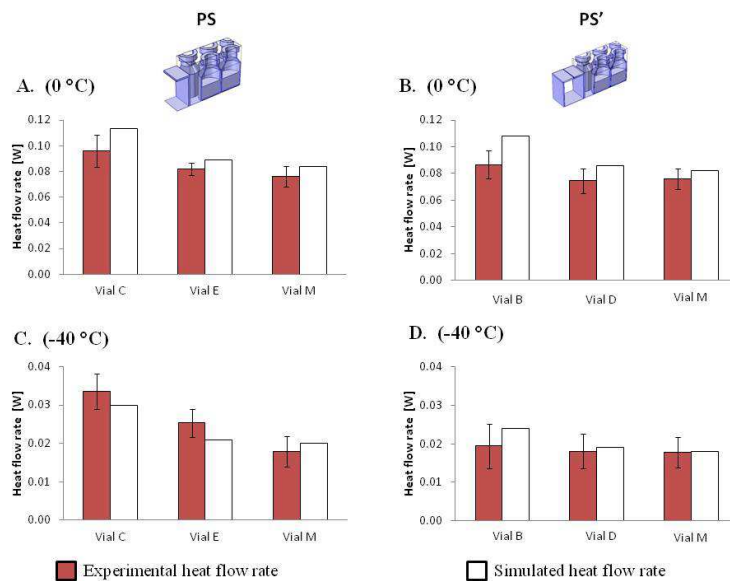


**Figure III.3.3:** Experimental (red bars) and simulated (white bars) heat flow rates in vials C, E, B, D and M in the PS configuration (Figures A and C) and in the PS' configuration (Figures B and D) at a chamber pressure of 4 Pa and two shelf temperatures of 0 °C and -40 °C. Error bars represent experimental standard deviations. PS: edge vials partially shielded by the rail; PS': vials partially exposed to the rail and located in the middle of the shelf. Significance of the abbreviations of vials C, E, B, D and M is reported in **Figure III.3.1**.

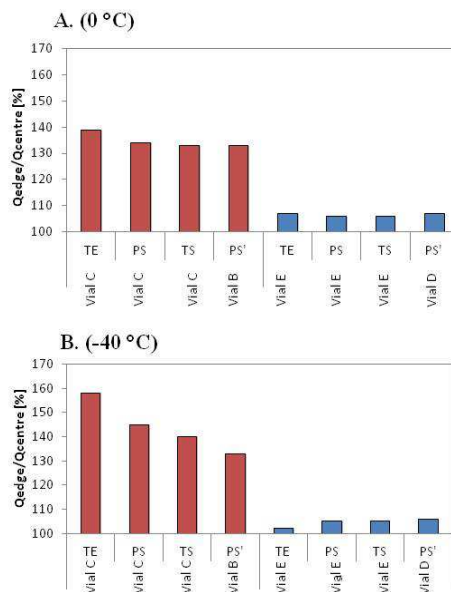


**Figure III.3.4:** Heat flow rates received by edge vials C and E or B and D ( $Q_{edge}$ ) relative to the heat flow rate received by central vial M ( $Q_{centre}$ ), evaluated for the four different loading configurations studied (TE, PS, TS, PS') and for two combinations of shelf temperature and chamber pressure: (A) 0 °C and 4 Pa, (B) -40 °C and 4 Pa. TE: edge vials totally exposed to the wall; PS: edge vials partially shielded by the rail; TS: edge vials totally shielded by the rail; PS': vials partially exposed to the rail and located in the middle of the shelf. Significance of the abbreviations of vials C, E, B, D and M is reported in **Figure III.3.1**.

The model satisfactorily predicted the experimental heat flow rates received by vials C, E, B, D and M in the PS configuration and in the PS' configuration, for all the operating conditions applied (relative mean error of about 13 % in both configurations).

However, the predicted heat flow rates (white bars) of the vials in contact with the rail (vials C and B) appeared to be slightly higher at high shelf temperature (0 °C) than the mean experimental value (red bars). Possible hypotheses on the origins of these differences include the following: (i) an experimental value of the wall temperature different than the one estimated by Scutellà *et al.* (Scutellà *et al.*, 2017b) and used in the model (**Table III.3.1**), which could impact on the estimation of the radiation and gas conduction in the drying chamber in the PS configuration, and (ii) a different position of the vial C and B on the shelf during the experiments respect the simulated ones (e.g., bigger distance between the rail and the vial), which may impact on the evaluation of the radiation and gas conduction between the rail and the vial in the PS and PS' configurations.

When considering shelf temperature of 0 °C (**Figure III.3.3A and III.3.3B**), the vials located at the vicinity of the rail, in contact (vials C and B) and not in contact (vials E and D) exhibited similar values of heat flow rate, regardless of the position of the rail on the shelf. When decreasing shelf temperature at -40 °C (**Figure III.3.3C and III.3.3D**), lower values of heat flow rates were observed for vials in the PS' configuration than for vials in the PS configuration, in particular for the vials in direct contact with the rail (vials B and C). The rail appeared thus to have a significant effect in heat transfer in vials located close to it, regardless of the position of the rail on the shelf. However, the effect of the position of the rail is dependent on process conditions, in particular on the shelf temperature.

Vials located at the middle of the shelf and in the vicinity of rail (vials B and D) could thus be considered as edge vials and the prediction of their heat flow rates appears as extremely valuable for cycle transfer between freeze-dryers of different size.

#### Effect of the vial loading configuration on the edge vial effect

**Figure III.3.4** presents the relative importance of the heat flow rate received by edge vials compared to the heat flow rate received by central vials (vial M) (expressed as the heat flow rate ratio  $Q_{edge}/Q_{centre}$ ). Four different vial loading configurations were investigated: edge vials partially shielded by the rail (PS), vials partially exposed to the rail and located in the middle of the shelf (PS'), edge vials totally shielded by the rail (TS) and vials totally exposed to the wall (TE). The simulations were run at chamber pressure of 4 Pa and two shelf temperatures, 0 °C and -40 °C.

Regardless of the loading configuration, vials in contact with the rail (vial C or B) exhibited a heat flow rate at least 30 % higher than central vials M. In contrast, the additional heat flow rate received by vials not in contact with the rail (vial E or D) compared to central vial M was lower than 10 %.

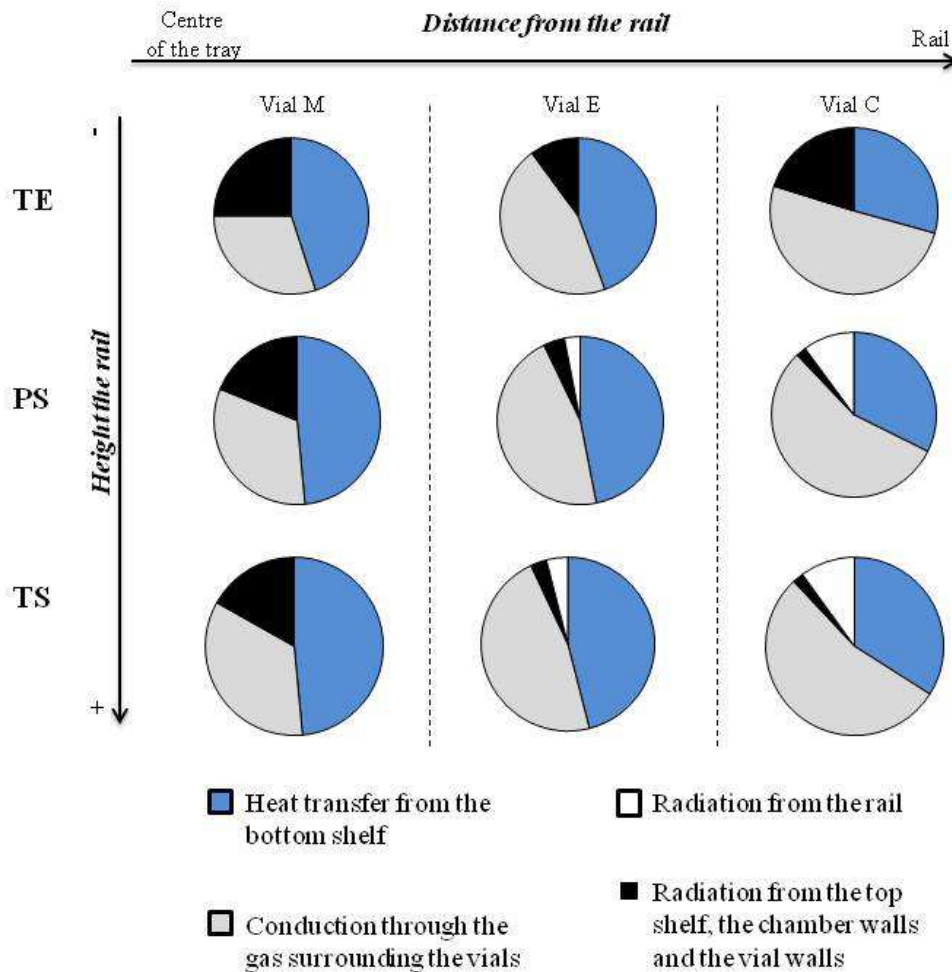


**Figure III.3.5:** Relative importance of various heat transfer mechanisms with respect to the total heat flow rate in four different loading configurations (TE, PS, TS) and at a chamber pressure of 4 Pa and a shelf temperature of -40 °C. TE: edge vials totally exposed to the wall; PS: edge vials partially shielded by the rail; TS: edge vials totally shielded by the rail. Significance of the abbreviations of vials C, E, B, D and M is reported in **Figure III.3.1**.

Furthermore, when considering shelf temperature of 0 °C (**Figure III.3.4A**), the vial loading configuration did not show a significant impact on the heat transfer ratio between edge and central vials (about 35 %), slightly higher (about 40 %) for the TE configuration. The influence of the loading configuration was more visible at low shelf temperatures (-40 °C, **Figure III.3.4B**). As the height of the rail increased (between TE, PS and TS configurations) the heat transfer ratio between edge vial C in contact with the rail and central vial M decreased.

Furthermore, when decreasing shelf temperature, the value of the heat flow rate ratio  $Q_{edge}/Q_{centre}$  increased in vial C for vial loading configurations including wall (TE, PS and TS), which was ascribed to an increased contribution of heat transfer by radiation (e.g., from 10 % at 0 °C to 20 % at -40 °C in configuration TE).

The vial B in PS' configuration showed the lowest value of heat flow rate ratio, as it was located in the middle of the shelf and thus it was not exposed to the radiation contribution from the wall. In order to better understand the effect of both vial position and loading configuration, the contributions to heat transfer of the shelves, the rail and the wall were evaluated. **Figure III.3.5** shows the relative importance of heat flow contributions of (i) heat transfer from the bottom shelf to the vial, including contact conduction, radiation, and gas conduction, (ii) conduction through the gas surrounding the sides and top of the vials, (iii) radiation from the rail and (iv) radiation from the top shelf, the chamber wall and other vial walls, in the four different configurations (TE, PS, TS, PS').

As expected, the heat flow rates from the bottom shelf played a major role on the total heat transfer and its relative importance decreased when distance between the vial and the rail decreased (from vial M to vial C). Conversely, the contribution of gas conduction increased when getting closer to the rail and was higher than radiation in all configurations. This finding confirmed the results of Scutellà et al. (Scutellà *et al.*, 2017b), that ascribed the additional heat flow rate received by edge vials mainly to the conduction through the water vapour contained in the drying chamber.

Furthermore, when considering the edge vials C and E, the use of shielding rails in the PS and TS configurations led to a lower contribution of radiation from the wall (represented in black in **Figure III.3.5**) with respect to the TE configuration. The rail contributed itself to the total heat flow rates by radiation heat transfer (represented in white in **Figure III.3.5**), which appeared to be significant especially for the edge vial C. However, total contribution of heat transfer by radiation including the rail, the wall, the shelves and the vial walls received by edge vials was significantly reduced when a shielding rail was used (PS and TS configuration compared to TE configuration).

When considering the central vial M, the use of the rail slightly decreased the importance of the radiation heat flow from the top shelf, the walls and the vial walls. This effect was probably due to the proximity of the simulated central vial M (located in the third row of the array) to the rail and the

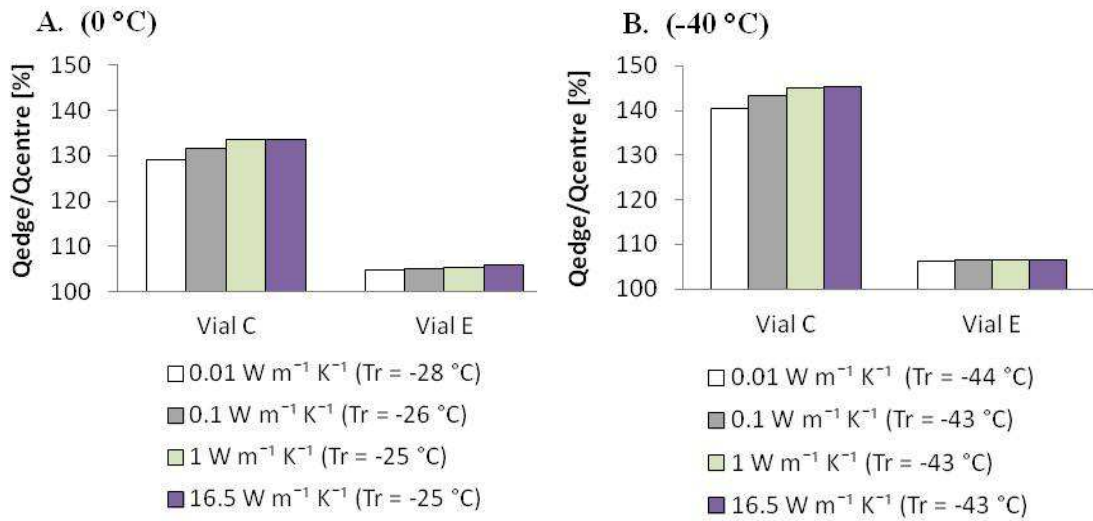


**Figure III.3.6:** Heat flow rate received by edge vials C or E ( $Q_{\text{edge}}$ ) relative to the heat flow rate received by central vial M ( $Q_{\text{centre}}$ ), evaluated in the TS configuration at (A) 0 °C and 4 Pa and (B) -40 °C and 4 Pa considering four different rail thermal conductivities.  $T_r$  represents the temperature of the rail evaluated for each value of thermal conductivity tested. TS: edge vials totally shielded by the rail. Significance of the abbreviations of vials C, E and M is reported in **Figure III.3.1**.

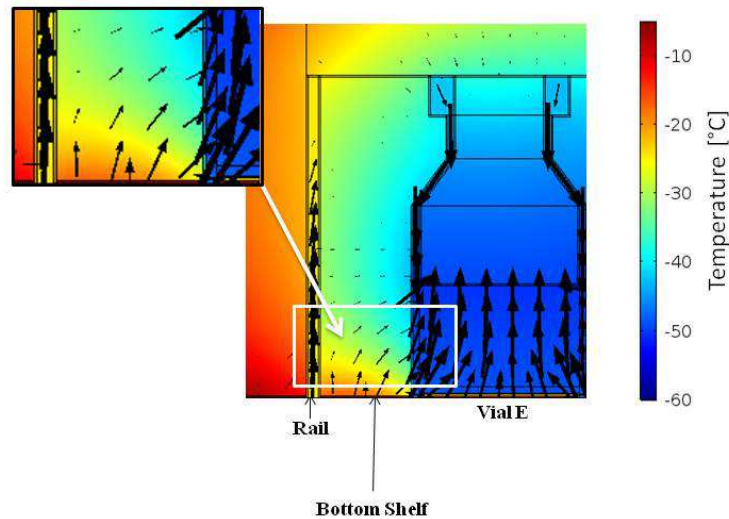


**Figure III.3.7:** Temperature profiles and heat fluxes in the TS configuration at a shelf temperature of 0 °C and a chamber pressure of 4 Pa for a rail thermal conductivity of 16.5 W m<sup>-1</sup> K<sup>-1</sup> and emissivity of 0.13. The view shows the gap between the rail, the bottom shelf and the edge vials (only vial E visible). Arrow dimension indicates heat flux magnitude on a logarithmic scale. The white rectangle and the inset to the figure indicates the lateral heat fluxes from bottom shelf to edge vials. TS: edge vials totally shielded by the rail. Vial E: edge vial not in contact with the rail.

edge of the shelf. In real systems, heat transfer in central vials located far from the rail should be almost unaffected by the rail.

#### Effect of the rail thermal conductivity and emissivity on the edge vial effect

As shown in **Figure III.3.5**, the presence of the rail in the vial loading configuration allows to shield the edge vials from the radiation of the chamber wall, but it still has a significant impact on the edge vial effect through radiation and gas conduction. Thus, the understanding of the effect of the thermal characteristics (i.e., emissivity and thermal conductivity) of the rail on the heat transfer in edge vials can guide the choice of the rail material and thus the design of the freeze-drying cycle.

Firstly, the impact of the rail emissivity on the heat transfer in edge vials was tested at a chamber pressure of 4 Pa in the TS configuration (totally shielded by the rail) by considering two shelf temperatures, 0 °C and -40 °C and a range of emissivity between 0.05 and 1. The variation of the emissivity of the rail did not modify the additional heat flow rates received by either the vial C or E (data not shown). This result is supported by the limited contribution of the radiation heat flow rates from the rail received by the edge vials (between 2 and 10 %, **Figure III.3.5**).

Then, the relative importance of the heat flow rate in vial C and E compared to the one received by the central vial M in the TS configuration was evaluated for different values of rail thermal conductivity (between 0.01 and 16.5 W m<sup>-1</sup> K<sup>-1</sup>). The thermal conductivity has an impact on the rail surface temperature (named  $T_r$ ), which in turn will influence the conduction through the gas contained in the gap between the rail and the vial. The results are presented in **Figure III.3.6**. A chamber pressure of 4 Pa and two shelf temperatures, 0 °C and -40 °C, were tested. The use of a material with an increasing thermal conductivity from 0.01 W m<sup>-1</sup> K<sup>-1</sup> to 1 W m<sup>-1</sup> K<sup>-1</sup> resulted in increasing the rail surface temperature  $T_r$  to a maximum of 3 °C. The increased rail temperature led to an increase of the heat flow rates ratio between edge vial C and edge vial M from 29 % to 34 % at 0 °C and from 41 % to 45 % at -40 °C. The use of rail with thermal conductivities higher than 1 W m<sup>-1</sup> K<sup>-1</sup> did not result in a further increase of the heat flow rate ratio between edge and central vials.

The effect of the rail thermal conductivity on the heat transfer was thus limited but not completely negligible for vial C. In contrast, the edge vial E was not affected by the thermal conductivity of the rail in the whole range tested, regardless of the shelf temperature considered. The limited effect of the rail thermal conductivity can be explained from the visualization of the heat fluxes in the system. **Figure III.3.7** presents a view of the drying chamber, in which is shown the gas contained in the gap between the rail, the bottom shelf and the edge vials (only vial E visible). The temperature is represented by the colour scale, whereas heat fluxes are represented by arrows, whose dimension is proportional to the flux magnitude on a logarithmic scale. A rail thermal conductivity of 16.5 W m<sup>-1</sup> K<sup>-1</sup> and an emissivity of 0.13 at 4 Pa and 0 °C were tested. The heat fluxes directed to the lateral side

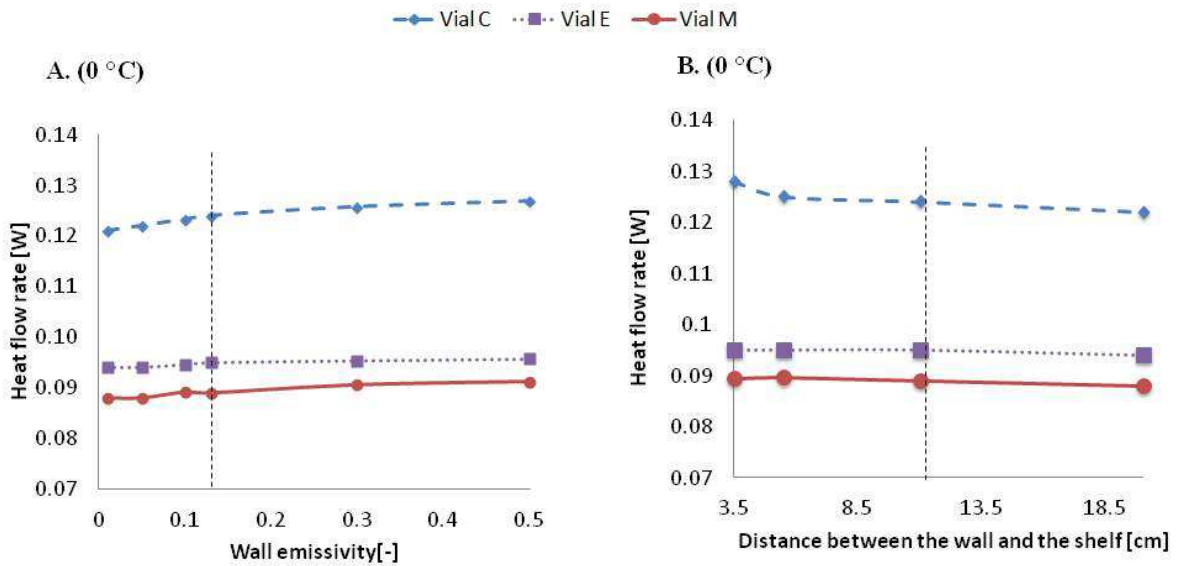


**Figure III.3.8:** Heat flow rates evaluated for edge vials C (dashed line) and E (dotted line) and for central vial M (solid line) in the TE configuration at 0 °C and 4 Pa for (A) different wall emissivities and (B) distances between the wall and the shelf. Vertical dotted lines represent the values characteristic of the freeze-dryer used. TE: edge vials totally exposed to the wall. Significance of the abbreviations of vials C, E and M is reported in **Figure III.3.1**.

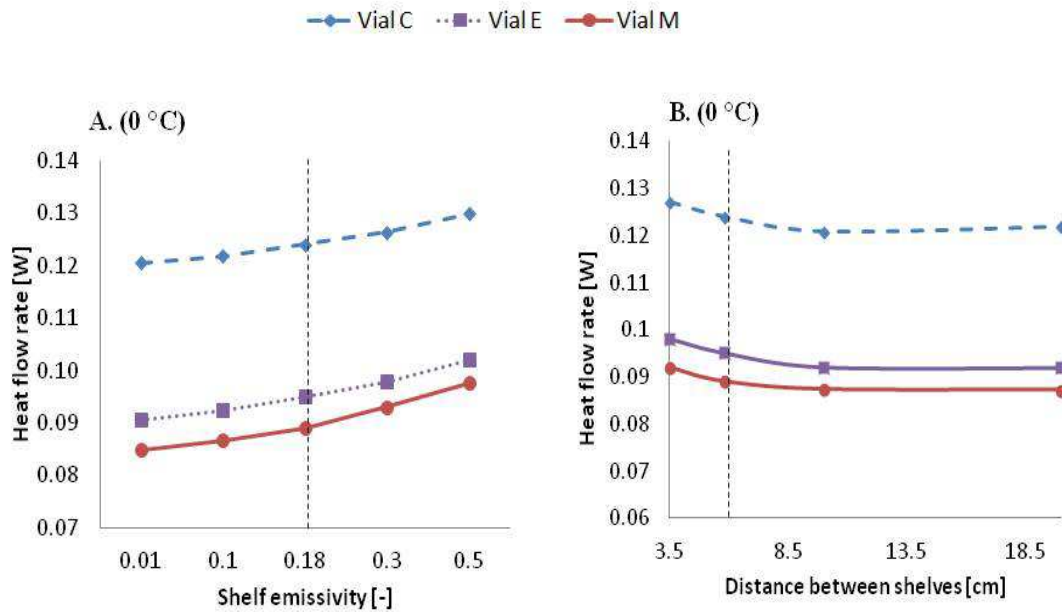


**Figure III.3.9:** Heat flow rates evaluated for edge vials C (dashed line) and E (dotted line) and for central vial M (solid line) in the TE configuration at 0 °C and 4 Pa for (A) different shelf emissivities and (B) for different distances between the top and bottom shelves. Vertical dotted lines represent the values characteristic of the freeze-dryer used. TE: edge vials totally exposed to the wall. Significance of the abbreviations of vials C, E, and M is reported in **Figure III.3.1**.

of the vials were mainly coming from the bottom shelf area between the vials and the rail (upward arrows) through gas conduction, as evidenced by the white rectangle and the inset. Thus, the rail's contribution to the lateral flux by gas conduction received by edge vials was small and modifications of the rail conductivity had only a limited impact on the lateral heat flux.

#### **Effect of the equipment dimensions and emissivity on the heat transfer in the drying chamber**

During scale-up, the cycle is transferred from pilot to commercial freeze-dryers which can have different dimensions (e.g., distances between the shelf and the wall and between shelves). Furthermore, measurements in several freeze-dryers of different scales have shown that the wall and shelf emissivity can vary in a range of 0.04-0.4. These features may modify the heat flow rates received by the vials respectively by gas conduction and radiation.

**Figure III.3.8** shows the heat flow rates received by vials C, E and M at 4 Pa and 0 °C in the TE configuration (totally exposed) considering different wall emissivities and different distances between the shelves and the wall. The dotted vertical lines represent the values for the freeze-dryer considered for the simulation (**Table III.3.1**). A variation of the wall emissivity between 0.01 and 0.5 resulted in an increase of the heat flow received by vials C, E and M of about 2, 4 and 5 %, respectively (**Figure III.3.8A**).

The heat flow rates in edge vials C decreased by about 5 % when the distance between the shelves and the wall increased from 3.5 cm to 20 cm (**Figure III.3.8B**), whereas vial E and M were not significantly affected. The variations of heat flow rate due to the wall emissivity and the distance between wall and shelves appears to have a minor impact on heat transfer, within measurement error and modelling uncertainty;

**Figure III.3.9** presents the heat flows received by the vials C, E and M at a pressure of 4 Pa and a shelf temperature of 0 °C in the TE configuration considering different shelf emissivities and different distances between the top and bottom shelves. An increase of the shelf emissivity from 0.01 to 0.5 caused an increase of the heat flow of about 5 % in vial C, 13 % in vial E and 15 % in vial M (**Figure III.3.9A**). However, considering a shelf temperature of -40 °C, the increase of shelf emissivity would lead to a less significant increase (maximum 6 %) of the heat flow rate in edge and central vials (data not shown). The impact of the shelf emissivity on the heat flow rates appeared to be more important than the wall emissivity for all the simulated vials C, E and M. This result pointed out that a variation of the shelf emissivity between one freeze-dryer and another cannot be neglected, and a precise thermal characterization (i.e., emissivity measurement) of the equipment may be necessary before performing scale-up. Furthermore, the heat flow decreased by about 5 % in all considered vials when the distance between the shelves increased from 3.5 cm to 10 cm (**Figure**

**III.3.9B).** Further increase of the distance (up to 20 cm) did not have any significant impact on the heat transfer. These results can be explained by a decrease of the gas conduction flow and of the view factor relevant to radiation at distances between the shelves higher than about 10 cm.

## CONCLUSIONS

In the present work, the 3D COMSOL model previously developed by our group was used to predict the impact of several factors on the variability of heat transfer between edge and central vials, such as the vial loading configurations, the thermal properties of the rail, the walls and the shelves and some characteristic dimensions of the drying chamber (i.e., distance between the shelf and the wall and distance between shelves). The analysis revealed that the loading configuration plays a significant role in the heat transfer variability between edge and central vials. The use of a rail shielding more than 70 % of the lateral side of vials located at the periphery of the shelf was found to significantly reduce the edge vial effect. However, the rail itself contributes to the heat transfer and its contribution has to be considered when it is present in the middle of a shelf, i.e., when several trays are used on a same shelf.

Furthermore, among the different thermal properties of the drying chamber components (rail, walls, shelves), the emissivity of shelf was found to significantly increase the heat flow received by both edge and central vials. Thus, a precise measurement of shelf emissivity is recommended to predict the heat transfer modification between equipments presenting different finish of the shelves. Among the explored geometric dimensions of the freeze-dryer, a distance between shelves less than about 5 cm slightly increased the heat transfer while the distance between shelves and walls had a negligible effect in the considered range.

The present model revealed to be a powerful tool, to be used during the cycle design and scale-up process to predict the heat transfer variability between edge and central vials, but also between different freeze-dryers.

## **ACKNOWLEDGMENTS**

The authors would like to thank Yves Mayeresse and Benoit Moreau (GSK Vaccines) for reviewing this work, Vincent Ronsse (technician) and Alain Philippart (operator) (GSK Vaccines) for their help in the data acquisition and Victor Rousseau and Gwenael Davaud (AgroParisTech students) for their help in developing the model.

## **CONFLICT OF INTEREST**

Erwan Bourlès is an employee of the GSK group of companies. Bernadette Scutellà participated in a postgraduate Ph.D. program at GSK Vaccines. Stephanie Passot, Fernanda Fonseca, Artemio Plana-Fattori, Denis Flick and Ioan Cristian Trelea report no financial conflicts of interest.

## **FUNDING**

This work was funded by GlaxoSmithKline Biologicals S.A., under a Cooperative Research and Development Agreement with INRA (Institut National de la Recherche Agronomique) via the intermediary of the UMR (Unité Mixte de Recherche) GMPA (Génie et Microbiologie des Procédés Alimentaires) at the INRA Versailles-Grignon research centre.

## **AUTHORS CONTRIBUTIONS**

All authors were involved in the conception of the model and design of the study. Bernadette Scutellà, Erwan Bourlès, acquired the data. Bernadette Scutellà, Stephanie Passot, Erwan Bourlès, Fernanda Fonseca and Ioan Cristian Trelea analyzed and interpreted the experimental results. Bernadette Scutellà, Artemio Plana-Fattori, Denis Flick, and Ioan Cristian Trelea were involved in the model development. All authors were involved in drafting the manuscript or revising it critically for important intellectual content. All authors had full access to the data and approved the manuscript before it was submitted by the corresponding author.

### III.3.3 Take-home message

- The vial loading configuration resulted to highly influence the heat transfer in edge vials. The presence of the rail reduced the additional heat flow rate received by edge vials, although it contributed to the heat transfer by gas conduction and radiation.
- Furthermore, the emissivity of the shelf was found to be the thermal property of the equipment that mainly impacted the heat transfer in both edge and central vials.
- The heat transfer in edge and central vial was not significantly influenced by the thermal characteristics of the rail, the emissivity of the walls and the geometry of the drying chamber.
- Our 3D mathematical model of heat transfer in freeze-drying revealed to be a powerful tool to predict the heat transfer variability between vials and between different equipments.

In these first **Papers III.1-3**, the mechanisms responsible for the heat transfer variability in vials differently located on the shelf were investigated. Vial geometry variability was found to be the main responsible for the heat transfer difference among vials located in the centre of the shelf. Furthermore, the use of a newly developed 3D mathematical model of heat transfer in freeze-drying identified the conduction through the gas in the drying chamber as the main responsible for the edge vial effect, rather than radiation from the chamber walls as usually stated.

The combination of these mechanisms may lead to significant differences of the product thermal history within the vial batch, and thus their predictions can help the design and scale-up of the freeze-drying cycles. However, variability of the mass transfer in the vial batch also may lead to differences in the product temperature and thus in the final product quality between vials. Identification and quantification of the mechanisms responsible for the mass transfer variability during primary and secondary drying will be the goal of the next **Papers III.4-5**.





### III.4 Determination of the product resistance variability and its influence on the product temperature in pharmaceutical freeze-drying

---

The present study was submitted to the *European Journal of Pharmaceutics and Biopharmaceutics*.

#### III.4.1 Context and objectives

During primary drying, the sublimed water vapour has to overcome three main barriers to go from the product interface to the condenser: the dried product layer, the elastomeric stopper (if present) and the pathway from the chamber and the condenser. Among these three barriers, the dried product layer is known to greatly limit the mass transfer during sublimation. The product resistance is influenced by the dimensions of the dried pores left after ice crystals sublimation, which in turn depends on the value of nucleation temperature during the freezing step. Furthermore, nucleation is a stochastic phenomenon and thus ice crystals of different size may form among vials processed following the same freeze-drying protocol, leading to differences in the mass transfer during sublimation.

#### Objective

The main objective of the following study was to investigate and quantify the product resistance variability and its impact on the product quality, through predictions of product temperature distributions, by the combined use of two experimental methods: the pressure rise test and the gravimetric method.



### III.4.2 Paper

#### TITLE

Determination of the product resistance variability and its influence on the product temperature in pharmaceutical freeze-drying

#### AUTHORS

B. Scutellà<sup>1,2</sup>, I.C. Trelea<sup>1</sup>, E. Bourlés<sup>2</sup>, F. Fonseca<sup>1</sup>, S. Passot<sup>1</sup>

#### AFFILIATION

<sup>1</sup> UMR GMPA, AgroParisTech, INRA, Université Paris Saclay, 78 850 Thiverval-Grignon, France

<sup>2</sup> GSK Vaccines, Rixensart, Belgium

<sup>3</sup> UMR Ingénierie Procédés Aliments, AgroParisTech, INRA, Université Paris-Saclay, 91300 Massy, France

#### ABSTRACT

During the primary drying step of the freeze-drying process, mass transfer resistance strongly affects product temperature, and consequently, the final product quality. The main objective of this study was to evaluate the variability of the mass transfer resistance due to the dried product layer ( $R_p$ ) in a manufacturing batch of vials, and its potential effect on the product temperature, from data obtained in a laboratory freeze-dryer. Freeze-drying cycles were run at -25 °C and 10 Pa in a pilot scale equipment using two different freezing protocols. Five repetitions of each condition were performed. Pressure rise test (PRT) and gravimetric methods were applied as complementary approaches to estimate  $R_p$ . PRT method allowed to estimate variability of the evolution of  $R_p$  with the dried layer thickness between different experiments whereas the gravimetric method determined  $R_p$  variability at a fixed time within the vial batch. Based on product resistance distribution calculated from PRT method, a product temperature safety margin of about  $\pm 5$  °C was defined for a product dried layer thickness of 5 mm. The present approach can be used to estimate the risk of failure of the process due to mass transfer variability based on product temperature distributions in cycle design and scale-up.

#### KEYWORDS

lyophilization, drying, mass transfer, product resistance, sublimation rate, controlled nucleation, heterogeneity, distribution, pressure rise test

**NOMENCLATURE**

$A$	Cross sectional area ( $m^2$ )
$df$	Degrees of freedom
$\Delta H$	Latent heat of sublimation ( $J\ kg^{-1}$ )
$K_V$	Vial heat transfer coefficient ( $W\ m^{-2}K^{-1}$ )
$l$	Layer thickness ( $m$ )
$m$	Water vapour mass ( $kg$ )
$M_W$	Molecular weight of water ( $kg\ kmol^{-1}$ )
$N_V$	Number of vials
$P$	Pressure ( $Pa$ )
$Q$	Heat flow rate ( $W$ )
$R_g$	Ideal gas constant ( $J\ K^{-1}kmol^{-1}$ )
$R_p$	Product resistance ( $Pa\ m^2\ s\ kg^{-1}$ )
$SD$	Standard deviation
$SE$	Standard error
$t_{sub}$	Sublimation time ( $s$ )
$T$	Temperature ( $K$ )
$V$	Volume ( $m^3$ )

**Greek**

$\lambda$	Thermal conductivity ( $W\ m^{-1}\ K^{-1}$ )
$\rho$	Product density ( $kg\ m^{-3}$ )

**Subscripts**

0,1	Index of parameters in <b>Equation III.4.5</b>
$B$	Vial bottom
$C$	Chamber
$d$	Dried
$f$	Frozen
$i$	Interface
$n$	Nucleation
$S$	Shelf
$V$	Vial

## INTRODUCTION

Freeze-drying is a soft-drying process which consists in the dehydration of the frozen product first by under-vacuum sublimation and then by desorption. Due to the use of very low temperature and pressure, freeze-drying is currently the method of choice in the pharmaceutical industry for the preservation of heat sensitive products such as vaccines, proteins or micro-organisms (Hansen *et al.*, 2015; Adams, 1991; Fonseca *et al.*, 2015). Several quality attributes of these product, e.g., the elegance of the dried cake, the reconstitution time and the moisture content, are governed by the temperature profile during the sublimation step (Johnson and Lewis, 2011; Patel *et al.*, 2017; Pikal and Shah, 1990). If the temperature of the sublimation interface exceeds a critical value, i.e., collapse temperature, the product may experience abrupt loss of quality due to the collapse of its structure (Pikal and Shah, 1990; Johnson and Lewis, 2011).

The thermal history of the product cannot be directly controlled but is governed by the heat and mass transfer taking place during the process. Theoretical models of these phenomena are nowadays largely used to predict critical process parameters, as the product temperature, for process design and scale-up (Trelea *et al.*, 2007; Velardi and Barresi, 2008; Giordano *et al.*, 2011; Lopez-Quiroga *et al.*, 2012; Pikal *et al.*, 2005). Freeze-drying models often involve the determination of heat and mass transfer parameters, such as the vial heat transfer coefficient  $K_V$  and the mass transfer resistance due to the product  $R_p$  (Pikal *et al.*, 1984; Giordano *et al.*, 2011; Pisano *et al.*, 2013; Trelea *et al.*, 2007; Pikal *et al.*, 2005). The correct evaluation of these model parameters and their variability is of paramount importance for a reliable prediction of the product temperature within the batch and between different freeze-dryers.

The vial heat transfer coefficient  $K_V$  is characteristic of the container, and depends on the chamber pressure and on the dimensions of the vial bottom geometry. Its determination is usually performed by the gravimetric method (Pikal *et al.*, 1984; Pisano *et al.*, 2011; Scutellà *et al.*, 2017a; Hibler *et al.*, 2012), which allows to have a detailed picture of the variability of this parameter among the vials on the shelf. In contrast, the product resistance  $R_p$  is characteristic of the formulation, and its value does not remain constant during sublimation as it is due to the growing dried layer thickness.

In literature, several methods were developed to measure the evolution of the product resistance with the dried layer thickness from the estimation of the mass flow rate value, such as the microbalance (Pikal *et al.*, 1983; Xiang *et al.*, 2004), the pressure rise test (PRT) (Fissore *et al.*, 2010; Oddone *et al.*, 2014; Tang *et al.*, 2006a), the tunable diode laser absorption spectroscopy (TDLAS) (Kuu *et al.*, 2011). Product resistance was also determined from the product temperature profile recorded by thermal sensors during the process by using mathematical models and soft sensors (i.e., software sensors) (Kuu *et al.*, 2006; Bosca *et al.*, 2013). Some of these techniques, such as the PRT and the TDLAS, allow to evaluate a global value of the product resistance in the vial batch, starting from



global measurement of the mass flow rate. Other methods allow to determine product resistance evolution in one vial (such as the microbalance) or in a limited number of vials (for example the use of thermocouples). Thus, the determination of the variability of the product resistance within a manufacturing batch of vials remains particularly challenging.

The product resistance value and variability is directly influenced by the freezing step. Some authors (Searles *et al.*, 2001b; Searles, 2010a; Konstantinidis *et al.*, 2011; Oddone *et al.*, 2014, 2016) have evidenced a direct correlation between nucleation temperature, ice crystal size, and mass transfer during primary drying. It was found that high values of nucleation temperature generate few and large ice crystals, which upon sublimation in primary drying leave larger pores and smaller specific surface area than low values of nucleation temperature. The dimension of the pores dramatically influences the resistance of the product due to the dried layer, and thus the sublimation rate (Searles, 2010a; Searles *et al.*, 2001b).

Furthermore, the stochastic nature of nucleation temperature leads to different kinetics of sublimation within a same vial batch (Searles *et al.*, 2001b; Searles, 2010a; Oddone *et al.*, 2014; Passot *et al.*, 2009; Oddone *et al.*, 2016), resulting in potentially high vial to vial variability that poses significant problems in achieving product quality homogeneity.

In the present work, an original approach was proposed to estimate the variability of the product resistance  $R_p$  in a manufacturing batch of vials during the primary drying step starting from data obtained at laboratory scale. Freeze-drying cycles were performed using a 5 % sucrose solution at 10 Pa and -25 °C in a laboratory scale freeze-dryer. Two different freezing protocols were used, i.e., the nucleation of ice crystals was either spontaneous or controlled using the nucleation agent Snomax. Five repetitions of each condition were carried out, in order to evaluate the product resistance variability between different laboratory scale batches. Furthermore, two additional cycles were carried with partially stoppered vials, to study the effect of the presence of the stopper on the product resistance. Two experimental methods were used for the determination of the product resistance: (1) a global one, namely the pressure rise test (PRT), to evaluate the average evolution of the product resistance with the dried layer thickness in single batches, and (2) a local one, namely the gravimetric method, to evaluate the variability of the mass loss at a given time of sublimation between single vials. The combination of the data provided by these methods was used to estimate the variability of the product resistance in a manufacturing batch of vials. Finally, the effect of  $R_p$  variability on the product quality was quantified by calculating the product temperature distribution and by assessing the risk of failure (potential percentage of rejected vials) of the process during the sublimation step.

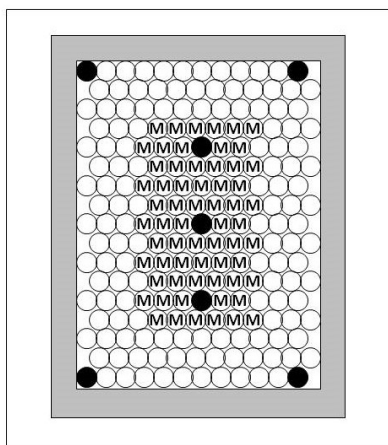


**Figure III.4.1:** Arrangement of the vials on the shelf. Symbols: black circle, vials in which the thermocouples are located; Letter 'M', gravimetrically-analyzed vials. All vials were filled with 1.8 mL of the selected product.

**Table III.4.1:** Description of the freeze-drying cycles performed in this study.

<i>Description</i>	<i>PRT method</i>	<i>Gravimetric+PRT method</i>
Vials filled with sucrose solution and processed without stoppers (S5)	S5-1	S5-4
	S5-2	S5-5
	S5-3	
Vials filled with sucrose solution and processed with partially inserted stoppers (S5s)	S5s-1	
	S5s-2	
Vials filled with sucrose solution + 0.1% of Snomax to control the nucleation and processed without stoppers (S5cn)	S5cn-1	S5cn-4
	S5cn-2	S5cn-5
	S5cn-3	

## MATERIALS AND METHOD

### Materials

Siliconized 3 mL tubing vials (Müller + Müller, Holzminden, Germany) filled with a 5 % w/w aqueous sucrose solution were used throughout this study.

The experiments were carried in the REVO laboratory scale freeze-dryer (Millrock Technology, Kingston, United States), equipped with three temperature controlled shelves and a condenser connected with the drying chamber by a butterfly valve. The drying chamber had a volume of 0.12 m<sup>3</sup>. Two pressure gauges, a capacitive manometer (MKS) and a thermal conductivity gauge (Pirani) were used to monitor the pressure in the chamber. In order to monitor the product temperature during the cycles, a number of 7 T-type Thermocouples were placed in the bottom centre of selected vials (**Figure III.4.1**). The accuracy of the product temperature measurement was estimated at  $\pm 0.5$  °C.

### Freeze-drying cycles

A number of 204 vials were arranged in hexagonal clusters (**Figure III.4.1**) in a bottomless tray and filled with 1.8 mL of the sucrose solution (i.e., 10 mm of filling height). In order to minimize the additional heat transfer at the border of the shelf, the vial batch was fully shielded by a polystyrene rail covered by aluminium tape. Three experimental conditions were investigated, as presented in **Table III.4.1**: vials filled with sucrose solution and processed without stoppers and with spontaneous nucleation (S5); vials filled with sucrose solution and processed with stoppers and with spontaneous nucleation (S5s); vials filled with sucrose and nucleating agent Snomax solution and processed without stopper and with controlled nucleation (S5cn).

Freeze-drying cycles with spontaneous nucleation (referred as S5) were performed in two successive steps: (1) a freezing step, performed firstly by cooling the shelf at 3 °C min<sup>-1</sup> from ambient temperature to -50 °C and then by holding the vials for 2 h at -50 °C, and (2) a sublimation step, carried out at a shelf temperature of -25 °C (heating rate of about 2.5 °C min<sup>-1</sup>) and a chamber pressure of 10 Pa. When controlled nucleation was applied, 0.1 % of the nucleation agent Snomax (Snomax LLC, Englewood, CO, US), an active protein derived from *Pseudomonas Syringae*, was added in the sucrose solution and the following freezing protocol was applied. The shelf temperature was first decreased from ambient temperature to -4 °C at about 3 °C min<sup>-1</sup>, then maintained at -4 °C for 1 hour to initiate ice nucleation and finally decreased to -50 °C at 3 °C min<sup>-1</sup>. During all the performed cycles (S5, S5s and S5cn), pressure rise tests (PRT) were performed to determine the mass flow rate. The PRT consisted in closing the valve between the drying chamber and the condenser at specified moments for a short time period of about 30s. The manometric pressure was recorded during the PRT every 0.1 s by a specially designed software. Some cycles (two of each condition without stopper) were stopped at about 30 % of the total sublimation time and the sublimed ice mass

**Table III.4.2:** Vial and freeze-dryer dimensions, physical properties and parameters used in this study

<i>Symbol</i>	<i>Significance</i>	<i>Value <math>\pm</math> SD</i>	<i>Units</i>
$A_{VB}$	Outer bottom area of the vial	$2.07 \cdot 10^{-4}$	$m^2$
$A_i$	Inner bottom area of the vial	$1.78 \cdot 10^{-4}$	$m^2$
$\Delta H$	Latent heat of sublimation of ice	$2.8 \cdot 10^6$	$J \cdot kg^{-1}$
$K_V$	Vial heat transfer coefficient <sup>a</sup>	$13.30 \pm 0.885$	$W \cdot m^{-2} \cdot K^{-1}$
$\lambda_f$	Ice thermal conductivity	2.23	$W \cdot m^{-1} \cdot K^{-1}$
$\rho$	Product density	917	$kg \cdot m^{-3}$
$R_g$	Ideal gas constant	$8.314 \cdot 10^3$	$J \cdot K^{-1} \cdot kmol^{-1}$
$T_C$	Temperature of the drying chamber	242	$K$
$M_W$	Water molecular weight	18	$kg \cdot kmol^{-1}$
$V_C$	Volume of the drying chamber	0.12	$m^3$

SD, standard deviation.

<sup>a</sup> Evaluated from Scutella et al. (Scutellà *et al.*, 2017a)

in 50 central vials (marked with the letter M in **Figure III.4.1**) was determined by the gravimetric method, as proposed by Scutella et al. (Scutellà *et al.*, 2017a). The selected vials were weighed before and after the cycle, and the water loss was calculated as difference between initial and final vial mass. Sublimation time was measured from the moment when shelf temperature exceeded product temperature, meaning that there was a net heat flux from the shelf towards the vials.

A summary of all the experiments performed is presented in **Table III.4.1**.

## THEORY AND DATA ANALYSIS

### Theoretical description of the product resistance

#### *Evaluation of the product resistance from the mass flow rate*

As widely reported in literature (Pikal, 2000; Pikal *et al.*, 1984; Overcashier *et al.*, 1999; Fissore and Pisano, 2015; Bosca *et al.*, 2013; Kodama *et al.*, 2013), the product resistance  $R_p$  can be calculated as:

$$R_p = \frac{A_i(P_i - P_{vC})}{\dot{m}} \quad \text{Equation III.4.1}$$

where  $\dot{m}$  is the mass flow rate,  $A_i$  is the sublimation interface area,  $P_{vC}$  is the partial pressure of the vapour in the drying chamber, usually assumed equal to the total chamber pressure during the sublimation step, and  $P_i$  is the vapour pressure at the sublimation interface, calculated using the Clausius-Clapeyron relation (Scutellà *et al.*, 2017a):

$$P_i = \exp \left( \frac{-6139.6}{T_i} + 28.8912 \right) \quad \text{Equation III.4.2}$$

In **Equation III.4.2**,  $T_i$  is the product temperature at the sublimation interface theoretically determined as follow:

$$\dot{Q} = A_i \frac{\lambda_f}{l_f} (T_i - T_{BV}) \quad \text{Equation III.4.3}$$

where  $\lambda_f$  is the conductivity of the frozen layer,  $A_i$  is the sublimation interface area, considered equal to the internal cross sectional area of the vial,  $l_f$  is the frozen dried layer thickness, evaluated as the difference between the initial product thickness and the dried layer thickness at given time,  $\dot{Q}$  is the heat flow rate, equal to the mass flow rate times the latent heat of sublimation ( $\Delta H \dot{m}$ ) considering the

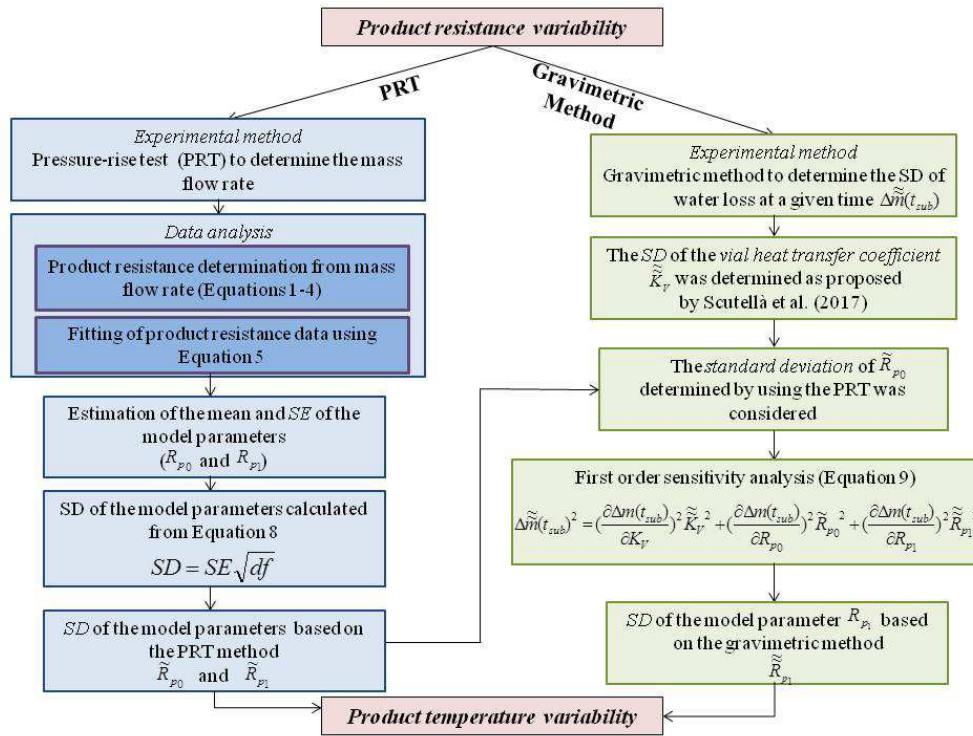


**Figure III.4.2:** Schematic flow of the strategy used to determine the product resistance variability by using the PRT and the gravimetric methods.

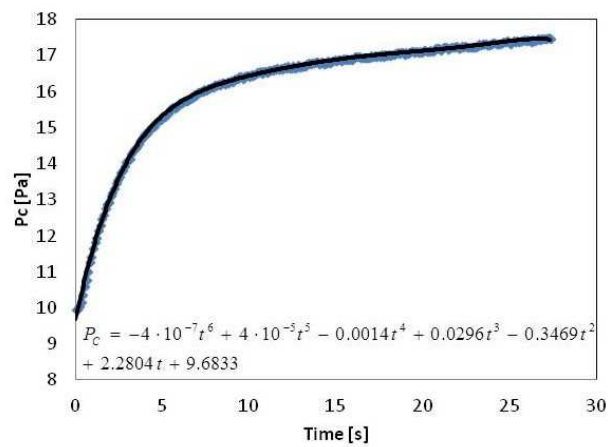


**Figure III.4.3:** Example of the increase of the chamber pressure in time during a PRT performed in the freeze-drying cycle S5-1.

pseudo-steady state during sublimation, and  $T_{BV}$  is the product temperature at the vial bottom, calculated as (Pikal *et al.*, 1984; Scutellà *et al.*, 2017a):

$$\dot{Q} = A_{BV} K_V (T_{BV} - T_S) \quad \text{Equation III.4.4}$$

where  $A_{BV}$  is the vial bottom area, considered equal to external cross sectional area of the vial,  $T_S$  is the temperature of the shelf, evaluated as the average between the inlet and outlet shelf fluid temperatures, and  $K_V$  is the vial heat transfer coefficient evaluated as proposed by Scutella *et al.* (Scutellà *et al.*, 2017a).

All relevant physical product properties and parameters used are reported in **Table III.4.2**.

*Dependence of the product resistance on the dried layer thickness  $l_d$*

The product resistance  $R_p$  can be described as a linear function of the dried layer  $l_d$  (Pikal *et al.*, 1984; Pikal and Shah, 1990):

$$R_p = R_{p_0} + R_{p_1} l_d \quad \text{Equation III.4.5}$$

where  $R_{p_0}$  and  $R_{p_1}$  are coefficients determined by data regression. The evolution of dried layer thickness in time ( $\frac{dl_d}{dt}$ ) can be calculated as:

$$\frac{dl_d}{dt} = \frac{1}{\rho A_i} \dot{m} \quad \text{Equation III.4.6}$$

where  $\rho$  is the density of the product (assumed equal to the density of the ice).

**Experimental evaluation of  $R_p$  and calculation of  $R_p$  distribution**

**Figure III.4.2** schematically represents the strategies used to evaluate the variability of the product resistance. Two experimental methods were used: the pressure rise test and the gravimetric methods.

*Evaluation of  $R_p$  using the pressure rise test*

The pressure rise tests were used to determine of the mass flow rate values during the sublimation step of all the freeze-drying cycles performed. **Figure III.4.3** shows an example of the evolution of the chamber pressure during a PRT. As soon as the valve between the chamber and the condenser was closed, the pressure inside the chamber increased, as result of the accumulation of the sublimed

water vapour, at first very rapidly and then more slowly when the chamber pressure approached the equilibrium value with the ice surface (Fissore *et al.*, 2010).

The initial slope of the pressure rise curve  $\frac{dP_c}{dt}$  was calculated by fitting the data with a 6<sup>th</sup> degree polynomial equation and performing the analytical derivative at the initial pressure rise time (equal to 0). Then,  $\frac{dP_c}{dt}$  was considered directly proportional to the sublimation flow rate  $\dot{m}$  through the ideal gas law:

$$\frac{dP_c}{dt} = \dot{m} \frac{R_g T_c N_V}{V_c M_W} \quad \text{Equation III.4.7}$$

where  $R_g$  is the ideal gas constant,  $V_c$  is the volume of the drying chamber,  $T_c$  is the temperature of the chamber, estimated as an average between the shelf temperature and product temperature at the interface (Pisano *et al.*, 2011),  $M_W$  is the molecular weight of the water vapour and  $N_V$  is the number of vials. The values of the relevant physical properties used in **Equation III.4.7** are reported in **Table III.4.2**. The mass flow rate values obtained from the PRT was then used to calculate the product resistance evolution with the dried layer thickness by using **Equations III.4.1-4**. For each condition tested (i.e., S5 and S5cn), five curves were obtained and considered as a single set of data to fit **Equation III.4.7** and to calculate the values and the standard errors (*SE*) of the parameters  $R_{p_0}$  and  $R_{p_1}$ . Finally, the standard deviations (*SD*) of the product resistance parameters  $R_{p_0}$  and  $R_{p_1}$  (named  $\widetilde{R}_{p_0}$  and  $\widetilde{R}_{p_1}$ ), were calculated from the *SE* by considering:

$$SD = SE \sqrt{df} \quad \text{Equation III.4.8}$$

where *df* is the number of the degrees of freedom, equal to the difference between the number of experimental points collected (i.e., the total number of PRTs performed during the five experiments for each condition) and the number of parameters ( $R_{p_0}$  and  $R_{p_1}$  for **Equation III.4.5**). Calculations were performed with Matlab R2014b software (The MathWorks, Inc., Natick, MA).

#### *Evaluation of $R_p$ using the gravimetric method*

The variability of the product resistance in a small batch of vials (i.e., 100) was also evaluated by performing a variance-based sensitivity analysis. Firstly, the gravimetric method was used to determine the distribution of the sublimed mass at a given time  $\Delta m(t_{sub})$  among vials in four freeze-drying cycles carried out with and without controlled nucleation. Differences in the sublimed mass between vials can be due to the variability of

the heat transfer to the vial and of the mass transfer in the dried layer. Thus, the total variance of the sublimed mass  $\Delta m(t_{sub})^2$  can be expressed as the sum of the fractions of variance due to the heat and mass transfer parameters  $K_V$ ,  $R_{p_0}$  and  $R_{p_1}$ , assuming that their effects are independent:

$$\Delta m(t_{sub})^2 = \left( \frac{\partial \Delta m(t_{sub})}{\partial K_V} \right)^2 \widetilde{K}_V^2 + \left( \frac{\partial \Delta m(t_{sub})}{\partial R_{p_0}} \right)^2 \widetilde{R}_{p_0}^2 + \left( \frac{\partial \Delta m(t_{sub})}{\partial R_{p_1}} \right)^2 \widetilde{R}_{p_1}^2 \quad \text{Equation III.4.9}$$

where  $\frac{\partial \Delta m(t_{sub})}{\partial K_V}$ ,  $\frac{\partial \Delta m(t_{sub})}{\partial R_{p_0}}$  and  $\frac{\partial \Delta m(t_{sub})}{\partial R_{p_1}}$  represent the sensitivities of  $\Delta m(t_{sub})$  to the parameters  $K_V$ ,  $R_{p_0}$  and  $R_{p_1}$  respectively and were estimated using a first order Taylor expansion:

$$\frac{\partial \Delta m(t_{sub})}{\partial \varphi_i} = \frac{\Delta m(t_{sub})(\varphi_i + \delta) - \Delta m(t_{sub})(\varphi_i)}{\delta} \quad \text{Equation III.4.10}$$

where  $\varphi_i$  represents each considered parameter ( $K_V$ ,  $R_{p_0}$  or  $R_{p_1}$ ) and  $\delta$  an increment equal to 5 % of  $\varphi_i$ . **Equation III.4.10** was solved as follow. Firstly, **Equations III.4.1-6** were used to calculate the mass flow rate by considering the mean value of  $R_{p_0}$  and  $R_{p_1}$  previously determined using the PRT method, and the  $K_V$  value calculated as proposed by Scutellà *et al.* (Scutellà *et al.*, 2017a) Then, the term  $\Delta m(t_{sub})$  was calculated by integrating the mass flow rate over time  $t_{sub}$  (sublimation time). The calculation was repeated considering the  $i$ -parameter incremented by  $\delta$ . The sensitivity terms obtained for each of the considered parameters were used in **Equation III.4.9** to calculate the standard deviation of  $R_{p_1}$  based on the gravimetric method (named  $\widetilde{R}_{p_1}$ ). The intra-batch standard deviation of  $K_V$  ( $\widetilde{K}_V$ ) was considered as mainly due to the vial bottom geometry and determined as proposed by Scutella *et al.* (Scutellà *et al.*, 2017a) (**Table III.4.1**). The least important term, namely the standard deviation of  $R_{p_0}$ , was taken into consideration to be approximately equal to  $\widetilde{R}_{p_0}$ , previously determined using the PRT method. Finally, normally distributed random values of  $R_{p_0}$  and  $R_{p_1}$  were used in **Equation III.4.5** to calculate the product resistance distribution for a given  $l_d$ . The software Matlab R2014b equipped with the Statistics Toolbox (The MathWorks, Inc., Natick, MA) was used to perform the calculations.

#### Evaluation of the product temperature $T_{BV}$ distributions

In order to assess the impact of the product resistance variability on the final product quality, distributions of the product temperature  $T_{BV}$  were calculated at a given  $l_d$  from the previously determined  $R_p$  distributions using **Equations III.4.1-4**. For this calculation,  $K_V$  was set equal to its

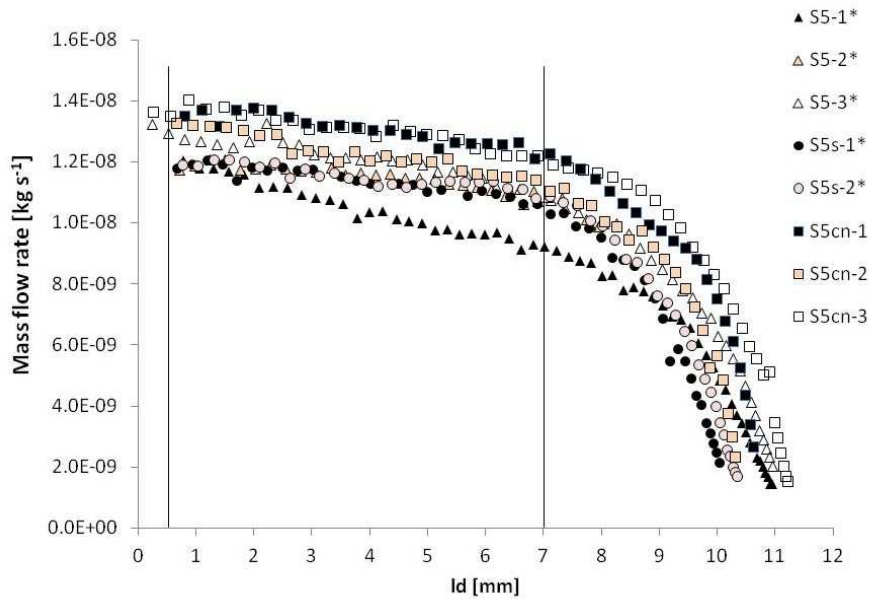


**Figure III.4.4:** Mass flow rates evolution in function of the dried thickness in freeze-drying tests of 5 % sucrose solution processed in vials without stoppers and spontaneous nucleation (S5, triangles), with partially inserted stoppers and spontaneous nucleation (S5s, circles) and without stoppers and controlled nucleation (S5cn, squares). The mass flow rates were determined by PRT method from **Equations III.4.7**. The solid lines represents the mass flow rates data range not affected by underestimation due to the PRT method and further considered in the analysis. Experiments marked with \* in the legend did not show a significant difference at 0.05 level (based on ANOVA tests).

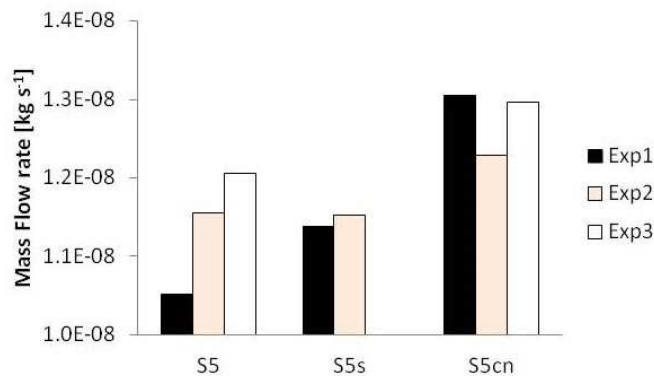


**Figure III.4.5:** Average values of the mass flow rates within a range of dried layer thickness between 0.5 mm and 7 mm in case of product in vials processed without stoppers and spontaneous nucleation (S5), with partially inserted stoppers and spontaneous nucleation (S5s) and without stoppers and with controlled nucleation (S5cn).

mean value. Chi-square goodness-of-fit tests were performed on the product temperature distributions, to verify that the simulated data were compatible with a normal distribution at a 0.05 significance level.

## RESULTS AND DISCUSSION

### Effect of the stopper and of the freezing protocol on the mass flow rate

**Figure III.4.4** shows the mass flow rates evolution with dried layer thickness  $l_d$  determined by PRT method for batches of vials processed with and without stoppers and frozen following two different protocols (spontaneous and controlled nucleation). The mass flow rate decreased as the dried layer thickness increased. However, at a dried layer thickness of about 7 mm, the mass flow rate started to decrease dramatically. This type of behavior of PRT data was previously reported in literature and was ascribed to batch heterogeneity (Fissore *et al.*, 2010). The vials in the batch completed sublimation progressively at different times, whereas a constant number of sublimating vials was continuously considered during the data analysis ( $N_V$  in **Equation III.4.7**).

**Figure III.4.5** reports the average values of the mass flow rate during sublimation (between dried layer thickness of 0.5 mm and 7 mm; total layer is of 10 mm) for each freeze-drying cycle performed with and without partially stoppered vials and with and without controlled nucleation during the freezing step. ANOVA test performed at 0.05 significance level did not revealed a significant difference among mass flow rates in cycles S5s and S5, carried out with and without partially stoppered vials. The presence of the stoppers on the vials did not appear to add a significant resistance to the mass transfer from the ice-vapour interface to the chamber. This finding is in agreement with an earlier work of Pikal *et al.* (Pikal *et al.*, 1984), who quantified the relative importance of the stopper resistance to about 3-10 % of the total mass transfer resistance, which is small compared to the product resistance (80-90 %). Conversely, ANOVA test performed at 0.05 significance level showed a significant difference among mass flow rates in cycles S5s and S5cn.

The mass flow rate resulted to be significantly higher in cycles in which ice nucleation was controlled during the freezing step (S5cn) than in the cycles in which ice nucleation was spontaneous (S5 and S5s).

As expected, the nucleation temperature  $T_n$  estimated from the thermocouple signals was found to be  $-4.12 \pm 0.36$  °C (coefficient of variation of 9 %), for cycles S5cn processed with controlled nucleation. Similarly, the nucleation temperature resulted to be  $-4.39 \pm 2.02$  °C in cycles S5 and S5s (coefficient of variation of about 45 %) processed with spontaneous nucleation. However, spontaneous nucleation is often reported to take place at temperature lower than  $-7$  °C (Konstantinidis *et al.*, 2011; Searles *et al.*, 2001b).

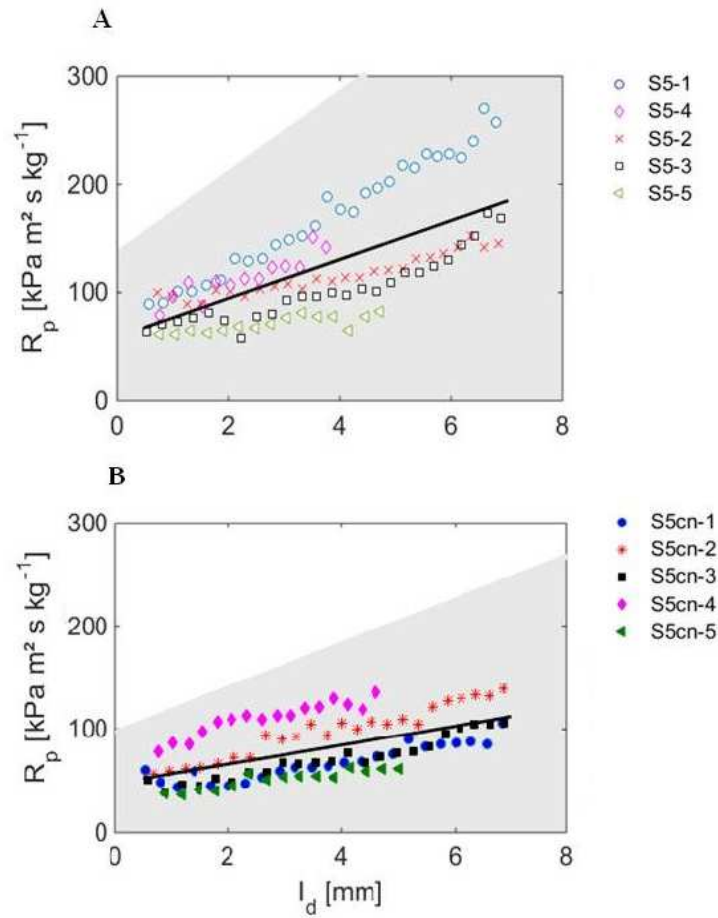


**Figure III.4.6:** Evolution of the product resistance with the dried layer thickness calculated from PRT data obtained in tests S5 performed with spontaneous nucleation (Figure A) and PRT data obtained in tests S5cn performed with controlled nucleation (Figure B). The grey area represents the range of  $R_p$  values considering the standard deviations of  $R_{p_0}$  and  $R_{p_1}$  (positive values only). Symbols: experimental data; Solid line: fitting of the experimental data with **Equation III.4.5**.

**Table III.4.3:** Mean  $\pm$  standard deviation (SD) for the sets of coefficients  $R_{p_0}$  and  $R_{p_1}$  (**Equation III.4.5**) from data of cycles S5 and S5cn.

Set of parameters	Pressure rise test				Gravimetric method	
	$R_{p_0}$ [ $\text{kPa s m}^2 \text{kg}^{-1}$ ]		$R_{p_1}$ [ $\text{kPa s m kg}^{-1}$ ]		$R_{p_1}$ [ $\text{kPa s m kg}^{-1}$ ]	
	Mean	$\frac{SD}{\overline{R_{p_0}}}$	Mean	$\frac{SD}{\overline{R_{p_1}}}$	Mean	$\frac{SD}{\overline{R_{p_1}}}$
S5	59	75	$1.8 \cdot 10^4$	$2.0 \cdot 10^4$	$1.8 \cdot 10^4$	$0.3 \cdot 10^4$
S5cn	47	48	$0.9 \cdot 10^4$	$1.2 \cdot 10^4$	$0.9 \cdot 10^4$	$0.2 \cdot 10^4$

In the present work, high nucleation temperature in uncontrolled vials was probably due to the high particulate level present in the laboratory environment and to the presence of the thermocouples into the monitored vials, which acted as nucleating agent. However, the coefficient of variability was significantly higher in cycles in which the nucleation was not controlled (S5+S5s). The high variability of the nucleation temperature may result in heterogeneous product structure and increased variability in mass flow rates between vials of the same or different batches.

#### Determination of the product resistance variability

The present analysis characterized the differences in mass transfer among 8 batches performed at pilot scale, constituted of about 200 vials each. However, manufacturing freeze-dryer often reach a capacity of 100,000 vials. The evaluation of the mass transfer variability within a batch of this size represents a real challenge. In the present work, the intra-batch mass transfer variability within a manufacturing batch was estimated by combining product resistance data from replicates of small batches processed in a laboratory scale freeze-dryer with and without controlled nucleation. To this end, the PRT method was used for the determination of the variability of the product resistance evolution with the dried layer thickness among laboratory scale batches. Finally, the gravimetric method was used to evaluate the inter-vial mass transfer variability of laboratory scale batch at a given time. The mass flow rate evolution with the dried layer thickness obtained using the PRT method in cycles performed with and without controlled nucleation (S5 and S5cn) were used to calculate the product resistance  $R_p$ . Five replicates of each condition were performed. The evolutions of  $R_p$  with the dried layer thickness  $l_d$  are presented in **Figure III.4.6**. The product resistance linearly increased with the dried layer thickness, regardless of the freezing protocol applied.

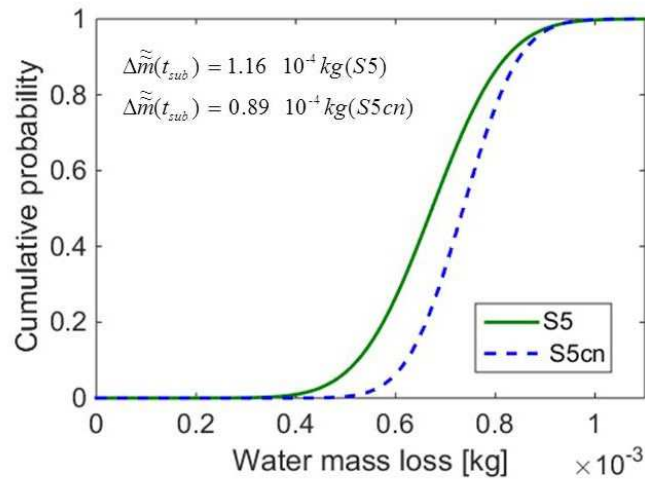
**Equation III.4.5** was then used to fit the product resistance data obtained from cycles S5 performed with spontaneous nucleation (**Figure III.4.6A**), and from cycles S5cn performed with controlled nucleation (**Figure III.4.6B**). The obtained value and standard deviation of two sets of parameters  $R_{p_0}$  and  $R_{p_1}$  are reported in **Table III.4.3**. Both the parameters  $R_{p_0}$  and  $R_{p_1}$  exhibited higher values and also higher standard deviations for cycles performed with spontaneous nucleation (data set S5) than for cycles performed with controlled nucleation (data set S5cn).

The determined value of  $R_{p_0}$  appeared to be of the same order of magnitude of previously reported values for sucrose-based model formulation (e.g.,  $51.2 \text{ kPa m}^2 \text{ s kg}^{-1}$  (Mortier *et al.*, 2016) and  $10 \text{ kPa m}^2 \text{ s kg}^{-1}$  (Pisano *et al.*, 2013), whereas  $R_{p_1}$  appeared to be lower than the value determined by Pisano *et al.* (Pisano *et al.*, 2013) ( $1.65 \cdot 10^5 \text{ kPa m}^2 \text{ s kg}^{-1}$ ).

**Table III.4.4:** Comparison of the product resistance value  $R_p$  obtained in this study with other reported in literature for a 5 % sucrose solution and a dried layer thickness of 5 mm.

Reference	Nucleation	Primary drying conditions	$R_p$ at $l_d = 5$ mm [kPa m <sup>2</sup> s kg <sup>-1</sup> ]
This work	Spontaneous	Performed at a shelf temperature of -25 °C and a chamber pressure of 10 Pa	149
	Controlled at -4 °C		92
(Konstantinidis <i>et al.</i> , 2011)	Spontaneous	Slow shelf ramping from -35 °C to -10 °C at 0.02 °C min <sup>-1</sup> , and chamber pressure of 13 Pa	125
	Controlled at -3 °C		91
(Bosca <i>et al.</i> , 2013)	Spontaneous	Performed at a shelf temperature of -20 °C and a chamber pressure of 10 Pa	145
(Rambhatla <i>et al.</i> , 2004) <sup>a</sup>	Controlled at -1 °C	Performed at a shelf temperature of -25 °C and a chamber pressure of 13 Pa	67
	Controlled at -6 °C		77
	Controlled at -11 °C		96
(Fissore and Pisano, 2015)	Spontaneous	Performed at a shelf temperature of -30 °C and a chamber pressure of 5 Pa	About 100

<sup>a</sup> Method II (improved ice fog technique)

**Figure III.4.7:** Cumulative probability of the water mass loss determined from data obtained by using the gravimetric method in cycles performed with spontaneous nucleation (S5, dotted line) and controlled nucleation (S5cn, dashed line). The standard deviation of the mass loss for the two sets of data is reported on the figure.

The range of  $R_p$  values defined by the determined standard deviations of  $R_{p_0}$  and  $R_{p_1}$  for different dried layer thicknesses is represented by the grey area in **Figure III.4.6** (positive values only). Furthermore, **Table III.4.4** compares the average value of the product resistance calculating by using **Equation III.4.5** at a dried layer thickness of 5 mm with value reported in literature, for the conditions considered (S5 and S5cn). Regardless the freezing protocol, the determined average value of  $R_p$  appeared to be in agreement with the other values reported and in particular with the  $R_p$  value reported by Bosca et al. (Bosca *et al.*, 2013) for spontaneous nucleation and with the  $R_p$  value reported by Konstantinidis et al. (Konstantinidis *et al.*, 2011) for controlled nucleation.

The gravimetric method was then used to evaluate the variability of the mass loss at a given time among vials for two replicates of cycles performed with and without controlled nucleation. The distributions of  $\Delta m(t_{sub})$  are reported in **Figure III.4.7**, as well as the standard deviation values of the mass loss  $\Delta \tilde{m}(t_{sub})$ . For product processed with controlled nucleation,  $\Delta \tilde{m}(t_{sub})$  appeared to be lower than in case of product processed with spontaneous nucleation. The values of  $\Delta \tilde{m}(t_{sub})$  determined from data obtained in cycles S5 and S5cn were then used in **Equation III.4.9** to calculate the value of standard deviation of  $R_{p_1}$  based on the gravimetric method ( $\tilde{R}_{p_1}$ ), which is reported in **Table III.4.3**.

The standard deviation  $\tilde{R}_{p_1}$  based on the gravimetric method represents about 15-20 % of the corresponding mean value of  $R_{p_1}$  which is comparable to the 10-25 % reported in the literature (Pisano *et al.*, 2013; Mortier *et al.*, 2016). Other studies often consider a 10 % variability for  $R_p$  (Bosca *et al.*, 2013; Giordano *et al.*, 2011; Pisano *et al.*, 2013). However, this standard deviation  $\tilde{R}_{p_1}$  based on the gravimetric method is representative of the variability in a small batch of about 100 vials. It was found to be about 5 to 6 times lower than the standard deviation  $\tilde{R}_{p_1}$  based on the PRT method, which was assumed representative of larger batches with several shelves loaded with vials and especially of the stochastic nature of spontaneous nucleation. For the following analysis of product temperature distribution, this larger variability based on  $\tilde{R}_{p_0}$  and  $\tilde{R}_{p_1}$  was used since it could better reflect the lack of homogeneity at manufacturing scale.

The value and standard deviation of the model parameters  $R_{p_0}$  and  $R_{p_1}$  determined by PRT method for cycles carried with and without controlled nucleation was then used to evaluate the distribution of the product resistance. The obtained cumulative distributions of  $R_p$  are shown in **Figure III.4.8** for a chamber pressure of 10 Pa and a shelf temperature of -25 °C.

Product processed during the freezing step with spontaneous (**Figure III.4.8A**) and controlled nucleation (**Figure III.4.8B**) were considered. Furthermore, two values of dried layer thickness  $l_d$  were simulated, 1 mm and 5 mm (total product thickness equal to 10 mm).

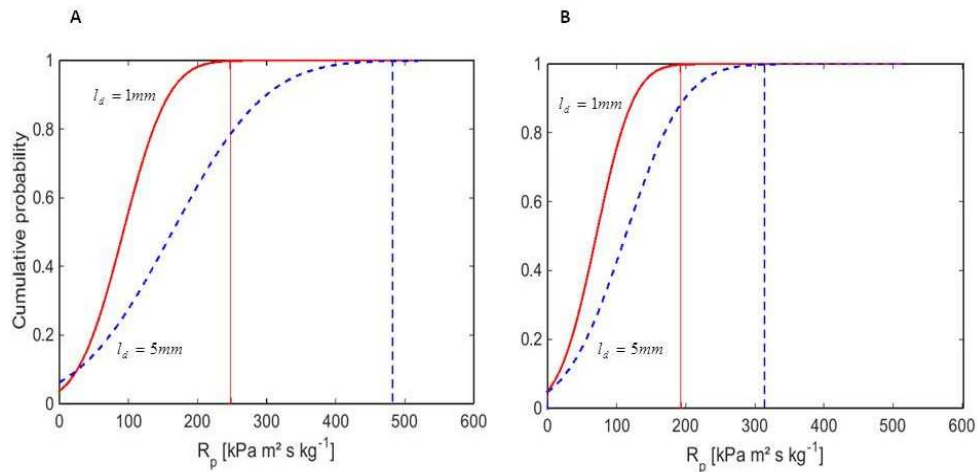


**Figure III.4.8:** Cumulative distributions of the product resistance obtained from the set of parameters S5 (Figure A) and S5cn (Figure B). Solid and dotted bold lines represent respectively the product resistance distribution at 1 mm and 5 mm. Solid and dotted thin lines includes approximately 99 % of values of the product resistance.

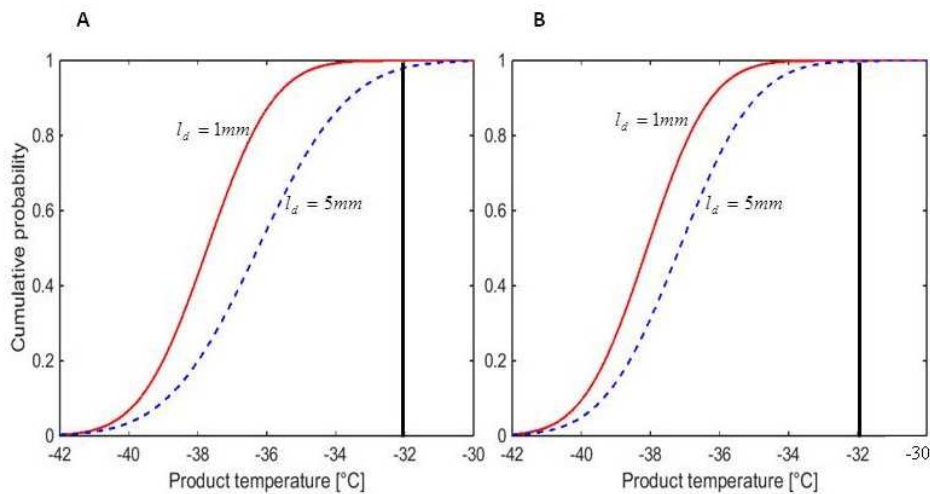


**Figure III.4.9:** Cumulative distributions of the product temperature obtained for freeze-drying cycles carried out with spontaneous nucleation (**Figure III.4.9A**) and without controlled nucleation (**Figure III.4.9B**). Solid and dotted lines represent the product resistance distribution at 1 mm and 5 mm respectively.

The results showed that the range of the product resistance values (calculated considering  $\pm 3$  times the SD limited to positive values, that includes approximately 99 % of the vials) significantly increased with  $l_d$ . In particular, product resistance values can be defined in a range of about  $\pm 160$  kPa s m<sup>2</sup> kg<sup>-1</sup> at 1 mm and of about  $\pm 320$  kPa s m<sup>2</sup> kg<sup>-1</sup> at 5mm for product processed with spontaneous nucleation (**Figure III.4.8A**, calculated considering  $\pm 3$  times the SD limited to positive values), and from  $\pm 119$  kPa s m<sup>2</sup> kg<sup>-1</sup> at 1 mm to about  $\pm 200$  kPa s m<sup>2</sup> kg<sup>-1</sup> at 5mm for product processed with controlled nucleation (**Figure III.4.8B**; calculated considering  $\pm 3$  times the SD limited to positive values).

#### **Impact of the product resistance variability on the product temperature distribution**

In order to optimize the primary drying step while maintaining an acceptable product quality, the product temperature has to be maintained close but below a critical value (e.g., glass transition temperature for amorphous product). The mass transfer heterogeneity due to differences in the product resistance among vials causes variability in the product temperature within the same batch or in different batches. Considering a constant value of the vial heat transfer coefficient (reported in **Table III.4.2**), the distributions of the product temperature due to the variability of the product resistance alone were calculated as reported in **Theory and data analysis**. Product resistance distributions previously determined for a 5 wt/wt sucrose solution processed with and without controlled nucleation and at -25 °C and 10 Pa during sublimation were considered, as shown in **Figure III.4.8**. Product temperature distributions were determined for two different dried layer thickness, i.e., 1 mm and 5 mm and are reported in **Figure III.4.9**. As expected, the value of product temperature increased at higher dried layer thickness, because of the higher product resistance value. Variability of the product temperature due to the product resistance distribution alone was estimated as  $\pm 3$  times the SD and was found to be approximately  $\pm 4.5$  °C at 1 mm and  $\pm 6$  °C at 5 mm for spontaneous nucleation (**Figure III.4.9**). If the controlled nucleation is used, the variability is  $\pm 4.5$  °C at 1 mm and  $\pm 5$  °C at 5 mm (**Figure III.4.9B**). This safety margin for the product temperature is significantly higher than the one estimated by Scutellà et al. (Scutellà *et al.*, 2017a), due to the inter-vial  $K_V$  variability in central vials, which was reported to be about  $\pm 1$  °C. Furthermore, previous works (Bosca *et al.*, 2015; Pisano *et al.*, 2013) reports product temperature margins due to the combined effect of the heat and mass transfer variability close to  $\pm 3$  °C, which is lower than the one estimated in this study.

Based on this analysis, the risk of failure of the process can be estimated. As example, considering the glass transition temperature of the sucrose (-32 °C), a 2 % of the vials processed with spontaneous nucleation will present a temperature higher than the critical value at a dried layer thickness of 5 mm (**Figure III.4.9**). Conversely, no vials processed with controlled nucleation will

present a temperature higher than the critical value. In order to assure that all the vials will present a temperature lower than the critical one, the shelf temperature should be reduced at about -28 °C (for a constant pressure of 10 Pa).

## CONCLUSIONS

The product resistance highly affects the value of the product temperature during the freeze-drying cycles. Thus, the value and variability of this parameter needs to be precisely evaluated for a reliable prediction of the product temperature. In this work, an original approach was proposed to estimate the variability of the product resistance by using two experimental methods, the pressure rise test and the gravimetric method. The impact on the mass transfer of the presence of the stoppers into the vial necks and of the freezing protocol was also considered. The presence of stoppers on the vials was not found to significantly modify the mass flow rate during sublimation. In contrast, the use of controlled nucleation during the freezing step of the freeze-drying cycle increased the mass flow rate with respect to cycles carried out with spontaneous nucleation and decreased its variability.

Then, product resistance data from 5 laboratory vial batches obtained using the pressure rise test were combined to estimate the product resistance variability in a manufacturing vial batch, which was expressed in terms of standard deviation of the parameters  $R_{p_0}$  and  $R_{p_1}$ . The standard deviations of  $R_{p_0}$  and  $R_{p_1}$  determined using the PRT method in batches processed with controlled nucleation resulted to be lower than the variability of the resistance in batch processed with spontaneous nucleation. Furthermore, the gravimetric method was used to estimate the variability of the product resistance between vials within a laboratory batch, which was found to be several times lower than the one obtained from the PRT method. The product resistance distributions determined from the PRT method was used to calculate the product temperature distributions, which resulted in a definition of a safety margin of about  $\pm 5$  °C. In order to assure the robustness of the method, an additional validation for the estimation of product resistance variability at manufacturing scale will be performed in the future.

Finally, as an example of practical application, the presented approach was used for the evaluation of the risk of failure of the process due to the mass transfer variability only, expressed as a percentage of potential vials showing a product temperature higher than the critical value. The proposed approach will be used in future works to investigate the variability of the product resistance among vials presenting low filling volume (e.g., 0.4-0.5 ml) and processed with spontaneous nucleation in environmental conditions similar to those of production scale GMP (i.e., less presence of particle in the air).

**ACKNOWLEDGMENTS**

The authors would like to thank Yves Mayeresse and Benoit Moreau (GSK Vaccines) for reviewing this work.

**CONFLICT OF INTEREST**

Erwan Bourlès is an employee of the GSK group of companies. Bernadette Scutellà participated in a postgraduate Ph.D. program at GSK Vaccines. Stephanie Passot, Fernanda Fonseca, and Ioan Cristian Trelea report no financial conflicts of interest.

**FUNDING**

This work was funded by GlaxoSmithKline Biologicals S.A., under a Cooperative Research and Development Agreement with INRA (Institut National de la Recherche Agronomique) via the intermediary of the UMR (Unité Mixte de Recherche) GMPA (Génie et Microbiologie des Procédés Alimentaires) at the INRA Versailles-Grignon research centre.

**AUTHORS CONTRIBUTIONS**

Bernadette Scutellà acquired the data. Bernadette Scutellà, Stephanie Passot, Erwan Bourlès, Fernanda Fonseca and Ioan Cristian Trelea analyzed and interpreted the experimental results. All authors were involved in drafting the manuscript or revising it critically for important intellectual content. All authors had full access to the data and approved the manuscript before it was submitted by the corresponding author.

### III.4.3 Take-home message

- The presence of the stopper on the vial neck did not strongly influence the mass flow rate during sublimation. In contrast, mass transfer resulted to be greatly influenced by the freezing protocol.
- The pressure rise test and the gravimetric method were used to evaluate the variability of the product resistance among vials (in terms of standard deviations of the product resistance parameters). The product resistance variability obtained by using the pressure rise test method was significantly higher than the one obtained by using the gravimetric method.
- The determined product resistance distribution led to the definition of a product temperature safety margin of about  $\pm 5$  °C, to be considered during the cycle design and scale-up.

The stochastic nature of nucleation in the freezing step leads not only to different dimensions of the pores between vials, but also to different specific surface areas of the product available for desorption of the remaining unfrozen water during secondary drying. The importance of the desorption kinetics variability on the heterogeneity of the product moisture content will be analyzed in **Paper III.5**.





### III.5 Can the desorption kinetics explain the residual moisture content heterogeneity observed in pharmaceuticals freeze-drying process?

The present study was object of an oral presentation at the *Eurodrying Conference 2017* (Liegi) and it was submitted for the *Eurodrying* special issue of the *Drying Technology* journal.

#### III.5.1 Context and objectives

During the freezing step, only a part of the water is frozen in form of ice crystals and removed by sublimation during primary drying. A small fraction of the water is bound to the interstitial matrix and removed by desorption during secondary drying. During the design of the secondary drying step, the shelf temperature and the operating time need to be selected in order to target the desiderate value of residual moisture content. The residual moisture content in the final product is one of the most important critical quality attribute of the freeze-dried vaccines and pharmaceuticals, as it influences the storage stability, the potency and shelf life of the product, and thus it has to be carefully controlled. However, a significant moisture content variability is often observed in the industrial practice between vials processed within the same batch. Understanding the mechanisms responsible for the moisture content distribution in the vial batch could help to perform the design of the secondary drying step.

#### Objective

In the present work, the desorption model proposed by Trelea et al. (Trelea *et al.*, 2016) was used (i) to evaluate the impact of the product temperature and structure on the desorption kinetics and (ii) to assess the importance of the desorption kinetics on the moisture content heterogeneity during the secondary drying step of freeze-drying process.



## III.5.2 Paper

### TITLE

Can the desorption kinetics explain the residual moisture content heterogeneity observed in pharmaceuticals freeze-drying process?

### SHORT TITLE

Model of desorption kinetics in freeze-drying

### AUTHORS

B. Scutellà<sup>1,2</sup>, E. Bourlès<sup>2</sup>, C. Tordjman<sup>1</sup>, F. Fonseca<sup>1</sup>, Y. Mayeresse<sup>3</sup>, I.C. Trelea<sup>1</sup>, S. Passot<sup>1</sup>

### AFFILIATIONS

<sup>1</sup> *UMR GMPA, AgroParisTech, INRA, Université Paris Saclay, 78850 Thiverval-Grignon, France*

<sup>2</sup> *GSK Vaccines, Rixensart, Belgium*

<sup>3</sup> *GSK Vaccines, Wavre, Belgium*

### ABSTRACT

Residual moisture is an important factor for the long-term stability of freeze-dried biopharmaceuticals. Significant moisture content heterogeneity is often reported within a batch of vials. This work aimed at investigating the role of the desorption kinetics on the moisture content variability in freeze drying. In this regard, the evolution of the moisture content of a sucrose formulation with time was experimentally determined for different product temperatures and structures. Then, the value and variability of the characteristic desorption times were assessed and included in a mathematical model in order to predict the final moisture content distribution in secondary drying at specific operating conditions.

### KEYWORDS

Lyophilisation, mathematical modelling, Karl-Fisher analysis, moisture content, controlled nucleation

**NOMENCLATURE**

$a_w$	Water activity ( $Pa Pa^{-1}$ )
$C, K$	GAB model parameters
$E_a$	Activation energy ( $kJ mol^{-1}$ )
$R$	Constant of ideal gas ( $kJ mol^{-1} K^{-1}$ )
$T_p$	Product temperature ( $K$ )
$t$	Current time ( $s$ )
$X$	Moisture content ( $kg kg^{-1} wb$ )

**Greek letters**

$\sigma_{meas}$	ncertainty of the measurement method ( $kg kg^{-1} wb$ )
$\tau$	Characteristic desorption time ( $s$ )

**Subscript and Superscripts**

$eq$	Equilibrium
$IN$	Initial (beginning of isothermal period during secondary drying)
$m$	Monolayer
$ref$	Reference

## INTRODUCTION

Freeze-drying (lyophilisation) is a drying operation widely used for stabilization of heat sensitive biological materials and pharmaceuticals, such as vaccines (Sadikoglu *et al.*, 2006; Hansen *et al.*, 2015). This process involves three successive steps: (i) freezing, to completely solidify the product, (ii) primary drying, in which the frozen water is removed by sublimation under vacuum and (iii) secondary drying, in which unfrozen water is removed by desorption (Jennings, 1999; Adams, 1991). Usually, primary drying is considered the most critical and longest step of the process. However, secondary drying governs one of the most important critical product quality attribute, the residual moisture content, which influences the product storage stability and shelf life (Pikal *et al.*, 1990; Passot *et al.*, 2012; Pikal *et al.*, 1991; Trelea *et al.*, 2016; Oddone *et al.*, 2017). Targeting the desiderate value of final product moisture content and its homogeneity in the batch is a very important quality control tool. However, monitoring the desorption kinetic during secondary drying may be a difficult task, due to the limited availability of technical solutions to measure the moisture content evolution in a non invasive way (Fissore *et al.*, 2011b; Schneid *et al.*, 2011). In this regards, mathematical modelling can be useful for the prediction of the moisture content evolution during the process. Most of the works in freeze-drying research have been devoted to optimization of primary drying, and few models are available in literature for the secondary drying (Trelea *et al.*, 2016; Sadikoglu and Liapis, 1997; Sahni and Pikal, 2017; Trelea *et al.*, 2007; Mayeresse, 2008; Sadikoglu *et al.*, 1998). Usually, a first order desorption kinetics is used to describe moisture content evolution in secondary drying (Sheehan and Liapis, 1998; Pisano *et al.*, 2012), but recently Sahni et al. (Sahni and Pikal, 2017) proposed a diffusion-like fractional order model and Trelea et al. (Trelea *et al.*, 2016) developed a dynamic model for desorption that accounts for monolayer and multilayer water state in the solid matrix, with very different desorption kinetics. Moreover, even if existing desorption models are able to predict the evolution of the average moisture content during the process, they do not give its distribution within the vial batch. Consequently, understanding the mechanisms leading to moisture content heterogeneity appears as a key point for ensuring reproducible final product quality and long-term stability.

The main objective of this work was to assess and quantify the effect of the desorption kinetics on the product moisture content distribution in secondary drying. The desorption kinetics of a sucrose formulation was studied at various product temperatures, by testing three different shelf temperatures (0 °C, 20 °C, 40 °C). Ice crystal size was modulated by adding the nucleation agent Snomax, an active protein derived from *Pseudomonas Syringae*, to the product formulation. Moisture content variability at different times during the process was determined by stoppering selected sets of vials. Then, the variability of the characteristic desorption time in a set of vials was calculated, and it was used to quantify the contribution of desorption kinetics to the moisture content distribution.

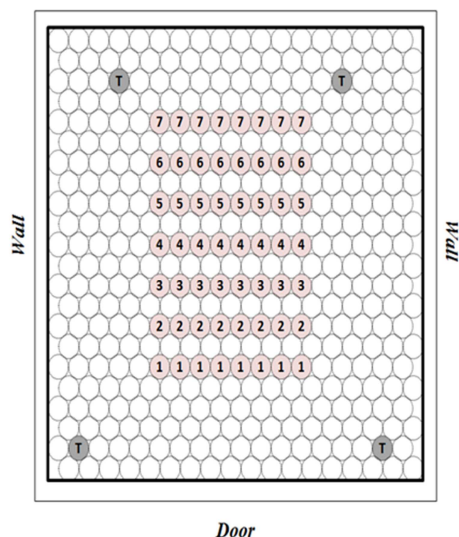


**Figure III.5.1:** Arrangement of the vials on the shelf. Numbered circles represent the vials in which the stoppers were inserted into the vial necks progressively from the end of the equilibration step to the end of the secondary drying. Vials in which the thermocouples were inserted are marked with the letter T.

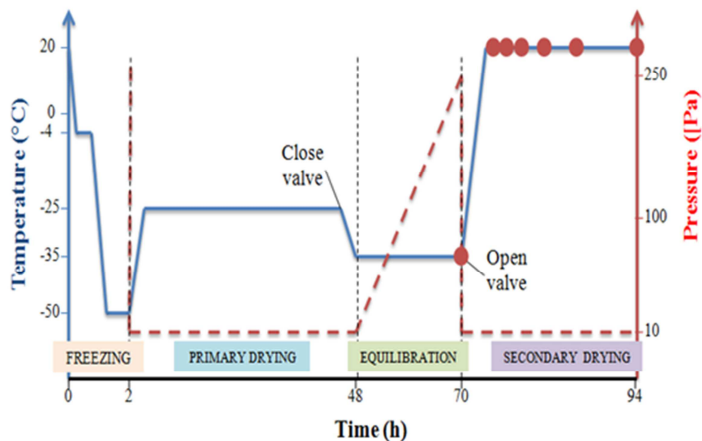


**Figure III.5.2:** Example of temperature and pressure profiles of a freeze-drying cycle with controlled nucleation, indicating stoppering and sampling times (red dots). Blue solid line represents shelf temperature (20 °C during secondary drying in this illustration), red dashed line represents chamber pressure.

Finally, as example of practical application, our approach was used to predict the risk of failure of the secondary drying step at fixed operating time and shelf temperature, expressed in terms of percentage of vial with a moisture content higher than the target value.

## MATERIALS AND METHODS

### Materials

A 5 % sucrose solution was used throughout the tests, prepared with distilled water and crystalline sucrose (VWR Chemicals Prolabo, Leuven, Belgium). The solution was processed in 3 mL siliconized glass tubing vials (Müller+Müller, Holzminden, Germany) for the desorption kinetics experiments, or in 50 mm diameter aluminium containers for the measurement variability experiments. Freeze-drying experiments were carried out in a pilot scale freeze-dryer (Millrock REVO, Kingstone, NY, US) equipped with 3 shelves and a condenser connected with the drying chamber by a butterfly valve. Capacitance and a thermal conductivity (Pirani) gauges were used to monitor the pressure in the drying chamber. Product temperature was monitored during the process by inserting T-type miniature thermocouples in the bottom centre of four vials. A "sample thief" mechanism was installed on the door of the freeze-dryer chamber to stopper selected vials.

### Freeze-drying procedure

A number of 385 vials were arranged in hexagonal clusters in a bottomless tray as shown in **Figure III.5.1**. A stainless steel rail was used to fully shield the vials from the chamber walls. The acrylic door of the freeze-dryer was covered by aluminium foil to avoid additional radiation from the external environment. The vials were filled with 1.4 mL of 5 % sucrose solution, and elastomeric stoppers were partially inserted in the neck of selected vials (numbered vials in **Figure III.5.1**). The vials were then loaded in the middle shelf of the freeze-dryer by using a metallic tray, which was removed immediately after to allow direct contact between the vials and the shelf during the cycle. Firstly, the freezing step was performed by decreasing the shelf temperature from ambient temperature to -50 °C at about 3 °C/min and holding the vials at constant temperature for 2 h. In some experiments, ice nucleation was controlled by adding 0.1 % of the nucleation agent Snomax (Snomax LLC, Englewood, CO, US). In this case, the freezing protocol was performed in four successive steps, as shown in **Figure III.5.2**: (i) a shelf temperature ramp from ambient temperature to -4 °C at about 3 °C/min, (ii) a holding step at -4 °C for 1 h, (iii) a further shelf temperature ramp from -4 °C to -50 °C at about 3 °C/min and (iv) a holding step at -50 °C of 2 h. In all cases, the primary drying step was performed at 10 Pa and -25 °C until the end of ice sublimation, determined by comparative pressure measurement using capacitance and Pirani gauges (Passot *et al.*, 2009).

After complete sublimation of ice crystals, an equilibration step was introduced in the cycle in order to reduce the moisture content heterogeneity at the end of the primary drying, as previously proposed (Schneid *et al.*, 2011). This step consisted in closing the valve between the chamber and the condenser and holding the vials at -35 °C for about 22 h. Finally, after opening the valve to decrease pressure back to 10 Pa, the shelf temperature was increased at 1 °C/min and the secondary drying step was performed for a period of about 24 h. Three constant values of shelf temperature during the secondary drying were investigated in different runs: 0 °C, 20 °C and 40 °C. At defined moments during the secondary drying (red dots in **Figure III.5.2**), the stoppers were completely inserted into the neck of selected vials located in the centre of the shelf by using the sample thief (8 vials per sampling time). Residual moisture content in all these vials was determined after the cycle. Some of these vials were also analysed in order to evaluate the water activity in the product, for the sorption isotherm determination.

Furthermore, additional freeze-dried sucrose samples were prepared. A number of 20 aluminium containers were filled with 5 mL of 5 % sucrose solution and freeze-dried by applying the same parameters as the cycle presented in **Figure III.5.1** without the equilibration step.

The produced samples were then used for evaluation of Karl Fisher measurement variability, as described in the following.

#### **Water activity and moisture content measurement**

The water activity in selected vials was determined by using the FMS-moisture/pressure headspace analyzer (Lighthouse, Charlottesville, VA, US). This non-destructive method enabled the measurement of water vapour in the vial headspace, by using a laser tuned to match the internal absorption frequency of water molecules. The amount of laser light absorbed was proportional to the water vapour concentration.

The moisture content of the samples was measured by the Karl Fisher titration method using a Metrohm KF 756 apparatus (Villebon-sur-Yvette, France) as previously described (Passot *et al.*, 2012). The variability of the Karl Fisher method was determined by performing 20 moisture content measurements on freeze-dried sucrose samples equilibrated at a known water activity. Sample equilibration was performed by reducing in powder 20 g of the dried sucrose and then placing it in a hermetic glass box containing saturated salt solutions with water activities of 0.11 (LiCl), 0.22 (CH<sub>3</sub>COOK) and 0.32 (MgCl<sub>2</sub>.6H<sub>2</sub>O) for one week at 25 °C.

## **THEORY AND DATA ANALYSIS**

### **Sorption isotherm**

The equilibrium moisture content  $X^{eq}$  at a given water activity  $a_w$  was described using the

Guggenheim-Anderson-Boer (GAB) model (Passot *et al.*, 2012; Trelea *et al.*, 2016):

$$X^{eq} = \frac{X_m K C a_w}{(1 - K a_w)(1 + K a_w (C - 1))} \quad \text{Equation III.5.1}$$

where  $X_m$  is the monolayer moisture content, and  $C$  and  $K$  are shape parameters, both determined by fitting in a least-squares sense the experimental data. Calculations were performed with Matlab R2014b software equipped with the Statistics Toolbox (The Mathworks Inc., Natick, MA, US).

### Desorption model

In the present study, the model proposed by Trelea *et al.* (Trelea *et al.*, 2016), was used to describe the desorption kinetic in secondary drying. This model is based on the consideration that moisture contained in biological products may exist in different states, such as mono or multilayer, which are more or less bound to the solid matrix. Considering the presence of 2 layers (with 1=monolayer, 2=multilayer), the total moisture content  $X$  in the product can be defined as the sum of the fractions  $X_i$  contained in each layer:

$$X = X_1 + X_2 \quad \text{Equation III.5.2}$$

Furthermore, water in different states may show a different desorption kinetic. For the  $i$ -layer this gives:

$$\frac{dX_i}{dt} = \frac{1}{\tau_i} (X_i^{eq} - X_i) \quad \text{Equation III.5.3}$$

where  $\tau_i$  is respectively the characteristic desorption time and  $X_i^{eq}$  the equilibrium moisture content of the water in the  $i$ -layer, which is determined from the sorption isotherm for a given water activity as proposed by Trelea *et al.* (Trelea *et al.*, 2016). In steady state operating conditions (i.e., constant values of shelf temperature and vapour pressure), **Equation III.5.3** has the solution:

$$X_i(t) = X_i^{eq} + (X_i^{IN} - X_i^{eq}) e^{-\frac{t}{\tau_i}} \quad \text{Equation III.5.4}$$

with  $X_i^{IN}$  equal to the moisture content contained in the  $i$ -layer at the beginning of the isothermal period. The total initial moisture content  $X^{IN}$  present in the product fills up successive layers until a maximum value. The maximum moisture content of layer 1 was successfully assumed to be equal to



$X_m$  (Trelea *et al.*, 2016), determined from the GAB sorption isotherm (**Equation III.5.1**). Thus, if  $X^{IN}$  is lower or equal to  $X_m$ , moisture will be present in the product only as monolayer, whereas if  $X^{IN}$  is higher than  $X_m$  the presence of the multilayer needs to be taken into consideration in the desorption kinetics.

### Temperature dependence

The characteristic desorption time  $\tau$  was assumed to depend on the product temperature  $T_p$  through an Arrhenius type equation (J.H. de Boer, 1953):

$$\tau_i = \tau_{ref_i} e^{-\frac{E_a}{R} \left( \frac{1}{T_p} - \frac{1}{T_{p_{ref}}} \right)} \quad \text{Equation III.5.5}$$

where  $E_a$  is the activation energy,  $R$  is the ideal gas constant,  $\tau_{ref}$  is the characteristic desorption time at a reference temperature  $T_{p_{ref}}$  (273.15 K in this study). Average values of  $E_a$  and  $\tau_{ref}$  were evaluated by fitting in a least-squares sense experimental data obtained as described in **Materials and Methods** section by using the software Matlab R2014b.

### Determination of the characteristic desorption time variability

**Equation III.5.4** states that the moisture content value and variability in time is influenced by (i) the variability of the characteristics desorption times ( $\tilde{\tau}_i$ ), which depends on the desorption mechanism and (ii) the variability of the initial product moisture content ( $\widetilde{X^{IN}}$ ), influenced by the variability of heat and mass transfer in primary drying. Furthermore, uncertainty of the measurement method  $\tilde{\sigma}_{meas}$  may also affect the measured moisture content distribution. Based on a first order sensitivity analysis and assuming variability sources independent, the variance of the measured moisture content  $\widetilde{X(t)}^2$  can be expressed as:

$$\widetilde{X(t)}^2 = \sum_{i=1}^2 \frac{\partial X(t)}{\partial \tau_i} \tilde{\tau}_i^2 + \frac{\partial X(t)}{\partial X^{IN}} \widetilde{X^{IN}}^2 + \tilde{\sigma}_{meas}^2 \quad \text{Equation III.5.6}$$

where  $\frac{\partial X(t)}{\partial \tau_i}$  and  $\frac{\partial X(t)}{\partial X^{IN}}$  represents the sensitivity of  $X(t)$  to the characteristic desorption times and to the initial value of moisture content, which can be calculated from the proposed model (**Equations III.5.2- 5**) by using a first order Taylor expansion.

In the present study,  $\widetilde{X(t)}$ ,  $\widetilde{X^{IN}}$  and  $\tilde{\sigma}_{meas}$  were experimentally determined and used to calculate the standard deviations of the characteristic desorption times  $\tilde{\tau}_i$  from **Equation III.5.6**.

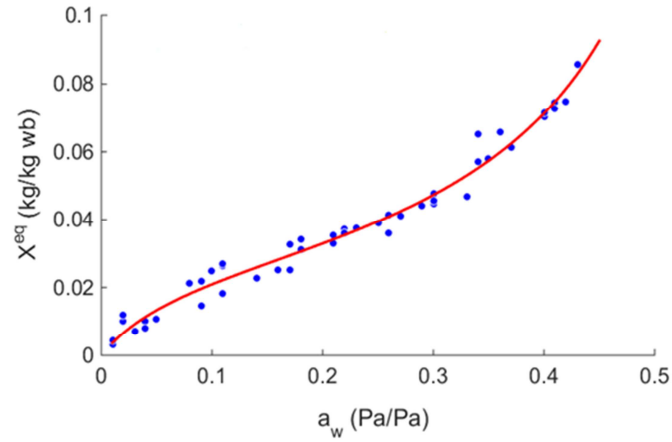


**Figure III.5.3:** Equilibrium moisture content of sucrose as a function of water activity. Symbols: experimental data, solid line: GAB model, **Equation III.5.1**.

**Table III.5.1:** Mean  $\pm$  standard error of the GAB model parameters (**Equation III.5.1**).

	<i>Value <math>\pm</math> Standard Error</i>
$X_m(kg\ kg^{-1}\ wb)$	$0.0278 \pm 0.0016$
$K$	$1.581 \pm 0.047$
$C$	$9.10 \pm 1.55$

Then, it was possible to quantify the impact of desorption kinetics on the moisture content distribution as well as the relative importance of the product temperature and structure by using the proposed model (**Equations III.5.2-5**).

## RESULTS AND DISCUSSION

### Sorption isotherm determination

**Figure III.5.3** shows the moisture content of sucrose as a function of the water activity. The GAB model (**Equation III.5.1**) fits the data satisfactorily. The value of the model parameters are reported in **Table III.5.1**. The parameters  $X_m$  and  $K$  shows an uncertainty of less than 6 % whereas the uncertainty of the shape parameter  $C$  remained large, since **Equation III.5.1** is less sensitive to this parameter. The obtained parameters are valid in the range of water activity 0-0.45.

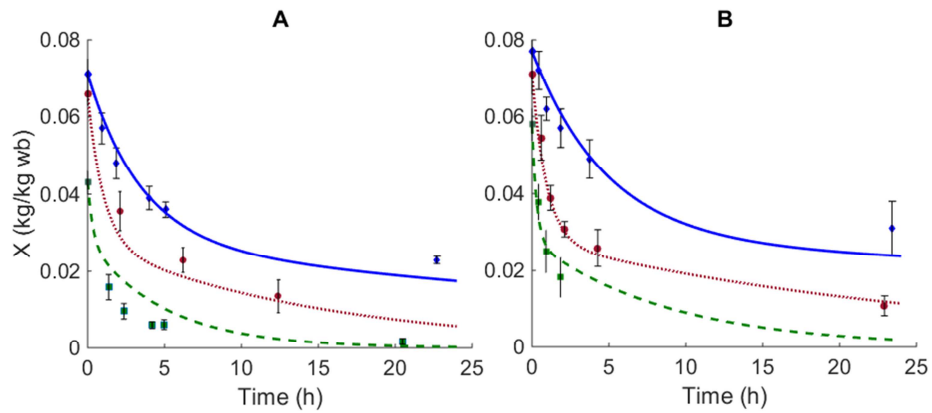


**Figure III.5.4:** Time evolution of moisture content for 5 % sucrose processed with uncontrolled (A) and controlled (B) nucleation at three shelf temperatures: 0 °C (blue solid line and diamonds), 20 °C (red dotted line and circles), 40 °C (green dashed line and squares). Symbols: experimental data, lines: multilayer model.

**Table III.5.2:** Characteristic desorption times at reference temperature and activation energy (mean  $\pm$  standard error) for product processed with uncontrolled and controlled nucleation.

	<i>Uncontrolled nucleation</i>	<i>Controlled nucleation</i>
$\tau_{\text{ref}_1}$ (h)	$56.39 \pm 15.61$	$149.88 \pm 60.89$
$\tau_{\text{ref}_2}$ (h)	$3.80 \pm 0.60$	$5.17 \pm 0.86$
$E_a$ (kJ mol <sup>-1</sup> )	$49.61 \pm 4.97$	

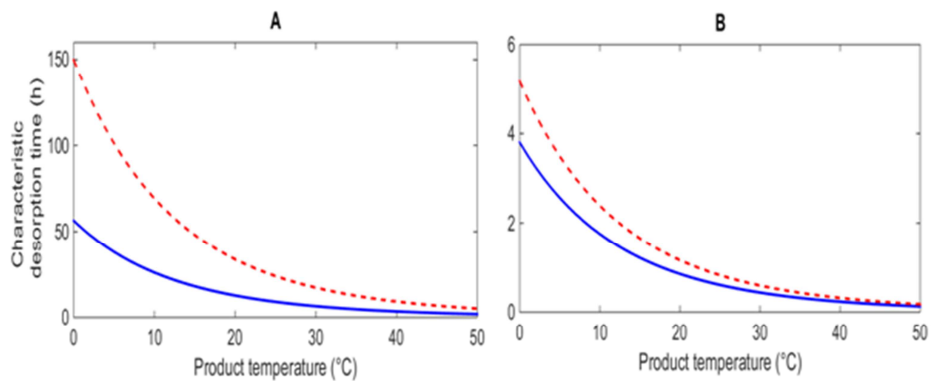


**Figure III.5.5:** Characteristic desorption times  $\tau_1$  (A) and  $\tau_2$  (B) in function of the product temperature for uncontrolled nucleation (solid line) and controlled nucleation (dotted line).

### Desorption kinetics

The moisture content values at the beginning of the isothermal period ( $X^{IN}$ ) were experimentally determined to be between 0.077 and 0.043 kg/kg in trials carried at shelf temperatures between 0 °C and 40 °C. These values appeared to be higher than the monolayer moisture content  $X_m$  (0.0278 kg/kg wb, **Table III.5.1**) and thus, the moisture was considered to be also present in the product as multilayer. The two layers model fits quite satisfactorily the experimental data, as shown in **Figure III.5.4**, especially in case of controlled nucleation. Two different drying kinetics, a fast initial one (roughly before 5 h) and a much slower subsequent one, are clearly visible and correspond respectively to the desorption of the multilayer (layer 2) and of the monolayer (layer 1). Determined desorption model parameters are reported in **Table III.5.2**. The characteristic desorption times for the mono and multilayer are quite different by a factor of almost 15 in case of uncontrolled nucleation and 30 in case of controlled nucleation. Furthermore, both  $\tau_{ref_1}$  and  $\tau_{ref_2}$  were found to be higher in case of controlled nucleation compared to uncontrolled nucleation.

It was found that a common value of activation energy for the two layers and for the product processed with and without controlled nucleation adequately described the desorption kinetics. The determined value of the activation energy was found to be slightly higher than previous reported values (Trelea *et al.*, 2016; Pisano *et al.*, 2012).

The obtained parameters were then used in **Equation III.5.5** to describe the dependence of the characteristic desorption time on the product temperature and structure, as presented in **Figure III.5.5**.

As previously reported (Trelea *et al.*, 2016; Pisano *et al.*, 2012), the increase of shelf temperature resulted in lower characteristic desorption times and thus in a faster desorption for both controlled and uncontrolled nucleation. In agreement with Trelea *et al.* (Trelea *et al.*, 2016), the characteristic desorption time for the monolayer (**Figure III.5.5A**) appears to be significantly higher than the multilayer (**Figure III.5.5B**). Furthermore, the kinetics of the uncontrolled nucleated product resulted to be faster than the controlled one. Controlled nucleation usually generates bigger ice crystals than uncontrolled nucleation, which results in a smaller specific surface area of the pores and in a slower desorption kinetics during secondary drying. This result points out that the desorption kinetics is highly dependent on both product temperature and structure, and its characterization is fundamental for the optimization of the secondary drying step.

**Table III.5.3:** Standard deviation of the characteristic desorption time at reference temperature for uncontrolled and controlled nucleation, calculated from **Equation III.4.6**.

	<i>Uncontrolled nucleation</i>	<i>Controlled nucleation</i>
$\overline{\tau_{\text{ref}_1}}$ (h)	12.40	46.50
$\overline{\tau_{\text{ref}_2}}$ (h)	0.83	1.60

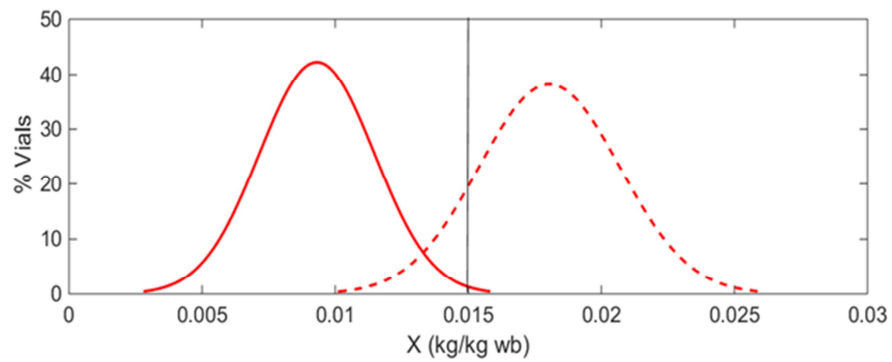


**Figure III.5.6:** Moisture content distribution after 15 h of desorption at a shelf temperature of 20 °C. Solid lines: uncontrolled nucleation; dotted lines: controlled nucleation.

### Desorption kinetics variability

The variability of the desorption kinetics was determined as standard deviation of the characteristic desorption times ( $\widetilde{\tau_{ref_1}}$  and  $\widetilde{\tau_{ref_2}}$ ) based on **Equation III.5.6**. In this analysis, the variability of moisture content value due to the Karl Fisher method ( $\tilde{\sigma}_{meas}$ ) was determined to be equal to 3.5 % (coefficient of variation) using 20 repeated measurements of samples equilibrated at different moisture contents. The calculated standard deviations of the parameters  $\tau_{ref_1}$  and  $\tau_{ref_2}$  for controlled and uncontrolled nucleation, shown in **Table III.5.3**, resulted to be quite comparable to the standard error of the parameters due to the fitting (**Table III.5.2**). This last value is higher because different sources of variability are mingled. The performed analysis can be used to simulate moisture content distributions at a specific time and shelf temperature and thus to estimate the importance of desorption kinetics on the success of the process for the selected operating variables. As example, **Figure III.5.6** shows the distributions of the moisture content after 15 h from the beginning of the isothermal period in secondary drying for a shelf temperature of 20 °C, in case of product processed with and without controlled nucleation. As an illustration, considering a target moisture content lower than e.g., 0.015 kg/kg wb in **Figure III.5.6**, the rejected vials will be about 1 % if uncontrolled nucleation is used. In contrast, due to the slower kinetics, the selected process time will not be sufficient to reach the target moisture content in most of the vials processed with controlled nucleation.

### CONCLUSIONS

Desorption in secondary drying was found to be influenced by the product temperature and structure. In particular, the desorption kinetics of both mono and multilayer appeared to be faster at higher shelf temperature and when nucleation was not controlled during the freezing step. The variance of the characteristic desorption times for mono and multilayer was estimated and used to predict the moisture content distribution in the vial batch for a fixed shelf temperature and operating time. The proposed approach can be used to perform a risk assessment-based design of the secondary drying step, by calculating the percentage of rejected vials with a final moisture content higher than the target value at specific operative conditions.

## **ACKNOWLEDGMENTS**

The authors would like to thank Benoit Moreau (GSK Vaccines) for reviewing this work and Olivier Despas (GSK Vaccines) for his help in the experimental work.

## **CONFLICT OF INTEREST**

Erwan Bourlès and Yves Mayeresse are employees of the GSK group of companies. Bernadette Scutellà participated in a postgraduate Ph.D. program at GSK Vaccines. Stephanie Passot, Fernanda Fonseca and Ioan Cristian Tréléa report no financial conflicts of interest.

## **FUNDING**

This work was funded by GlaxoSmithKline Biologicals S.A., under a Cooperative Research and Development Agreement with INRA (Institut National de la Recherche Agronomique) via the intermediary of the UMR (Unité Mixte de Recherche) GMPA (Génie et Microbiologie des Procédés Alimentaires) at the INRA Versailles-Grignon research centre.

## **AUTHORS CONTRIBUTIONS**

Bernadette Scutellà, Stephanie Passot, Erwan Bourlès, Fernanda Fonseca and Ioan Cristian Trelea were involved in the conception and the design of the study. Bernadette Scutellà and Cassandre Tordjman acquired the data. Bernadette Scutellà, Stephanie Passot, Erwan Bourlès, Fernanda Fonseca and Ioan Cristian Trelea analyzed and interpreted the experimental results. All authors were involved in drafting the manuscript or revising it critically for important intellectual content. All authors had full access to the data and approved the manuscript before it was submitted by the corresponding author.

### III.5.3 Take-home message

- The multilayer model of Trelea et al. (Trelea *et al.*, 2016) was used to describe the evolution of the moisture content in the product during desorption in secondary drying. Desorption of the monolayer, stronger bound to the product matrix, resulted to be much slower than the multilayer.
- The use of a higher shelf temperature during secondary drying led to a faster desorption of both mono and multilayer. Furthermore, desorption is product processed with controlled nucleation resulted to be slower than in product processed with uncontrolled nucleation.
- The variability of the characteristic desorption times for mono and multilayer was determined and used to predict the moisture content distribution in the vial batch for a fixed shelf temperature and operating time. Finally, thus original approach was used in the design of the secondary drying step to evaluate the risk of failure of the process (% of vials rejected).

The research conducted until now was focused on the understanding and quantification of the mechanisms responsible for the heat and mass transfer variability during primary and secondary drying, and thus causing heterogeneity in the final product quality. The next and last step of this Ph.D. project (presented in **Paper III.6**) will consist in the implementation of all the previously studied mechanisms responsible for heat and mass transfer variability in a multi-vial, dynamic mathematical model.



## III.6 Multi-vial, dynamic mathematical model to design freeze-drying process of pharmaceuticals through a risk-based approach

---

### III.6.1 Context and objectives

The ultimate aim of the application of the FDA's Quality by Design approach in freeze-drying is to obtain safe, effective and high quality pharmaceutical products. One of the most useful tool to pursue this goal is the design space, which is the multidimensional combination and interaction of input variables and process parameters leading to the target quality attributes within the vial batch under a controlled risk. Nowadays, construction of the design space is more and more often performed by using mathematical models, which are often based on average values of the model parameters (e.g., vial heat transfer coefficient, product resistance, characteristic desorption time). However, the work performed during this Ph.D. project (presented in **Papers III.1-5**) showed that several mechanisms are responsible for the heat and mass transfer variability during freeze-drying. These mechanisms were quantified and implemented into the mathematical model used to predict the variability of the product temperature, ice fraction and moisture content, for a more conscious selection of the operating conditions of freeze-drying cycles.

#### Objective

The aim of this work was to develop a multi-vial dynamic mathematical model of freeze-drying process, including all the previously analysed mechanisms responsible for heat and mass transfer variability (**Papers III.1-5**) during the process and thus for the product quality heterogeneity. The model was used to predict the product temperature, the ice fraction, and the moisture content evolution during the process for several vials in the batch, and to propose an approach for design of the freeze-drying cycle of pharmaceuticals at known risk of failure. In the near future, the model will be used for the definition of the design space of the process.

## NOMENCLATURE

$a_w$	Water activity
$A$	Cross sectional area ( $m^2$ )
$C_1$	Parameter of <b>Equation III.6.5</b> ( $W m^{-4} K^{-1}$ )
$C_2$	Parameter of <b>Equation III.6.5</b> ( $W m^{-2} K^{-1} Pa^{-1}$ )
$C_p$	Heat capacity ( $J K^{-1}$ )
$E_a$	Activation energy ( $J kg^{-1} K^{-1}$ )
$\Delta H$	Latent heat of sublimation ( $J kg^{-1}$ )
$f_I$	Mass fraction of ice in the product
$K$	Heat transfer coefficient ( $W m^{-2} K^{-1}$ )
$k_{GT}$	Gordon-Taylor constant ( <b>Equation III.6.24</b> )
$l$	Layer thickness ( $m$ )
$\dot{m}$	Water vapour flow rate ( $kg s^{-1}$ )
$m$	Mass of solids in the product ( $kg$ )
$M_W$	Molecular mass of water ( $g mol^{-1}$ )
$N_V$	Number of vials
$P$	Pressure ( $Pa$ )
$\dot{Q}$	Heat flow rate ( $W$ )
$R_g$	Ideal gas constant ( $J K^{-1} kmol^{-1}$ )
$R_p$	Product resistance ( $Pa m^2 s kg^{-1}$ )
$R_{p_0}$	Parameter of <b>Equation III.6.10</b> ( $Pa m^2 s kg^{-1}$ )
$R_{p_1}$	Parameter of <b>Equation III.6.10</b> ( $Pa m s kg^{-1}$ )
$t$	Time ( $s$ )
$T$	Temperature ( $K$ )
$V$	Volume ( $m^3$ )
$X$	Fraction of moisture content

## Greek

$\beta$	Mass transfer parameter ( $s kg^{-1} K^{-1}$ )
$\theta_1, \theta_2$	Shape parameters of <b>Equation III.6.14</b>
$\lambda$	Thermal conductivity ( $W m^{-1} K^{-1}$ )
$\tau$	Characteristic desorption time ( $s$ )

**Subscripts and Superscript**

<i>0</i>	Initial
<i>B</i>	Bottom
<i>c</i>	Contact
<i>C</i>	Chamber
<i>CN</i>	Condenser
<i>d</i>	Dried
<i>des</i>	Desorption
<i>eq</i>	Equilibrium
<i>f</i>	Frozen
<i>i</i>	Interface
<i>I</i>	Ice
<i>M</i>	Monolayer
<i>P</i>	Product
<i>r</i>	Radiation
<i>R</i>	Rail
<i>ref</i>	Reference
<i>s</i>	Solute
<i>S</i>	Shelf
<i>sub</i>	Sublimation
<i>T</i>	Top
<i>v</i>	Vapour
<i>V</i>	Vial
<i>w</i>	Water
<i>W</i>	Wall



## III.6.2 Paper

### INTRODUCTION

Freeze-drying is a batch process used to dry heat sensitive products by means of sublimation of the previously frozen product (primary drying), followed by desorption of the unfrozen water (secondary drying) (Jennings, 1999; Adams, 1991). Due to the use of low temperature and pressure, freeze-drying process is often the only solution to produce pharmaceutical and biological products (e.g., vaccines) with acceptable characteristics of stability, shelf-life, and potency. In order to meet the patient needs and the regulatory requirements regarding product quality, product and process development department in freeze-drying process development is presently shifting from the traditional Quality-by-Testing (QbT) to the new Quality-by-Design (QbD) approach (Nail and Searles, 2008; Mockus *et al.*, 2011; Yu, 2008), which states that the quality has to be built into the process by design and not only tested into final product (Nail and Searles, 2008).

In this regard, the concept of "design space" is gaining popularity as a tool for cycle development and scale-up as well as for the implementation of QbD in freeze-drying of pharmaceutical products. The design space is defined in the guidance ICH Q8 (Food and Drug Administration, 2009) as: "the multidimensional combination and interaction of input variables and process parameters that have been demonstrated to provide assurance of quality". Design spaces can be developed for both the primary and secondary drying steps of the freeze-drying process. The classical design space of the primary drying step illustrates the relationship of two critical process parameters, the product temperature and the sublimation rate, with the operating variables of the process, i.e., the chamber pressure and shelf temperature, usually at the end of sublimation. In order to define the "safe area" of the design space for the process development, two specific constraints have to be considered: (i) the maximum capability of the equipment, that is the maximum sublimation rate supported by the equipment at a given pressure and (ii) the maximum allowed product temperature to avoid product damage (i.e., the collapse of the product cake). Furthermore, Pisano *et al.* (Pisano *et al.*, 2012) developed a design space for the secondary drying step, which was described in terms of shelf temperature and operating time leading to a product temperature lower than the maximum allowed value and a moisture content lower than the target one.

Recently, several mathematical models (Giordano *et al.*, 2011; Pisano *et al.*, 2013; Fissore *et al.*, 2011a; Pisano *et al.*, 2012a; Mortier *et al.*, 2016) were developed for the prediction of the product temperature, the sublimation rate and the desorption rate during freeze-drying and used for the calculation of the design spaces of primary drying and secondary drying. Most of these models were based on average values of the model parameters (e.g., product resistance, vial heat transfer coefficient, characteristic desorption time) over the vial batch, whereas only few of them took into account the uncertainty of the parameters due to differences in heat and mass transfer mechanisms

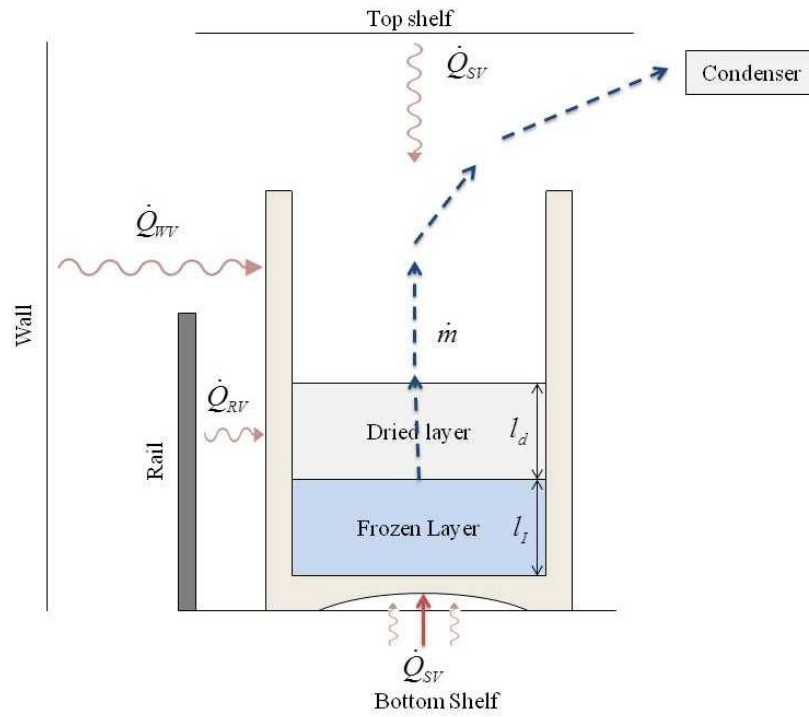


**Figure III.6.1:** Schematic representation of heat and mass transfer during primary drying

between vials processed in the same or in different batches (Mortier *et al.*, 2016; Pisano *et al.*, 2013; Giordano *et al.*, 2011). The understanding and quantification of these mechanisms responsible for product quality variability, previously performed in **Papers III.1-5**, led to a better prediction of the process parameters distribution and consequently of the risk of failure associated to the process.

Our goal in the present study was to develop a multi-vial dynamic mathematical model for freeze-drying for the process design, taking into account sources responsible for heat and mass transfer variability among vials, previously presented in dedicated **Papers (III.1-5)**. The developed model was then used to predict the evolution of the product temperature, the ice fraction and the moisture content in about 100 vials during primary and secondary drying for three given cycles considering a 5 % sucrose solution and a pilot freeze-dryer.

Finally, a new risk-based approach for the design of the primary and secondary drying steps of the freeze-drying process was proposed, which includes the evaluation of the percentage of vials potentially rejected for specific combinations of operating variables. In future work, model predictions of the product temperature, sublimation rate and desorption rate will be validated with experimental data and the model will be used to construct the design space of the process.

## MATHEMATICAL MODEL

### Hypotheses

A dynamic mathematical model simulating a large number of vials during freeze-drying was developed based on the following assumptions:

*H1 - Heat and mass transfer mechanisms considered:* **Figure III.6.1** gives a schematic representation of the considered heat and mass transfer phenomena. Heat transfer was described to take place between some key points of the system: from the shelf to the top and bottom of the vial (heat flow contributions  $\dot{Q}_{SV}$ , **Figure III.6.1**) and from the wall and the rail to the lateral vial wall exposed to them (respectively heat flow contributions  $\dot{Q}_{WV}$  and  $\dot{Q}_{GV}$ , **Figure III.6.1**). Mass transfer in primary drying was considered to take place from the sublimation front, through the dried product, the drying chamber, and finally to the condenser (mass flux  $\dot{m}$ , dotted blue arrow in **Figure III.6.1**);

*H2 - Process dynamics:* Transfer phenomena characterized by a fast dynamics, e.g., heat transfer in the frozen and dried layer, the mass transfer in the gas, are assumed to be in pseudo-steady state and thus are described by algebraic equations. Slow dynamics phenomena, e.g., sublimation front movement and desorption, are considered to be time dependent and are described by differential equations;

*H3 - Desorption during primary drying:* At the temperature commonly used in primary drying (usually  $< -10$  °C for pharmaceutical products), the desorption kinetics of the water bound to the dried structure is very slow. Thus, desorption was not assumed to take place until completion of sublimation during the primary drying step, as stated by the following condition:

$$\dot{m}_{des} = 0 \text{ if } f_I > 0 \quad \text{Equation III.6.1}$$

where  $\dot{m}_{des}$  is the desorption flow rate and  $f_I$  is the fraction of ice. Based on previous experimental data (**Paper III.5**), an average initial moisture content of 0.07 kg/kg wb was considered at the beginning of secondary drying (i.e., after the shelf temperature ramp from the primary drying set point to the secondary drying set point).

*H4 - Sublimation interface:* A flat sublimation frozen-dried layer interface was considered;

*H5 - Convection heat transfer:* Convection heat transfer was not considered. A recent work of Pikal et al. (Pikal *et al.*, 2016), and the use of our previous developed model of heat transfer during sublimation (**Paper III.2**) showed that convection can be considered as negligible at the low pressures typically encountered during the freeze-drying of pharmaceuticals (usually below 10 Pa);

*H6 - Presence of the stopper:* Based on our previous data (**Paper III.4**) and in agreement with a study of Pikal et al. (Pikal *et al.*, 1984), the presence of the stopper was considered to add negligible resistance and only the dried product layer was considered to impose a resistance to the water vapour flow rate from the sublimation interface to the drying chamber;

*H7 - Radiation phenomena:* It was considered that the solid surfaces are opaque, that the radiation and the absorption occur in the same spectral range and that the absorption and radiation of the low pressure water vapour are negligible. Under these conditions, the Stefan-Boltzmann equation was used to describe the radiation heat transfer between selected drying chamber components and the vials.

### Operating variables

The shelf and the total chamber pressure were assumed to be defined by the freeze-drying protocol and known at any moment.

### Main equations of the model

The heat flux received during the process by the vial is assumed to mainly serve for the ice sublimation during primary drying and for the water desorption in secondary drying. The evolution of product temperature  $T_p$  during primary and secondary drying for a vial can be determined as:

$$C_p \frac{dT_p}{dt} = \dot{Q}_{SV} - \Delta H_{sub} \dot{m}_{sub} - \Delta H_{des} \dot{m}_{des} \quad \text{Equation III.6.2}$$

where  $\dot{m}_{sub}$  and  $\dot{m}_{des}$  are the mass flow rates respectively during sublimation and desorption,  $\Delta H_{sub}$  and  $\Delta H_{des}$  are the latent heat of sublimation and desorption,  $\dot{Q}_{SV}$  is the heat flow rate between the shelf and the vial, and  $C_p$  is the heat capacity of the vial with the product contained therein.

*Heat transfer between the shelf and the vial*

The heat transfer between the shelf and the vial  $\dot{Q}_{SV}$  depends on the difference between shelf and product temperature  $T_S$  and  $T_p$ , and can be expressed in term of heat transfer coefficient  $K_{SV}$ :

$$\dot{Q}_{SV} = K_{SV} A_{BV} (T_S - T_p) \quad \text{Equation III.6.3}$$

being  $A_{BV}$  the bottom cross sectional area of the vial. The heat transfer coefficient  $K_{SV}$  can be defined as:

$$K_{SV} = \left( \frac{1}{K_V(P_C)} + \frac{l_I(t)}{\lambda_I} \right)^{-1} \quad \text{Equation III.6.4}$$

where  $\frac{l_I(t)}{\lambda_I}$  is the heat transfer resistance of the ice layer, defined as the apparent thickness of the frozen layer over the thermal conductivity of the frozen product, whereas  $\frac{1}{K_V(P_C)}$  is the resistance to heat transfer through the vial bottom. The term  $K_V(P_C)$ , known as vial heat transfer coefficient, includes three heat transfer contributions (Pikal *et al.*, 1984; Pisano *et al.*, 2011; Hibler and Gieseler, 2012; Scutellà *et al.*, 2017a): (i) the contact conduction between the bottom shelf and the vial via points of direct contact, (ii) the radiation from the top and bottom shelves and (iii) the conduction through the gas entrapped in the vial bottom curvature, which will depend on the vial depth of bottom curvature and the chamber pressure  $P_C$ . Thus, the vial heat transfer coefficient  $K_V(P_C)$  will depend on the vial bottom dimensions (contact area between the shelf and the vial  $A_c$  and depth of bottom curvature  $l_{BV}$ ) and the chamber pressure  $P_C$  as:

$$K_V = C_1 A_c + K_r + \frac{C_2 P_C}{1 + C_2 \frac{l_{BV} P_C}{\lambda_v}} \quad \text{Equation III.6.5}$$

In **Equation III.6.5**,  $K_r$  represents the radiation contribution of the top and bottom shelf defined as:

$$K_r = (F_{TS \rightarrow V} + F_{BS \rightarrow V})(T_S + T_p)(T_S^2 + T_p^2) \quad \text{Equation III.6.6}$$

with  $F_{BS \rightarrow V}$  calculated in function of the parallel plate configuration between the shelf and the vial,  $F_{TS \rightarrow V}$  considered to be equal to the emissivity of the vial, as defined in **Paper III.1**.

*Mass transfer during primary drying*

During primary drying the sublimation flux can be defined by the difference between the equilibrium pressure at the ice-vapour interface  $P_{vi}$  and the partial vapour pressure in the chamber  $P_{vC}$ :

$$\dot{m}_{sub} = \frac{A_i}{R_p} (P_{vi} - P_{vC}) \quad \text{Equation III.6.7}$$

where  $P_{vi}$  can be calculated from the Clausius Clapeyron equation:

$$P_{vi} = \exp \left( \frac{-6139.6}{T_p} + 28.8912 \right) \quad \text{Equation III.6.8}$$

$P_{vC}$  is defined as:

$$\frac{dP_{vC}}{dt} = \frac{R_g T_C}{V_C M_W} (\sum_1^{N_V} (\dot{m}_{sub} + \dot{m}_{des}) - \dot{m}_{CN}) \quad \text{Equation III.6.9}$$

with  $T_C$  and  $V_C$  are the chamber temperature and volume,  $R_g$  is the ideal gas constant,  $\dot{m}_{CN}$  is the mass flow rate from the chamber to the condenser and  $M_W$  is the molecular mass of the water. Only the mass transfer resistance of the dried layer  $R_p$  was considered, which depends linearly on the dried layer thickness (**Paper III.4**) (Pikal *et al.*, 1984; Pikal and Shah, 1990):

$$R_p = R_{p0} + l_d R_{p1} \quad \text{Equation III.6.10}$$

Finally, the fraction of ice  $f_I$  contained in the product evolves with time as a function of the sublimation rate  $\dot{m}_{sub}$  as:

$$m_{I_0} \frac{df_I}{dt} = -\dot{m}_{sub} \quad \text{Equation III.6.11}$$

with  $m_{I_0}$  equal to the initial mass of ice in the product.

*Mass transfer during secondary drying*

The multilayer model, previously presented by Trelea et al. (Trelea *et al.*, 2016), and in **Paper III.5**, was used to describe the desorption kinetics in secondary drying. The main hypothesis of this model is that the moisture may be contained into the product in different layers more or less bound to the solid matrix, which may present different desorption kinetics. Considering the presence of 2 layers (with 1=monolayer, 2=multilayer), the total moisture content  $X$  in the product can be defined as the sum of the moisture fractions  $X_i$  contained in each layer:

$$X = \sum_{i=1}^2 X_i \quad \text{Equation III.6.12}$$

The desorption kinetics for the  $i$ -layer was described as:

$$i = 1,2 \quad \frac{dX_i}{dt} = \frac{1}{\tau_i} (X_i^{eq} - X_i) \quad \text{Equation III.6.13}$$

where  $\tau_i$  is the characteristic desorption time, and  $X_i^{eq}$  the equilibrium moisture content of the water in the  $i$ -layer determined from the sorption isotherm. In this model, the equilibrium moisture content  $X^{eq}$  at a given water activity  $a_w$  was described by using the Guggenheim-Anderson-Boer (GAB) model:

$$X^{eq} = \frac{X_M \theta_1 \theta_2 a_w}{(1 - \theta_1 a_w)(1 + \theta_1 a_w (\theta_2 - 1))} \quad \text{Equation III.6.14}$$

with  $X_M$  equal to the monolayer moisture content and  $\theta_1$  and  $\theta_2$  shape parameters of the model.

Furthermore, the characteristic desorption time  $\tau_i$  of each compartment is assumed to depend on the product temperature through an Arrhenius type equation:

$$\tau_i = \tau_{ref_i} e^{-\frac{E_a}{R_g} \left( \frac{1}{T_p} - \frac{1}{T_{ref}} \right)} \quad \text{Equation III.6.15}$$

where  $\tau_{ref_i}$  is the characteristic desorption time of the  $i$ -layer at reference temperature and  $E_a$  is the activation energy, considered equal for the two layers.

Finally, the desorption flow rate  $\dot{m}_{des}$  can be defined as:

$$\dot{m}_{des} = m_s \frac{1}{(1-X)^2} \frac{dX}{dt} \quad \text{Equation III.6.16}$$



**Table III.6.1:** Parameters used in the model. SD: standard deviation. Parameters for which the SD is given are considered as normal distributed in the model. (*continued*)

	<i>Symbol</i>	<i>Value ± SD</i>	<i>Units</i>	
<i>Vial characteristics</i>	Vial bottom area	$A_{BV}$	$2.07 \cdot 10^{-4}$	$m^2$
	Vapour-product interface area	$A_i$	$1.78 \cdot 10^{-4}$	$m^2$
	Vial-shelf contact area	$A_c$	$(1.67 \pm 0.4) \cdot 10^{-5}$	$m^2$
	External radius of the vial	$r_R$	$16.25 \cdot 10^{-3}$	$m^2$
	Depth of bottom curvature	$l_{BV}$	$(1.23 \pm 0.34) \cdot 10^{-4}$	$m$
	Height of the vial	$\square_V$	$31 \cdot 10^{-3}$	$m$
<i>Freeze-dryer characteristics</i>	Volume of the chamber	$V_C$	0.12	$m^3$
	Height of the rail	$\square_R$	$22 \cdot 10^{-3}$	$m$
	Number of vials	$N_V$	2310	-
	Emissivity of the shelves and rail	$\varepsilon_S, \varepsilon_R$	0.113	-
	Emissivity of the wall	$\varepsilon_W$	0.084	-
	Temperature of the walls	$T_C$	276	$K$
<i>Physical properties and constants</i>	Latent heat of sublimation	$\Delta H_{sub}$	$2.8 \cdot 10^6$	$J \cdot kg^{-1}$
	Latent heat of desorption	$\Delta H_{des}$	$2.3 \cdot 10^6$	$J \cdot kg^{-1}$
	Ice conductivity	$\lambda_I$	2.23	$W \cdot m^{-1} \cdot K^{-1}$
	Gordon-Taylor constant (Equation III.6.24)	$k_{GT}$	0.2721	
	Vapour conductivity at ambient pressure	$\lambda_v$	0.025	$W \cdot m^{-1} \cdot K^{-1}$
	Ideal gas constant	$R_g$	8.314	$kJ \cdot K^{-1} \cdot kmol^{-1}$
Stefan-Boltzmann constant	$\sigma$	$5.67 \cdot 10^{-8}$	$W \cdot K^{-4} \cdot m^{-2}$	

**Table III.6.1:** Parameters used in the model. SD: standard deviation. Parameters for which the SD is given are considered as normal distributed in the model.

	<i>Symbol</i>	<i>Value ± SD</i>	<i>Units</i>	
<i>Physical properties and constants</i>	Glass transition temperature of the solids ( <b>Equation III.6.22</b> )	$T_{g,s}$	347 K	
	Glass transition temperature of the water ( <b>Equation III.6.22</b> )	$T_{g,w}$	135 K	
	Glass transition temperature of maximally freeze-concentrated solution	$T_g'$	-32 °C	
<i>Heat transfer</i>	Vial heat transfer coefficient	$C_1$	$2.20 \cdot 10^5$ $W m^{-4} K^{-1}$	
	parameters ( <b>Equation III.6.5</b> )	$C_2$	0.667 $W m^{-2} K^{-1} Pa^{-1}$	
	Visualization factors for central vials	$F_{S \rightarrow V}$	0.11 -	
		$F_{W \rightarrow V}$	0 -	
		$F_{R \rightarrow V}$		
	Visualization factors for edge vials	$F_{S \rightarrow V}$	0.11 -	
		$F_{R \rightarrow V}$		
		$F_{W \rightarrow V}$	0.08 -	
	<i>Mass transfer</i>	Product resistance parameters ( <b>Equation III.6.9</b> )	$R_{p_0}$	$59 \pm 75$ $kPa m^2 s kg^{-1}$
			$R_{p_1}$	$(1.8 \pm 2.0) \cdot 10^4$ $kPa m s kg^{-1}$
Characteristic desorption time at reference temperature for mono (1) and multilayer (2)		$\tau_{ref_1}$	$56.39 \pm 12.40$ s	
		$\tau_{ref_2}$	$3.80 \pm 0.83$ s	
Activation energy		$E_a$	49.61 $kJ mol^{-1}$	
Monolayer moisture content		$X_M$	0.028 $kg kg^{-1}(wb)$	
Parameters <b>Equation III.6.13</b>		$\theta_1$	1.581 -	
	$\theta_2$	9.10 -		
	Mass transfer parameter	$\beta$	$4 \cdot 10^4$ $s kg^{-1} K^{-1}$	

*Mass transfer from the chamber to the condenser*

The mass transfer from the drying chamber to the condenser was described by using a dynamic model proposed by Trelea et al. (Trelea *et al.*, 2015), in which the mass flux from the chamber to the condenser depends on the total chamber pressure  $P_C$  and on the water vapour partial pressure at the interface in the vial ( $P_{vV}$ ) and in the condenser ( $P_{vCN}$ ) as :

$$\dot{m}_{CN} = \frac{1}{\beta T_C} \ln\left(\frac{P_C - P_{vCN}}{P_C - P_{vV}}\right) \quad \text{Equation III.6.17}$$

where  $\beta$  is a parameter that depends on the geometry of the pathway between the freeze-dryer chamber and the condenser, and  $T_C$  is the temperature of the chamber considered equal to the temperature of the wall.

Values of relevant coefficients and parameters used in the model are reported in **Table III.6.1**.

**Analysis of the heat and mass transfer variability in freeze-drying**

Four sources of inter-vial product quality variability were identified:

- a) *Variability of the vial geometry*: The vial heat transfer coefficient between the shelf and the vial is influenced by two vial bottom dimensions, the shelf-vial contact area  $A_c$  and the depth of bottom curvature  $l_{BV}$ , as shown by **Equation III.6.5**. Thus, differences in these dimensions among the vials can result in a variability of the heat transfer among the vials on the shelf. In the present study, the distributions of  $K_V$  at different chamber pressures over the vial batch were calculated based on the normal distributions of  $A_c$  and  $l_{BV}$ , as previously proposed in **Paper III.1**.
- b) *Edge vial effect*: It is well known that the heat flow rate received by the vials depends on the position of the vials on the shelf. Vials located at the periphery of the shelf receive an additional heat transfer by radiation from the wall and the rail (if present) and conduction through the gas between the chamber wall, the rail and the wall of the vials, as previously analyzed in **Paper III.2**. This phenomenon is known in literature as edge vial effect. In the present study, the conduction through the gas between the chamber wall, the rail and the wall of the vials was not taken into consideration, whereas the additional radiation heat flow rates from the wall and rail to the edge vials were predicted. Thus, **Equation III.6.2** becomes for edge vials:

$$C_p \frac{dT_V}{dt} = \dot{Q}_{SV} + \dot{Q}_{WV} + \dot{Q}_{RV} - \Delta H_{sub} \dot{m}_{sub} - \Delta H_{des} \dot{m}_{des} \quad \text{Equation III.6.18}$$

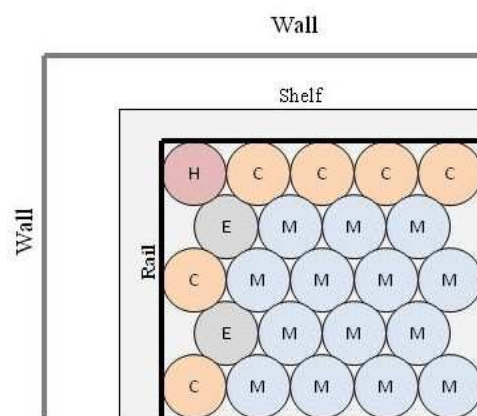


**Figure III.6.2:** Loading configuration ("bottomless tray") of the vials on the shelf considered in the simulations

The contributions  $\dot{Q}_{WV}$  and  $\dot{Q}_{RV}$  are the radiation heat flow rates from the wall and the rail, defined through the Stefan-Boltzmann equation:

$$\dot{Q}_{RV} = F_{R \rightarrow V} \sigma A_{LR} (T_R^4 - T_P^4) \quad \text{Equation III.6.19}$$

$$\dot{Q}_{WV} = F_{W \rightarrow V} \sigma A_{LW} (T_W^4 - T_P^4) \quad \text{Equation III.6.20}$$

with  $A_{LR}$  and  $A_{LW}$  are the lateral area of the vial exposed to the rail and the wall:

$$A_{LR} = 2\pi\phi r_V (h_R) \quad \text{Equation III.6.21}$$

$$A_{LW} = 2\pi\phi r_V (h_V - h_R) \quad \text{Equation III.6.22}$$

where  $\phi$  is equal to the fraction of vial lateral area exposed to both the wall or to the rail (if present).

The terms  $\dot{Q}_{WV}$  and  $\dot{Q}_{RV}$  may be more or less important in **Equation III.6.18**, depending on the vial loading configuration used.

As example, **Figure III.6.2** shows an array of vials disposed in a typical hexagonal arrangement and loaded by using a "bottomless tray" configuration: a rail surrounds the vial batch and shields 70 % of the lateral wall of edge vials. In this configuration, the vials receive radiations from both the walls and the rail. Furthermore, the vials can be classified in four different groups: edge vials located at the corner of the shelf (H,  $\phi = 0.75$ ), edge vials more exposed to the wall and/or rail (C,  $\phi = 0.50$ ), vials less exposed to the wall and/or the rail (E,  $\phi = 0.30$ ), vials located in the centre of the shelf and not exposed to the wall and rail (M,  $\phi = 0$ ). The visualization factors between the rail and the vial  $F_{R \rightarrow V}$  and between the wall and the vial  $F_{W \rightarrow V}$  were calculated considering the parallel plate configuration (according to the simplified radiation model for vial freeze-drying proposed in **Paper III.2**):

$$i = R, W \quad F_{i \rightarrow V} = \frac{1}{\frac{1}{e_i} + \frac{1}{e_V} - 1} \quad \text{Equation III.6.23}$$

where  $e_R$ ,  $e_W$  and  $e_V$  represents the emissivity of the rail, the wall and the vial glass.

- c) *Variability of the mass transfer resistance*: In **Paper III.4** the product resistance variability in a large batch of vials was quantified in terms of normal distributions of the parameters  $R_{p_0}$  and  $R_{p_1}$  (**Equation III.6.10**). The normal distribution of these parameters was truncated to positive values.

**Table III.6.2:** Description of the cycles I, II and III simulated in this work

Cycle	Primary Drying			Secondary drying		
	Time	$P_C$	$T_S$	Maximum time considered	$P_C$	$T_S$
I			-40 °C			0 °C
II	84 h	6 Pa	-27 °C	45 h	6 Pa	18 °C
III			-10 °C			40 °C

- d) *Variability of the desorption kinetics*: The variability of the desorption kinetics responsible for the final moisture content heterogeneity was previously quantified in terms of normal distributions of the characteristic desorption times at reference temperature  $\tau_{ref_i}$  (**Equation III.6.15**), as proposed in **Paper III.5**.

All the average values and the standard deviations of relevant coefficients used in the model, reported in **Table III.6.1**, were experimentally validated in previous dedicated studies (**Paper III.1-5**).

### Prediction of the risk of the process

The developed mathematical model was used to propose a risk-based approach for the design of the primary and secondary drying steps of the freeze-drying process. Firstly, the model was used to calculate the product temperature, ice fraction and moisture content evolution for a wide range of combinations of operating variables (i.e., chamber pressure and shelf temperature), considering the selected freeze-dryer and loading configuration. Then, the risk of failure of the primary drying step was calculated in terms of vials potentially rejected by considering two main constraints: (i) the product temperature had to be maintained below a critical value (i.e., the glass transition temperature of maximally freeze-concentrated solution  $T'_g$  of the selected product); (ii) the sublimation had to be completed at the end of primary drying, i.e., the fraction of ice had to be equal to zero. Hence, the range of acceptable combinations of operating variables (i.e., chamber pressure and shelf temperature) was identified based on the target level of risk.

For the design of the secondary drying step, the constraints considered were: (i) the final moisture content had to be equal or lower than the target moisture content and (ii) the temperature at any moment had to be lower than the glass transition temperature for dry product  $T_g$ . The value of  $T_g$  strongly depends on the current moisture content and was calculated by using the Gordon-Taylor equation as previously proposed in literature (Pisano *et al.*, 2012; Passot *et al.*, 2012).

$$T_g = \frac{XT_{g,w} + k_{GT}(1-X)T_{g,s}}{X + k_{GT}(1-X)} \quad \text{Equation III.6.24}$$

where  $T_{g,w}$  and  $T_{g,s}$  are the glass transition temperature of the water and the solute and  $k_{GT}$  is a constant. Hence, the range of acceptable combinations of operating variables (i.e., shelf temperature and operating time) was identified based on the target level of risk. The chamber pressure was not considered for the design of the secondary drying, as it does not have a significant effect on desorption for the range of pressure typically used in freeze-drying (< 10 Pa) (Pikal *et al.*, 1990).

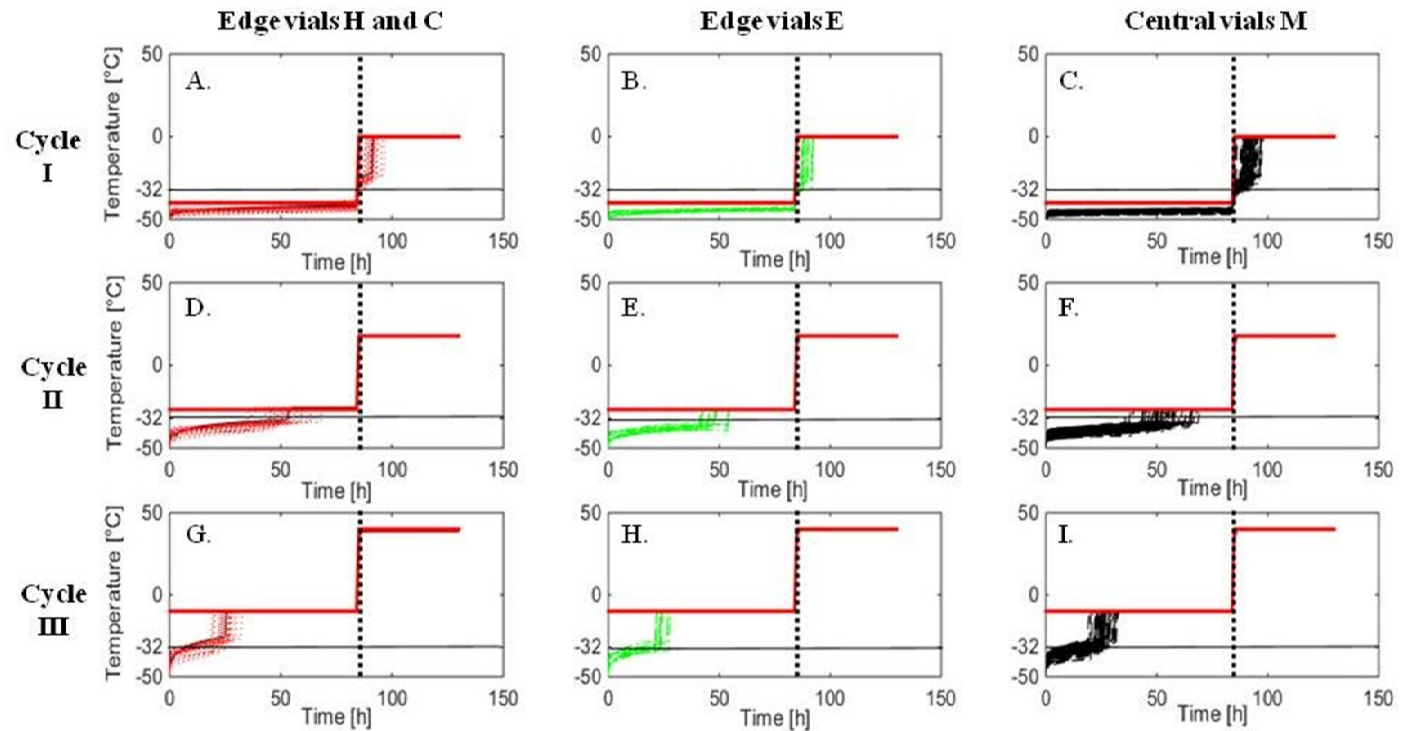


**Figure III.6.3:** Product temperature profiles predicted during the freeze-drying cycles performed at a chamber pressure of 6 Pa and at a shelf temperature during the primary and secondary drying steps respectively of  $-40\text{ }^{\circ}\text{C}$  and  $0\text{ }^{\circ}\text{C}$  (cycle I),  $-27\text{ }^{\circ}\text{C}$  and  $18\text{ }^{\circ}\text{C}$  (cycle II) and  $-10\text{ }^{\circ}\text{C}$  and  $40\text{ }^{\circ}\text{C}$  (cycle III). The black solid thin lines represent the corner vials (Figures A, D, G), the red dotted lines the edge vials C in contact with the rail (Figures A, D, G), the green dashed lines the edge vials E not in contact with the rail (Figures B, E, H), the black dashed lines the central vials M (Figures C, F, I), the red bold solid line the shelf temperature. The vertical dotted black lines represent the end of primary drying. The temperature  $-32\text{ }^{\circ}\text{C}$  corresponds to the glass transition temperature  $T_g'$  of the product.

### Numerical solution

The developed model was solved by means of Matlab R2014b software equipped with the Statistics Toolbox (The MathWorks, Inc., Natick, MA). This commercial software was ran on a PC, equipped with Intel(R) Core(TM) i7-4600U CPUs, at 2.1 GHz, 64-bits, with 8 Gb of RAM, under Windows 10. The function *ode15s*( ) in Matlab was used to solve the set of ordinary differential equations of the model. The analysis on the effect of the heat and mass transfer variability on the process parameters relevant for product quality (e.g., product temperature) during freeze-drying was performed by using the Monte Carlo method, which is often used in literature to simulate uncertainty of the parameters in mathematical model of freeze-drying (Mortier *et al.*, 2016; Bosca *et al.*, 2015; Giordano *et al.*, 2011). This method consisted in simulation of batches of 100 vials with random normal distributions of the considered model parameters ( $A_C$ ,  $l_{BV}$ ,  $R_{p_0}$ ,  $R_{p_1}$ ,  $\tau_{ref_1}$  and  $\tau_{ref_2}$ ). Due to computer limitations, the number of simulated vials (100) was significantly smaller than the actual number of vials in the freeze-dryer (2310, **Table III.6.1**). The number of simulated representative vials in each category (corner vial H, edge vial C in contact with the rail, edge vial E not in contact with the rail, central vial M; **Figure III.6.2**) was proportional to the real number in the considered loading configuration and their contributions to the total mass flux was weighted accordingly.

### Simulated system

In the present work, the model was used to simulate freeze-drying process performed in the pilot freeze-dryer REVO (Millrock Technology, Kingston, United States). The equipment was constituted of a drying chamber equipped with three shelves and a condenser running at temperature of  $-75$  °C. A number of 770 glass tubing vials (Müller + Müller, Holzminden, Germany) were supposed to be loaded on each shelf. The vials had a total volume of 3 mL and were all filled with 1.8 mL of 5 % aqueous sucrose solution. Furthermore, the vial array was surrounded by a metallic rail (shielding 70 % of the lateral wall of the vials) and arranged on the shelf as previously shown in **Figure III.6.2**. The shelf was considered to be at a temperature of  $-50$  °C at the beginning of primary drying. Relevant characteristic of the equipment and vial geometry, as well as product properties are reported in **Table III.6.1**. Then, the evolution of product temperature, ice fraction, vapour pressure in the chamber and moisture content during desorption were predicted for three main cycles (named I, II and III), performed at a chamber pressure of 6 Pa and different shelf temperatures. The cycles are described in **Table III.6.2**. Finally, the risk of failure of primary and secondary drying, expressed as percentage of vials potentially rejected, was calculated for the selected product and freeze-dryer and for selected combinations of chamber pressure and shelf temperature. Chamber pressures between 4 and 10 Pa and shelf temperatures between  $-40$  °C to  $-10$  °C in primary drying, and  $0$  °C and  $40$  °C in secondary drying were considered.

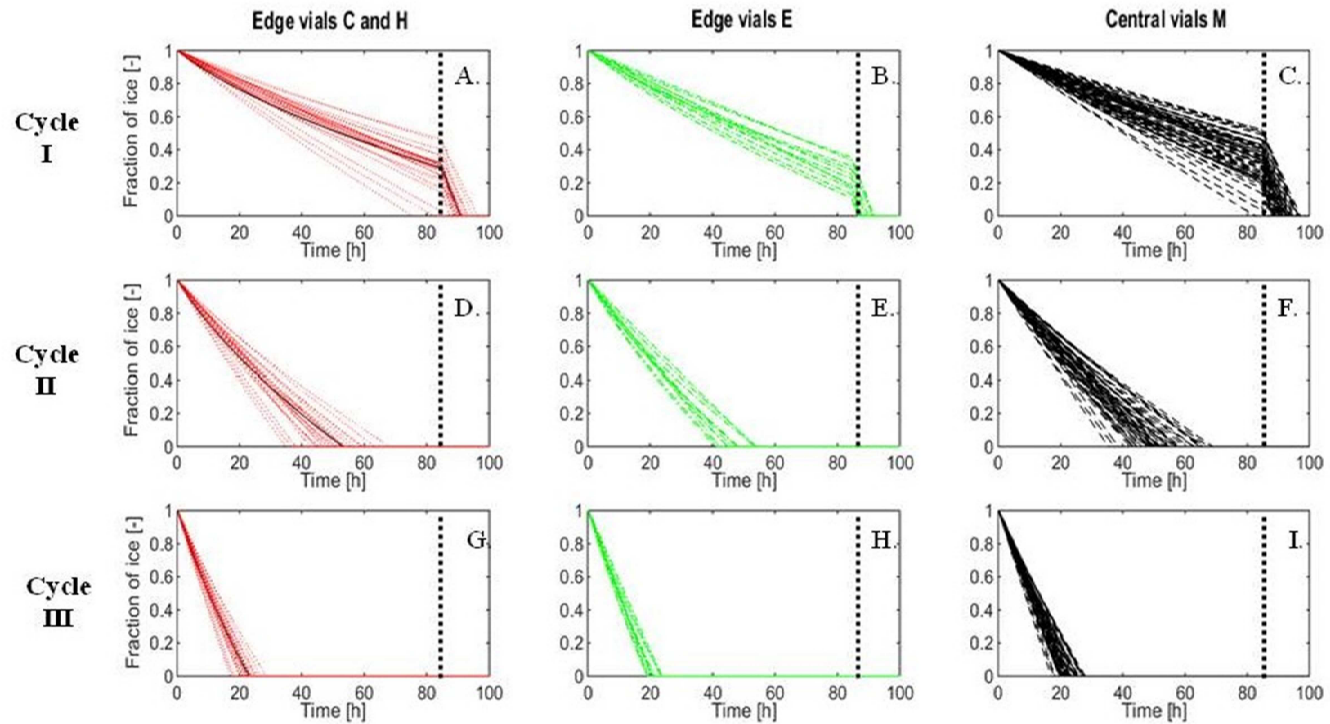


**Figure III.6.4:** Predicted values of ice fraction contained in the product during the primary drying step of freeze-drying cycles performed at a chamber pressure of 6 Pa and at a shelf temperature during the primary drying step of  $-40\text{ }^{\circ}\text{C}$  (cycle I),  $-27\text{ }^{\circ}\text{C}$  (cycle II) and  $-10\text{ }^{\circ}\text{C}$  (cycle III). The black solid thin lines represent the corner vials (Figures A, D, G), the red dotted lines the edge vials C in contact with the rail (Figures A, D, G), the green dashed lines the edge vials E not in contact with the rail (Figures B, E, H), the black dashed lines the central vials M (Figures C, F, I). The vertical dotted black lines represent the end of primary drying.

The capability of the pilot freeze-dryer was not considered to be limiting in the selected cycles.

## PRELIMINARY RESULTS

### Prediction of process parameters

**Figure III.6.3** shows the simulated product temperature during the cycle I, II and III for a corner vial (H), edge vials in contact (C) and not in contact with the rail (E), and central vials (M). Single lines represent the thermal history evolution for each simulated vial. The product temperature in edge vials (and especially in vials H and C) was found to be higher than in most of the central vials, as they received additional radiation contributions from the wall and the rail. However, the model does not take into account the additional conduction through the gas taking place between the chamber walls, the rail and the walls of the edge vials, which strongly contributes to the heat transfer variability between edge and central vials, as previously found in **Paper III.2**. Additional heat flux received by the edge vials is thus underestimated in these simulations.

When the product temperature rose and approached the shelf temperature, sublimation was completed as the heat received by the vials served to increase the product temperature. The abrupt increase of product temperature at the end of sublimation was due to the assumption of the planar interface, as no intra-vial heterogeneity was considered for the heat and mass transfer. Among the three simulated cycles, the sublimation was not completed for all vials within the fixed primary drying time only in cycle I performed at  $-40\text{ }^{\circ}\text{C}$  (**Figure III.6.3A, B and C**), and it continued for the remaining vials during the secondary drying step at higher shelf temperature ( $0\text{ }^{\circ}\text{C}$ ). In contrast, in cycle II and III carried out at higher shelf temperatures ( $-27\text{ }^{\circ}\text{C}$  and  $-10\text{ }^{\circ}\text{C}$ ), sublimation was completed within 84 h or less, and the vials approached the temperature of the shelf before the transition between primary and secondary drying. However, the shelf temperature and chamber pressure used in cycle III led to a product temperature in most of the vials above the critical value (i.e., above  $-32\text{ }^{\circ}\text{C}$ ), which may cause the collapse of the product.

The primary drying step can be well described also by the evolution of the ice fraction in time, as shown in **Figure III.6.4**. Sublimation can be defined as completed when no more ice is contained into the product ( $f_I=0$ ). Edge vials (and especially vials C in contact with the rail) completed sublimation in primary drying before most of the central vials, because they were processed at higher product temperature. As previously evidenced by the product temperature in **Figure III.6.3**, sublimation in cycle I carried out at lower shelf temperature ( $-40\text{ }^{\circ}\text{C}$ ) was not completed and ice was still present in most of the vials at the end of primary drying. In contrast, the ice fraction  $f_I$  was found to approach 0 in 84 h or less in cycle II and III when higher shelf temperatures ( $-27\text{ }^{\circ}\text{C}$  and  $-10\text{ }^{\circ}\text{C}$ ) were applied.

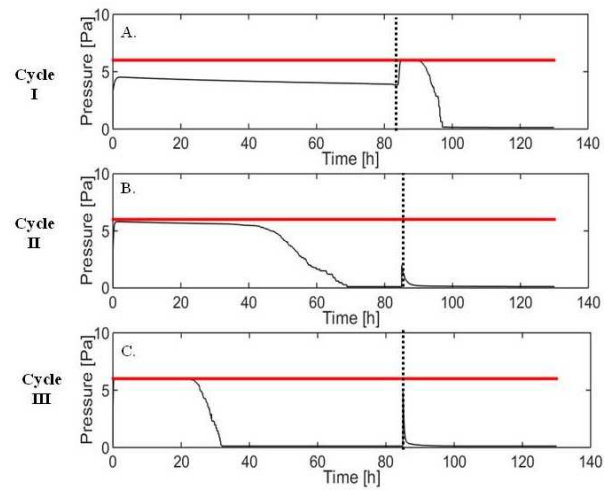


**Figure III.6.5:** Predicted values of total chamber pressure (bold red line) and the partial vapour pressure (dotted black line) during the primary and secondary steps of freeze-drying cycles performed at a chamber pressure of 6 Pa and a shelf temperature of  $-40\text{ }^{\circ}\text{C}$  and  $0\text{ }^{\circ}\text{C}$  (cycle I),  $-27\text{ }^{\circ}\text{C}$  and  $18\text{ }^{\circ}\text{C}$  (cycle II) and  $-10\text{ }^{\circ}\text{C}$  and  $40\text{ }^{\circ}\text{C}$  (cycle III).

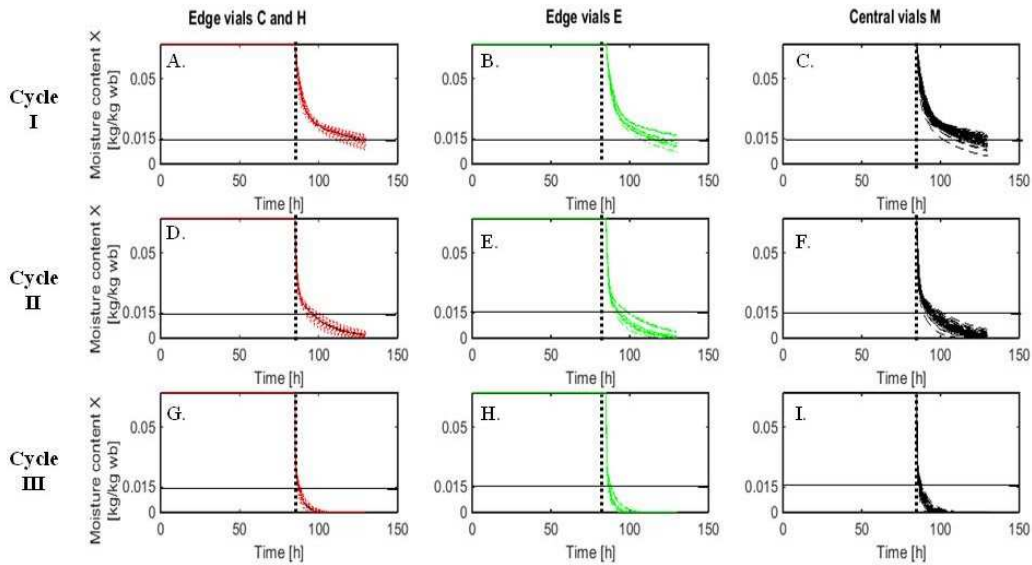


**Figure III.6.6:** Predicted moisture content profile during the secondary drying step of cycles performed at a chamber pressure of 6 Pa and at a shelf temperature of  $0\text{ }^{\circ}\text{C}$  (cycle I),  $18\text{ }^{\circ}\text{C}$  (cycle II) and  $40\text{ }^{\circ}\text{C}$  (cycle III). The black solid thin lines represent the corner vials (Figures A, D, G), the red dotted lines the edge vials C in contact with the rail (Figures A, D, G), the green dashed lines the edge vials E not in contact with the rail (Figures B, E, H), the black dashed lines the central vials M (Figures C, F, I), the red bold solid line the shelf temperature. The vertical dotted black lines represent the beginning of secondary drying.

The model was also used to predict the evolution of the partial vapour pressure  $P_{v_c}$  during the process for the three considered cycles, as shown in **Figure III.6.5**. The partial vapour pressure  $P_{v_c}$  value is usually close to the total chamber pressure during primary drying, as the gas in the drying chamber is mostly water vapour. For the cycle I (performed at low shelf temperature and chamber pressure), the model simulation showed that the  $P_{v_c}$  remained lower than the total chamber pressure during primary drying, as the drying chamber was not saturated with water vapour. At 84 h, when the temperature of the shelf rose for the transition to secondary drying, sublimation continued and the equilibrium vapour pressure increased close to the chamber pressure values. In contrast, in cycle II and III the drying chamber was saturated with water vapour in primary drying and the  $P_{v_c}$  value was close to the total chamber pressure. At the end of primary drying, the value of  $P_{v_c}$  decreases slowly due to the heterogeneity in the batch, as vials differently located on the shelf completed sublimation at different times. Finally, the model was used to predict the evolution of the moisture content  $X$  in the vial batch during secondary drying of cycles I, II and III respectively performed at 6 Pa and at a shelf temperature of 0 °C, 18 °C and 40 °C. Results are shown in **Figure III.6.6**. In all the simulated cycles, vials presented different profiles of moisture content due to the variability in the desorption kinetics. **Figure III.6.6A, B and C** shows that the target moisture content (1.5 %) was not reached in most of the vials within the specified secondary drying time (45 h) in cycle I. In contrast, in cycles II and III desorption was successfully carried within a secondary step of 45 h and all the vials reached a moisture content lower than the target value of 1.5 %.

#### Risk assessment for a freeze-drying cycle

The developed model was used to predict the risk of failure of the process in terms of percentage of vials potentially rejected for different combinations of operating variables (shelf temperature, chamber pressure, operating time). Four different risks responsible for vial rejection were considered in primary and secondary drying: (i) product temperature higher than the critical value ( $T'_g$ ) during primary drying; (ii) sublimation not completed at the end of primary drying; (iii) product temperature higher than the critical value ( $T_g$ ) during secondary drying; (iv) final moisture content in the product higher than the target value at the end of secondary drying. Based on these constraints, potential vial rejection of the primary and secondary drying steps were defined to select the best cycle at the maximum allowed risk (set in the present work as 1 %). **Figure III.6.7** shows the vial rejection for a primary drying step, due to a product temperature higher than  $T'_g$  (**Figure III.6.7A**) and to the sublimation not completed at the end of primary drying (**Figure III.6.7B**) in function of the chamber

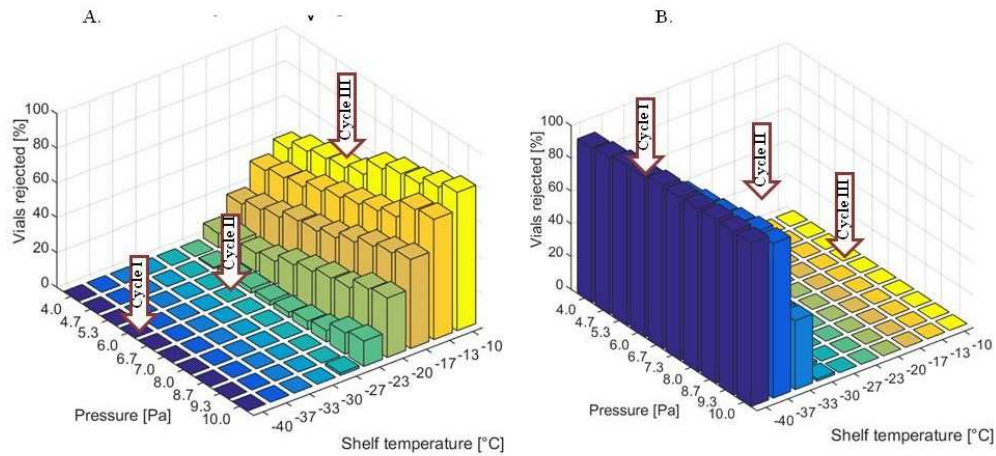


**Figure III.6.7:** Potential vial rejection (%) in primary drying performed at different chamber pressures and shelf temperatures due to (A) a product temperature higher than the critical value ( $T_g'$ ) and (B) sublimation not completed after 84 h of primary drying. The arrows evidence the cycles I, II, and III.

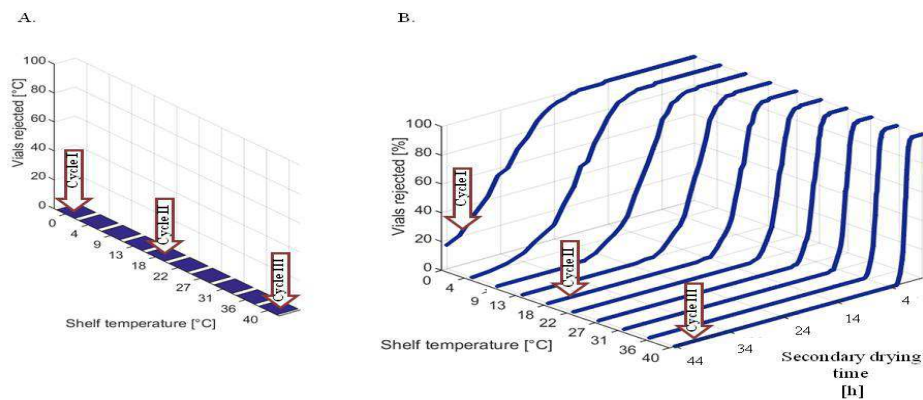


**Figure III.6.8:** Potential vial rejection (%) due to (A) a product temperature higher than the critical value ( $T_g$ ) during the whole duration of the secondary drying step and (B) product moisture content higher than the target value (1.5 %) for different shelf temperatures and operating times. Red arrows evidence the cycles I, II, and III.

pressure and shelf temperature and for a given operating time (84 h). Typical ranges of chamber pressure and shelf temperature used in the pharmaceutical industry were explored, respectively between 4 and 10 Pa, and -40 °C and -10 °C. **Figure III.6.7A** shows that, if a shelf temperature higher than -27 °C is used during primary drying, the vial rejection become higher than 1 % for most of the pressures tested. The vial rejection can be evaluated for the previously considered cycles I, II and III (shown by the white arrows in **Figure III.6.7**). Cycle I and II will not lead to a temperature higher than the critical value during primary drying, and no vials will be rejected. In contrast, in cycle III the product temperature will be higher than  $T'_g$  for about 55 % of the vials.

Furthermore, for the primary drying time specified (84 h), a shelf temperature higher than -30 °C has to be considered to avoid the presence of ice at the end of the primary drying time. The sublimation will be completed in all the vials in the batch in the cycles II and III, whereas ice will be still present in 97 % of the vials in cycle I.

**Figure III.6.8** presents the risk of vial rejection of the secondary drying step due to a product temperature higher than  $T_g$  (**Figure III.6.8A**) and to a final moisture content in the product higher than the target value of 1.5 % (**Figure III.6.8B**). A range of shelf temperature between 0 °C and 40 °C was explored, and the pressure maintained constant at 6 Pa.

Results show that the product temperature remains below the critical value whatever the shelf temperature tested during the whole secondary drying step. In contrast, the use of a shelf temperature of 0 °C in cycle I will lead to a vial rejection of 17 % due to a high final moisture content at the end of the secondary drying step (i.e., 45 h), whereas all the vial processed in cycles II and III will present a moisture content lower than 1.5 %. Thus, cycle II appeared to be the best cycle for the product and equipment selected, as will result in no vial rejection in both primary and secondary drying.

The present work presents an original approach for the definition of the risk of failure of the process, i.e., the evaluation of the percentage of vials potentially rejected. Previous works included the uncertainty of the model parameters into mathematical models to predict the variability of the process parameters of primary drying step (i.e., product temperature and sublimation rate) (Pisano *et al.*, 2013; Mortier *et al.*, 2016; Giordano *et al.*, 2011). However, the risk of failure of the process was usually defined as probability that the temperature at the sublimation front exceed the critical value (e.g.,  $T'_g$ ).

Moreover, to our knowledge, the impact of the variability of the desorption kinetics parameter (i.e., characteristic desorption time) on the risk of failure of the secondary drying step (i.e., moisture

content higher than the target value and/or product temperature higher than the critical value) has never been investigated.

The calculation of design spaces of primary and secondary drying based on this mathematical model, including the percentage of vials potentially rejected (similar to those shown in **Figure III.6.7** and **III.6.8**) could be a powerful tool for the process design and scale-up. However, further work needs to be performed to validate model predictions by comparison with experimental data.

## CONCLUSIONS AND PERSPECTIVES

In this work, a multi-vial, dynamic mathematical model of the primary and secondary drying steps of the freeze-drying process was developed, including the heterogeneity of process parameters due to vial dimensions, position on the shelf and random nucleation process. Several mechanisms responsible for heat and mass transfer and thus for differences in the product quality were included in the model, in order to predict the variability of product temperature, ice fraction and moisture content among the vials on the shelf. The value and the distribution of key model parameters (i.e., the vial heat transfer coefficient, the product resistance, the characteristic desorption time at reference temperature and the different view factors between the vial and the wall, the shelf and the rail), were experimentally validated in previous works.

The ultimate aim of the proposed model is the process development and optimization based on a risk assessment approach. In this regard, as an example of practical application, the model was used to calculate the risk of failure of the primary and secondary drying steps for a 5 % sucrose solution processed in a pilot freeze-dryer, expressed in terms of percentage of vials potentially rejected. The risks of the process considered were: the product temperature higher than the maximum allowed value in primary and secondary drying, the sublimation not completed within the selected operating time and a moisture content value higher than the target one at the end of secondary drying.

In the future, the number of vials simulated will be increased and the sensitivity of the predicted percentage of vials potentially rejected to the number of simulated vials will be assessed. The model will be validated at pilot scale, in order to assure the robustness of the prediction of both the critical process parameters (e.g., product temperature) and of the percentage of vials potentially rejected. Design spaces of primary and secondary drying will be then calculated, to be used for the cycle transfer and scale-up of the process, e.g., by simulating different vial loading configurations and considering different equipment characteristics (e.g., equipment capability).

### III.6.3 Take-home message

- In this work, a multi-vials, dynamic mathematical model of freeze-drying process (i.e. primary and secondary drying steps) was developed including the variability of the heat and mass transfer parameters previously quantified in **Papers III.1 and III.4-5** (i.e.  $A_c, l_{BV}, R_{p_0}, R_{p_1}, \tau_{ref_0}, \tau_{ref_1}$ ). The additional heat transfer contribution by radiation from the chamber walls and the rail to edge vials was also considered (**Papers III.2-3**);
- The model was used to predict the variability of process parameters (e.g. product temperature) in three freeze-drying cycles performed at different shelf temperatures;
- Finally, a new approach was proposed for the risk-based design of primary and secondary drying steps of the freeze-drying process based on different constraints, i.e. maximum allowed product temperature in primary and secondary drying, completion of the sublimation of the ice crystals at the end of primary drying and value of the final moisture content lower than the target one at the end of secondary drying.
- In the future, the model will be validate with experimental data and used for the calculation of the design space of primary and secondary drying at known level of risk.



— IV —

## GENERAL CONCLUSIONS



## GENERAL CONCLUSIONS

---

*"There are two possible outcomes: if the result confirms the hypothesis, then you've made a measurement. If the result is contrary to the hypothesis, then you've made a discovery".*

*- Enrico Fermi*

### **Objectives of this study**

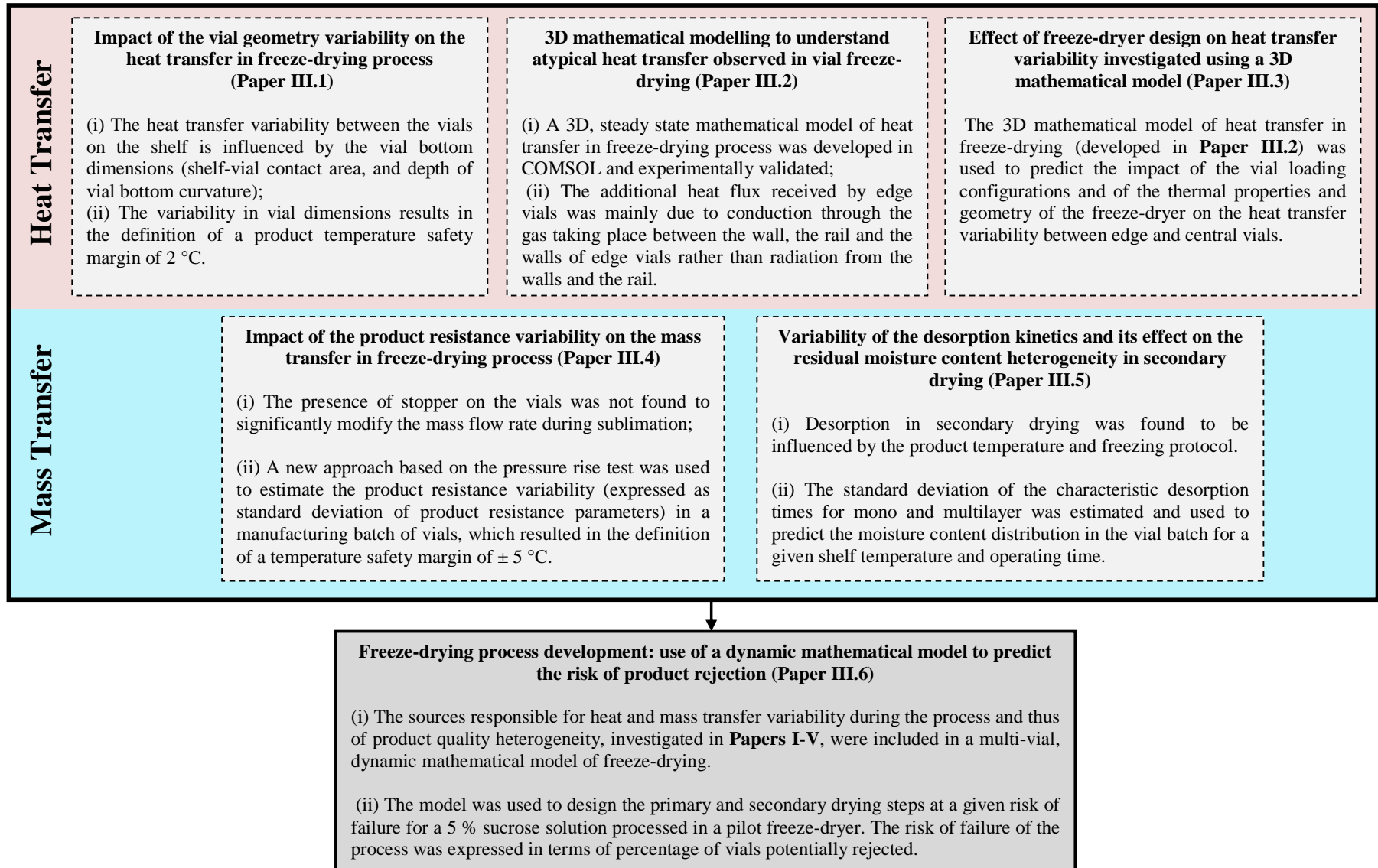
Vaccines continuously make a significant contribution to prevent serious diseases worldwide and to improve the human health. Most of the produced vaccines are stable at very low residual moisture content, thus their production process involves a drying step. As the formulation of the vaccines is very heat sensitive, this drying step is generally performed at very low temperature by means of the freeze-drying process.

To address the regulatory expectations regarding the quality of the product, the Quality-by-Design approach proposed by the US Food and Drug Administration is more and more often implemented into the production process of vaccines by pharmaceutical companies. The Quality-by-Design philosophy is based on the idea that the quality should be built into the product during the production process. To achieve this goal, it is of paramount importance to understand which are the critical parameters of the process that impact on the critical quality attributes of the product. With regard to the freeze-drying step, the main parameters that influences the critical quality attributes of a vaccine formulation (e.g., the potency of the product, the elegance of the dried cake, the final moisture content) are the product temperature, the sublimation rate and the desorption rate. An accurate prediction of the value and variability of these critical parameters could guide the selection of the operating variables of the process to obtain product batch of desired quality.

In this context, this Ph.D. work focused on:

1. Providing new insights in the understanding and quantification of the main sources responsible for the variability of the critical process parameters, and thus of the heterogeneity of the quality attributes in the final batch of products;
2. Using the acquired knowledge to deliver operational protocols and tools to the industrial partner (GlaxoSmithKline Vaccines), in order to guide the design and scale-up of the freeze-drying process of vaccines.

Figure IV.1: Schematic presentation of the main results obtained in this Ph.D. project.



### Main conclusions

The variability of the critical process parameters, such as the product temperature, the sublimation rate and the desorption rate, is due to differences in the heat and mass transfer phenomena between the vials. Based on the literature review, the variability of heat and mass transfer mechanisms during the process was potentially ascribed to: (i) the variability of the vial bottom dimensions and the position of the vial on the shelf of the freeze-dryer, which could lead to differences in the heat flow rate received by the vials; (ii) the modification of the cake structure during the freezing step (e.g., dimensions of the pores, of the specific surface area), which result to difference in the sublimation and desorption kinetics during primary and secondary drying, respectively. These potential sources of heat and mass transfer variability were thus investigated, and their impact on critical process parameters was quantified.

#### *Variability of the heat transfer during the freeze-drying process*

During freeze-drying process, vials receive three main heat transfer contributions from the bottom and top shelves: (i) by contact conduction *via* points of contact between the vial and the shelf, (ii) by radiation and (iii) by conduction through the gas entrapped in the vial bottom concavity. The contact conduction depends on the bottom area of the vial directly in contact with the shelf (Cannon and Semeley, 2004; Kuu *et al.*, 2009). Conversely, the conduction through the gas takes place under Knudsen regime in the range of low pressures typically used in freeze-drying (<10 Pa), and it depends on the depth of the vial bottom curvature and on the chamber pressure (Brülls and Rasmuson, 2002; Nail, 1980; Pikal, 2000; Pikal *et al.*, 1984; Pisano *et al.*, 2011; Ybema *et al.*, 1995). In literature, several examples of the dependence of the heat transfer (expressed in terms of vial heat transfer coefficient  $K_V$ ) on the chamber pressure are reported (Hibler *et al.*, 2012; Kuu *et al.*, 2009; Pikal *et al.*, 1984; Pisano *et al.*, 2011). However, the impact of the variability of the contact area and of the depth of bottom curvature on the heat transfer has never been quantified. Thus, in a first part of this Ph.D. work, the attention was focused on investigating the *impact of the vial bottom dimensions variability on the heat transfer* in vials located in the centre of the shelf and surrounded by other vials in the same conditions (**Paper III.1**). The importance of freeze-dryer design and operating variables (chamber pressure and shelf temperature) was also investigated. In agreement with the literature (Hibler *et al.*, 2012; Pikal *et al.*, 1984; Pisano *et al.*, 2011), the determined vial heat transfer coefficient  $K_V$  strongly depended on the value of chamber pressure. However, the dependence of  $K_V$  on shelf temperature was found to be negligible. Furthermore, no relevant differences were found among vial heat transfer coefficients evaluated in freeze-dryers of different design, but similar shelves emissivity) at chamber pressure lower than 10 Pa. Then, importance of the contact area between the shelf and the vial and the depth of bottom curvature on the heat transfer was determined

by calculating the  $K_V$  distributions at different chamber pressures. The variability of  $K_V$  between central vials was nearly completely explained by the combined variability of these two vial bottom dimensions. The contact area was found to highly influence the  $K_V$  distribution at chamber pressure lower than 30 Pa. In contrast, the bottom curvature played a non negligible role on the  $K_V$  distribution only at chamber pressures higher than 30 Pa. The results of this study can guide the choice of the vial design and provider. At pressures commonly used in freeze-drying of vaccines (< 10 Pa), particular attention should be devoted to the tolerance of the contact area between the shelf and the vial during the selection of the container. Furthermore, this original approach led also to the definition of a product temperature safety margin only due to the variability of the vial bottom geometry, quantified as about 2 °C, which should be taken into account during the cycle design.

The heat transfer variability during freeze-drying process depends also on the position of the vial on the shelf. It is well known that vials located in the periphery of the shelf present higher heat flow rates than vials located in the centre. This *edge vial effect* is classically ascribed in literature to the additional radiation from the wall and the rail received by the edge vials (Pikal *et al.*, 1984; Pisano *et al.*, 2011; Rambhatla and Pikal, 2003). However, the experimental works of Rambhatla *et al.* (Rambhatla and Pikal, 2003), and the mathematical model of Gan *et al.* (Gan *et al.*, 2005), evidenced that the presence of a metallic rail surrounding the vials may play also a non negligible role in the heat transfer received by edge vials. Thus, a 3D mechanistic mathematical of heat transfer during sublimation was developed in **Paper III.2** by using the software COMSOL Multiphysics in order to accurately predict the heat transfer variability related to the position of the vial on the shelf, and to understand the relative importance of the different heat transfer mechanisms on the edge vial effect. The model was experimentally validated for a broad range of chamber pressures (4 to 15 Pa) and shelf temperatures (0 °C and -40 °C). Conversely to literature, the use of this model revealed that the conduction through the gas taking place between the wall, the rail and the lateral walls of edge vials is the main mechanism responsible for the additional heat flow rate received by edge vials. Radiation from the walls and the rail had a minor but non-negligible contribution in the heat flow rate received by edge vials in the configuration considered (vials partially shielded by the rail).

Successively, the developed 3D mathematical model of heat transfer during sublimation was used in **Paper III.3** to investigate *the impact of design characteristics of the equipment on the heat transfer variability between edge and central vials*, such as the vial loading configuration, the geometry and the thermal characteristics of the equipment. Model simulations showed that the use of the rail can significantly reduce the differences in heat transfer between edge and central vials, as it decrease the radiation contribution received by the lateral walls of edge vials. Thus, prediction of the differences in heat flow rate received by the edge vials can play a key role for a successful cycle transfer among freeze-dryers in which different vial loading configurations can be used. Furthermore, difference in

the emissivity of the rail and the drying chamber wall did not significantly impact the heat transfer in edge vials, due to the relative small importance of the radiation on the total heat transfer. In contrast, higher emissivity of the shelf significantly increase the heat flow rate received by both edge and central vials, and thus a precise measurement of shelf emissivity is recommended to predict modifications in heat transfer between equipments presenting different finish of the shelves.

Relevant dimensions of the chamber, i.e., differences of the distance between the shelves and the distance between the shelf and the wall, did not significantly impacted on the heat transfer in edge and central vials for a chamber pressure of 4 Pa. This result is in agreement with the previous experimental data presented in **Paper III.1**, where it was shown that equipment of similar emissivity but different dimensions did not impact on the heat transfer in central vials (*via* vial heat transfer coefficient) at chamber pressure lower than 10 Pa.

In conclusion, the developed model revealed to be a powerful tool to be used for the prediction the heat transfer variability between edge and central vials in different devices during the cycle design and scale-up.

#### *Variability of the mass transfer during the freeze-drying process*

Part of the work presented in this thesis concerns *the evaluation of variability of the mass transfer during the sublimation step and its effect on the product temperature (Paper III.4)*. It is well known in literature that the value of the nucleation temperature influences the ice crystals size, the size of pores in the dried layer of the product and finally of the mass flow rate during the sublimation step (Konstantinidis *et al.*, 2011; Oddone *et al.*, 2014; Searles *et al.*, 2001b). However, nucleation is a stochastic phenomenon and thus ice crystals of different size can form during the freezing step within different vials, which led to an inter-vial variability of the mass flow rates. The estimation of the mass transfer variability within a batch, especially of manufacturing size (i.e., about 100,000 vials), can be really difficult. Moreover, the devices available for the determination of the mass flow rate give usually either a global value for all the vials in the batch (e.g., the pressure rise test) or a local value within one or very few vials (e.g., microbalance). The value of the coefficient of variation of product resistance is often quantified as about 10 % and estimated in laboratory batches from the uncertainty of the product temperature measurement (Pisano *et al.*, 2013) or from the variation of product temperature among few vials, measured by using thermocouples (Bosca *et al.*, 2015). In this study, a new approach was proposed to estimate the variability of the mass transfer for a 5 % sucrose solution, expressed in terms of product resistance distribution, by using two experimental methods: the pressure rise test (PRT) and the gravimetric method. This procedure was used on freeze-drying cycles performed with different freezing protocols, i.e., spontaneous and controlled nucleation. A 5 % sucrose solution and a filling volume of 1.8 ml (filling height of 1 cm) were considered during the

experiments.

Firstly, the PRT method was used to compare the impact of the presence of the stopper into the vial neck and of the freezing protocol on the mass transfer during sublimation. The presence of the stopper did not significantly modified the mass flow rate conversely to the freezing protocol. Then, the PRT method was used to evaluate the average product resistance evolution with the dried layer thickness in 5 laboratory vial batches. These data were then combined to estimate the product resistance variability within a manufacturing vial batch. Finally, the PRT product resistance data and local information provided by the gravimetric method were combined to assess the intra-batch product resistance variability at laboratory scale. The variability of the product resistance (expressed as standard deviation of the product resistance parameters) determined by using the PRT method in batches processed with controlled nucleation resulted to be lower than the one determined considering batches processed with spontaneous nucleation. Furthermore, the variability of the product resistance between vials within a laboratory batch estimated by using the gravimetric method was found to be significantly lower than the one among different batches obtained from the PRT method.

The product resistance distributions determined from the PRT method were used to calculate the product temperature distributions, and resulted in the definition of a safety margin of the product temperature of about  $\pm 5$  °C due to the mass transfer variability only. This safety margin resulted to be higher if compared with other value reported in literature for central vials, which were close to  $\pm 3$  °C and included the combined effect of the heat and mass transfer variability (Bosca *et al.*, 2015; Pisano *et al.*, 2013). A further validation of the proposed method used for the estimation of product resistance variability at manufacturing scale will be performed in the future.

The stochastic nature of nucleation during the freezing step influences not only the dimensions of the pores in the dried layer thickness but also the specific surface area available for desorption during secondary drying (Pikal *et al.*, 1990; Rambhatla *et al.*, 2004). In **Paper III.5**, *the variability of desorption kinetics during secondary drying* was quantified (in terms of standard deviation of the characteristic desorption time) and its impact on the final moisture content heterogeneity was evaluated. The multilayer desorption model previously proposed by Trelea *et al.* (Trelea *et al.*, 2016) adequately described the evolution of the moisture content during the secondary drying step. In agreement with the results of Trelea *et al.* (Trelea *et al.*, 2016), the desorption of the multilayer was found to be significantly faster than the desorption of the monolayer of about 30 times (for spontaneous nucleation). Higher values of product temperature during the secondary drying step led to a faster desorption kinetics for both mono and multilayer. Furthermore, the freezing protocol strongly impacted on the desorption kinetics. In particular, the use of controlled nucleation during the

freezing step led to a slower desorption kinetics than the use of spontaneous nucleation. The standard deviation of the characteristic desorption time was then quantified from experimental data. Finally, the proposed approach in this study was used to predict the moisture content distribution in final batch and to quantify the risk of failure of the process (expressed as percentage of vials potentially rejected due to a high residual moisture content).

*Multi-vial, dynamic mathematical model of freeze-drying*

The analysis performed in **Papers III.1-5** provided a comprehensive understanding of the sources responsible for the heat and mass transfer variability during freeze-drying process. In the last step of the project (presented in **Paper III.6**), the previously investigated heat and mass transfer mechanisms were included in a dynamic mathematical model developed in Matlab in order to predict the value and distribution of the product temperature, the ice fraction and the moisture content during the process for different operating conditions (shelf temperature, chamber pressure, operating time) and for 100 vials filled with 5 % sucrose solution and differently located on the shelf of a pilot scale freeze-dryer. The evolution of partial vapour pressure was also predicted.

The developed model was then used to design the primary and secondary drying steps of the process at specified level of risk. Four main constraints were considered: (i) a product temperature lower than the glass transition temperature during primary and (ii) during secondary drying, (iii) the completion of sublimation at given primary drying time and (iv) a moisture content value in the final product lower than the target value. The equipment capability was not considered to be limiting in this preliminary analysis. Then, acceptable combinations of the operating variables of the process were defined in function of the maximum allowed percentage of vials rejected.

In line with the Quality by Design philosophy, this study provided new and significant contributions for the understanding of the sources responsible for heat and mass transfer differences during freeze-drying process, and thus of the final product quality variability within the same or different vial batches. The work performed during this Ph.D. project contributed to improve the approach used by the industrial partner (GSK) for the development and scale-up of freeze-drying cycles in two different ways:

- By delivering experimental protocols for (i) the definition of product temperature safety margins due to the variability of relevant dimensions of the vial bottom, and to the variability of the mass transfer resistance due to the dry layer of the product, and (ii) for the prediction of moisture content distribution during secondary drying based on the variability of the desorption kinetics;
- By developing two mathematical models of freeze-drying: (i) a 3D steady state mathematical model for the description of heat transfer variability between edge and central vials during sublimation, and (ii) a multi-vial, dynamic model of freeze-drying for the development of cycles at known risk of failure.

The results obtained during the present project open several perspectives on short and medium-long term.

## Perspectives

### *Short term perspectives*

The short term perspectives here proposed concern the improvement of the two mathematical models developed during this thesis: the 3D, static mathematical model of heat transfer during the sublimation step and the multi-vial, dynamic mathematical model of freeze-drying.

The *3D, static mathematical model of heat transfer in freeze-drying* developed by using COMSOL Multiphysics allows the evaluation of the heat flow rate variability between edge and central vials for different vial loading configurations and equipment features. However, in **Paper III.3** it was observed that the simulated vial located in the third row of the array in the geometry of the model still receive a non-negligible contribution by radiation from the walls and the rail. Thus, the addition of other rows of vials in the original geometry of the model could allow to simulate the "real" central vial.

Furthermore, the developed model simulates only pure ice. Inclusion of the product resistance into

the model could allow to predict also the product temperature and to define a product temperature safety margin for the difference in heat transfer between edge and central vials.

The *multi-vial, dynamic mathematical model of freeze-drying* developed in Matlab (**Paper III.6**) is very promising as it could allow the determination of design spaces of primary and secondary drying based on different constraints (e.g., maximum allowed product temperature, target residual moisture content). However, some improvements should be performed to assure the robustness of the model predictions. Future work should focus on two key aspects:

- *Contribution of the additional gas conduction to the edge vials*: despite the inclusion of several heat and mass transfer mechanisms responsible for product quality variability, the additional contribution of conduction through the gas between the wall, the rail and the lateral walls of edge vials was not taken into account in this first version of the model. This heat transfer mechanism revealed to be the major responsible for the additional heat flow rates received by edge vials (**Paper III.2**), and thus its inclusion in the developed dynamic mathematical model would be important for a correct evaluation of the product temperature profile in edge vials.

- *Experimental validation*: the physical parameters used in the model (e.g.,  $K_V$ ,  $R_p$ ,  $\tau_{ref}$ ) and their distributions were experimentally determined in the due course of this project (**Papers III.1-5**). However, to ensure the robustness of the model and consequently of the performed risk assessment analysis, a further experimental validation should be performed focusing on four main points: (i) firstly, the proposed approach for the estimation of the product resistance variability by using the PRT method should be validated in a manufacturing or medium scale freeze-dryer. Furthermore, to fully understand the role played by the presence of the stopper into the vial neck in the mass transfer, experiments with and without stopper should be performed by using a low filling volume (e.g., 0.04-0.05 ml); (ii) the distribution of product temperature profiles and of moisture content for vials differently located on the shelf predicted by the model should be compared with experimental data, for a range of chamber pressures and shelf temperatures typically used in freeze-drying of vaccines (e.g., shelf temperatures between -40 °C and -10 °C, and chamber pressures lower than 10 Pa). Validation of the partial vapour pressure decrease obtained from the Pirani gauge should also be considered since it is a good indicator of the overall batch heterogeneity; (iii) it would be of interest to quantify the importance of the desorption taking place during sublimation step in the dried layer of the product, in order to estimate the variability of the initial moisture content during the desorption step and its effect on the final moisture content heterogeneity. Furthermore, description of the desorption kinetics in time-varying operating conditions (e.g., shelf temperature not constant), as proposed by Trelea et al. (Trelea *et al.*, 2016), will be integrated in the model in order to evaluate the importance of the ramp between primary and secondary drying on the desorption; (iv) the percentage

of vials rejected predicted by the model should be compared with the actual one. Different scenarios should be tested, e.g., cycle in which the product temperature is higher than the glass transition temperature in primary and secondary drying, moisture content higher than the target value etc. Visual inspection of the vials should be performed and the percentage of vial collapse and/or presenting a high moisture content should be evaluated.

Finally, in order to use the model for the design and scale-up of the freeze-drying process, the maximum equipment capability should be considered as a constraint in the calculation of the design space of primary drying and equipment capability data (previously determined for various pilot and manufacturing scale freeze-dryers during this Ph.D. project) should be integrated into the model.

### *Medium-long term perspectives*

#### *- Development of an user-friendly software based on the multi-vial, dynamic mathematical model:*

Once that the model will be validated, it will be of great interest to use it for the design of freeze-drying cycle of vaccine formulations. The selection of the operating conditions of the cycle (chamber pressure, shelf temperature and process time) can be performed directly from the calculated design spaces of primary and secondary drying in function of the risk of failure and of the level of optimization of the process (i.e., duration of the process). Furthermore, the model could be used to perform the scale-up between pilot and manufacturing scale. The proposed risk assessment-based design spaces could be calculated for different freeze-dryers by providing relevant information about the dimension of the vial batch, the equipment capability, the characteristic of the freeze-dryer (e.g., emissivities) and the vial loading configuration used. The comparison of the design space at pilot and commercial scale will allow to perform a rational choice of the process parameters for a successful scale-up with a significantly reduced experimental effort. Finally, an user-friendly software for the cycle design and scale-up could be developed based on proposed model for the less expert users. In conclusion, in line with the Quality-by-Design approach, the developed model/software could be used as smart tool to perform a risk assessment based cycle design and scale-up while guaranteeing the final product quality.

#### *- Describe and understand the mechanisms of collapse:*

the collapse of the product cake during primary and secondary drying due to a product temperature higher than the critical value is a phenomenon of paramount importance, as it led to the rejection of the vial due to lack of pharmaceutical elegance of the cake and high moisture content in the product. A better understanding of the relation between the dynamics of the cake collapse (and possibly microcollapse) and the product temperature appears to be important for a correct prediction of the percentage of vials rejected due to this phenomenon.

- *Development of a 3D mathematical model for describing the mass transfer between the chamber and the condenser:* it would be of great interest to deeply explore the mass transfer from the sublimation interface to the condenser to monitor the partial vapour pressure during the drying process by using COMSOL. These mass transfer phenomena were already described in a 1D dimensional model (Trelea *et al.*, 2015). However, a 3D mathematical model could describe mass transfer in more complex geometries, where 1D assumption cannot be applied, for different operating conditions and/or different mixtures of inert gas and water vapour inside the chamber.

- *Investigation of the heat transfer variability in other type of containers:* The experimental and theoretical analysis performed in this project focused on the investigation of the mechanisms responsible for quality heterogeneity for product processed within glass tubing vials. However, other type of containers are often used in pharmaceutical industries, such as syringes and dual-chamber cartridges. The geometry of the container could significantly change the contribution of the different heat transfer phenomena taking place during the process. On a long term, the strategy here proposed to evaluate the importance of the variability of the container dimensions could be adapted and applied to other types of containers. Moreover, the geometry of the 3D mathematical model of heat transfer in freeze-dryer developed in COMSOL could be modified in function of the geometry of the considered system to simulate differences in heat transfer between containers differently located on the shelf.











— SMALL GLOSSARY —



## SMALL GLOSSARY OF FREEZE-DRYING

---

Some of the terms recurring in freeze-drying science and often used in the present work:

**AMORPHOUS MATERIAL:** Most of the pharmaceutical products that are freeze-dried do not crystallize during the freezing step but form a solid with amorphous (or glassy) interstitial structure with a very high viscosity. In this state, most of the biochemical reactions are stopped and the product stability (shelf life) is significantly increased. The temperature at which the glass exhibits a change in viscosity is termed the *glass transition temperature*.

**BOUND WATER:** Fraction of water that is present in the formulation as essential component to various materials. It can be distinguished from *free water* by its inability to form ice crystals. This fraction of water is partially removed from the matrix during *secondary drying*, in order to produce a final product with a target value of *moisture content*.

**CAKE:** The porous and spongy structure resulting from the freeze-drying process in a *vial* after sublimation of the ice crystals.

**CENTRAL VIALS:** Vials located in the centre of the shelf and surrounded by other vials in the same conditions.

**CHOKED FLOW:** When the sublimation rate becomes higher than the *maximum equipment capability*, the chamber pressure rises above the set point and the process runs out of control. The maximum speed at which the water vapour can flow in the duct from the chamber to the condenser is the velocity of sound, which can be reached at very high sublimation rates. Under this specific condition, the vapour flow rate becomes independent of the pressure on the condenser side of the duct connecting the chamber and the condenser. The equipment capability highly depends on the duct geometry between the chamber and the condenser and on the condenser performance.

**COLLAPSE:** Viscous flow of the porous structure of the product. Collapse can happen during primary drying when material reaches a critical temperature known as *collapse temperature*, and

during secondary drying when the product reaches temperature higher than the *glass transition temperature* for the dried product.

**COLLAPSE TEMPERATURE:** the temperature above which collapse occurs during primary drying (see *Collapse*).

**CRITICAL PROCESS PARAMETERS (CPPs):** The CPPs are the process parameters whose variability has an impact on one or more critical quality attributes of the product and therefore should be monitored or controlled to ensure that the process produces the desiderate quality. Examples of CPPs in freeze-drying are the product temperature, the sublimation rate and the desorption rate.

**CRITICAL QUALITY ATTRIBUTES (CQAs):** The CQAs are the physical, biological, chemical and biological properties of a product that should be within appropriate limits, range or distribution to assure the desiderate product quality. CQAs are defined in function of the *Quality Target Product Profile*. Examples of CQAs are the aspect of the product cake, reconstitution time and the final moisture content.

**CYCLE:** Sequence of the steps of the freeze-drying process, i.e., freezing, primary drying and secondary drying.

**DESIGN SPACE:** The multidimensional combination and interaction of input variables (e.g., material attributes) and process parameters that have been demonstrated to provide assurance of quality. Typical coordinates of the classical design space in freeze-drying are the shelf temperature, chamber pressure, sublimation rate and product temperature.

**DESORPTION:** Mass transfer mechanism through which the bound water contained in the dried product at the end of sublimation is partially removed during *secondary drying* by increasing the temperature of the product.

**EDGE VIAL EFFECT:** Difference between the heat flow rate received by vials located in the centre of the shelf and surrounded by other vials in the same conditions, and vials located at the periphery of the shelf, due to position dependent heat transfer mechanisms (e.g., radiation from the walls to edge vials).

**EDGE VIALS:** Vials located at the periphery of the shelf and exposed to different drying chamber

components, e.g., walls, rail, door.

**FREE WATER:** Fraction of water in a solution that is not chemically or physically bound. It forms ice crystals during the freezing step and is has to be removed during primary drying by means of sublimation.

**FREEZING:** First step of the freeze-drying process during which the solidification of the solution occurs. The freezing point is the temperature at which solid and liquid are in equilibrium.

**GLASS TRANSITION TEMPERATURE:** The temperature at which the material goes from a glassy state to a rubbery state (see *glass transition*). The value of  $T_g$  depends on the concentration of solutes.

**GLASS TRANSITION:** The reversible transition in amorphous materials from a hard and "glassy" state into a rubber-like state.

**NUCLEATION:** The process by which the nuclei of the ice crystals are formed. Usually, nucleation is a stochastic phenomenon if not controlled. The use of *controlled nucleation* during the freezing step allows to increase and homogenize the nucleation temperature value. In the present work, controlled nucleation was performed in some experimental analysis by adding the nucleation agent *Snomax* to the initial formulation.

**PARENTERAL:** refers to pharmaceuticals product which are administrated in other ways than by the alimentary tract, e.g., by injection.

**PRIMARY DRYING:** It is the second step of freeze-drying process, and consists in removing of the ice crystals by sublimation.

**QUALITY TARGET PRODUCT PROFILE (QTPP):** The QTPP define the design criteria of the product and forms the basis of design for its development. Considerations should include dosage, container system, drug quality criteria (e.g., potency).

**QUALITY-BY-DESIGN (QBD):** A new systematic approach for product development that begins with predefined objectives on the product quality characteristics and emphasizes product and process understanding.

**QUALITY-BY-TESTING (QBT):** A regulatory framework in which product quality is ensured by the use of fixed product manufacturing process and by tests on the raw materials, the in-process materials and on the end-product.

**RECIPE:** A recipe describes in terms of operating variables, such as shelf temperature, chamber pressure and operating time, the entire freeze-drying process in a stepwise manner. The recipe of a *freeze-drying cycle* is usually programmed directly into a freeze dryer control system and recorded electronically for recall whenever required.

**RECONSTITUTION:** The act of adding a solvent (usually water) into the freeze-dried product, in order to return it to the liquid state.

**RESIDUAL MOISTURE:** The amount of *bound water* that remains into the freeze dried product after sublimation in primary drying. The amount of residual moisture in a freeze dried product is reduced during secondary drying.

**SECONDARY DRYING:** It is the third and last step of freeze-drying process and consists in reducing the amount of *bound water* (or *residual moisture*) in the dried product by desorption.

**STOPPER:** The stoppers are elastomeric caps for vials, usually presenting one or two openings. A stopper is usually only partially inserted into the *vial* neck, to allow water vapour to leave the vial during primary and secondary drying. The vials are then completely "stoppered" (i.e., fully inserted into the vial neck) at the end of the process.

**SUBLIMATION:** It is the transition from a solid to a gas phase with no intermediate liquid stage. Ice crystals present in the frozen product sublime in water vapour during *primary drying*.

**SUPERCOOLING:** The process of cooling a liquid below its freezing point, without it becoming a solid. The *supercooling degree* is the difference between the nucleation temperature and the equilibrium freezing point.

**VACCINE:** A biological product aimed to improve immunity to a specific disease.

**VIAL:** Small glass container (available in a wide range of size) used as primary packaging in freeze-

drying of *vaccines* and other *parenteral products*. The vials usually present a "champagne-like" bottom with a concavity in which gas is entrapped.



— RÉSUMÉ SUBSTANTIEL —



## RÉSUMÉ SUBSTANTIEL EN FRANÇAIS

---

### Contexte

La vaccination est largement considérée comme l'une des plus grandes réalisations de la recherche médicale. Depuis le premier développement par Edward Jenner du vaccin contre la variole, la vaccination a permis de réduire considérablement la propagation de plusieurs maladies mortelles, comme la poliomyélite, le tétanos, la coqueluche ou la diphtérie. De nos jours, les vaccins existants peuvent être classés dans différents groupes en fonction de leur ingrédient actif (antigène). Les vaccins vivants atténués sont connus pour être les plus réussis et efficaces. Ils sont réalisés réduisant la virulence des virus ou plus rarement de bactéries. En outre, ils sont généralement plus stables sous forme sèche (1-3 % de la teneur en eau) que dans les solutions aqueuses et donc leur procédé de production implique une phase de séchage. Cependant, les vaccins sont des produits très sensibles à la chaleur et peuvent être endommagés s'ils sont exposés à des températures de séchage élevées.

Ainsi, en raison de l'utilisation combinée du vide et de basses températures, la lyophilisation est généralement la méthode de choix utilisée pour la production de vaccins. Ce procédé de stabilisation se déroule en trois étapes successives: (i) la congélation de la formulation de vaccin, préalablement remplie dans des flacons de verre, avec formation de cristaux de glace et d'une matrice cryo-concentrée; (ii) dessiccation primaire, dans laquelle les cristaux de glace sont éliminés par sublimation; (iii) dessiccation secondaire, dans laquelle la désorption de l'eau liée à la matrice solide permet d'atteindre la teneur en eau résiduelle cible dans le produit. Malgré son utilisation importante dans l'industrie pharmaceutique, la lyophilisation reste un processus long et coûteux, difficile à mettre au point et à changer d'échelle, ce qui entraîne souvent des lots de produits de qualité non homogène.

De nos jours, la sécurité des vaccins et l'efficacité de la vaccination attirent de plus en plus l'attention du public. Le besoin d'assurer la qualité du produit a conduit à des procédures réglementaires plus rigoureuses pour toutes les étapes du développement et de la production des vaccins. L'une des approches les plus récentes pour améliorer la qualité des produits pharmaceutiques tout en réduisant le fardeau réglementaire est la mise en œuvre de l'initiative "Quality by Design" (QdB, en français "Qualité par la Conception") proposée au

début de 2000 par la Food and Drug Administration aux États-Unis. La philosophie de l'approche QdB stipule que la qualité du produit ne doit pas être uniquement testée sur le produit final, mais intégrée au processus de production grâce à la détermination de cibles de qualité et à une compréhension approfondie de la façon dont le produit et le procédé interagissent. L'une des étapes essentielles de la mise en œuvre de la qualité par la conception dans le procédé de production des vaccins est la définition des "critical quality attributes" (CQA, en français "attributs de qualité critiques") du produit, par exemple la stabilité de l'antigène, la teneur finale en eau du produit le produit et l'élégance pharmaceutique du gâteau. Ces CQA dépendent fortement de l'étape de lyophilisation, pendant laquelle la température du produit doit être maintenue en dessous d'une valeur maximale autorisée pour éviter la perte de la structure poreuse du produit, c'est-à-dire l'effondrement du produit. L'effondrement provoque généralement une teneur en eau finale élevée du produit, un temps de reconstitution du produit long et en particulier la perte de l'élégance pharmaceutique du gâteau nécessaire pour l'acceptation du produit par les autorités et les utilisateurs. Cependant, une température du produit trop éloignée de l'optimum conduit à une augmentation significative du temps de lyophilisation et donc à une diminution de l'efficacité du processus.

Les conditions optimales de fonctionnement d'un procédé de lyophilisation peuvent aujourd'hui être définies en construisant le "design space" (en français, l'espace de conception). Le *design space*, concept clé de QdB, est défini comme la combinaison multidimensionnelle de variables de commande (e.g. attributs du produit) et de paramètres du procédé qui assurent la qualité du produit. La construction du *design space* peut être effectuée par deux approches : soit par la réalisation d'une vaste campagne expérimentale, soit par la modélisation des phénomènes de transfert de chaleur et de matière ayant lieu pendant la lyophilisation, ce qui permet de prédire une valeur moyenne de la température du produit et de la vitesse de sublimation dans un lot de flacons.

Malheureusement, les transferts de chaleur et de matière se produisant pendant la lyophilisation dépendent non seulement des conditions opératoires du procédé (e.g. de la pression de la chambre, de la température de l'étagère), mais aussi de plusieurs facteurs, tels que les propriétés du produit, la géométrie des flacons, les caractéristiques de l'équipement utilisé. Comprendre l'impact de ces facteurs sur les transferts de chaleur et de matière ayant lieu dans des flacons situés à différents endroits sur l'étagère du lyophilisateur est d'une

importance primordiale pour une meilleure définition du *design space* et pour prédire la variabilité de la qualité du produit. La prédiction de la qualité du produit, permet, à son tour, d'effectuer une analyse de risque du procédé lors de la conception et pendant les étapes de changement d'échelle.

Dans ce contexte, le présent projet de thèse a été réalisé avec l'appui scientifique et financier de la société pharmaceutique GlaxoSmithKline Vaccines (Belgique).

### **Objectif de la thèse**

L'objectif principal de ce travail était de développer une nouvelle approche pour la conception, l'optimisation et le changement d'échelle des cycles de lyophilisation pour un risque connu, conformément à l'approche *Qualité by Design*. À cet égard, l'attention a porté sur (i) l'étude et la quantification des mécanismes responsables de la variabilité des transferts de chaleur et de matière dans le même lot de flacons ou entre de lots, à différentes échelles, pendant la dessiccation primaire et secondaire et sur (ii) l'intégration des phénomènes étudiés dans un modèle mathématique mécanistique décrivant le procédé de lyophilisation en flacon.

### **Principaux résultats**

Dans ce contexte, le présent travail s'est focalisé sur l'étude qualitative et quantitative de quatre sources potentiellement responsables de la variabilité des paramètres critiques du procédé de lyophilisation: (1) la variabilité de la géométrie du fond du flacon, responsable des différences observées dans le transfert de chaleur et dans la température du produit, (2) le rayonnement du rail utilisé pour maintenir les flacons et des parois, ainsi que la conduction thermique du gaz contenu entre la paroi du lyophilisateur, le rail et la paroi latérale du flacon, en tant que mécanismes responsables du flux de chaleur additionnel reçu par les flacons situés sur le bord; (3) la variabilité de la résistance produit due à la couche sèche formée pendant le procédé, responsable des différences de transfert de matière et de température pendant la dessiccation primaire et enfin (4) l'impact de la variabilité de la cinétique de désorption pendant la dessiccation secondaire sur l'hétérogénéité de la teneur en eau finale dans un batch.

La première partie de ce travail (présenté dans la **Publication III.1** dans ce manuscrit) a porté sur l'étude de l'impact de la variabilité des dimensions du fond du flacon (*i.e.* l'aire de contact entre l'étagère et le flacon et la profondeur de la concavité du fond du flacon) sur le

transfert de chaleur dans des flacons situés au centre de l'étagère et entourés d'autres flacons. La variabilité dans les dimensions des flacons peut être due aux conditions de production et dépend de la conception et du fournisseur. Ainsi, l'importance de deux dimensions du fond du flacon sur le transfert de chaleur a été déterminée en calculant les distributions du  $K_V$ . La variabilité du coefficient de transfert de chaleur du flacon  $K_V$  entre les flacons centraux a été presque complètement expliquée par la variabilité combinée de ces deux dimensions du fond du flacon. L'aire de contact a fortement influencé la distribution de  $K_V$  pour des pressions de chambre inférieures à 30 Pa. En revanche, la variabilité de la concavité du fond du flacon joue un rôle non négligeable sur la distribution de  $K_V$  uniquement à des pressions de chambre supérieures à 30 Pa. Ainsi, à des pressions couramment utilisées dans la lyophilisation des vaccins (<10 Pa), une attention particulière devrait être accordée à l'aire de contact entre l'étagère et le flacon pour la sélection des flacons. Par ailleurs, l'approche proposée a également conduit à la définition d'une marge de sécurité pour la température du produit en fonction de la variabilité de la géométrie du fond du flacon, qui a été quantifiée à environ  $\pm 1$  °C.

Dans cette première partie, seules les différences de transfert de chaleur entre les flacons situés au centre de l'étagère ont été considérées. Cependant, les flacons situés à la périphérie de l'étagère et exposés aux composants de l'enceinte de lyophilisation, tels que la paroi ou le rail de maintien des flacons, présentent habituellement un flux de chaleur et une température de produit significativement plus élevés que les flacons centraux. Ainsi, une attention particulière a été portée à la compréhension des mécanismes responsables des flux de chaleur supplémentaires reçus par les flacons du bord.

Un modèle mathématique en trois dimensions (3D) a été développé en utilisant le logiciel COMSOL Multiphysics (présenté dans la **Publication III.2** dans ce manuscrit), et validé expérimentalement pour une large gamme de pressions de chambre (4 à 15 Pa) et des températures d'étagère (0 °C et -40 °C). L'utilisation du modèle a révélé que la conduction à travers le gaz entre la paroi de l'enceinte de lyophilisation, le rail et la paroi latérale du flacon est le mécanisme dominant. Contrairement à ce qui est affirmé habituellement dans la littérature, le rayonnement provenant du mur et du rail a eu une contribution mineure sur le flux de chaleur reçu par les flacons du bord. Le modèle mathématique 3D développé a fourni des informations utiles concernant l'impact de certains éléments de l'équipement sur la variabilité du transfert de chaleur entre les flacons de bord et les flacons centraux, tels que la

configuration de chargement des flacons, la géométrie et la caractéristique thermique de l'équipement (présenté dans la **Publication III.3** dans ce manuscrit). Les simulations réalisées avec le modèle ont montré que l'utilisation du rail peut réduire considérablement les différences de transfert de chaleur entre les flacons du bord et les centraux, malgré sa contribution au rayonnement sur les flacons du bord. Ainsi, la prédiction des différences de flux de chaleur reçu par les flacons de bord paraît essentielle pour réussir un transfert de cycle entre lyophilisateurs présentant différentes configurations de chargement de flacons. De plus, la différence de l'émissivité du rail et de la paroi de l'enceinte de lyophilisation n'a pas eu d'impact significatif sur le transfert de chaleur dans les flacons du bord. En revanche, une plus grande émissivité de l'étagère augmente de manière significative le flux de chaleur reçus par les flacons du bord et du centre. Par conséquent, une mesure précise de l'émissivité des étagères est recommandée pour prévoir les variations du transfert de chaleur entre les équipements présentant une finition différente des étagères. Le modèle développé s'est révélé être un outil puissant pour la prédiction de la variabilité du transfert de chaleur entre les flacons du bord et ceux du centre dans différents dispositifs pendant la conception du cycle de lyophilisation et le changement de l'échelle.

La variabilité du transfert de matière pendant l'étape de sublimation et son effet sur la température du produit ont été également étudiés (présenté dans la **Publication III.4** dans ce manuscrit). Tout d'abord, l'impact de la présence du bouchon dans le col du flacon et de l'utilisation de différents protocoles de congélation sur le flux de vapeur d'eau pendant la dessiccation primaire ont été étudiés. La présence du bouchon n'a pas modifié de manière significative le flux massique pendant la sublimation, alors que des flux massiques plus élevés ont été observés lorsque la nucléation a été contrôlée pendant l'étape de congélation. Il est largement admis dans la littérature que la valeur de la température de nucléation influence la taille des cristaux de glace, la taille des pores dans la couche sèche du produit et le flux massique pendant l'étape de sublimation. Cependant, la nucléation est un phénomène stochastique et, par conséquent, des cristaux de glace de taille différente peuvent se former dans différents flacons pendant la congélation, ce qui conduit à une variabilité de flux massiques entre les flacons. La quantification de la variabilité de transfert de matière dans un lot, en particulier de taille commerciale (environ 100,000 flacons), peut être vraiment difficile à réaliser. De plus, les dispositifs disponibles pour la détermination du flux

massique donnent habituellement soit une valeur globale parmi tous les flacons dans le lot (e.g. le test d'élévation de pression), soit une valeur locale dans un ou dans un ou un nombre réduit de flacons (e.g. microbalance).

Dans ce travail, une nouvelle approche a été proposée pour estimer la variabilité du transfert de matière, exprimée en termes de distribution de la résistance du produit, en utilisant deux méthodes expérimentales: le test de remonté de pression (PRT) et la méthode gravimétrique. Ces approches ont été utilisées pour des cycles de lyophilisation effectués avec différents protocoles de congélation, c'est-à-dire une nucléation spontanée et contrôlée.

La méthode PRT a été utilisée pour évaluer l'évolution de la résistance du produit avec l'épaisseur de la couche sèche dans 5 lots de flacons de laboratoire. Ces données ont ensuite été combinées pour estimer la variabilité de la résistance du produit dans un lot de flacons. La variabilité de la résistance du produit déterminée en utilisant la méthode PRT dans des lots ayant subi une nucléation contrôlée a été plus faible que dans les lots avec nucléation spontanée. En outre, la variabilité de la résistance du produit entre les flacons au sein d'un même estimée en utilisant la méthode gravimétrique s'est avérée significativement inférieure à celle entre différents lots, obtenue à partir de la méthode PRT. Les distributions de résistance des produits déterminées à partir de la méthode PRT ont été utilisées pour calculer les distributions de température du produit et ont abouti à la définition d'une marge de sécurité de la température du produit d'environ  $\pm 5$  °C en raison uniquement de la variabilité du transfert de matière.

La nature stochastique de la nucléation influence non seulement les dimensions des pores dans l'épaisseur de la couche sèche, mais aussi la surface spécifique disponible pour la désorption pendant la dessiccation secondaire. L'impact de la variabilité de la cinétique de désorption sur la teneur en eau du produit pendant la dessiccation secondaire a été évalué et exprimé en termes d'écart type du temps caractéristique de désorption (présenté dans la **Publication III.5** dans ce manuscrit). Le modèle de désorption multicouche proposé précédemment a décrit de manière adéquate l'évolution l'humidité pendant l'étape de séchage secondaire. La désorption de la multicouche s'est révélée significativement plus rapide que la désorption de la monocouche. De plus, la température et la structure du produit ont eu un impact significatif sur la cinétique de désorption. L'écart-type du temps caractéristique de désorption a été quantifié à partir de données expérimentales et utilisé avec succès pour

prédire la distribution de la teneur en eau dans le lot de produit final ainsi que le risque associé au procédé, exprimé en % de flacons potentiellement rejetés en raison d'une trop forte humidité résiduelle.

Dans la dernière étape du projet, les mécanismes précédents de transfert de chaleur et de matière ont été inclus dans un modèle mathématique dynamique développé dans Matlab (présenté dans la **Publication III.6** dans ce manuscrit) afin de prédire la température du produit, la pression de vapeur partielle, la fraction de glace résiduelle et les évolutions du taux d'humidité pour différentes conditions opératoires (température d'étagère, pression de la chambre, temps de séchage), pour 100 flacons remplis de solution de saccharose à 5 % situés aux différents endroits de l'étagère. Le modèle développé a ensuite été utilisé pour concevoir les étapes de séchage primaire et secondaire du processus au niveau de risque spécifié. Quatre contraintes principales ont été considérées comme définissant les limites de l'espace de conception: (i) une température du produit inférieure à la température de transition vitreuse pendant la dessiccation primaire et (ii) pendant la dessiccation secondaire, (iii) l'achèvement de la sublimation à la fin de la dessiccation primaire et (iv) une valeur de teneur en eau dans le produit final inférieure à la valeur cible. Le modèle développé a ensuite été utilisé pour concevoir les étapes de séchage primaire et secondaire du processus au niveau de risque spécifié.

### **Perspectives**

Les perspectives à court terme ici proposées concernent l'amélioration des deux modèles mathématiques développés au cours de cette thèse: le modèle mathématique 3D de transfert de chaleur en régime permanent pour les flacons du bord de l'étagère et le modèle dynamique multi-flacon incluant les différentes sources de variabilité étudiées.

Le modèle mathématique 3D du transfert de chaleur dans la lyophilisation développé à l'aide de COMSOL Multiphysics permet d'évaluer la variabilité du flux de chaleur entre les flacons du bord et centraux pour différentes configurations de chargement de flacons et de caractéristiques de l'équipement. Il a été observé par simulation que le flacon situé dans la troisième rangée reçoit encore une contribution non négligeable des parois et du rail. Ainsi, l'inclusion d'autres lignes de flacons dans la géométrie d'origine du modèle pourrait permettre de simuler des vrais flacons "centraux". Par ailleurs, l'inclusion de la résistance du produit, et plus généralement le transfert de matière entre le front de sublimation des flacons

et le condenseur, pourrait permettre de prédire également la température du produit et de définir une marge de sécurité en termes de température.

Le modèle mathématique dynamique de lyophilisation développé est très prometteur car il permet de déterminer des *design spaces* basés sur l'évaluation des risques de dessiccation primaire et secondaire en fonction de différentes contraintes (par exemple, la température maximale admissible du produit, la teneur en eau résiduelle cible). Cependant, certaines améliorations devraient être effectuées pour assurer la robustesse des prédictions du modèle. Les travaux futurs devraient porter surtout sur la validation expérimentale. Les paramètres physiques utilisés dans le modèle (par exemple  $K_V$ ,  $R_p$ ) et leurs distributions ont été déterminés expérimentalement au cours de ce projet. Cependant, pour assurer la robustesse du modèle et, par conséquent, de l'analyse de l'évaluation des risques effectuée, une validation expérimentale complémentaire. Tout d'abord, le profil de température du produit et l'évolution du taux d'eau pour les flacons situés aux différents endroits sur l'étagère prédite par le modèle devraient être comparés aux données expérimentales. La validation de la pression de vapeur partielle dans la chambre à partir des données obtenues de la jauge Pirani devrait également être envisagée car cette grandeur décrit bien l'hétérogénéité globale des conditions de lyophilisation. Enfin, le pourcentage de flacons rejetés prévu par le modèle devrait être comparé à celui actuel. Différents scénarios devraient être testés, par exemple cycle dans lequel la température du produit est supérieure à la température de transition vitreuse pendant la dessiccation primaire et secondaire ; un taux d'eau supérieur à la valeur cible, etc. L'inspection visuelle des flacons doit être effectuée et le pourcentage de flacons s'effondrant et / ou présentant une teneur élevée en eau devrait être évalué.





**— REFERENCES —**



## REFERENCES

- Abdelwahed, W., Degobert, G., Stainmesse, S. and Fessi, H. (2006). 'Freeze-drying of nanoparticles: Formulation, process and storage considerations☆'. *Advanced Drug Delivery Reviews*, 58 (15), pp.1688–1713
- Adams, G. D. J. (1991). 'Freeze-Drying of Biological Materials'. *Drying Technology*, 9 (4), pp.891–925
- Akers, M. J. (2016). *Sterile drug products: formulation, packaging, manufacturing and quality*. 1st ed. London, UK: CRC Press
- Akhilesh, B. and Babu, M. M. (2010). 'Selection of Containers/Closures for Use in Lyophilization Applications: Possibilities and Limitations'. *American Pharmaceutical Review*, 13 (4)
- Amestoy, P. R., Duff, I. S., L'Excellent, J.-Y. and Koster, J. (2001). 'MUMPS: A General Purpose Distributed Memory Sparse Solver'. In: Sørøvik, T., Manne, F., Gebremedhin, A. H. and Moe, R. (eds.), *Applied Parallel Computing. New Paradigms for HPC in Industry and Academia: 5th International Workshop, PARA 2000 Bergen, Norway, June 18–20, 2000 Proceedings*, Berlin, Heidelberg: Springer Berlin Heidelberg, pp.121–130
- Barresi, A. A., Ghio, S., Fissore, D. and Pisano, R. (2009a). 'Freeze Drying of Pharmaceutical Excipients Close to Collapse Temperature: Influence of the Process Conditions on Process Time and Product Quality'. *Drying Technology*, 27 (6), pp.805–816
- Barresi, A. A., Velardi, S. A., Fissore, D. and Pisano, R. (2009b). 'Monitoring and controlling processes with complex dynamics using soft-sensors'. In: Ferrarini, L. and Veber, C. (eds.), *Modeling, Control, Simulation and Diagnosis of Complex Industrial and Energy Systems*, Ottawa, CA: O3NEDIA - ISA, pp.139–162
- Béal, C. and Fonseca, F. (2015). 'Freezing of Probiotic Bacteria'. In: Foerst, P. and Santivarangkna, C. (eds.), *Advances in Probiotic Technology*, Boca Raton, FL: CRC Press, pp.179–212 (Accessed: 19 September 2017).
- Bird, R. B., Stewart, W. E. and Lightfoot, E. N. (2002). *Transport phenomena*. 2nd ed. New York: Wiley
- Bosca, S., Barresi, A. A. and Fissore, D. (2013). 'Use of a soft sensor for the fast estimation of dried cake resistance during a freeze-drying cycle'. *International Journal of Pharmaceutics*, 451 (1–2), pp.23–33
- Bosca, S., Barresi, A. A., Fissore, D. and Deamichele, M. (2015). 'Risk-Based Design of a Freeze-Drying Cycle for Pharmaceuticals'. In: *EMChIE 2015 Conference Proceedings*, 1, 2015, Tarragona: Arts Gràfiques Rabassa, S.A., pp.265–270
- Broadwater, R. P., Shaalan, H. E., Fabrycky, W. J. and Lee, R. E. (1994). 'Decision evaluation with interval mathematics: a power distribution system case study'. *IEEE Transactions on power delivery*, 9 (1), pp.59–67

- Brülls, M. and Rasmuson, a. (2002a). 'Heat transfer in vial lyophilization'. *International Journal of Pharmaceutics*, 246 (1–2), pp.1–16 [Online]. doi:10.1016/S0378-5173(02)00353-8.
- Brülls, M. and Rasmuson, A. (2002b). 'Heat transfer in vial lyophilization'. *International Journal of Pharmaceutics*, 246 (1–2), pp.1–16
- Cannon, A. and Semeley, K. (2004). 'Statistical evaluation of vial design features that influence sublimation rates during primary drying'. *Pharmaceutical research*, 21 (3), pp.536–542
- Chang, B. S. and Fischer, N. L. (1995). 'Development of an efficient single-step freeze-drying cycle for protein formulations'. *Pharmaceutical Research*, 12 (6), pp.831–837
- Dushman, S. and Lafferty, M. J. (eds.). (1962). *Scientific foundations of vacuum technique*. 2nd ed. New York: Wiley
- Fissore, D. and Barresi, A. A. (2011). 'Scale-up and process transfer of freeze-drying recipes'. *Drying Technology*, 29 (14), pp.1673–1684
- Fissore, D. and Pisano, R. (2015). 'Computer-Aided Framework for the Design of Freeze-Drying Cycles: Optimization of the Operating Conditions of the Primary Drying Stage'. *Processes*, 3 (2), pp.406–421
- Fissore, D., Pisano, R. and Barresi, A. A. (2010). 'On the Methods Based on the Pressure Rise Test for Monitoring a Freeze-Drying Process'. *Drying Technology*, 29 (1), pp.73–90
- Fissore, D., Pisano, R. and Barresi, A. A. (2011a). 'Advanced approach to build the design space for the primary drying of a pharmaceutical freeze-drying process'. *Journal of Pharmaceutical Sciences*, 100 (11), pp.4922–4933
- Fissore, D., Pisano, R. and Barresi, A. A. (2011b). 'Monitoring of the Secondary Drying in Freeze-Drying of Pharmaceuticals'. *Journal of Pharmaceutical Sciences*, 100 (2), pp.732–742
- Fissore, D., Pisano, R. and Barresi, A. A. (2015). 'Using Mathematical Modeling and Prior Knowledge for QbD in Freeze-Drying Processes'. In: Jameel, F., Hershenson, S., Khan, M. A. and Martin-Moe, S. (eds.), *Quality by Design for Biopharmaceutical Drug Product Development*, 18, New York, NY: Springer New York, pp.565–593
- Fonseca, F., Cenard, S. and Passot, S. (2015). 'Freeze-Drying of Lactic Acid Bacteria'. In: Wolkers, W. F. and Oldenhof, H. (eds.), *Cryopreservation and Freeze-Drying Protocols*, 1257, New York, NY: Springer New York, pp.477–488
- Fonseca, F., Passot, S., Cunin, O. and Marin, M. (2008). 'Collapse Temperature of Freeze-Dried *Lactobacillus bulgaricus* Suspensions and Protective Media'. *Biotechnology Progress*, 20 (1), pp.229–238
- Food and Drug Administration. (2009). *Guidance for Industry, Q8(R2) Pharmaceutical Development*. Rockville, US: U.S. Dept. of Health and Human Services, Food and Drug Administration, Center for Drug Evaluation and Research [Online]. Available at: <http://purl.access.gpo.gov/GPO/LPS117887> (Accessed: 26 September 2017).
- Franks, F. (1998). 'Freeze-drying of bioproducts: putting principles into practice'. *European Journal of Pharmaceutics and Biopharmaceutics*, 45 (3), pp.221–229

- Fukusako, S. (1990). 'Thermophysical properties of ice, snow, and sea ice'. *International Journal of Thermophysics*, 11 (2), pp.353–372
- Gan, K. H., Bruttini, R., Crosser, O. K. and Liapis, A. I. (2005). 'Freeze-drying of pharmaceuticals in vials on trays: effects of drying chamber wall temperature and tray side on lyophilization performance'. *International Journal of Heat and Mass Transfer*, 48 (9), pp.1675–1687
- Ganguly, A., Nail, S. L. and Alexeenko, A. (2013). 'Experimental Determination of the Key Heat Transfer Mechanisms in Pharmaceutical Freeze-Drying'. *Journal of Pharmaceutical Sciences*, 102 (5), pp.1610–1625
- Gieseler, H., Kessler, W. J., Finson, M., Davis, S. J., Mulhall, P. A., Bons, V., Debo, D. J. and Pikal, M. J. (2007). 'Evaluation of tunable diode laser absorption spectroscopy for in-process water vapor mass flux measurements during freeze drying'. *Journal of Pharmaceutical Sciences*, 96 (7), pp.1776–1793
- Giordano, A., Barresi, A. A. and Fissore, D. (2011). 'On the Use of Mathematical Models to Build the Design Space for the Primary Drying Phase of a Pharmaceutical Lyophilization Process'. *Journal of Pharmaceutical Sciences*, 100 (1), pp.311–324
- Hansen, L. J. J., Daoussi, R., Vervaet, C., Remon, J.-P. and De Beer, T. R. M. (2015). 'Freeze-drying of live virus vaccines: A review'. *Vaccine*, 33 (42), pp.5507–5519
- Haynes, W. M., Lide, D. R. and Bruno, T. J. (eds.). (2014). *CRC Handbook of Chemistry and Physics*. 93rd ed. Boca Raton, FL: CRC Press
- Heldman, D. R. (ed.). (2010). *Encyclopedia of Agricultural, Food, and Biological Engineering*. 2nd ed. New York, NY: Marcel Dekker, Inc
- Hibler, S. and Gieseler, H. (2012). 'Heat transfer characteristics of current primary packaging systems for pharmaceutical freeze-drying'. *Journal of Pharmaceutical Sciences*, 101 (11), pp.4025–4031
- Hibler, S., Wagner, C. and Gieseler, H. (2012). 'Vial Freeze-Drying, part 1: New Insights into Heat Transfer Characteristics of Tubing and Molded Vials'. *Journal of Pharmaceutical Sciences*, 101 (3), pp.1189–1201
- Hottot, A., Peczalski, R., Vessot, S. and Andrieu, J. (2006). 'Freeze-Drying of Pharmaceutical Proteins in Vials: Modeling of Freezing and Sublimation Steps'. *Drying Technology*, 24 (5), pp.561–570
- Hottot, A., Vessot, S. and Andrieu, J. (2005). 'Determination of mass and heat transfer parameters during freeze-drying cycles of pharmaceutical products'. *PDA journal of pharmaceutical science and technology / PDA*, 59 (2), pp.138–153
- Jennings, T. A. (1999). *Lyophilization: introduction and basic principles*. Englewood, CO: Interpharm Press
- J.H. de Boer. (1953). *The dynamic character of adsorption*. Oxford, UK: Clarendon Press
- Johnson, R. and Lewis, L. (2011). 'Freeze-drying protein formulations above their collapse temperatures: Possible issues and concerns'. *American Pharmaceutical Review*, 14 (3), pp.50–54

- Kasper, J. C. and Friess, W. (2011). 'The freezing step in lyophilization: Physico-chemical fundamentals, freezing methods and consequences on process performance and quality attributes of biopharmaceuticals'. *European Journal of Pharmaceutics and Biopharmaceutics*, 78 (2), pp.248–263
- Kochs, M., Körber, C., Nunner, B. and Heschel, I. (1991). 'The influence of the freezing process on vapour transport during sublimation in vacuum-freeze-drying'. *International Journal of Heat and Mass Transfer*, 34 (9), pp.2395–2408
- Kodama, T., Sawada, H., Hosomi, H., Takeuchi, M., Wakiyama, N., Yonemochi, E. and Terada, K. (2013). 'Determination for dry layer resistance of sucrose under various primary drying conditions using a novel simulation program for designing pharmaceutical lyophilization cycle'. *International Journal of Pharmaceutics*, 452 (1–2), pp.180–187
- Koganti, V. R., Shalaev, E. Y., Berry, M. R., Osterberg, T., Youssef, M., Hiebert, D. N., Kanka, F. A., Nolan, M., Barrett, R., Scalzo, G., Fitzpatrick, G., Fitzgibbon, N., Luthra, S. and Zhang, L. (2011). 'Investigation of Design Space for Freeze-Drying: Use of Modeling for Primary Drying Segment of a Freeze-Drying Cycle'. *AAPS PharmSciTech*, 12 (3), pp.854–861
- Konstantinidis, A. K., Kuu, W., Otten, L., Nail, S. L. and Sever, R. R. (2011). 'Controlled nucleation in freeze-drying: Effects on pore size in the dried product layer, mass transfer resistance, and primary drying rate'. *Journal of Pharmaceutical Sciences*, 100 (8), pp.3453–3470
- Kremer, D. M., Pikal, M. J., Petre, W. J., Shalaev, E. Y., Gatlin, L. A. and Kramer, T. (2009). 'A procedure to optimize scale-up for the primary drying phase of lyophilization'. *Journal of Pharmaceutical Sciences*, 98 (1), pp.307–318
- Kuu, W., Hardwick, L. and Akers, M. (2006). 'Rapid determination of dry layer mass transfer resistance for various pharmaceutical formulations during primary drying using product temperature profiles'. *International Journal of Pharmaceutics*, 313 (1–2), pp.99–113
- Kuu, W. Y., Nail, S. L. and Sacha, G. (2009). 'Rapid determination of vial heat transfer parameters using tunable diode laser absorption spectroscopy (TDLAS) in response to step-changes in pressure set-point during freeze-drying'. *Journal of Pharmaceutical Sciences*, 98 (3), pp.1136–1154
- Kuu, W. Y., O'Bryan, K. R., Hardwick, L. M. and Paul, T. W. (2011). 'Product mass transfer resistance directly determined during freeze-drying cycle runs using tunable diode laser absorption spectroscopy (TDLAS) and pore diffusion model'. *Pharmaceutical Development and Technology*, 16 (4), pp.343–357
- Liapis, A. I. and Bruttini, R. (1994). 'A theory for the primary and secondary drying stages of the freeze-drying of pharmaceutical crystalline and amorphous solutes: comparison between experimental data and theory'. *Separations Technology*, 4 (3), pp.144–155
- Liapis, A. I. and Litchfield, R. J. (1979). 'Optimal control of a freeze dryer—I Theoretical development and quasi steady state analysis'. *Chemical Engineering Science*, 34 (7), pp.975–981
- Liu, Y., Zhao, Y. and Feng, X. (2008). 'Exergy analysis for a freeze-drying process'. *Applied Thermal Engineering*, 28 (7), pp.675–690
- Lopez-Quiroga, E., Antelo, L. T. and Alonso, A. A. (2012). 'Time-scale modeling and optimal control of freeze-drying'. *Journal of Food Engineering*, 111 (4), pp.655–666

- Lu, X. and Pikal, M. J. (2004). 'Freeze-Drying of Mannitol–Trehalose–Sodium Chloride-Based Formulations: The Impact of Annealing on Dry Layer Resistance to Mass Transfer and Cake Structure'. *Pharmaceutical Development and Technology*, 9 (1), pp.85–95
- Mascarenhas, W. J., Akay, H. U. and Pikal, M. J. (1997). 'A computational model for finite element analysis of the freeze-drying process'. *Computer Methods in Applied Mechanics and Engineering*, 148 (1–2), pp.105–124
- Mayeresse, Y. (2008). *Moisture content in freeze-dried product*. San Diego, California
- Millman, M. J., Liapis, A. I. and Marchello, J. M. (1985). 'An analysis of the lyophilization process using a sorption-sublimation model and various operational policies'. *AIChE Journal*, 31 (10), pp.1594–1604
- Milton, N., Pikal, M. J., Roy, M. L. and Nail, S. L. (1997). 'Evaluation of manometric temperature measurement as a method of monitoring product temperature during lyophilization'. *PDA Journal of Pharmaceutical Science and Technology*, 51 (1), pp.7–16
- Mockus, L. N., Paul, T. W., Pease, N. A., Harper, N. J., Basu, P. K., Oslos, E. A., Sacha, G. A., Kuu, W. Y., Hardwick, L. M., Karty, J. J., Pikal, M. J., Hee, E., Khan, M. A. and Nail, S. L. (2011). 'Quality by design in formulation and process development for a freeze-dried, small molecule parenteral product: a case study'. *Pharmaceutical Development and Technology*, 16 (6), pp.549–576
- Monchau, J.-P., Candau, Y. and Ibos, L. (2013). *Device for Measuring the Emissivity or Reflectivity of a Surface*. Patent WO2013EP53112 20130215. [Online]. Available at: [http://worldwide.espacenet.com/publicationDetails/biblio?DB=worldwide.espacenet.com&II=1&ND=3&adjacent=true&locale=en\\_EP&FT=D&date=20130822&CC=WO&NR=2013121013A1&KC=A1](http://worldwide.espacenet.com/publicationDetails/biblio?DB=worldwide.espacenet.com&II=1&ND=3&adjacent=true&locale=en_EP&FT=D&date=20130822&CC=WO&NR=2013121013A1&KC=A1) (Accessed: 25 September 2017).
- Mortier, S. T. F. C., Van Bockstal, P.-J., Corver, J., Nopens, I., Gernaey, K. V. and De Beer, T. (2016). 'Uncertainty analysis as essential step in the establishment of the dynamic Design Space of primary drying during freeze-drying'. *European Journal of Pharmaceutics and Biopharmaceutics*, 103, pp.71–83
- Nail, S. L. (1980). 'The Effect of Chamber Pressure on Heat Transfer in the Freeze Drying of Parenteral Solutions'. *PDA Journal of Pharmaceutical Science and Technology*, 34 (5), pp.358–368
- Nail, S. L. and Searles, J. A. (2008). 'Elements of quality by design in development and scale-up of freeze parenterals'. *Biopharm International*, 21 (1), pp.44–52
- Oddone, I., Barresi, A. A. and Pisano, R. (2017). 'Influence of controlled ice nucleation on the freeze-drying of pharmaceutical products: the secondary drying step'. *International Journal of Pharmaceutics*, 524 (1–2), pp.134–140
- Oddone, I., Pisano, R., Bullich, R. and Stewart, P. (2014). 'Vacuum-Induced Nucleation as a Method for Freeze-Drying Cycle Optimization'. *Industrial & Engineering Chemistry Research*, 53 (47), pp.18236–18244
- Oddone, I., Van Bockstal, P.-J., De Beer, T. and Pisano, R. (2016). 'Impact of vacuum-induced surface freezing on inter- and intra-vial heterogeneity'. *European Journal of Pharmaceutics and Biopharmaceutics*, 103, pp.167–178

## REFERENCES

---

- Overcashier, D. E., Patapoff, T. W. and Hsu, C. C. (1999). 'Lyophilization of protein formulations in vials: Investigation of the relationship between resistance to vapor flow during primary drying and small-scale product collapse'. *Journal of pharmaceutical sciences*, 88 (7), pp.688–695
- Passot, S., Cenard, S., Douania, I., Tréléa, I. C. and Fonseca, F. (2012). 'Critical water activity and amorphous state for optimal preservation of lyophilised lactic acid bacteria'. *Food Chemistry*, 132 (4), pp.1699–1705
- Passot, S., Fonseca, F., Barbouche, N., Marin, M., Alarcon-Lorca, M., Rolland, D. and Rapaud, M. (2007). 'Effect of Product Temperature During Primary Drying on the Long-Term Stability of Lyophilized Proteins'. *Pharmaceutical Development and Technology*, 12 (6), pp.543–553
- Passot, S., Tréléa, I. C., Marin, M., Galan, M., Morris, G. J. and Fonseca, F. (2009). 'Effect of Controlled Ice Nucleation on Primary Drying Stage and Protein Recovery in Vials Cooled in a Modified Freeze-Dryer'. *Journal of Biomechanical Engineering*, 131 (7), pp.074511
- Patel, S. M., Chaudhuri, S. and Pikal, M. J. (2010a). 'Choked flow and importance of Mach I in freeze-drying process design'. *Chemical Engineering Science*, 65 (21), pp.5716–5727
- Patel, S. M., Jameel, F. and Pikal, M. J. (2010b). 'The effect of dryer load on freeze drying process design'. *Journal of Pharmaceutical Sciences*, 99 (10), pp.4363–4379
- Patel, S. M., Nail, S. L., Pikal, M. J., Geidobler, R., Winter, G., Hawe, A., Davagnino, J. and Rambhatla Gupta, S. (2017). 'Lyophilized Drug Product Cake Appearance: What Is Acceptable?'. *Journal of Pharmaceutical Sciences*, 106 (7), pp.1706–1721
- Patel, S. M. and Pikal, M. J. (2013). 'Lyophilization Process Design Space'. *Journal of Pharmaceutical Sciences*, 102 (11), pp.3883–3887
- Perry, R. H., Green, D. W. and Maloney, J. O. (eds.). (1997). *Perry's Chemical Engineering Handbook*. 7th ed. New York, NY: McGraw-Hill
- Pikal, M. J. (1985). 'Use of laboratory data in freeze drying process design: heat and mass transfer coefficients and the computer simulation of freeze drying'. *Journal of Parenteral Science and Technology: A Publication of the Parenteral Drug Association*, 39 (3), pp.115–139
- Pikal, M. J. (1994). 'Freeze-Drying of Proteins: Process, Formulation, and Stability'. In: Cleland, J. L. and Langer, R. (eds.), *Formulation and Delivery of Proteins and Peptides*, 567, Washington, DC: American Chemical Society, pp.120–133
- Pikal, M. J. (2000). 'Heat and mass transfer in low pressure gases: applications to freeze drying'. *Drugs and the Pharmaceutical Sciences*, 102, pp.611–686
- Pikal, M. J., Bogner, R., Mudhivarthi, V., Sharma, P. and Sane, P. (2016). 'Freeze-Drying Process Development and Scale-Up: Scale-Up of Edge Vial Versus Center Vial Heat Transfer Coefficients, Kv'. *Journal of Pharmaceutical Sciences*, 105 (11)
- Pikal, M. J., Dellerman, K. M., Roy, M. L. and Ralph M. Riggin. (1991). 'The Effects of Formulation Variables on the Stability of Freeze-Dried Human Growth Hormone'. *Pharmaceutical Research*, 8 (14), pp.427–436
- Pikal, M. J., Mascarenhas, W. J., Akay, H. U., Cardon, S., Bhugra, C., Jameel, F. and Rambhatla, S. (2005). 'The Nonsteady State Modeling of Freeze Drying: In-Process Product Temperature and

- Moisture Content Mapping and Pharmaceutical Product Quality Applications'. *Pharmaceutical Development and Technology*, 10 (1), pp.17–32
- Pikal, M. J., Roy, M. L. and Shah, S. (1984). 'Mass and heat transfer in vial freeze-drying of pharmaceuticals: role of the vial'. *Journal of Pharmaceutical Sciences*, 73 (9), pp.1224–1237
- Pikal, M. J. and Shah, S. (1990). 'The collapse temperature in freeze drying: Dependence on measurement methodology and rate of water removal from the glassy phase'. *International Journal of Pharmaceutics*, 62 (2–3), pp.165–186
- Pikal, M. J., Shah, S., Senior, D. and Lang, J. E. (1983). 'Physical chemistry of freeze-drying: Measurement of sublimation rates for frozen aqueous solutions by a microbalance technique'. *Journal of pharmaceutical sciences*, 72 (6), pp.635–650
- Pikal, M., Shah, S., Roy, M. and Putman, R. (1990). 'The secondary drying stage of freeze drying: drying kinetics as a function of temperature and chamber pressure☆'. *International Journal of Pharmaceutics*, 60 (3), pp.203–207
- Pisano, R., Barresi, A. A. and Fissore, D. (2011). 'Heat transfer in freeze-drying apparatus'. In: dos Santos Bernardes, M. (ed.), *Developments in Heat Transfer*, Rijeka, Croatia: INTECH, pp.91–114 [Online]. Available at: <http://cdn.intechweb.org/pdfs/19886.pdf> (Accessed: 26 September 2017).
- Pisano, R., Fissore, D. and Barresi, A. A. (2012a). 'Quality by Design in the Secondary Drying Step of a Freeze-Drying Process'. *Drying Technology*, 30 (11–12), pp.1307–1316
- Pisano, R., Fissore, D. and Barresi, A. A. (2012b). 'Quality by Design in the Secondary Drying Step of a Freeze-Drying Process'. *Drying Technology*, 30 (11–12), pp.1307–1316
- Pisano, R., Fissore, D., Barresi, A. A., Brayard, P., Chouvenec, P. and Woinet, B. (2013). 'Quality by design: optimization of a freeze-drying cycle via design space in case of heterogeneous drying behavior and influence of the freezing protocol'. *Pharmaceutical Development and Technology*, 18 (1), pp.280–295
- Rambhatla, S. and Pikal, M. J. (2003). 'Heat and mass transfer scale-up issues during freeze-drying, I: atypical radiation and the edge vial effect'. *Aaps Pharmscitech*, 4 (2), pp.22–31
- Rambhatla, S., Ramot, R., Bhugra, C. and Pikal, M. J. (2004). 'Heat and mass transfer scale-up issues during freeze drying: II. Control and characterization of the degree of supercooling'. *Aaps Pharmscitech*, 5 (4), pp.54–62
- Rasetto, V., Marchisio, D. L., Fissore, D. and Barresi, A. A. (2008). 'Model-based monitoring of a non-uniform batch in a freeze-drying process'. In: *Proceedings of 18th European Symposium on Computer Aided Process Engineering–ESCAPE18 (edited by B. Braunschweig, X. Joulia)*, 2008, pp.1–4 [Online]. Available at: [https://www.researchgate.net/profile/Davide\\_Fissore/publication/268049257\\_Model\\_based-monitoring\\_of\\_a\\_non-uniform\\_batch\\_in\\_a\\_freeze-drying\\_process/links/5551ad3708ae12808b392e00.pdf](https://www.researchgate.net/profile/Davide_Fissore/publication/268049257_Model_based-monitoring_of_a_non-uniform_batch_in_a_freeze-drying_process/links/5551ad3708ae12808b392e00.pdf) (Accessed: 18 October 2016).
- Ratti, C. (2001). 'Hot air and freeze-drying of high-value foods: a review'. *Journal of food engineering*, 49 (4), pp.311–319
- Riedel, S. (2005). 'Edward Jenner and the history of smallpox and vaccination'. *Proceedings (Baylor University. Medical Center)*, 18 (1), pp.21–25

- Roos, Y. H. (1997). 'Frozen state transitions in relation to freeze drying'. *Journal of thermal analysis*, 48 (3), pp.535–544 [Online]. doi:10.1007/BF01979500.
- Roos, Y. H. (2010). 'Glass Transition Temperature and Its Relevance in Food Processing'. *Annual Review of Food Science and Technology*, 1 (1), pp.469–496
- Roos, Y. and Karel, M. (2007). 'Amorphous state and delayed ice formation in sucrose solutions'. *International Journal of Food Science & Technology*, 26 (6), pp.553–566
- Sadikoglu, H. and Liapis, A. I. (1997). 'Mathematical Modelling of the Primary and Secondary Drying Stages of Bulk Solution Freeze-Drying in Trays: Parameter Estimation and Model Discrimination by Comparison of Theoretical Results With Experimental Data'. *Drying Technology*, 15 (3), pp.791–810
- Sadikoglu, H., Liapis, A. I. and Crosser, O. K. (1998). 'Optimal Control of the Primary and Secondary Stages of Bulk Solution Freeze-Drying in Trays'. *Drying Technology*, 16 (3–5), pp.399–431
- Sadikoglu, H., Ozdemir, M. and Seker, M. (2006). 'Freeze-Drying of Pharmaceutical Products: Research and Development Needs'. *Drying Technology*, 24 (7), pp.849–861
- Sahni, E. K. and Pikal, M. J. (2017). 'Modeling the Secondary Drying Stage of Freeze Drying: Development and Validation of an Excel-based Model'. *Journal of Pharmaceutical Sciences*, 106 (3), pp.779–791
- Schneid, S. C., Gieseler, H., Kessler, W. J., Luthra, S. A. and Pikal, M. J. (2011). 'Optimization of the Secondary Drying Step in Freeze Drying Using TDLAS Technology'. *AAPS PharmSciTech*, 12 (1), pp.379–387
- Schoen, M. P., Braxton, B. K., Gatlin, L. A. and Jefferis, R. P. (1995). 'A simulation model for the primary drying phase of the freeze-drying cycle'. *International Journal of Pharmaceutics*, 114 (2), pp.159–170
- Scutellà, B., Passot, S., Bourlés, E., Fonseca, F. and Trélea, I. C. (2017a). 'How Vial Geometry Variability Influences Heat Transfer and Product Temperature During Freeze-Drying'. *Journal of Pharmaceutical Sciences*, 106 (3), pp.770–778
- Scutellà, B., Plana-Fattori, A., Passot, S., Bourlés, E., Fonseca, F., Flick, D. and Trelea, I. C. (2017b). '3D mathematical modelling to understand atypical heat transfer observed in vial freeze-drying'. *Applied Thermal Engineering*, 126, pp.226–236
- Searles, J. A. (2010a). 'Freezing and Annealing Phenomena in Lyophilization'. In: Rey, L. and May, J. C. (eds.), *Freeze Drying/ Lyophilization of Pharmaceutical and Biological Products*, Drugs and the pharmaceutical sciences, 3rd ed, 206, London, UK: CRC Press, pp.52–81
- Searles, J. A. (2010b). 'Optimizing the Throughput of Freeze-Dryers Within a Constrained Design Space'. In: Rey, L. and May, J. C. (eds.), *Freeze Drying/ Lyophilization of Pharmaceutical and Biological Products*, Drugs and the pharmaceutical sciences, 3rd ed, 206, London, UK: Informa Healthcare
- Searles, J. A., Carpenter, J. F. and Randolph, T. W. (2001a). 'Annealing to optimize the primary drying rate, reduce freezing-induced drying rate heterogeneity, and determine Tg' in pharmaceutical lyophilization'. *Journal of pharmaceutical sciences*, 90 (7), pp.872–887

- Searles, J. A., Carpenter, J. F. and Randolph, T. W. (2001b). 'The ice nucleation temperature determines the primary drying rate of lyophilization for samples frozen on a temperature-controlled shelf'. *Journal of Pharmaceutical Sciences*, 90 (7), pp.860–871
- Sheehan, P. and Liapis, A. I. (1998). 'Modeling of the primary and secondary drying stages of the freeze drying of pharmaceutical products in vials: Numerical results obtained from the solution of a dynamic and spatially multi-dimensional lyophilization model for different operational policies'. *Biotechnology and Bioengineering*, 60 (6), pp.712–728
- Tang, X. C., Nail, S. L. and Pikal, M. J. (2006a). 'Evaluation of manometric temperature measurement (MTM), a process analytical technology tool in freeze drying, part III: heat and mass transfer measurement'. *AAPS PharmSciTech*, 7 (4), pp.E105–E111
- Tang, X. C. and Pikal, M. J. (2004). 'Design of freeze-drying processes for pharmaceuticals: practical advice'. *Pharmaceutical research*, 21 (2), pp.191–200
- Tang, X., Nail, S. L. and Pikal, M. J. (2006b). 'Evaluation of manometric temperature measurement, a process analytical technology tool for freeze-drying: Part I, product temperature measurement'. *AAPS PharmSciTech*, 7 (1), pp.E95–E103
- Tchessalov, S., Dixon, D. and Warne, N. W. (2007). 'Principles of lyophilization cycle scale-up'. *American Pharmaceutical Review*, 10 (2)
- Trelea, I. C., Fonseca, F. and Passot, S. (2016). 'Dynamic modeling of the secondary drying stage of freeze drying reveals distinct desorption kinetics for bound water'. *Drying Technology*, 34 (3), pp.335–345
- Trelea, I. C., Fonseca, F., Passot, S. and Flick, D. (2015). 'A Binary Gas Transport Model Improves the Prediction of Mass Transfer in Freeze Drying'. *Drying Technology*, 33 (15–16), pp.1849–1858
- Trelea, I. C., Passot, S., Fonseca, F. and Marin, M. (2007). 'An Interactive Tool for the Optimization of Freeze-Drying Cycles Based on Quality Criteria'. *Drying Technology*, 25 (5), pp.741–751
- Tsinontides, S. C., Rajniak, P., Pham, D., Hunke, W. A., Placek, J. and Reynolds, S. D. (2004). 'Freeze drying—principles and practice for successful scale-up to manufacturing'. *International Journal of Pharmaceutics*, 280 (1–2), pp.1–16
- Varshney, D. and Singh, M. (2015). 'History of Lyophilization'. In: Varshney, D. and Singh, M. (eds.), *Lyophilized Biologics and Vaccines: Modality-Based Approaches*, New York, NY: Springer New York, pp.3–10 [Online]. doi:10.1007/978-1-4939-2383-0\_1.
- Velardi, S. A. and Barresi, A. A. (2008). 'Development of simplified models for the freeze-drying process and investigation of the optimal operating conditions'. *Chemical Engineering Research and Design*, 86 (1), pp.9–22
- Velardi, S. A., Rasetto, V. and Barresi, A. A. (2008). 'Dynamic Parameters Estimation Method: Advanced Manometric Temperature Measurement Approach for Freeze-Drying Monitoring of Pharmaceutical Solutions'. *Industrial & Engineering Chemistry Research*, 47 (21), pp.8445–8457
- Xiang, J., Hey, J. M., Liedtke, V. and Wang, D. . (2004). 'Investigation of freeze–drying sublimation rates using a freeze–drying microbalance technique'. *International Journal of Pharmaceutics*, 279 (1–2), pp.95–105

## REFERENCES

---

Ybema, H., Kolkman-Roodbeen, L., te Booy, M. P. and Vromans, H. (1995). 'Vial lyophilization: calculations on rate limitation during primary drying'. *Pharmaceutical Research*, 12 (9), pp.1260–1263

Yu, L. (2001). 'Amorphous pharmaceutical solids: preparation, characterization and stabilization'. *Advanced drug delivery reviews*, 48 (1), pp.27–42

Yu, L. X. (2008). 'Pharmaceutical Quality by Design: Product and Process Development, Understanding, and Control'. *Pharmaceutical Research*, 25 (4), pp.781–791

Zhai, S., Su, H., Taylor, R. and Slater, N. K. H. (2005). 'Pure ice sublimation within vials in a laboratory lyophiliser; comparison of theory with experiment'. *Chemical Engineering Science*, 60 (4), pp.1167–1176





**— APPENDIX —**



## APPENDIX

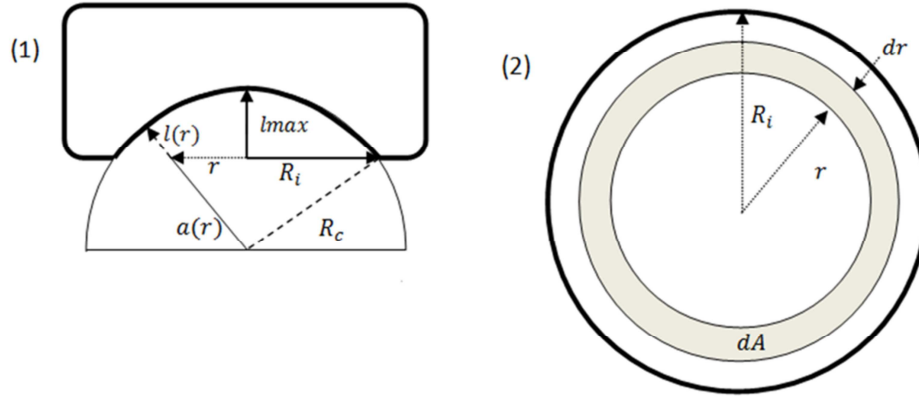


**Figure A.** Side (1) and top (2) view of the vial bottom represented as a semi-spherical calotte.

The evaluation of the mean bottom curvature depth  $l$  was performed from geometrical considerations on the semi-spherical calotte at the vial bottom, as represented in **Figure A**.

The bottom curvature depth depends on the radius of the vial bottom as follows:

$$l(r) = R_c - a(r) \quad \text{Equation A1}$$

where  $R_c$  is the radius of the calotte and  $a(r)$  is the distance between the shelf and the vial bottom, measured normal to the vial bottom:

$$a(r) = \sqrt{(R_c - l_{max})^2 + r^2} \quad \text{Equation A2}$$

$R_c$  can be calculated as a function of the maximum bottom curvature depth  $l_{max}$  and the inner vial bottom radius  $R_i$ :

$$R_c^2 = R_i^2 + (R_c - l_{max})^2 \quad \text{Equation A3}$$

The area-mean bottom curvature depth can be defined as the integral of  $l(r)$  on the calotte, divided by the area:

$$l = \frac{1}{A} \int l(r) dA \quad \text{Equation A4}$$

The relevant area for heat transfer by gas conduction is:

$$A = \pi R_i^2 \quad \text{Equation A5}$$

and the area element:

$$dA = 2\pi r dr \quad \text{Equation A6}$$

Combining **Equations A1-A6**,  $l$  was calculated as:

$$l = \frac{2}{R_i^2} \int_0^{R_i} (R_c - \sqrt{(R_c - l_{max})^2 + r^2}) r dr \quad \text{Equation A7}$$







**Title :** *Freeze-drying of vaccines: Contribution of mathematical modelling for assessing product heterogeneity and scale-up risks*

**Keywords :** drying; heat and mass transfer; scale-up; Quality-by-Design; mathematical modelling.

**Abstract:** Freeze-drying is the process of choice in pharmaceutical industry for the stabilization of heat sensitive products such as vaccines. However, due the product pre-conditioning in individual vials, this process is difficult to design and often results in batches presenting a significant heterogeneity in the quality of the final product. The main goal of this Ph.D. project was the development of a mathematical model making it possible to predict the risk of failure when designing the freeze-drying process, i.e., the percentage of "rejected vials". To this end, the work focused on the understanding and quantification of the sources responsible for heat and mass transfer variability during the process. Firstly, the vial-to-vial heat transfer variability was investigated by taking the vial bottom dimensions and the vial position on the shelf of equipment into account. The variability of geometrical dimensions observed within a batch of vials (i.e., contact area between the shelf and the vial and the mean bottom curvature depth) moderately influenced the heat transfer coefficient distribution among vials (by less than 10 %). Secondly, a original 3D mathematical model was developed in COMSOL Multiphysics to explain and predict atypical heat transfer observed in vials located at the border of the shelf during the freeze-drying process. Conduction through low-pressure water vapour appeared as the dominant mechanism explaining the additional heat transfer to border vials rather than as reported in literature radiation from the walls of the drying chamber. Furthermore, this 3D mathematical model was used to investigate the effect of the vial loading configuration and of the equipment characteristics on heat transfer variability. In a second part, mass transfer variability was quantified on a 5% sucrose solution and by focusing on two parameters, the resistance of the dried layer to mass transfer during sublimation and the characteristic desorption time. The dried layer resistance was assessed by combining complementary approaches, the pressure rise test and gravimetric methods. The estimated variability of the dried layer resistance was found to have a higher impact on the product temperature distribution than the heat transfer coefficient variability. The value and variability of characteristic desorption time was evaluated for different temperatures and made it possible to simulate moisture content heterogeneity between vials in the batch. In the last part of the work, the main quantified sources of heat and mass transfer variability were integrated in a mathematical model of freeze-drying process. This multi-vial, dynamic model was used not only to predict the evolution of product temperature and moisture content during freeze-drying for a batch of 100 vials, but also to estimate the percentage of vials that could potentially be rejected. The proposed approach, extended to a greater number of simulated vials, could be applied to calculate design spaces of the primary and secondary drying steps of freeze-drying process at a known risk of failure.

**Titre :** *La lyophilisation des vaccins: contribution de la mod lisation math matique   l' valuation de l'h t rog n it  des produits et des risques de changement d' chelle*

**Mots cl s :** s chage; transfert de masse et chaleur; changement d' chelle; Quality-by-Design; mod lisation math matique.

**R sum  :** La lyophilisation est le proc d  de choix dans l'industrie pharmaceutique pour la stabilisation de produits thermosensibles tels que les vaccins. Cependant, en raison du pr -conditionnement du produit dans des flacons individuels, ce processus est difficile   concevoir et aboutit souvent   des lots pr sentant une h t rog n it  significative dans la qualit  du produit final. L'objectif principal de ce doctorat a  t  le d veloppement d'un mod le math matique pour la conception du processus de lyophilisation   un niveau de risque donn , c'est   dire un pourcentage de flacons potentiellement non conformes. Le travail a port  sur la compr hension et la quantification des sources possibles responsables de la variabilit  des transferts de chaleur et de mati re lors du processus. Dans un premier temps, la variabilit  du transfert de chaleur entre les flacons a  t   tudi e en consid rant les dimensions du flacon et sa position sur l' tag re de l' quipement. La variabilit  des dimensions g om triques observ es dans un lot de flacons (i.e., l'aire de contact entre l' tag re et le flacon et la profondeur de concavit  du fond) a influenc  la distribution du coefficient de transfert de chaleur entre les flacons. De plus, un mod le math matique original en 3D a  t  d velopp  dans COMSOL Multiphysics pour expliquer et pr dire les transferts de chaleur atypiques observ s dans les flacons situ s sur les bords de l' tag re lors du processus de lyophilisation. Les ph nom nes conductifs   basse pression au sein de la vapeur d'eau ont  t  report s comme un m canisme dominant expliquant ces transferts de chaleur atypiques alors que les ph nom nes radiatifs li s   la pr sence des parois de l' quipement ont toujours  t  cit s dans la litt rature. Par ailleurs, ce mod le math matique en 3D a  t  utilis  pour  tudier l'effet de la configuration de chargement du lyophilisateur et des caract ristiques de l' quipement sur la variabilit  du transfert de chaleur. Dans un deuxi me temps, la variabilit  des transferts de mati re a  t   valu e sur une solution de saccharose   5 % en consid rant deux param tres, la r sistance de la couche s che au transfert de mati re pendant la sublimation et le temps caract ristique de d sorption. La r sistance   la couche s che a  t   valu e en combinant deux approches compl mentaires, les tests de remont e de pression et la m thode gravim trique. La variabilit  estim e de la r sistance   la couche s ch e a eu un impact plus important sur la distribution de la temp rature du produit que la variabilit  du coefficient de transfert de chaleur. La valeur et la variabilit  du temps caract ristique de d sorption ont  t   valu es pour diff rentes temp ratures et ont permis de simuler l'h t rog n it  de la teneur en eau finale entre les flacons. Dans la derni re partie du travail, les principales sources quantifi es de variabilit  des transferts de chaleur et de mati re ont  t  int gr es dans un mod le math matique de lyophilisation. Ce mod le dynamique multi-flacons a  t  utilis  non seulement pour pr dire l' volution de la temp rature et de la teneur en eau du produit pendant la lyophilisation pour un lot de 100 flacons, mais aussi pour estimer le pourcentage de flacons potentiellement non conformes. L'approche de mod lisation propos e,  tendue   un plus grand nombre de flacons simul s, pourrait  tre utilis e pour calculer les "design spaces" (espaces de travail) des  tapes de dessiccation primaire et secondaire du processus de lyophilisation   un risque connu de pourcentage de flacons non conformes.